UNIVERSITEIT VAN PRETORIA
UNIVERSITY OF PRETORIA
YUNIBESITHI YA PRETORIA

FINITE ELEMENT MODELLING OF CRACKING IN CONCRETE GRAVITY DAMS

Q. CAI

UNIVERSITEIT VAN PRETORIA
UNIVERSITY OF PRETORIA
YUNIBESITHI YA PRETORIA

Finite element modelling of cracking in concrete gravity dams

QINGBO CAI

A thesis submitted in partial fulfilment of the requirements for the degree of

PHILOSOPHIAE DOCTOR (ENGINEERING)

In the

FACULTY OF ENGINEERING, BUILT ENVIRONMENT AND INFORMATION TECHNOLOGY

UNIVERSITY OF PRETORIA

June 2007

THESIS SUMMARY

Finite element modelling of cracking in concrete gravity dams

by

Q. CAI

Supervisor: Professor B.W.J. van Rensburg

Co-Supervisor: Dr. J.M. Robberts

Department: Civil Engineering

University: University of Pretoria

Degree: Philosophiae Doctor (Engineering)

Evaluating the safety of unreinforced concrete structures, such as concrete dams, requires an accurate prediction of cracking. Developing a suitable constitutive material model and a reliable computational procedure for analysing cracking processes in concrete has been a challenging and demanding task.

Although many analytical methods based on fracture mechanics have been proposed for concrete dams in the last few decades, they have not yet become part of standard design procedures. Few of the current research findings are being implemented by practising engineers when evaluating dam safety.

This research is focused on the development of a suitable crack modelling and analysis method for the prediction and study of fracturing in concrete gravity dams, and consequently, for the evaluation of dam safety against cracking. The research aims to contribute to the continuing research efforts into mastering the mechanics of cracking in concrete dams.

An analytical method for the purpose of establishing a crack constitutive model and implementing the model for the fracture analysis of concrete structures, in particular massive concrete gravity dams under static loading conditions, has been developed, verified and applied in the safety evaluation of a concrete gravity dam.

The constitutive material model is based on non-linear fracture mechanics and assumes a bilinear softening response. The crack model has various improved features: (1) an enhanced mode I bilinear strain-softening approach has been put forward; (2) a new formula for bilinear softening parameters has been developed and their relation with linear softening has been outlined; (3) the influence of bilinear softening parameters on the cracking response has been studied; and (4) an enhanced modification to the shear retention factor which depends on the crack normal strain is included.

The material model has been incorporated into a finite element analysis using a smeared crack approach. A sub-program was specially coded for this research.

The validity of the proposed cracking model and the computational procedure developed for the purpose of analyzing the tensile fracture behaviour of concrete structures has been confirmed by verification on various concrete structures, including beams, a dam model and actual gravity dams.

The crack modelling technique developed was successfully used in evaluating the safety of an existing concrete gravity dam in South Africa and adequately predicted the cracking response of the dam structure under static loadings.

The main conclusions drawn are as follows:

- Both mode I and mode II fracture have been modelled successfully.
- The proposed bilinear softening model remains relatively simple to implement but significantly improves on predicting the softening response of “small-scale” concrete structures.
- Both plane stress and plane strain crack analyses have been considered and can be confidently adopted in two-dimensional applications.

- The proposed method is mesh objective.
- The crack modelling method developed can correctly predict the crack propagation trajectory and the structural behaviour with regard to fracturing in concrete structures.
- If not considering shear stress concentration near the tip of a crack, constitutive crack analysis normally indicates a higher safety factor and a higher Imminent Failure Flood (IFF) than the classical methods in the analysis of concrete gravity dams for safety evaluation.

Keyterms: Concrete gravity dams, constitutive crack model, non-linear fracture mechanics, crack modeling, dam safety, computational procedure, crack propagation, bilinear softening, smeared crack approach.

ACKNOWLEDGEMENTS

I wish to express my appreciation to the following organization and people who made this thesis possible:

(a) Professor B.W.J. van Rensburg, my supervisor, and Dr. J.M. Robberts, my co-supervisor, for their constant guidance, profound interest in and valuable advice with this difficult research topic.

(b) Dr. C. Oosthuizen for his support and encouragement during the course of the study.

(c) Mr. P. Nightingale for his assistance on finding the information on the Van Ryneveld's Pass Dam.

(d) My family for their support, sacrifices and patience during the study.

(e) The permission of the Director-General of the Department of Water Affairs and Forestry (DWAF) to publish this thesis is gratefully acknowledged. The views expressed are those of the author, and not necessarily those of the Department.

TABLE OF CONTENTS

LIST OF TABLES

LIST OF FIGURES

NOTATION

Given below is a list of the principal symbols and notations used in the thesis. All symbols and notations are defined in the text when they appear.

Stresses and Strains

σ_{ij}	Stress tensor
S_{ij}	Stress deviator tensor
σ_m	Mean normal (hydrostatic) stress
σ	Stress
$\sigma_1, \sigma_2, \sigma_3$	Principal stresses
σ_x	Normal stress in *x* direction
σ_y	Normal stress in *y* direction
σ_z	Normal stress in *z* direction
σ_{xy}	Shear stress in *xy* plane
σ_{yz}	Shear stress in *yz* plane
σ_{zx}	Shear stress in *zx* plane
σ_{nn}	Stress normal to crack
σ_{ss}	Stress parallel to crack
σ_{ns}	Shear stress in crack
$\{\sigma\}$	Stress vector in global coordinate
$\{\sigma'\}$	Stress vector in local coordinate
S^{cr}	Crack stresses in local coordinate
S_n^{cr}, S_{nn}^{cr}	Mode I normal stress in local coordinate
S_{ns}^{cr}	Mode II shear stress in local coordinate
S_{nt}^{cr}	Mode III shear stress in local coordinate
ε_{ij}	Strain tensor
ε	Strain

$\varepsilon_1, \varepsilon_2$	Principal strains
ε_x	Normal strain in *x* direction
ε_y	Normal strain in *y* direction
ε_z	Normal strain in *z* direction
ε_{xy}	Shear strain in *xy* plane
ε_{yz}	Shear strain in *yz* plane
ε_{zx}	Shear strain in *zx* plane
ε_u	Ultimate normal tensile strain of no-tension resistance
$\varepsilon_n, \varepsilon_{nn}$	Strain normal to crack
$\varepsilon_s, \varepsilon_{ss}$	Strain parallel to crack
ε_{ns}	Shear strain in crack
ε^{co}	Intact concrete strain in global coordinate
$\varepsilon^{cr}, \varepsilon_i^{cr}$	Crack strain in global coordinate
$\{\varepsilon\}$	Strain vector in global coordinate
$\{\varepsilon'\}$	Strain vector in local coordinate
e_n	Normal strain of cracked concrete in local coordinate
e_n^e	Elastic normal strain of concrete at the tensile strength
e_n^u	Ultimate normal strain of crack concrete
e_n^f	Ultimate normal crack strain in local coordinate
e_i^{cr}	Crack strain in local coordinate
e_{nn}^{cr}	Mode I normal crack strain in local coordinate
γ_{ns}^{cr}	Mode II shear crack strain in local coordinate
γ_{nt}^{cr}	Mode III shear crack strain in local coordinate
I_1	First invariant of stress tensor
J_2	Second invariant of stress deviator tensor
J_3	Third invariant of stress deviator tensor

Material Parameters

D^{co}	Constitutive matrix of the intact concrete
D^{cr}	Constitutive matrix of cracks
D_i^I	Mode I stiffness of a crack(i)
D^{II}, D_i^{II}	Mode II stiffness
D^{III}	Mode III stiffness
$D_{i,l}^I$	Mode I stiffness of a crack(i) for linear strain softening
$D_{i,bl}^I$	Mode I stiffness of a crack(i) for bilinear strain softening
$\underline{D}$	Constitutive matrix
E	Young's modulus
E_s	Strain softening modulus
E_n	Secant modulus
f_c	Compressive strength of concrete
f_t	Tensile strength of concrete
f_t^c, f_t^r	Tensile strength of concrete or rock
G	Shear modulus
G_f	Specific fracture energy
G_f^c, G_f^r	Fracture energy of concrete or rock
h_c	Crack characteristic length
$\underline{K}^e$	Stiffness matrix of an element
$\underline{K}$	Overall structural stiffness matrix
$[K]$	Constitutive matrix in global coordinate
$[K']$	Constitutive matrix in local coordinate
K	Stress intensity factor
K_{IC}	Fracture toughness
p	Constant defining shear softening shape
α_1, α_2	Bilinear softening shape parameters

β	Shear retention factor
β_{max}	Maximum shear retention factor
μ	Normal retention factor
ν	Poisson's ratio
w_c	Crack band width

Miscellaneous Symbols

a	Depth of crack
$\underline{a}^e$	Nodal point displacement of an element
$\underline{a}$	Overall nodal displacement vector
$\underline{B}$	Stress-displacement operator
d	Depth of beam
Gr	Self weight
$\underline{f}^e$	Loads on an element
$\underline{f}$	Overall structural load vector
h	Width of dam at the level of initial notch
$\underline{L}$	Differential operator
l_1, l_2, l_3	Direction cosines of local axes (n, s, t) to global x axis
n_1, n_2, n_3	Direction cosines of local axes (n, s, t) to global y axis
m_1, m_2, m_3	Direction cosines of local axes (n, s, t) to global z axis
$\underline{N}(\underline{x})$	Shape functions
N, N_i	Transformation matrix of crack quantities between the global and local coordinate
MPa	Megapascals stress or pressure
n	Direction normal to crack
s	Direction parallel to crack
t	Direction parallel to crack
P_0	Load to cause crack-tip tensile stress equal to the tensile strength
P_u	Peak load

$[R]$	Transformation matrix of stress, strain and stiffness between the global and local coordinate systems
$\underline{u}(\underline{x})$	Displacement field
ΔT	Temperature drop in degree Celsius
Tol	Convergence tolerance
W, W_1, W_2	Crack opening
x, y, z	Cartesian coordinates
Δ	Increment of quantities
φ	Frictional angle
ϕ	Threshold angle of a crack
θ	Angle of the local axis system with the global coordinate system
U_x	Displacement in x-direction
U_y	Displacement in y-direction

Abbreviations and Acronyms

BLS	Bilinear softening
B&L(1993)	Bhattacharjee & Leger (1993)
B&L(1994)	Bhattacharjee & Leger (1994)
CBM	Crack band model
CMOD	Crack mouth opening displacement
CMSD	Crack mouth sliding displacement
CS	Cornelissen et al's softening
DWAF	Department of Water Affairs & Forestry
FE	Finite element
FM	Fracture mechanics
F.O.S	Factor of safety
FPZ	Fracture process zone
FSL	Full supply level
FU	Full uplift
H:V	Slope ratio of horizontal to vertical
ICM	Interface crack model
ICOLD	International Congress on Large Dams

IFF	Imminent failure flood
LEFM	Linear elastic fracture mechanics
LS	Linear softening
ISCM	Interfaced smeared crack model
NLFM	Non-linear fracture mechanics
NOC	Non-overspill crest
NW-IALAD	Network Integrity Assessment of Large Concrete Dams
PU	Partial uplift
R&B(1989)	Rots & Blaauwendraal (1989)
R&D(1987)	Rots & de Borst (1987)
RDD	Recommended design discharge
RDF	Recommendation design flood
RL	Reduced level
RMF	Regional maximum flood
SEF	Safety evaluation flood
TW	Tailwater level
OBE	Operationally based earthquake
MCE	Maximum credible earthquake

CHAPTER I - INTRODUCTION

1.1 Background and overview

Concrete, as a material of low tensile strength, has been subject to cracking problems since it was first used in structural applications. Recognition of the importance of cracking in concrete structures has prompted great interest in research on the fracture modelling of concrete. Classical (strength-based) mechanics of materials have been proved to be inadequate to handle severe discontinuities, such as cracks in a material. With the advance of powerful finite element (FE) analysis techniques, intensified research efforts have been made over the past few decades in the application of fracture mechanics (FM) in the modelling of cracking phenomena in concrete and concrete structures. Plain and reinforced concrete structures have been extensively analyzed using this broad FE, FM approach.

For example, Valente (2003) used a crack band model to analyze statically and dynamically the collapsed baroque Noto Cathedral in Italy for the purpose of rebuilding the 60-m-high structure.

Shi, Ohtsu, Suzuki & Hibino (2001) extended the discrete crack approach to the numerical analysis of multiple cracks in a real-size tunnel specimen which had been experimentally tested.

The sudden collapse of the New York Schoharie Creek Bridge in 1987 due to the unstable cracking in the reinforced piers, caused by the rapid flow of a flood, led Swenson & Ingraffea (1991) to adopt discrete cracking models, including linear and non-linear FM, to evaluate the initiation, stability and propagation profile of the crack that caused the failure. The deadly (loss of ten lives) cracking problems of the bridge can be rationally explained by the use of FE-based models.

Other types of plain or reinforced concrete structures that experienced fracture-controlled problems, such as the pullout of anchor bolts, the thick-walled ring, beams, panels, frames,

containment vessels and shells, have also been analyzed in the past using FE, FM models (ACI 1997).

In an important effort to apply the FM approaches that have been developed to problems of practical significance, concrete dams (which are normally huge, fracture-sensitive concrete structures) have received special attention from researchers and have formed an essential part of this broad area of research on concrete crack modelling.

Uncontrolled crack propagation in concrete caused the disastrous failures of Malpasset Dam in France in 1959 (SimScience website). The rapid crack propagation as evidenced in the failure process of the above dam, has emphasized the importance of developing an accurate crack modelling method to safeguard dams. The Kölnbrein arch dam in Austria and Koyna gravity dam in India are representative of the two main types of dam structures which have attracted most research efforts for FM crack modelling of concrete dams.

Gravity dams are structures that rely on their own weight for resistance against sliding and overturning to maintain stability. In ancient times dated back as early as 4000 years BC, gravity dams were built using masonry materials such as earth, rock and cut blocks, with both the upstream and downstream faces sloped and the base thickness being many times the height of the dam. Concrete was first used in building a 47-m-high gravity dam called the Lower Crystal Springs Dam in the USA which was completed in 1889. Because they are relatively simple to design and build, concrete gravity dams have become a major dam type throughout the world. With the development of design and analytical expertise, as well as of construction techniques and equipment, dams have become ever larger with regard to both height and volume, e.g. the world's largest gravity dam so far, Three Gorges Dam in China, has a height of 185 m and a water-storage volume of 39.2 billion m^3. If a dam on this scale were to fail and collapse, this could lead to probably the greatest disaster in human history. Therefore, the safety of huge structures such as concrete gravity dams is of the utmost concern to the engineers involved in the design, construction and post-built safety evaluation of dams.

A great deal of research on the numerical modelling of the cracking behaviour of concrete has been carried out during the past few decades. In the process, many concrete crack

propagation models have been developed and applied in concrete cracking analyses. The early strength-based model, in which the crack was assumed to propagate when the calculated tensile stresses at the crack tip exceed a specified tensile strength of the concrete, has seldom been used in any recent concrete analyses due to its inherent lack of mesh objectivity (FE mesh discretization has a significant influence on the results). Linear elastic fracture mechanics (LEFM), in which crack growth occurs when the effective stress intensity factor exceeds the material's fracture toughness, has been widely used in the analysis of concrete in the past. Models based on non-linear fracture mechanics (NLFM) have now become popular for analysing concrete cracking due to the existence of a fracture process zone (FPZ) at the front of the crack tip.

Many concrete gravity dams, which are generally massive, plain concrete structures, have experienced cracking problems to various extents. Crack formation and propagation in concrete gravity dams could influence their structural stability and endanger the safety of the dams. Normally, the huge size of a concrete dam excludes direct experimental tests on the structural cracking behaviour under various loading conditions. Therefore, evaluation of the possible cracking trajectory in concrete dams by means of an accurate constitutive model, in order to simulate the cracking response of the concrete effectively, becomes vital and would be a useful tool for practising engineers to ensure the safety of dam structures. This requires developing a numerical model and techniques that can accurately analyse and appraise a dam structure, either for the purpose of designing a new dam or for evaluating the safety of an existing concrete dam.

The need for methods that can accurately predict the behaviour of cracking in concrete dams has led to intensified research in this field. In fact, many attempts have been made to develop a rigorous model to simulate the cracking mechanisms in and the behaviour of concrete dams, especially concrete gravity dams. To name a few, Ingraffea (1990) performed a case study on the Fontana Dam, a gravity dam in the United States, to elucidate the mechanisms for crack initiation and to predict the observed crack trajectory employing a 2-D discrete LEFM method. Bhattacharjee & Leger (1994) applied a 2-D smeared crack model based on NLFM crack propagation criteria to study the static fracture behaviour of the Koyna Dam, a gravity dam in India. A more detailed review of these attempts will be given in Chapter II.

Although many analytical methods based on fracture mechanics have been proposed for concrete dams in the last few decades, they have not yet become part of standard design procedures. In fact, few of the current researches from all over the world are being implemented by practising engineers when evaluating dam safety. Current practice for crack analysis in concrete dams is to implement either the traditional "no-tension" gravity design method, which is based on rigid body equilibrium and strength of materials to determine crack length, assuming horizontal planar crack extension, linear stress distribution and zero stress at crack tip, or a non-linear FE analysis including plasticity models and contact simulation.

There are several FE programs that can be used to analyse the cracking response of concrete structures, e.g. MSC.Marc, ABAQUS, ANSYS, DIANA, LUSAS, FRANC2D/3D, FRACDAM and MERLIN, etc. At the Department of Water Affairs and Forestry (DWAF) – the dam authority in South Africa, MSC.Marc is currently the main FE tool used for non-linear analysis, including crack prediction on concrete dams. The cracking analysis in MSC.Marc is limited to linear tensile strain softening and the constant shear retention factor. This means that MSC.Marc lacks the flexibility in analysing cracking behaviour that is offered by more advanced crack models (including multi-linear or non-linear softening, shear retention factor varied with the crack's normal strain, etc.). Although some commercial FE programs, such as DIANA include advanced crack models, the codes of these programs are not generally available to be modified/enhanced for research purposes. In addition, the existing programs yield significantly different results on the crack response of a concrete gravity dam, as demonstrated in the benchmark exercise carried out by the European Thematic Network Integrity Assessment of Large Dams between 2003 and 2005 (refer to http://nw-ialad.uibk.ac.at). The different results with regard to peak load, displacement and stress given by the different programs highlight the need to improve the cracking analysis capacity of the existing FE packages by developing, perhaps, a better method of crack analysis and its numerical implementation in an FE program. An improved crack model and method could give a more accurate crack response (crack profile, horizontal crest displacement, etc.) in concrete dams which could be used to evaluate the safety of dams.

1.2 Motivations and objectives of this study

This research aims to contribute to the continuing research efforts on mastering the mechanics of cracking in concrete dams.

In order to evaluate the stability and safety of concrete dams more accurately, it is necessary to develop a better model and method for analysing cracking problems in concrete dams.

The objectives of the research are as follows:

- To evaluate the existing constitutive crack models critically and to adopt a suitable constitutive crack model using non-linear smeared fracture mechanics for simulating and investigating the cracking process in concrete dam structures.
- To develop a more accurate strain softening relation and to calibrate the parameters.
- To develop a numerical program specially for implementing the constitutive model in order to carry out fracture analysis of concrete dams under static loading conditions.
- To validate the constitutive model and numerical techniques by investigating the cracking behaviour of concrete structures that have been researched experimentally and/or numerically in the past.
- To investigate dam concrete softening parameters.
- To investigate the cracking behaviours of concrete gravity dams for better evaluation of dam safety.

1.3 Scope of this study

This research is focused on the development of a suitable crack modelling and analysis method for the prediction and study of fracturing in concrete gravity dams, and consequently, for the evaluation of dam safety against cracking. The research is limited to the two-dimensional (2-D) static cracking analysis of concrete gravity dams. The following areas are not covered in this research:

- Three-dimensional (3-D) cracking, although the research could be extended from 2-D to 3-D with some additional effort.
- Dynamic cracking.
- The water pressure that develops inside the crack as the crack grows.
- The coupling between different crack modes, and different cracks.
- Time dependent behaviour such as creep and shrinkage.

1.4 Methodology of this study

The research begins with a thorough literature review of previous investigations into the subject area and similar research. The theory and development of constitutive crack models are followed to establish the material crack model used in this study. The implementation of the proposal crack model is undertaken through the development of a sub-program specially coded for this research. The constitutive crack model proposed and the implementation procedure of the proposed crack model in an FE program are validated by analyzing and comparing the results obtained with the previously investigated concrete beams, gravity dams and model dam. After the verification process, the crack model and the sub-program are applied to analyze and predict the fracture response and to evaluate the related dam safety against the cracking of an existing, full-size concrete gravity dam. Finally, conclusions are drawn and recommendations are made based on this study.

1.5 Organization of this study

Chapter I gives the background, motivation, objectives, scope and methodology of this study. Chapter II is a comprehensive literature review of the development of crack models for application with concrete, especially concrete dams. The review focuses mainly on the evolution of the crack models proposed by other researchers in the world during the past few decades and gives a critical appraisal of the pros and cons of the crack models. A brief description of the analytical and design methods adopted for concrete gravity dams is given for readers who are not familiar with the design and safety evaluation procedure for concrete gravity dams. Past investigations into the fracture analysis of concrete dams are also discussed in Chapter II.

Chapter III presents the constitutive crack model adopted for smeared crack analysis of concrete structures in this research. It describes the crack onset criterion and direction, strain softening during the fracture process and post-crack features (such as non-orthogonal crack criteria for a new crack to occur, and whether the crack is fixed or rotating, definition of crack closing and reopening, and crack mechanisms for unloading and reloading), etc. A bilinear strain softening diagram for mode I and a shear softening relationship for mode II are proposed.

In Chapter IV, a numerical program capable of constitutive modelling crack initiation and the crack propagation of mixed modes is developed specially for smeared crack analysis of fracture behaviours in concrete dams. The program is incorporated into a commercial general-purpose code called MSC.Marc in order to carry out a complete FE analysis from the pre-processing involved in setting up the mesh and the loading/boundary conditions etc., and the solving of equilibrium equations, to post-processing of the results obtained. Preliminary verification of the program that has been developed is carried out on some elementary specimens. Three cracking verification cases in DIANA are selected to further benchmark the program that has been developed in this chapter.

In Chapter V, the proposed crack model and the numerical techniques that have been developed are thoroughly evaluated and benchmarked in static fracture analyses of different plain concrete beam structures under either mode I or mixed mode loading conditions. The fracture response of the beams and the parameter study on the proposed bilinear softening relationship are discussed in this chapter.

The proposed crack modelling techniques are needed to be evaluated and benchmarked in static fracture analyses of concrete dams. For this purpose, in Chapter VI, a scaled-down model of a gravity dam, a full-scale “benchmark” gravity dam and an existing gravity dam (the Koyna Dam in India) under static loading conditions are selected to do the benchmark because these dams were previously investigated for fracture behaviours by other researchers.

With confidence in the crack modelling techniques developed in this research having been built up by means of the benchmark exercises detailed in the previous chapters, Chapter VII is devoted to using the crack model to predict the static fracture response of a concrete

gravity dam in South Africa and to evaluate the safety of the dam – the stability of the dam has been a matter of concern for the dam safety authority.

The last chapter, Chapter VIII, gives the conclusions of this research and makes recommendations for further study and application of concrete crack models.

Figure 1.1 gives a schematic outline of the organization of this study.

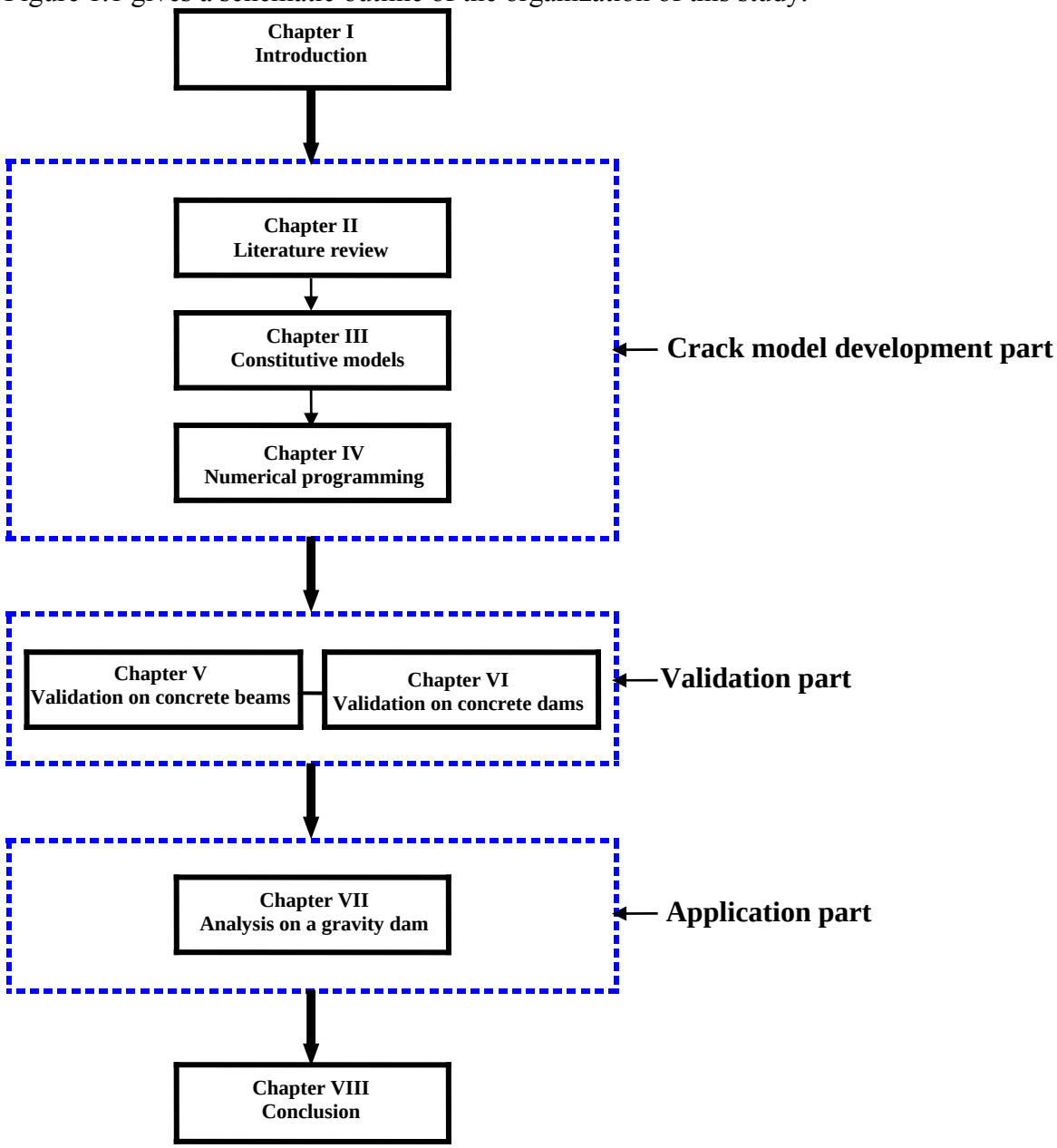

Figure 1.1 - Outline of the research

CHAPTER II - LITERATURE REVIEW ON GRAVITY DAM DESIGN AND ON THE DEVELOPMENT IN FRACTURE ANALYSIS OF CONCRETE DAMS

The constitutive modelling of cracking behaviours and crack representations in numerical implementation are the two main issues in the study of cracking in concrete structures. Crack modelling in concrete structures has undergone great development in the past, especially with regard to smeared constitutive models. The general development of research into the crack modelling of concrete, especially smeared constitutive modelling of concrete cracking and its application to concrete dams, is presented. This review of past and current research into the modelling of concrete cracking should provide a clear background to and platform for any further research in this field.

The methodology adopted to date for analyzing the cracking problems of concrete dams is reviewed to show the historical trends in the development of analysis methods for correctly predicting fracturing behaviours in concrete dams. Current research efforts to improve the modelling of cracking in concrete dams are also pointed out.

The use of finite element (FE) analysis for modelling cracks is an important step in developing crack models suitable for the accurate simulation of the cracking process in concrete structures. Much effort has been put into finding appropriate ways to represent cracking in FE formulation. The main methods proposed so far are presented.

Accurate determination of the fracture energy (a material parameter of fracture mechanics) of massive dam concrete, which uses large aggregates, has a significant influence on the fracture analysis of concrete dams. For this reason, research on this key material parameter for fracture in concrete dams is described.

Past investigations into cracking analyses for concrete gravity dams under static loadings are discussed to highlight the human pursuit of complete safety for dam structures, even under cracking situations.

2.1 Causes of cracking in concrete gravity dams

The low tensile resistance of concrete is the main reason why cracking is a common phenomenon in concrete dams. There are many causes that could contribute to cracking in concrete dams, either individually or collectively. A broad classification of these causes is given below (Linsbauer 1990).

Inadequate design and construction methods: Geometrical "flaws or defects" such as notches, corners, jagged interface between dam and foundation, and inadequate preparation of the construction joints and concrete block joints. All these defects can lead to local stress concentration and deformation restraint.

Material problems: Volume changes due to shrinkage, creep, heat of hydration or chemical changes such as alkali-aggregate reaction.

Structural behaviour: Tensile stresses induced by varied static loadings, earthquake loadings, temperature changes and differential settlement of the foundation. Uplift pressure and overflow can also cause severe cracking in dams and endanger their safety.

Normally, surface cracks caused by, e.g., concrete shrinkage or creep cannot really threaten the structural safety of concrete dams and are not the type of cracks that dam engineers regard as a concern for structural safety. Cracks penetrating deep inside dams, caused by excessive stresses or strains (which develop as a result of load application) or by material volume changes (such as alkali-aggregate reaction), are the main concern for engineers because these cracks can lead to considerable changes to the structural behaviour and failure resistance of the dam structure. In general, the state of stress and strain in the concrete mass will determine and control the fracture mechanism in concrete.

2.2 Brief description of methods of analysis and design criteria for concrete gravity dams

For the design of concrete dams, it is necessary to determine the forces that can be expected to affect the stability of the structure. The forces (shown in Figure 2.1) that must

be considered for the design and analysis of concrete gravity dams under static loadings are those due to:

- Hydrostatic pressure (including tailwater loading) H, H', V, V'
- Silt pressure (sediment loading) S
- Uplift forces U
- Weight of structure (self weight) Gr

Other loads, including wind and waves, ice and temperature loading, are sometimes considered in design.

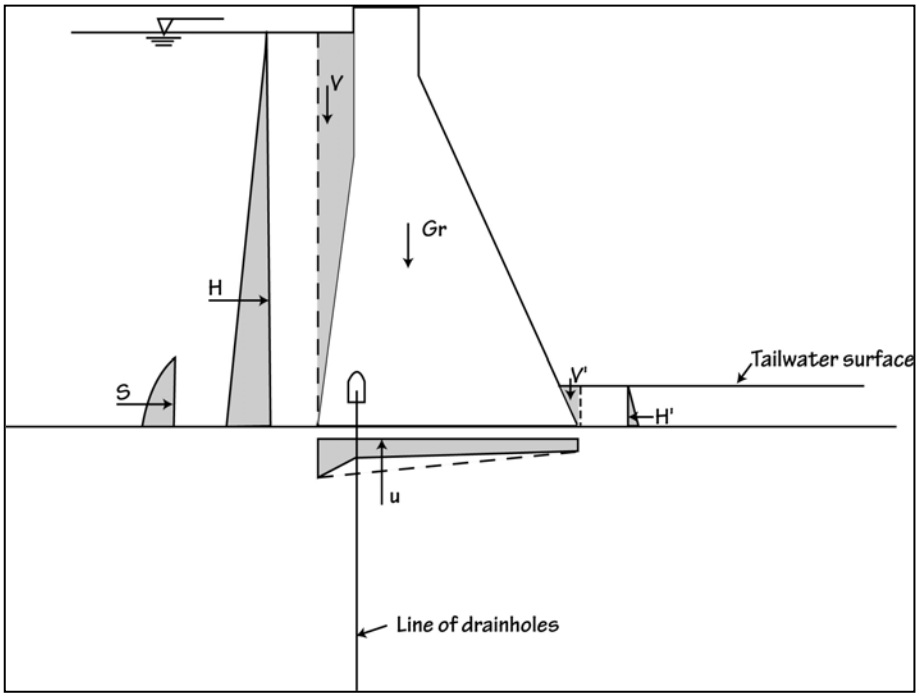

Figure 2.1 - Forces acting on a gravity dam

In addition to the normal static loading conditions, it may be necessary to apply earthquake loads. It is not likely, however, that all of these loads will occur at the same time. Table 2.1 below lists the load combinations for concrete dam design in South Africa (Chemaly 1995).

TABLE 2.1 - Definition of load combinations in South Africa

Load category	**Load combinations**
Normal loading	A. RDD + Gr + PU + S + TW
Abnormal loading	B. FSL + Gr + PU + S + OBE
	C. RDD + Gr + FU + S + TW
	D. RMF + Gr + PU + S + TW
Extreme loading	E. FSL + Gr + PU + S + TW + MCE

FSL: Water level at full supply level
FU: Full uplift (relief holes blocked or no drainage system)
Gr: Self weight of dam
MCE: Maximum credible earthquake
OBE: Operationally based earthquake
PU: Partial uplift (with pressure-relief holes functioning)
RDD: Water level at recommended design discharge (1 in 200-year flood)
RMF: Water level at regional maximum flood
S: Silt loading (after 100 years' deposition)
TW: Tailwater level

Over the years, methods of analyzing concrete gravity dams have been developed and improved – from the classical method based on linear elastic calculations to the FE method which can carry out far more accurate non-linear analysis under more complex loading conditions.

The classical method of calculating stresses is based on the assumption of a linear stress distribution on a horizontal plane. The gravity dam is idealized as a cantilever beam. The stresses are computed by applying the following classical formula:

$$\sigma = \frac{P}{A} \pm \frac{My}{I} \tag{2.1}$$

Where

P Normal force acting on the selected cross-section

A Area of the cross-section

M Bending moment acting on the cross-section

y Distance to the centre of the cross-section

I Moment of inertia of the cross-section.

The calculated stresses in a horizontal plane are limited to meet the design criteria for permissible stresses in a concrete dam. The design criteria for stress distribution in a concrete gravity dam in South Africa are shown in Table 2.2 (Kroon 2002):

TABLE 2.2 - Design criteria for normal stresses in concrete gravity dams (South Africa)

	Normal loading (A)	**Unusual loadings (B, C, D and E)**
Tensile stresses	None	0,2 MPa
Compressive stresses	$0{,}25\,f_c$	$0{,}25\,f_c$

Note: f_c is the compressive strength of the concrete in a standard cube after one year. The maximum tensile stress of 0,2 MPa can only be allowed on a dam site where the foundation rock is sound and not excessively horizontally jointed.

A gravity dam is also designed to be safe against sliding and overturning. The stability of a gravity dam against overturning is guaranteed by dimensioning the dam so that the resultant of all forces acting on any horizontal plane within the dam and foundation, intersects the corresponding base plane within its middle third of the length. This will effectively prevent tensile stresses in a dam.

The stability of a dam against sliding is of major concern to dam engineers. The factor of safety against sliding is defined using the following formula:

$$F.O.S = \frac{CA + P\tan\varphi}{H} \qquad (2.2)$$

Where

C Ultimate cohesion of concrete or rock

φ Angle of internal friction

A Area of the basis of contact

P Sum of the vertical forces, including the uplift forces

H Sum of the horizontal forces.

The design criteria adopted in South Africa for safety against sliding of concrete dams are listed in Table 2.3.

TABLE 2.3 - Design criteria for safety against sliding in concrete gravity dams (South Africa)

	Normal loading (A)	**Abnormal loadings (B, C, D)**	**Extreme loading (E)**
F.O.S. for peak	2,0 – 4,0	1,5 – 2,0	> 1,0 – 1,2
F.O.S. for residual	1,5 – 2,0	> 1,0 – 1,2	> 1,0

Note: Peak is the maximum shear properties (such as C and φ) in the interface between the wall concrete and foundation rock. Residual means the remained shear properties in the interface for long term.

The development of computing power and the FE method allowed engineers to analyse non-linearity in concrete dam behaviour, including dam-foundation interactions, material plasticity, thermal stresses, etc. The FE method and numerical techniques have been improved and gradually introduced into the codes of practice, leading to better and safer designs (Galvez *et al*. 1996). Currently, two principal analytical methods, namely the classical method and the FE method, are being used in the design of concrete dams.

2.3 Analysis of cracking in concrete dams

With the conventional design methodology described in Section 2.2, concrete dams are usually designed to have “no tension” in any part of the dam under normal service loads and to withstand minimum tensile stresses only under extreme loading cases. However this “no tension” design has never been justified theoretically. The work of Bažant (1990) reveals that even apparently conservative “no tension” design cannot always be regarded as safe if a certain size (e.g. base width) of dam is exceeded. In his paper, Bažant used a simple example of a dam model with a predefined horizontal crack at the base to demonstrate that the “no tension” solution could yield a higher maximum load than linear

elastic fracture mechanics (LEFM). The size effect plot also shows that there is a critical size of dam after which the "no tension" design gives a higher maximum load than LEFM. In reality, most, if not all, of the existing concrete dams in the world cannot really be said to be in a perfect crack-free condition, even if many of these were designed to have "no tension".

The rigid body equilibrium strength-based criterion was initially adopted where it was assumed that a crack would propagate whenever the principal tensile stress at the crack tip exceeded a specified tensile strength of the concrete. This was the only criterion for determining crack growth in concrete dams before the late 1970s (Saouma, Bruhwiler & Boggs 1990).

The strength criterion for crack analysis of concrete dams is based on the assumption that a crack will propagate horizontally in a plane and extend to a point where the stress becomes zero, and that the stress distribution is linear along the uncracked length of the dam wall in that plane. This kind of cracking analysis method suffers from the following shortcomings:

- The shear stress cannot be considered.
- Strictly speaking, this shallow beam theory cannot be applied to concrete dams which usually have low aspect (height/base width) ratios.
- The stress singularity at the tip of a crack cannot be taken into account.

The analysis of cracking based on this rather arguable assumption is not compatible with continuum mechanics (Linsbauer 1990). The diagram in Figure 2.2 is an illustrative example of the forces and stress distribution in a cracked concrete gravity dam analyzed by means of the conventional method.

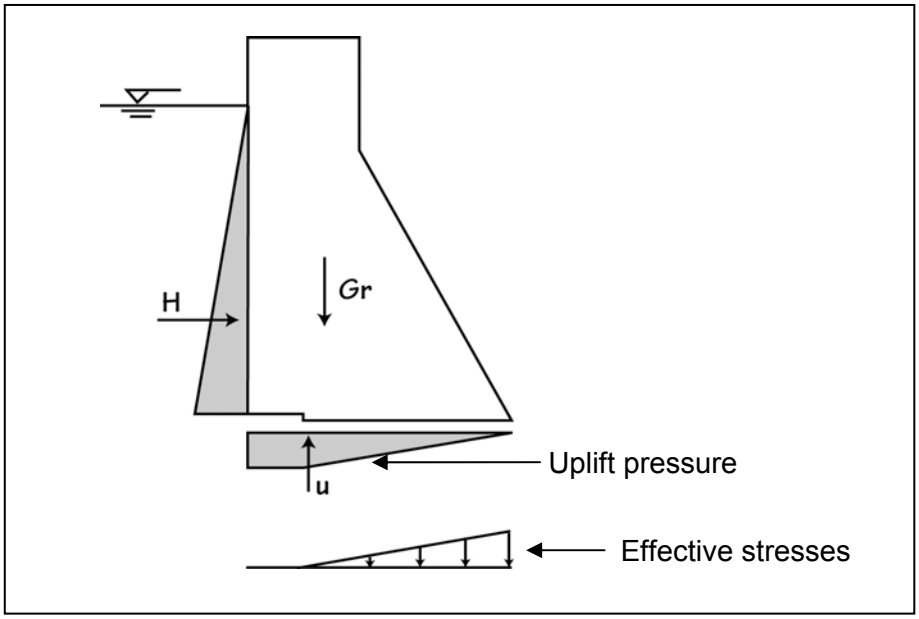

Figure 2.2 - Diagram of the forces and stresses used in the classical analysis method for a concrete gravity dam

Significant advances in the FE method make it a very useful tool for investigating cracking in concrete dams. However, when the strength-based approach is applied in the FE method, it is often found that if the mesh around the crack tip is refined, the stresses become progressively larger and the results are said to be “mesh-unobjective”. This leads to the conclusion that strength-based models are unsuitable for modelling the stress singularities at a crack tip and that they are inadequate for analyzing cracking in concrete structures.

It is well known that cracking in concrete is a dominant source of the non-linearity experienced in concrete dams. To study cracking behaviour in a dam and to gain an understanding of how the cracking that is normally caused by high stress concentrations can redistribute the stress in a dam, non-linear FE analysis using material plasticity models (such as Drucker-Prager and Mohr-Coulomb) and contact simulation of the cracks has been adopted. This approach allows prediction of the scope of the cracking and the potential effect on leaking in concrete dams.

Fracture mechanics, based on fracture energy principles, deals with cracking in materials and is ideally suited for studying crack development and propagation in concrete structures. The application of fracture mechanics to modelling the cracking process in

concrete dams for the purpose of safety evaluation has drawn a great deal of interest and attention world-wide. At the 15th International Congress on Large Dams (ICOLD) conference held in Lausanne in 1985, researches on the analysis of cracking responses in concrete dams using fracture mechanics were accepted and presented (Linsbauer 1990). Although many analytical methods based on fracture mechanics have been proposed for concrete dams in the last decades, they have not yet been introduced into standard design procedures.

During the past decades, LEFM has been widely used in the analysis of concrete dams, especially gravity dams. Due to the existence of a fracture process zone (FPZ) (refer to Figure 2.3) at the front of the crack tip, although sometimes, small compared with the size of the dam, strictly speaking, a model based on non-linear fracture mechanics (NLFM) should be adopted in all cracking analyses of concrete dams. NLFM has gained recognition among the researchers and become the main trend for the fracture analysis of concrete dams.

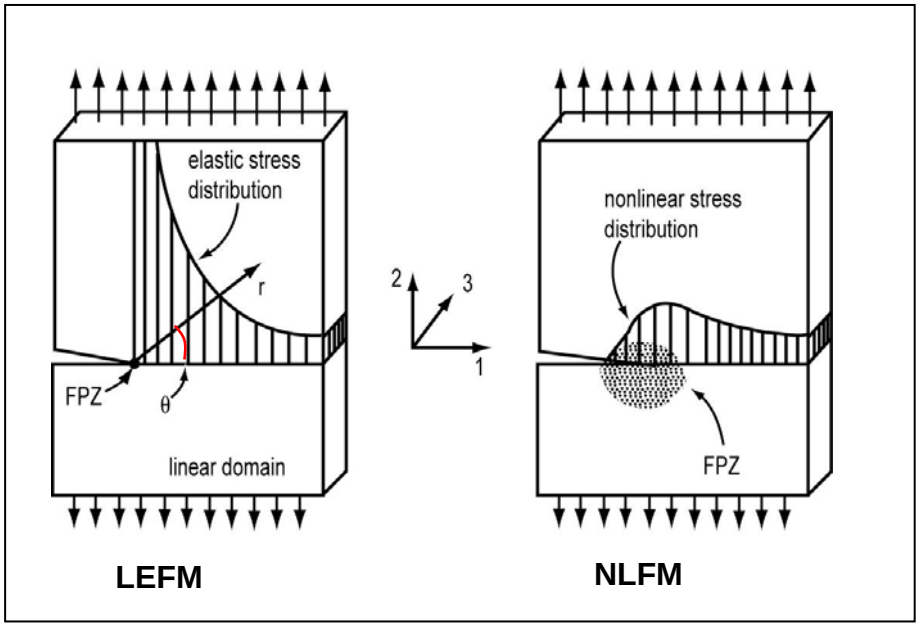

Figure 2.3 - Fracture process zone in LEFM and NLFM (Bhattacharjee & Leger 1992)

Detailed descriptions of LEFM and NLFM, the crack models based on them and their past application in the analysis of concrete dams are given in later sections (2.5.3, 2.5.4 and 2.7) of this chapter.

2.4 Finite element approaches for modelling cracking in concrete

Constitutive modelling of the crack behaviour of concrete relies on the FE program's ability to install the constitutive model and simulate the cracking profile. At present, the methods most frequently adopted in FE analysis to model cracking are as discussed below.

Discrete crack approach: This approach represents a crack as a discrete gap along the inter-element boundary. Inter-element boundaries are separated to simulate cracking. This involves the addition of nodes which influence element connectivity and the stiffness matrix. The analysis is complicated by a continuous change of the FE topology during the analysis (Bhattacharjee & Leger 1992). A pre-defined crack path is sometimes needed beforehand to define the orientation of the cracks.

Smeared crack approach: In this approach, the stiffness of the material in an element (or at an integration point) is modified to simulate an infinite number of closely spaced cracks 'smeared' over the region under consideration. The advantage of the method lies in its simplicity and cost-effectiveness since the topology of the FE mesh remains unchanged and no restrictions are imposed on the orientation of the crack (Bhattacharjee & Leger 1992). This approach still has several deficiencies, namely its tendency to cause diffused crack patterns, the directional bias and stress locking.

There are other FE approaches that could be used to model cracking in concrete. For example, Kuo (1982) proposed an interfaced smeared crack model (ISCM) which combines the advantages of the discrete and smeared approaches. Graves & Derucher (1987) proposed an improved interfaced smeared crack model on the basis of Kuo's work to find a satisfactory 'pushing-back' procedure (by altering the local element displacements until the stresses at the cracking interface are brought close to zero through an iteration process) at the local level. Other authors have mentioned the lattice approach as another numerical method with possibilities (Galvez, Cervenka, Cendon & Saouma 2002; Cai, Robberts & van Rensburg 2004).

2.5 Crack modelling of concrete

Concrete is made up of different constituents (or phases) and is by nature a heterogeneous material. The cracking process in concrete is very complicated and the crack surface is tortuous (see Figure 2.7). To model this complex process adequately demands continued research efforts to find methods capable of accurately predicting and simulating the cracking response in concrete.

A non-linear static analysis of cracked concrete requires a constitutive model that is able to represent the locations phenomenon (i.e. to identify locations where cracks will initiate, predict crack growth and model crack coalescence) and to model this process up to collapse of the structure. In general, five main phases can be identified and these are discussed in the following sections:

- pre-fracture material stress-strain behaviour
- crack (fracture) initiation
- crack propagation criteria
- crack modelling, and
- post-crack behaviour.

2.5.1 Pre-fracture material stress-strain behaviour

Before cracking, concrete in tension can be sufficiently modelled as an isotropic, linear elastic material. The behaviour of concrete under high compressive loading is normally modelled as non-linear. However, in structures such as concrete gravity dams, the compression stresses are low enough that it is adequate to assume a linear elastic constitutive law. It is true that some non-elastic softening close to the peak tensile stress, before a crack is initiated, will be ignored in the above assumption. Nevertheless, a non-linear, plastic stress-strain law can always be adopted due to the rapid advance of FE analysis capacity. Most of the previous investigations into concrete cracking, especially in concrete gravity dams, have assumed a pre-cracking linear, elastic behaviour under both tensile and compressive loadings.

For concrete cracking analysis, the plane stress state is probably the analysis most often adopted for verification. In plane stress analysis, the linear, elastic incremental stress–incremental strain relationship is expressed as follows:

$$\begin{Bmatrix} \Delta\sigma_x \\ \Delta\sigma_y \\ \Delta\sigma_{xy} \end{Bmatrix} = \begin{bmatrix} \frac{E}{1-\nu^2} & \frac{\nu E}{1-\nu^2} & 0 \\ \frac{\nu E}{1-\nu^2} & \frac{E}{1-\nu^2} & 0 \\ 0 & 0 & \frac{E}{2(1+\nu)} \end{bmatrix} \begin{Bmatrix} \Delta\varepsilon_x \\ \Delta\varepsilon_y \\ \Delta\gamma_{xy} \end{Bmatrix} \tag{2.3}$$

Where

E Young's modulus

ν Poisson's ratio

x the global horizontal direction

y the global vertical direction.

2.5.2 Crack initiation

To study the non-linearity caused by cracking in concrete, it is necessary to know where the cracking starts. Thus it is important to set up crack initiation criteria in the model. Researchers have proposed various criteria to indicate crack initiation:

- The conventional criterion for a homogeneous structure is to assume that a new crack will initiate when the principal tensile stress reaches the uniaxial tensile strength of the concrete. Bhattacharjee & Leger (1993) have pointed out that this criterion is not entirely satisfactory in a 2-D or 3-D FE analysis, because: (i) the material stress-strain response is non-linear prior to reaching the peak strength, and (ii) the principal stress and strain, used as the response indicators, are not directly proportional due to Poisson's effect.

- In a 3-D analysis, cracking can be assumed to occur when the stress reaches a failure surface (or more specifically, the crack detection surface) on a meridian plane (Chen 1982).

- Difficulty in finding the uniaxial tensile strength experimentally has led to the modulus of rupture, as obtained from a beam test, being used as a crack initiation criterion (Linsbauer, Ingraffea, Rossmanith & Wawrzynek 1989a).

- Another crack initiation criterion states that a linear elastic relationship is assumed until the tensile strain energy density in the analysis equals the pre-peak area under a uniaxial stress-strain diagram as obtained from a laboratory specimen, as shown in Figure 2.4 (Bhattacharjee & Leger 1993; Bhattacharjee & Leger 1994).

$$½\sigma_1\varepsilon_1 \geq \int_0^{\varepsilon} \sigma \, d\varepsilon = ½\sigma_i\varepsilon_i = \frac{\sigma_i^2}{2E} \tag{2.4}$$

To obtain the tensile strain energy, $½\sigma_1\varepsilon_1$, we need to know the maximum principal stress, σ_1, and strain, ε_1, at a material point. σ_i is the apparent tensile strength, defined as 25 ~ 30% higher than the tensile strength of concrete, σ_t, while ε_i is the corresponding strain.

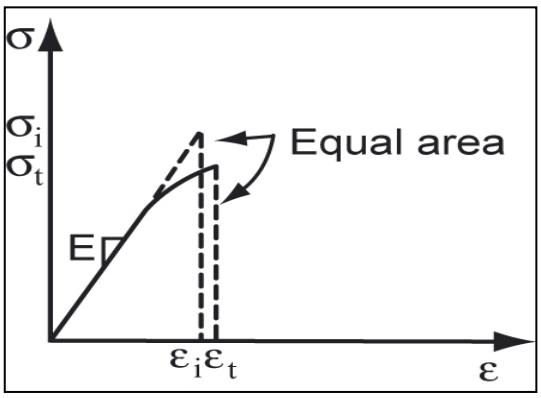

Figure 2.4 – Crack initiation criterion (Bhattacharjee & Leger 1994)

- Onate, Oller, Oliver & Lubliner (1988) used a fully elasto-plastic model for the concrete and assumed that cracking occurred where the effective plastic strain was greater than zero. It was further assumed that the crack developed in a direction orthogonal to the direction of the maximum principal strain at the point.

The conventional crack initiation criterion remains the most accepted due to its simplicity and conceptual straightforwardness (Araujo & Awruch 1998; Leclerc, Leger & Tinawi 2003; Planas, Elices, Guinea, Gomez, Cendon & Arbilla 2003, etc). Most researchers also agree that the crack direction should be orthogonal to the maximum principal stress or strain.

2.5.3 Crack propagation criteria

- Strength-based criterion

As discussed in Section 2.3, the strength-based criterion assumes that a crack will propagate when the predicted stress at the tip of the crack exceeds the tensile strength of the material. In this way, the criterion is identical to the conventional crack initiation criterion.

- Fracture mechanics criteria

Fracture mechanics predicts the propagation of cracks on the basis of the energy dissipated by the structure during fracturing. It is now well established that fracture in concrete is not concentrated in a point at the crack tip, but rather occurs within a finite zone ahead of the crack, defined as the FPZ. Micro-cracking of the material in the FPZ helps to explain the observed softening behaviour of material in this region.

The non-homogeneous nature of concrete causes further complications:

(i) Cracks do not propagate along a straight line, but rather follow a tortuous path.

(ii) The exact position of the crack tip is difficult to determine because of aggregate bridging in the crack and variations in the size of the FPZ.

Fracture mechanics can be broadly classified into two categories: LEFM and NLFM. Models based on LEFM assume a linear elastic material and that crack extension is accompanied by a sudden release of surface stresses. At the tip of a crack, the stress becomes singular. Crack growth occurs when the effective stress intensity factor

(including the appropriate modes of I – opening, II – sliding and III – tearing – see Figure 2.5) equals the material fracture toughness.

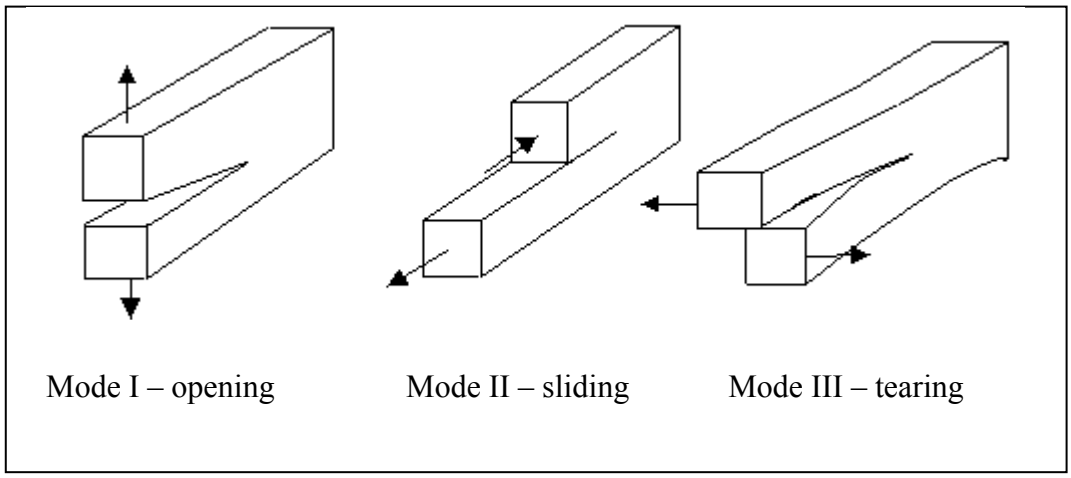

Figure 2.5 - Modes of fracture

Since the presence of FPZ is ignored, LEFM should be applied only to concrete structures in which the FPZ is much smaller than the dimensions of the structure under consideration. LEFM can, therefore, successfully be applied to most parts of a large concrete structure, such as a gravity dam. However, a concrete gravity dam, normally a very stiff structure, may have long and narrow (small opening displacement) cracks. In this case, the FPZ cannot be treated as small and be ignored, which means that sometimes LEFM cannot be applied, even to large gravity dams.

NLFM recognizes the non-linear material behaviour by including the strain-softening behaviour of the concrete in the FPZ. In 1990, Saouma *et al*. adopted that crack propagation occurs when the stress at the tip of the FPZ reaches the tensile strength. Since the 1980s, research into crack analysis models based on NLFM has been intensified. The following section, Section 2.5.4, focuses mainly on the development of smeared cracking models based on NLFM, although the other crack models based on, for example, discrete fracture, LEFM and strength-based criteria, are also addressed.

2.5.4 Crack models

Strain softening has been modelled by various types of constitutive laws. Apart from NLFM, endochronic theory, plastic-fracturing theory, plasticity with decreasing yield limit and, recently, continuum damage theory are also used (Pijaudier-Cabot & Bažant 1987; Bažant & Kim 1979; Ghrib & Tinawi 1995).
Various crack propagation criteria and fracture models based on these criteria have been proposed in the literature, but only the major developments are presented here.

Two major categories of crack models – discrete and smeared – are described in this section, which shows the development of the major fracture models. The overall development of cracking models is illustrated in Figure 2.10.

➢ Discrete fracture models

- **Discrete model 1: Linear elastic fracture mechanics (LEFM)**

The criterion for crack growth in LEFM, which is applicable only to cracked structures, is as follows:

$$K \geq K_{IC} \tag{2.5}$$

Where K is the stress intensity factor, which is a measure of the strength of the singularity around the tip of a crack. K can be expressed and computed by:

$$K = f_{ij}(\theta)\sigma_{ij}\sqrt{2\pi r} \tag{2.6}$$

As shown in Figure 2.6, σ_{ij} are the stresses at a distance, r, from the crack tip and at an angle, θ, from the crack plane. $f_{ij}(\theta)$ are known trigonometric functions of θ (depending on the specimen, crack geometry and loading, etc.). At the crack tip, the stress is theoretically singular. Thus, as the crack tip is approached, the stress asymptotically approaches infinity. Hence:

$$K = \sqrt{\pi a}\,\sigma \qquad (\theta = 0;\ r \to 0)$$

Where

a the crack size

σ the applied stress.

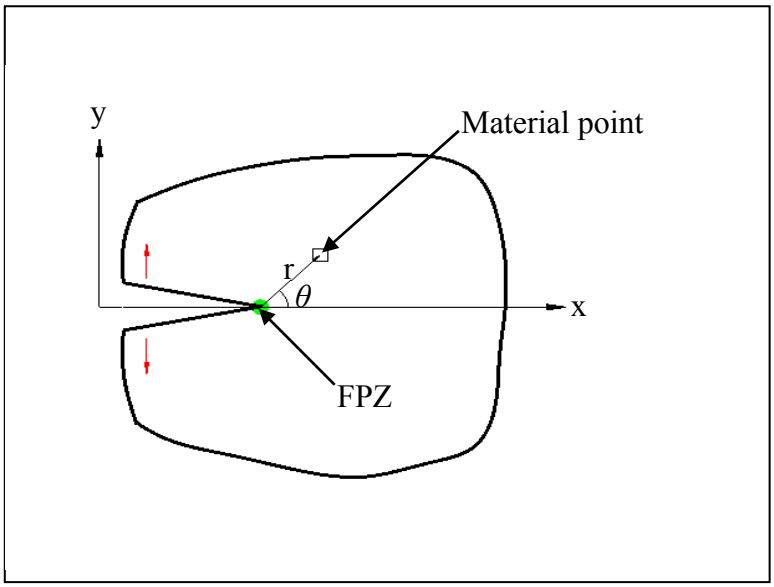

Figure 2.6 - Crack in an arbitrary body and coordinate system (LEFM)

K_{IC} is the fracture toughness, which is a measure of the material's resistance to cracking and can be determined experimentally.

The stress intensity factor, K, and the fracture toughness, K_{IC}, should be determined in accordance with the three different fracture modes (I – opening, II –sliding and III – tearing). For 2-D analysis, modes I and II are normally considered, although mode I – opening is usually the dominant mode in concrete fracturing.

- **Discrete model 2: Fictitious crack model** (Hillerborg, Modeer & Petersson 1976)

As can be seen in Figure 2.7, the FPZ is characterized as a fictitious crack lying ahead of the actual crack tip. Three material parameters are required in this model: tensile strength f_t, specific fracture energy G_f, and the shape of the softening curve $\sigma(\delta)$. G_f is

regarded as a material property and represents the energy absorbed per unit area of crack:

$$G_f = \int_0^{\delta_f} \sigma(\delta)\, d\delta \tag{2.7}$$

where δ_f is the critical crack separation displacement when the softening stress is equal to zero.

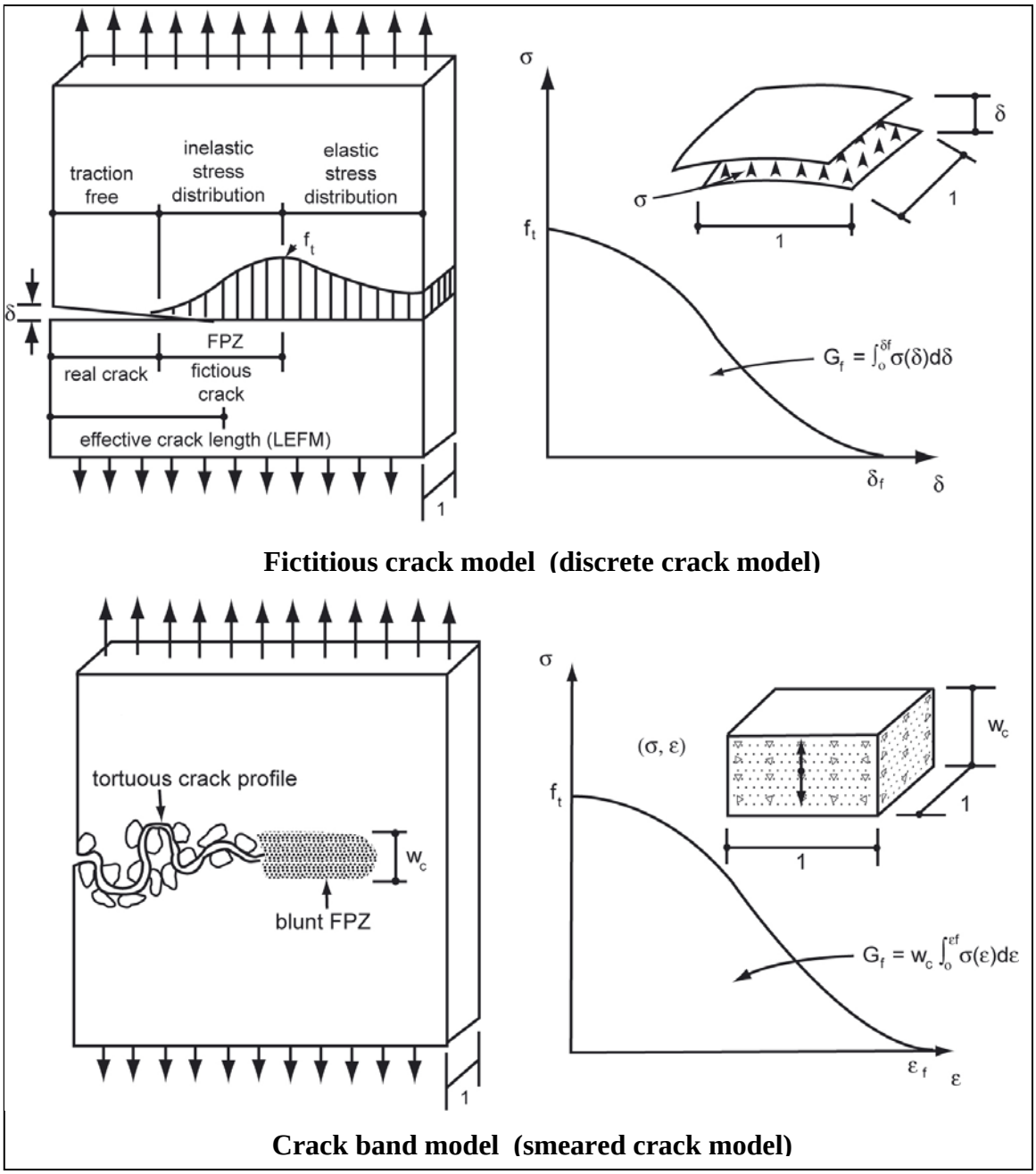

Figure 2.7 - Representative NLFM discrete and smeared crack models (Bhattacharjee & Leger 1992)

- **Discrete model 3: Effective elastic crack approach**

  The FPZ in concrete can also be modelled by a single Griffith-Irwin energy dissipation mechanism. By setting $\sigma(\delta) = 0$, it is implied that no energy is required to overcome the cohesive pressure in separating the crack surfaces. A two-parameter fracture model by Jenq & Shah (1985) and a size effect model by Bažant & Kazemi (1990) are typical examples.

The following three discrete models have also been proposed (Rots 2002):

- Decomposed crack model (Rots 1988)
- Plasticity-based interface model (Lourenco 1996)
- Model based on total relative displacement (Rots 1988)

➢ Smeared fracture and constitutive models

- **Smeared model 1: Orthotropic stress-strain relations** (Rashid 1968)

  The classical smeared crack model was based on the conventional strength-based crack initiation/propagation criterion, with zero post-cracking strength perpendicular to the crack. Although good results were obtained for many practical applications, the method proved to be mesh-unobjective and converged to an incorrect failure mode, with zero energy dissipation. The model's results did not reflect the size effect seen in test results. The constitutive law of this model in 2-D application is as follows (Rots 1989).

$$\begin{Bmatrix} \Delta\sigma_{nn} \\ \Delta\sigma_{ss} \\ \Delta\sigma_{ns} \end{Bmatrix} = \begin{bmatrix} 0 & 0 & 0 \\ 0 & \mathrm{E} & 0 \\ 0 & 0 & 0 \end{bmatrix} \begin{Bmatrix} \Delta\varepsilon_{nn} \\ \Delta\varepsilon_{ss} \\ \Delta\varepsilon_{ns} \end{Bmatrix} \tag{2.8}$$

  Where

  n the direction normal to the crack (mode I – opening)

s the direction tangential to the crack (mode II – shearing).

In this model, both the normal and shear stiffness of the crack become zero immediately after the crack is formed. The orientation of the crack is fixed upon crack formation.

- **Smeared model 2: Mode II shear retention improvement** (based on Rashid's orthotropic model)

Numerical difficulties and distorted crack patterns were sometimes experienced with the application of the above orthotropic model (Rots 1989). Retaining a reduced shear stiffness across the crack can improve the performance of the model which has the following stress-strain relation:

$$\begin{Bmatrix} \Delta\sigma_{nn} \\ \Delta\sigma_{ss} \\ \Delta\sigma_{ns} \end{Bmatrix} = \begin{bmatrix} 0 & 0 & 0 \\ 0 & \mathrm{E} & 0 \\ 0 & 0 & \beta G \end{bmatrix} \begin{Bmatrix} \Delta\varepsilon_{nn} \\ \Delta\varepsilon_{ss} \\ \Delta\varepsilon_{ns} \end{Bmatrix} \tag{2.9}$$

A constant shear retention factor is usually adopted in the application of the model. A more realistic, crack-opening-dependent shear retention factor was also applied previously in order to reflect the fact that shear stress transferred in a crack would decrease as the crack propagated further, with an increase in the crack's normal strain.

The shear retention factor β ($0 \le \beta \le 1$) is used to account for aggregate interlock in the concrete cracking process, which can reduce the numerical difficulties.

- **Smeared model 3: Mode I tension softening improvement** (based on the above smeared model 2)

$$\begin{Bmatrix} \Delta\sigma_{nn} \\ \Delta\sigma_{ss} \\ \Delta\sigma_{ns} \end{Bmatrix} = \begin{bmatrix} E_S & 0 & 0 \\ 0 & \mathrm{E} & 0 \\ 0 & 0 & \beta G \end{bmatrix} \begin{Bmatrix} \Delta\varepsilon_{nn} \\ \Delta\varepsilon_{ss} \\ \Delta\varepsilon_{ns} \end{Bmatrix} \tag{2.10}$$

$$E_S = \mu E$$

A sudden drop in the tensile strength to zero in the above smeared crack model 2 may also cause numerical difficulties similar to those caused by shear drop to zero (Rots 1989). Many displacement-controlled tensile tests reveal a gradual softening in the stress-strain relation after crack initiation. For this reason, further improvements were made to introduce a normal strain-softening concept into the fixed crack model. By doing this, 'over-stiff' results can be reduced; such results are often seen despite the effort of adopting mode II shear retention β. Linear strain softening is often used by inserting a negative normal retention factor μ ($-1 \le \mu \le 0$).

- **Smeared model 4: Extended crack band model (CBM)** (proposed by Bažant & Oh 1983)

Bažant & Oh (1983) improved the above fixed crack models by taking Poisson coupling after crack formation into consideration. In their original crack band model, they ignored the shear retention effect by not including the shear modulus term ($\beta G = 0$). The following extended crack band model was proposed to reinsert the shear modulus on a retention basis (βG).

$$\begin{Bmatrix} \Delta\sigma_{nn} \\ \Delta\sigma_{ss} \\ \Delta\sigma_{ns} \end{Bmatrix} = \begin{bmatrix} \frac{\mu E}{1-\nu^2\mu} & \frac{\nu\mu E}{1-\nu^2\mu} & 0 \\ \frac{\nu\mu E}{1-\nu^2\mu} & \frac{E}{1-\nu^2\mu} & 0 \\ 0 & 0 & \beta G \end{bmatrix} \begin{Bmatrix} \Delta\varepsilon_{nn} \\ \Delta\varepsilon_{ss} \\ \Delta\varepsilon_{ns} \end{Bmatrix} \qquad (2.11)$$

Where

$$\mu = \frac{E_s}{E}$$

ν Poisson's ratio

E_s the strain-softening modulus (negative value).

It is assumed that the FPZ develops within a fixed bandwidth, propagating as a blunt front. A typical value for the bandwidth, w_c, would be three times the size of the

aggregate. Although the CBM (see Figure 2.7) has shown good agreement with all the basic experimental data for concrete specimens, it has the following disadvantages (Bažant & Lin 1988):

(i) The bandwidth determines the element size and subdivision of the bandwidth is not allowed.
(ii) If the crack follows a zigzag path, the rugged opposite sides of the crack could incorrectly transfer stresses that would normally not be present in an open crack – a phenomenon referred to as 'stress locking'.
(iii) The choice of mesh could influence the direction of fracture propagation.
(iv) The bandwidth of the cracking zone cannot be altered.

For the linear strain-softening relationship shown in Figure 2.8, which is often assumed, the E_s can be obtained using the following formula:

$$G_f = h_c\left(1-\frac{E}{E_s}\right)\frac{f_t^2}{2E} \quad \Rightarrow \quad E_s = \frac{f_t^2 E}{f_t^2 - \dfrac{2EG_f}{h_c}} \tag{2.12}$$

Where

f_t the tensile strength

E the elastic modulus

G_f the fracture energy

h_c the crack characteristic length (in CBM, $h_c = w_c$).

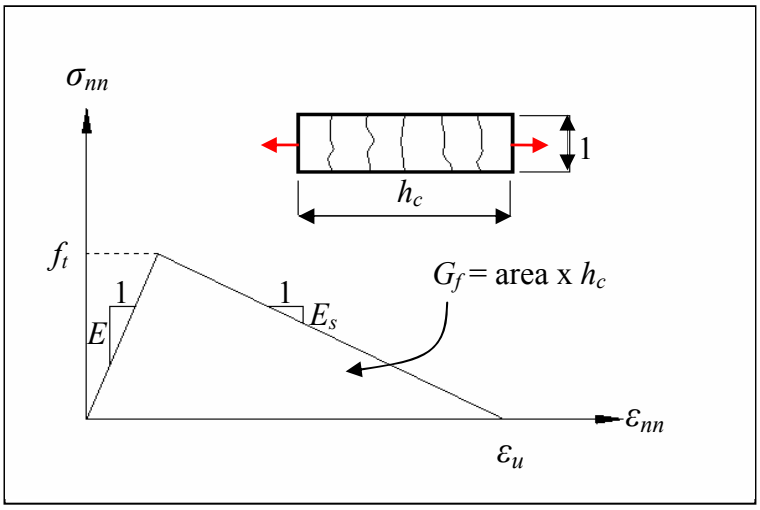

Figure 2.8 - Stress-strain diagram for the crack band model

- **Smeared model 5: Non-orthogonal model** (de Borst & Nauta 1985)

In this non-orthogonal smeared crack model, the total strain increment is considered to be composed of an intact concrete strain increment $\Delta\varepsilon^{co}$ and a cracked strain increment $\Delta\varepsilon^{cr}$:

$$\Delta\varepsilon = \Delta\varepsilon^{co} + \Delta\varepsilon^{cr} \tag{2.13}$$

The constitutive relationship for the cracked concrete is given by:

$$\Delta\sigma = \left\{D^{co} - D^{co}N\left(D^{cr} + N^T D^{co} N\right)^{-1} N^T D^{co}\right\}\Delta\varepsilon \tag{2.14}$$

Where

D^{co} the constitutive matrix for the intact concrete between cracks

D^{cr} the constitutive matrix for the cracks (in the local coordinate direction)

N a transformation matrix.

The model has the following advantages:

- A mixed-mode crack matrix can be formed.
- Non-orthogonal multi-crack formation can be modelled.
- Crack formation can be combined with other non-linear phenomena, such as plasticity, creep and thermal effects.

Rots (2002) also pointed out two disadvantages of this model:

- Difficulty of implementation due to the complicated algorithms involving internal iterations.
- Difficulty of choosing parameters for the shear retention functions and the threshold angles. There is no theoretical or experimental guideline to determine these values for different applications.

- **Smeared model 6: Non-local crack constitutive model** (Bažant & Lin 1988)

  The principal idea of this non-local crack model is to use the non-local concept only for those variables that control 'damage' and not for the strains or stresses in the constitutive relation. The disadvantages of the above smeared model 4 (CBM) can be eliminated by using a non-local constitutive model. Variables causing strain softening are treated as non-local, while all other variables are treated as local. The most important feature of this model is that the effect of structure size on the ultimate capacity and on the post-peak slope of the load–deflection diagram can be correctly presented (ACI 1997). The application of a non-local model in the analysis of a dam may be limited since at least three elements are required on the crack band, resulting in a very fine mesh. The analysis is complicated by the spatial averaging of local response quantities (Bhattacharjee & Leger 1994).

  When the model was used for practical applications, the following inconveniences became apparent (Pijaudier-Cabot & Bažant (1987):

  - The non-local concept is applied for all responses, including the elastic or plastic hardening behaviour.
  - An overlay with a local continuum is necessary for avoiding certain zero-energy periodic modes of instability.

  Pijaudier-Cabot & Bažant (1987) developed a modified non-local formation which avoids these two inconveniences.

- **Smeared model 7: Localized smeared fracture models** (Bhattacharjee & Leger 1994)

  The models of plane stress use a simplified definition of the constitutive material behaviour and have been shown to be computationally economical. A local axis system *ns* is selected for the fractured material, where the direction *n* is normal to the smeared cracks (refer to Figure 2.9). If E_n is the secant modulus of the fractured material, then the 2-D constitutive matrix relating local stresses and strains is defined as:

$$[D]_{ns} = \frac{E}{1-\eta\nu^2}\begin{bmatrix} \eta & \eta\nu & 0 \\ \eta\nu & 1 & 0 \\ 0 & 0 & \mu\dfrac{1-\eta\nu^2}{2(1+\nu)} \end{bmatrix} \tag{2.15}$$

Where

$$\eta = \frac{E_n}{E}; \qquad \mu = \frac{1+\nu}{1-\eta\nu^2}\left(\frac{\eta\varepsilon_n - \varepsilon_s}{\varepsilon_n - \varepsilon_s} - \eta\nu\right)(0 \le \mu \le 1)$$

ε_n and ε_s normal strain components in the local axis normal to and parallel with the fractured plane respectively.

The local constitutive relationship matrix $[D]_{ns}$ can be transformed to the global coordinate directions as follows:

$$[D]_{xy} = [T]^T [D]_{ns} [T] \tag{2.16}$$

Where

[T] strain transformation matrix defined as follows in terms of the inclination of the normal to a crack plane, θ:

$$[T] = \begin{bmatrix} \cos^2\theta & \sin^2\theta & \cos\theta\sin\theta \\ \sin^2\theta & \cos^2\theta & -\cos\theta\sin\theta \\ -2\cos\theta\sin\theta & 2\cos\theta\sin\theta & \cos^2\theta - \sin^2\theta \end{bmatrix} \tag{2.17}$$

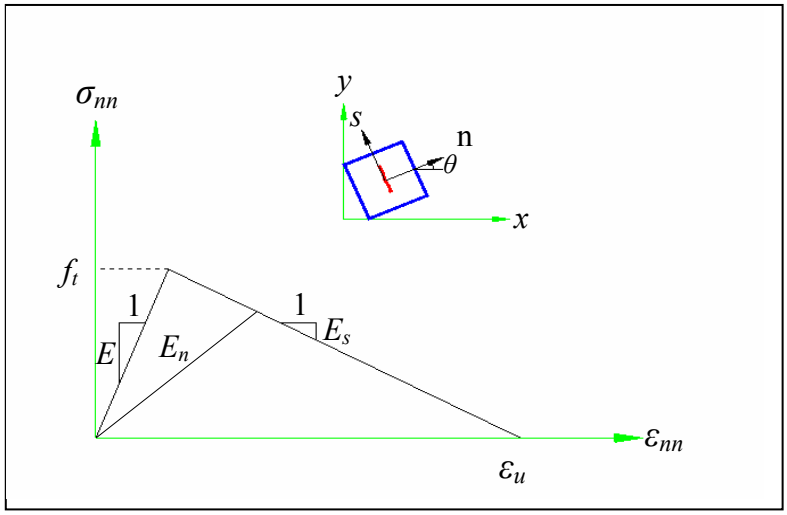

Figure 2.9 - Stress-strain diagram in local coordinates for smeared crack model 7

- **Other smeared models**

Rots (2002) also listed and elaborated on three other smeared crack models with their merits and demerits.

- Total-strain based model (Feenstra *et al*. 1998): In this model, material is modelled by stress-total strain relations.
- Plasticity based model (Feenstra 1993): The tension and compression of the model are approached in a unified way.
- Micro-plane crack model (Bažant & Oh 1985): The model is similar to the non-orthogonal crack model.

Two other smeared crack models were also proposed (Planas, Elices, Guinea, Gomez, Cendon & Arbilla 2003):

- Strong singularity crack model (Oliver *et al*. 2002): This model is similar to the classical local models (such as the crack band model) with an improvement in the strong singularity kinematics, which is able to make a jump in displacements appear naturally in a solution of the continuum approach.

- Gradient crack model (Peerlings *et al*. 2001): This model is similar to the non-local model. It assumes that the stress at a material point is derived from both the strain at that point and its spatial derivatives.

To summarize the available crack models, the flow chart in Figure 2.10 categorizes and lists them into a systematic way.

2.5.5 Summary of crack models discussed

Since the late 1960s, many concrete crack propagation criteria have been developed and applied to analyze cracking in concrete structures. The early strength-based criterion has seldom been used in recent analyses due to its inherent lack of mesh objectivity. LEFM has been widely used in the analysis of concrete dams, in particular gravity dams, as shown in Section 2.7 below. NLFM manages to account for the FPZ in front of the crack tip, providing improved modelling of cracking in concrete. Most of the recent models proposed in the literature are based on NLFM.

Concrete dams are huge structures and models requiring a fine FE mesh, such as the CBM (Bažant & Oh 1983) and non-local models (e.g. Bažant & Lin 1988), are not recommended. The use of a cohesive (fictitious) discrete crack model seems to be gaining popularity, although the computational costs are very high. The non-orthogonal smeared crack model proposed by de Borst & Nauta (1985) appears to be very promising due to its ability to handle simultaneously non-linear concrete behaviour and cracking, non-orthogonal multi-crack formation and crack rotation, and due to it having no stringent mesh size requirement.

Some features that should be considered in concrete cracking models are briefly discussed below.

- **Mixed mode:** In the papers by Planas *et al*. (2003) and Rots & de Borst (1987), although it is pointed out that fractures predominantly form and propagate in mode I, both sets of researchers agree that pure mode I fractures do not occur, which means that mode II cannot be totally ignored.

Galvez *et al.* (2002) further investigated mixed-mode fracturing and their numerical results agreed quite well with those from two experimental sets of mixed-mode fracture of concrete beams. The benchmark results showed that a mode II parameter change has little influence on the numerical predictions. They suggested further research on the influence of the parameters of mode II in the mixed-mode (I/II) fracture of concrete.

- **Crack direction:** The direction of crack propagation has been determined predominantly in the literature to be orthogonal to the direction of maximum principal stress or strain. Martha, Llorca, Ingraffea & Elices (1991) described and compared three crack-direction criteria, namely (i) maximum circumferential stress theory, (ii) minimum strain energy density theory and (iii) maximum energy release rate theory, and concluded that a suitable criterion had still not been found and that further research was necessary. Feng, Pekau & Zhang (1996) adopted the strain energy density factor criterion, which assumes that the direction of crack propagation is towards the minimum region of strain energy density factor. Two assumptions (hypotheses) had to be made in order to obtain a simplified model of 3-D crack propagation for arch dams.

- **Coupling effect:** In most of the cracking models, the coupling effect between the shear stiffness and normal stiffness is generally ignored due to the fact that most applications are restricted to small crack strains. 2-D modelling of the crack shear transferred in rough cracks and the influence of the crack width and normal stresses, etc. on crack shear has been done by various researchers – Bažant & Gambarova (1984); Riggs & Powell (1986); Yoshikawa, Wu & Tanabe (1989) and Divakar & Fafitis (1992), etc. To the authors' knowledge, 3-D crack shear modelling is still an untouched area, at least in the field of concrete dams.

- **Crack closing and reopening:** Most crack models adopt the secant modulus approach for unloading (crack closing). For reloading, the constitutive models follow the same route of unloading until the normal strain in the crack exceeds the previously reached strain. Bhattacharjee & Leger (1992) reviewed a few available studies on this matter and suggested further rational investigation.

2.5.6 Shear resistance of fractured concrete

Fracture could lead to a significant change in the direction of the principal stresses. Aggregate interlocking on the rough crack surfaces results in the development of shear stresses in the cracked concrete. Shear transfer along rough cracks is known to be pressure-sensitive and to cause dilation. Three boundary conditions for the normal pressure imposed on a rough crack are usually considered in the modelling of shear resistance in a crack. They are:

- Constant normal stress condition
- Constant crack width condition
- Variable normal stress and crack width conditions.

Divakar & Fafitis (1992) developed a micro-mechanical interface shear model to predict the shear transfer under the above three boundary conditions. Four mechanisms (sliding; interlocking, overriding and fracturing) of shear transfer were considered. This micro-mechanical model, which took into account the internal structure of the material and the nature of the rough surface, was satisfactorily verified by the experimental results. Bažant & Gambarova (1984) introduced a crack band micro-plane model to describe crack shear in concrete.

A simple shear retention factor, β, is often used to reduce the shear modulus in the constitutive matrix. However, this ignores shear dilation and the dependence of shear on the crack opening displacement. A constant shear modulus fails to account for the variation in shear strain, caused by the strain normal to the crack, which has been observed experimentally. To overcome this problem, Rots & de Borst (1987) adopted a bilinear shear modulus approach and Balakrishnan & Murray (1988) proposed a method of decreasing the shear modulus linearly with increasing normal strain.

2.5.7 Post-crack behaviour

The post-fracture behaviour forms an important part of the crack constitutive model. A crack is normally assumed to propagate in a direction perpendicular to the maximum

principal stress that initiated the first cracking. Fixed orthogonal crack models assume that an additional crack plane will only form orthogonally to the first crack plane. Later developments (Rots & Blaauwendraad 1989) resulted in the rotating crack model and the fixed, multi-directional (non-orthogonal) crack model.

Cervera, Oliver & Herrero (1990) presented an elastic-fracturing constitutive model, of which the post-fracture concrete behaviour is the most important part, for progressive cracking in large dams due to the swelling of concrete. The model allows for one or two independent sets of cracks appearing at the same point in two scenarios, as follows:

- Two cracks will be orthogonal if they are formed simultaneously and no further cracking will be allowed at that point.
- If one crack occurs first, further loading may cause a sequential, second crack to occur, which can be allowed to form in a non-orthogonal direction to the first (primary) crack.

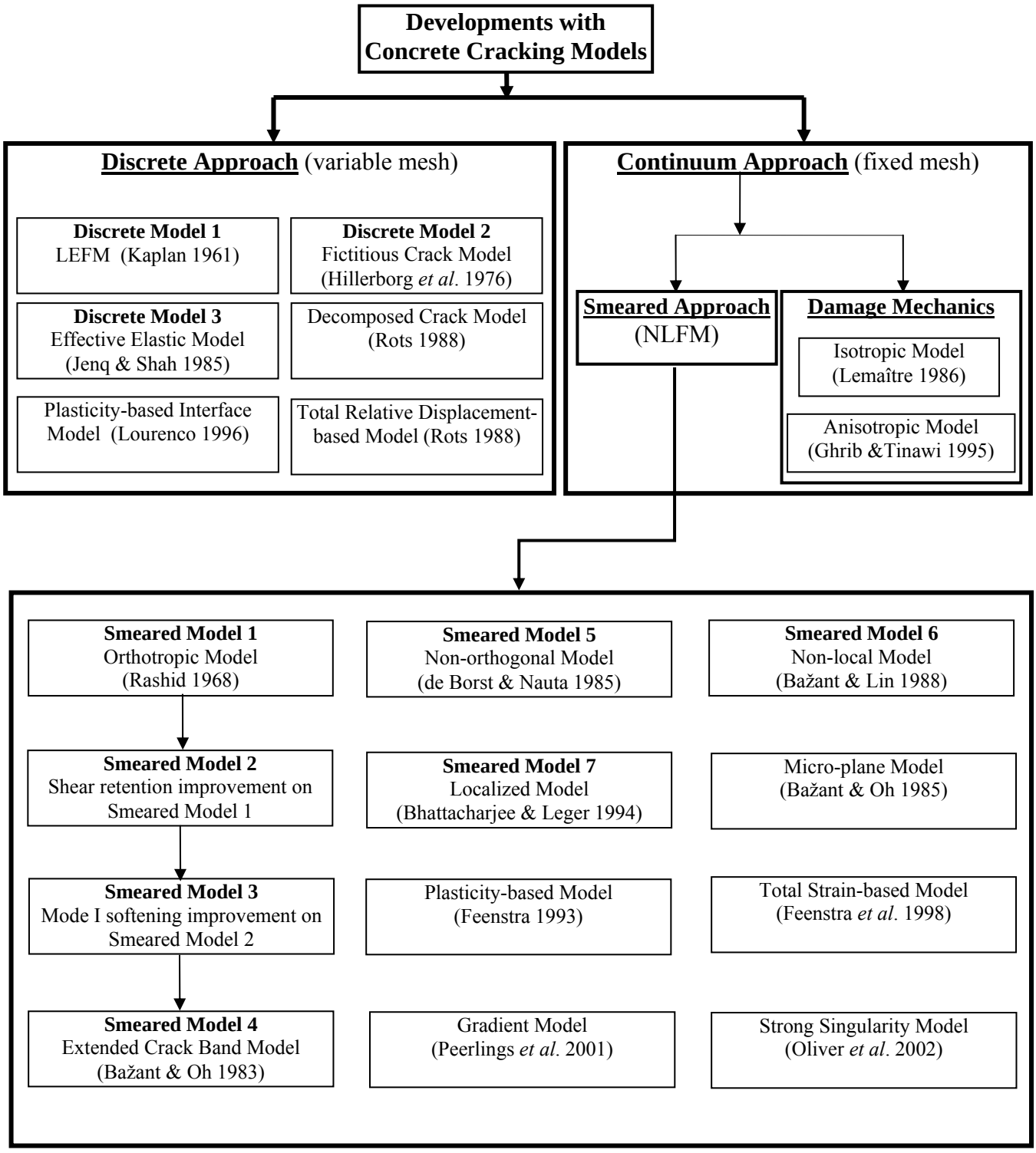

Figure 2.10 - Flowchart of overall cracking models proposed for concrete fracture

2.6 Fracture energy G_f of dam concrete

Accurate determination of the fracture energy of concrete, especially dam concrete, is not an easy task because the amount of the fracture energy G_f will vary with many factors, namely type and size of specimen, type of aggregates, maximum grain size, concrete strength and moisture, type of cement and additives, loading rate, etc. Dam concrete is usually different from normal concrete in the following ways:

- Large aggregate size: maximum aggregate size is usually 100 ~ 150 mm
- Low water-cement ratio: to improve strength
- Low cement content: to reduce thermal cracking and shrinkage during curing.

Very high discrepancies of the fracture energy G_f of dam concrete have been reported, as discussed below.

Trunk & Wittmann (1998) conducted a series of tests on normal and dam concrete with different specimen sizes up to 3 200 mm. For normal concrete, a fracture energy G_f of 121 ~ 322 N/m was obtained. For dam concrete, a fracture energy G_f of 219 ~ 482 N/m was determined.

Brühwiler (1988) carried out wedge-splitting tests on different specimens – cylindrical, drilled cores from three existing concrete dams. Fracture energies G_f of 175, 235 and 257 N/m were obtained for these three dam concrete specimens which had diameters of 200 ~ 300 mm.

Espandar & Lotfi (2000) adopted a fracture energy G_f of 600 N/m in the analysis of the Shahid Rajaee arch dam in Iran.

Espandar & Lotfi (2003) stated that RILEM gave a fracture energy G_f in the range of 70 ~ 200 N/m for normal concrete and suggested that the fracture energy of dam concrete should be three times higher than that of normal concrete. A higher fracture energy has often been used in the practical analysis of dam concrete. Fracture energies G_f of as high as 1 375 and 2 200 N/m have been seen to be used before.

Bhattacharjee & Leger (1994) pointed out that the fracture energy generally observed for dam concrete is typically in the range of 100 ~ 200 N/m.

The ICOLD report (2001) stated that fracture energy increases with the maximum aggregate size. For normal concrete, if the maximum grain size is in the range of 2 ~ 38 mm, the fracture energy was found to be in the range of 50 ~ 200 N/m. Fracture energies of up to 280 N/m were obtained for the maximum grain size of 76 mm. The maximum aggregate size normally used in concrete dams is in the range of 100 ~ 150 mm, which would result in an even higher fracture energy.

Saouma, Broz, Bruhwiler & Boggs (1991) obtained fracture energy G_f of 80 ~ 140 N/m for dam concrete.

The fracture energy of concrete increases with the size of the specimens and becomes a constant value after a critical large specimen size is reached. Therefore, sufficiently large specimens have to be used for any experiments to accurately determine the fracture energy. The fracture energy obtained on small specimens needs to be corrected for the size effect.

Bažant and his co-workers (Bažant, Kim & Pfeiffer 1986; Bažant & Pfeiffer 1987) proposed a 'size effect law' for the correct determination of the fracture energy G_f as follows:

$$G_f = \frac{g(\alpha)}{AE} \qquad (\alpha = \frac{a_0}{d}) \tag{2.18}$$

Where

$g(\alpha)$	the non-dimensionalized energy-release rate, known for the chosen specimen shape from LEFM
A	the slope of the size-effect regression line of σ_N^{-2} versus d
σ_N	nominal stress at maximum load
d	the characteristic dimension (depth) of the specimen

a_0 the traction-free crack length (notch length).

Linsbauer (1991) carried out the wedge-splitting tests on drilling core samples of dam concrete with two diameters, 150 mm and 190 mm. The diameter of each sample allowed ten drilling cores to be tested. A large spread of fracture energies were reported to have been obtained from the experiment. For the samples of 150 mm in diameter, the fracture energy ranged from 59.9 to 177.3 N/m, with an average value of 109.1 N/m. The larger samples of 190 mm in diameter samples gave fracture energies in the range of 109.1 to 230.8 N/m, with an average value of 155.4 N/m.

He, Plesha, Rowlands & Bažant (1992) also carried out large-scale wedge-splitting compact tension tests on dam concrete in order to study the fracture mechanics properties of dam concrete for different loading rates and specimen sizes. Dam concrete specimens were cast with a maximum aggregate size of 76 mm. The size-effect law presented by Bažant *et al*. (1986) discussed above was adopted to compute the fracture energy of the dam concrete from the test data. The experimental results showed that the fracture energy falls within the range of 200 to 300 N/m for dam concrete.

It is also reported from experiments that the fracture energy G_f increases with the compressive strength of the concrete and the loading rate.

Three test methods are usually employed for the determination of the concrete fracture energy G_f, namely the uniaxial tensile test, the bending test and the wedge-splitting test. The double cantilever-beam test, the compact tension specimen test and the double torsion specimen test have also been used in the past.

In conclusion, the fracture energy of dam concrete with large maximum aggregates is much higher than that of normal concrete. The past investigations and experiments yielded huge discrepancies in the magnitudes of the fracture energy of the dam concrete (mostly between 80 and 600 N/m), which would make the choice of fracture energy for the crack modelling of concrete dams a rather uncertain matter. Therefore, a sensitivity study on this fracture parameter should be considered in the fracture analysis of a concrete dam. The

fracture energy G_f = 100 ~ 300 N/m is probably the most possible value for concrete dams.

2.7 Past investigations of the static cracking problems of concrete gravity dams

Over the past decades, many attempts have been made to investigate the cracking problems in concrete gravity dams by using various cracking analysis methods. Discrete LEFM seems to be the most popular approach for dam fracture analysis and it is used extensively in modelling the cracking of gravity dams. Ayari (1988), in his PhD study, adopted the discrete LEFM approach in analyzing the static fracture response of concrete gravity dams.

Chappell & Ingraffea (1981) used LEFM to model fracture in the Fontana gravity dam (USA) which had experienced the first traces of cracking in 1949. The cracking problem in this dam was formally acknowledged in 1972. Reasonably accurate predictions of crack trajectory and stability were obtained (SIMSCIENCE website). Again, Ingraffea (1990) used a 2-D mixed-mode, discrete LEFM model as a forensic tool to analyze crack propagation in the Fontana Dam. The observed crack profile, which started from the middle of the downstream face (caused by a combination of cyclic, reversible thermal expansion and concrete growth due to the alkali-silica reaction) and then dipped down through the gallery, was reproduced by this mixed-mode LEFM crack analysis. He further used the method in a generic gravity dam for the purpose of evaluating the dam's design and analyzing its stability. The factor of safety against sliding predicted by LEFM is, in general, less conservative (i.e. has a higher value) than that of the classical method.

Linsbauer (1990) developed a diagram (critical crack vs. depth of crack level and fracture toughness) based on LEFM for assessing cracking in gravity dams which can be applied in determining "the stability of horizontal cracks in the top three quarters of any gravity dam" with a triangular dam profile of width-to-height ratio of 0.8. The value of LEFM in analyzing cracking in concrete dams has therefore been demonstrated.

Gioia, Bažant & Pohl (1992) carried out a 2-D mixed-mode discrete LEFM analysis on an identical model of the Koyna Dam – a concrete gravity dam in India. FRANC – a discrete

LEFM program, was adopted for the prediction of crack growth. Curves of overflow-displacement at the top were plotted to compare the results obtained from analyses of no-tension, plasticity and fracture mechanics. The conclusions drawn from the analysis are that the classical no-tension design criterion is not always safe and that the safety of dams should be evaluated on the basis of fracture mechanics.

Kumar & Nayak (1994) carried out a 2-D mixed-mode, discrete LEFM analysis in a case study of the Lakhwar gravity dam. Seven load cases with six different cracks at different locations were used to study the effect of parameters such as dam height, B/H (base-height ratio), type of singularity at the heel, etc. The results show that the most significant parameters affecting the tensile stress and the stress intensity factor are E_R/E_C (ratio of Young's modulus of foundation rock and concrete), B/H and the type of singularity at the heel. LEFM can "successfully" determine the location of cracks.

Plizzari, Waggoner & Saouma (1995) experimentally tested and numerically analyzed (using LEFM) cracking in gravity dam models in order to establish a centrifugal testing technique for modelling fracturing in concrete gravity dams.

Plizzari (1997) further used LEFM to predict crack propagation in concrete gravity dams. A parametric study of triangular-shaped dams was performed, assuming a horizontal crack at the dam/foundation interface. He proposed a scale law to determine the maximum hydrostatic pressure that a cracked gravity dam can carry.

Compared with the wide applications of LEFM in the analysis of the cracking of concrete dam structures, the NLFM criterion was applied much less in the past to concrete structures, apparently due to the complexity of applying it. Nevertheless, Bhattacharjee & Leger (1994) used the NLFM criterion in a 2-D smeared crack model for analyzing a model gravity dam and the Koyna gravity dam in India. A rotating crack model and a fixed crack model with variable shear resistance factors (FCM-VSRF) were used to analyze the Koyna Dam. The relation of overflow and displacement at the top was plotted to allow comparison with the results of LEFM and plasticity analyses. The crack profile predicted was good. Sensitivity studies of the response to fracture parameters, such as fracture energy and initial crack depth, and to different crack models (rotating or fixed)

were carried out. The FCM-VSRF model normally provides a stiffer response due to significant stress-locking. The fracture energy G_f and the initial crack depth a_0 do not have much influence on the ultimate structural response.

Bhattacharjee & Leger (1995) again employed a rotating smeared crack model to predict the static fracture behaviour of the Koyna Dam. They proposed the concept of 'effective porosity' to model the water intrusion and the consequent uplift pressure inside the cracks which was found to greatly reduce the ultimate resistance of the dam structure. Comparison with the conventional 'no-tension' gravity method revealed that this method of analysis for concrete dams may not always be as conservative as is usually thought.

Ghrib & Tinawi (1995) presented damage mechanics models based on anisotropic formulation to predict the static response of concrete dams. A 1:40 reduced model of a gravity dam tested by Carpinteri, Valente, Ferrara & Imperato (1992) was used to verify the accuracy of the proposed model. The damage models provide an accurate prediction of the ultimate load. They also provide crack profiles "similar" to the experimental results. The Koyna Dam was also used to compare the proposed damage mechanics models with the other numerical investigations under overflow hydrostatic loading. It is stated that the proposed models are mesh-objective and accurate, and can be used for assessing the ultimate capacity of a concrete dam and the dam's safety margin.

Saouma & Morris (1998) used a 2-D LEFM and NLFM interface crack model (ICM) to analyze the Greyrock gravity dam in the USA. The program MERLIN was coded so that the criterion for crack propagation was a strength-based one in which the tensile stress could not exceed the tensile strength. Fracture mechanics analysis was employed to evaluate the dam safety and to highlight the need for practice engineers to accept this method for evaluating dam safety. Two crack orientations – straight and kinking – were considered. The analysis based on fracture mechanics revealed that the classical rigid body equilibrium is more conservative and that it would be more economical to use the method based on fracture mechanics.

Araújo & Awruch (1998) adopted both discrete NLFM crack model and continuum damage theory in an analysis of the cracking of the Tucuruí gravity dam in Brazil, which

was due to thermal effects during the construction phase, and verified the dam's safety against cracking.

Cervera *et al*. (1990) used 2-D and 3-D elastic-fracturing models in the analysis of a 79-m-high gravity dam in Spain, called the Mequinenza Dam, which had experienced cracking on the upstream wall and the interior corridors. Fracture due to swelling of the concrete was modelled, including the mechanism of water intrusion, concrete extension, tensile fracturing and seasonal thermal straining.

Cervera, Oliver & Galindo (1992) again developed an FE constitutive model to study cracking due to concrete hydration in the large Mequinenza gravity dam. For short-term behaviour, a continuum damage constitutive model was used. For long-term creep behaviour, visco-elastic effects were modelled and considered. Good agreement between the numerical simulation and the measurements was obtained.

Barpi & Valente (2001) used a 1:40-scale gravity dam model previously tested by Carpinteri *et al*. (1992) to verify the capability of the cohesive crack model to correctly predict the size effect, using fuzzy parameters. They found that the cohesive crack model could indeed predict the size effect, thus explaining the behaviour of a dam model based on experimental results from much smaller specimens.

Shi, Suzuki & Nakano (2003) used an extended fictitious crack model to model multiple cracks in concrete dams. Only mode I cracks were considered for simplicity. Bi-linear strain softening was adopted. Three FE models of generic gravity dams with initial notches were used to verify the analytical procedure developed for the cracking analysis of concrete dams. They demonstrated that the model is able to investigate the ultimate response of concrete dams, identify the potentially damaging cracks and predict the crack profile, without any restrictions on the numbers and locations of cracks.

Saouma *et al*. (1990) gave a detailed review of the application of fracture mechanics to concrete dams. The applicability of various models to concrete dams, and the limitations of the models, were discussed and practical examples of fracture mechanics models were

presented. Compared with the classical method, the fracture mechanics approach is less conservative and the results are less sensitive to material properties.

2.8 Concluding remarks and recommendations

It is a demanding and challenging task to develop a constitutive model that effectively includes all the characteristics of cracking in concrete, yet remains sufficiently simple for practical implementation. An accurate model should include the tortuous crack path and the non-linear inelastic material behaviour in the FPZ.

Constitutive modelling of the tensile resistance of concrete using the FE method has progressed from conventional strength-based models to models based on fracture mechanics and energy-conserving principles. Current trends in research show a movement from 2-D to 3-D modelling, from LEFM to NLFM, and from a single crack with a predefined location to multiple cracks with unbiased location and taking into consideration the effect of water pressure inside the cracks. The complexity of the problem seems to be the reason why a generally accepted 3-D fracture model for concrete has not yet been presented. However, the constitutive model proposed by de Borst & Nauta (1985) appears to be very promising.

From the literature review, it can be concluded that further research is needed into developing a constitutive model of concrete dams, to be implemented into FE analysis. The following aspects should be addressed:

- The fracture strain softening has been well studied, but further attention should be given to the multi-linear and non-linear mode I softening diagram for the concrete normally used in concrete dams.
- The post-cracking treatment of shear in the constitutive model requires more attention. The influence of normal displacements (or strains) on the shear modulus should be investigated both experimentally and numerically.
- Mixed-mode criteria should be used to address the complex stresses often encountered in dams.

- The smeared crack model is recommended for incorporation into the existing FE programs.
- More research effort into crack propagation direction criteria in concrete dams is needed.

CHAPTER III - CONSTITUTIVE MODELS AND PARAMETERS STUDY

As shown in Chapter II, the constitutive modelling of concrete cracking phenomena has undergone tremendous development. Many constitutive models have been proposed in the past for analyzing concrete fracture, mainly for small-scale concrete structures such as single- or double-notched beams of mode I or mixed-mode fracturing.

Concrete dams are normally huge in size and are subjected to both normal and shear loadings, which results in a complex state of stress within the structures. As stated in Chapter II, the non-orthogonal crack model proposed by de Borst & Nauta (1985) is an ideal model to form the basis for the further development of models to simulate the cracking process in concrete dams under both normal and shear loadings. The constitutive relationships adopted in this research for the different deformation phases, such as the stages before and during softening, are outlined in the sections below.

In this research a smeared constitutive model has been established which has the advantages of preserving the topology of the finite element (FE) mesh and of easy determination of the crack orientation by aligning the crack perpendicular to the direction of principal stress during analysis. This model can be used to analyze the entire process of concrete cracking, including

- Pre-softening: Structural behaviour before a crack is initiated
- During softening: Structural behaviour during crack formation
- Structural behaviour for unloading/reloading and closing/reopening of cracks.

3.1 Pre-softening constitutive relationship

In this study, linear elastic behaviour in tension before the onset of a tensile fracture is assumed. For compression, linear elasticity is also assumed due to the fact that the research is focused on the local strain-softening behaviour of tensile fractured concrete and because the structures involved in this study, such as concrete gravity dams, are governed by cracking, not crushing. As a consequence, some non-elastic softening close to the peak

stress before a crack is initiated will be ignored by the above assumption. If required, a non-linear, plastic stress-strain law could be included later.

The incremental stress – incremental strain relationship is expressed as follows.

$$\Delta\sigma = D^{co}\,\Delta\varepsilon \tag{3.1}$$

- For 3-D FE analysis, equation (3.1) can be expressed as follows:

$$\begin{Bmatrix} \Delta\sigma_x \\ \Delta\sigma_y \\ \Delta\sigma_z \\ \Delta\sigma_{xy} \\ \Delta\sigma_{yz} \\ \Delta\sigma_{zx} \end{Bmatrix} = \frac{E}{(1+\nu)(1-2\nu)} \begin{bmatrix} 1-\nu & \nu & \nu & 0 & 0 & 0 \\ \nu & 1-\nu & \nu & 0 & 0 & 0 \\ \nu & \nu & 1-\nu & 0 & 0 & 0 \\ 0 & 0 & 0 & \frac{1-2\nu}{2} & 0 & 0 \\ 0 & 0 & 0 & 0 & \frac{1-2\nu}{2} & 0 \\ 0 & 0 & 0 & 0 & 0 & \frac{1-2\nu}{2} \end{bmatrix} \begin{Bmatrix} \Delta\varepsilon_x \\ \Delta\varepsilon_y \\ \Delta\varepsilon_z \\ \Delta\gamma_{xy} \\ \Delta\gamma_{yz} \\ \Delta\gamma_{zx} \end{Bmatrix} \tag{3.2}$$

Where

E	Young's modulus
ν	Poisson's ratio
x, y, z	Global Cartesian coordinates

- For plane stress analysis, the above equation (3.1) can be expressed as follows:

$$\begin{Bmatrix} \Delta\sigma_x \\ \Delta\sigma_y \\ \Delta\sigma_{xy} \end{Bmatrix} = \begin{bmatrix} \frac{E}{1-\nu^2} & \frac{\nu E}{1-\nu^2} & 0 \\ \frac{\nu E}{1-\nu^2} & \frac{E}{1-\nu^2} & 0 \\ 0 & 0 & G \end{bmatrix} \begin{Bmatrix} \Delta\varepsilon_x \\ \Delta\varepsilon_y \\ \Delta\gamma_{xy} \end{Bmatrix} \tag{3.3}$$

Where

G shear modulus, $G = \dfrac{E}{2(1+\nu)}$

- For plane strain analysis, the above equation (3.1) can be expressed as follows:

$$\begin{Bmatrix} \Delta\sigma_x \\ \Delta\sigma_y \\ \Delta\sigma_z \\ \Delta\sigma_{xy} \end{Bmatrix} = \frac{E}{(1+\nu)(1-2\nu)} \begin{bmatrix} 1-\nu & \nu & 0 & 0 \\ \nu & 1-\nu & 0 & 0 \\ \nu & \nu & 0 & 0 \\ 0 & 0 & 0 & \frac{1-2\nu}{2} \end{bmatrix} \begin{Bmatrix} \Delta\varepsilon_x \\ \Delta\varepsilon_y \\ \Delta\varepsilon_z = 0 \\ \Delta\gamma_{xy} \end{Bmatrix} \tag{3.4}$$

3.2 Crack onset criterion and crack direction

The crack onset criterion in this research is defined by assuming that the concrete will crack when the maximum tensile principal stress σ_1 exceeds the concrete tensile strength f_t at a Gauss point. The crack direction is then perpendicular to the direction of the maximum principal stress (see Figure 3.1).

This is a simple and effective conventional criterion which will ignore the effects of the second and third principal stresses under multi-axial loading conditions. For a 2-D application, the criterion is shown in straight lines in Figure 3.2. A more accurate crack initiation criterion (red curve in the Figure 3.2) depends on the second principal stress of the perpendicular direction, such as the criterion based on tensile strain energy density proposed by Bhattacharjee & Leger (1993).

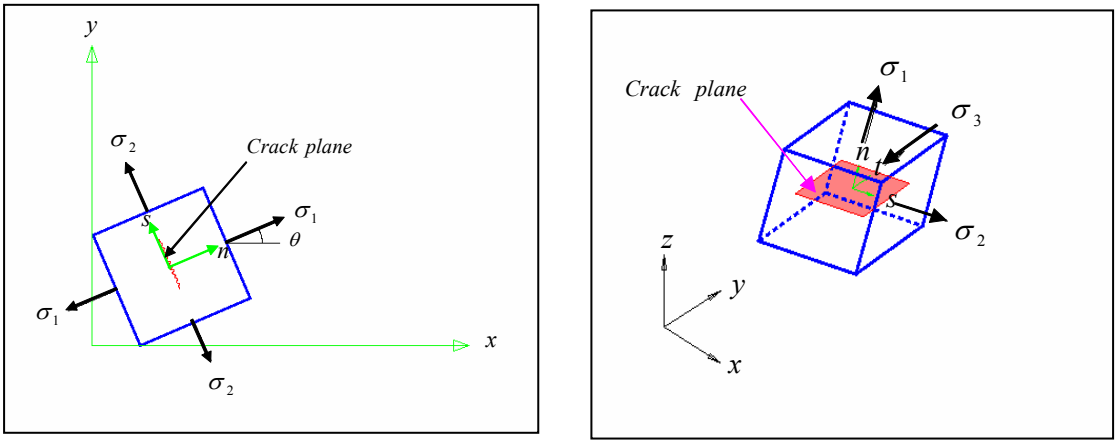

Figure 3.1 - Crack direction and local axis system for 2-D and 3-D applications

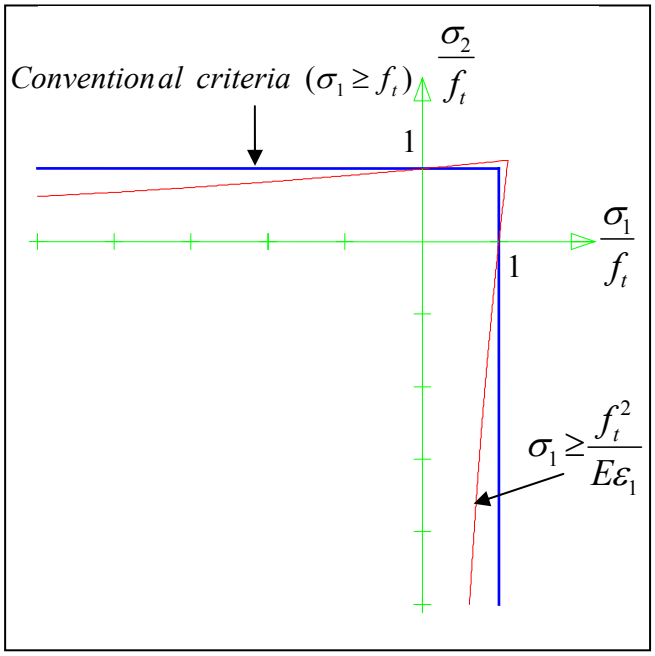

Figure 3.2 - Crack initiation criteria for a 2-D application

3.3 Constitutive relationship during concrete cracking

The early orthogonal crack models limited the crack formation and directions. Following cracking at one point, a second crack can be only allowed to form in the perpendicular direction of the first crack and so on. In 3-D modelling, a third crack may only develop perpendicular to the first two cracks. To improve cracking behaviour, de Borst and Nauta (1985) developed a non-orthogonal crack model, which allows a subsequent crack at a point to develop at any angle to a prior crack. This approach is ideal for simulating the cracking process in concrete structures. One of the main features of the model is that it decomposes the total crack strain increment into a strain increment for the uncracked concrete between cracks $\Delta\varepsilon^{co}$ and a strain increment at the crack $\Delta\varepsilon^{cr}$ as follows:

$$\Delta\varepsilon = \Delta\varepsilon^{co} + \Delta\varepsilon^{cr} \tag{3.5}$$

The crack strain increment $\Delta\varepsilon^{cr}$ in equation (3.5) is further contributed to by all the individual cracks at a particular Gauss point:

$$\Delta\varepsilon^{cr} = \Delta\varepsilon_1^{cr} + \Delta\varepsilon_2^{cr} + \cdots \tag{3.6}$$

Where $\Delta\varepsilon_1^{cr}$ is the strain increment of a first (primary) crack; $\Delta\varepsilon_2^{cr}$ is the strain increment of a secondary crack, and so on.

The strain increment of individual crack (i), $\Delta\varepsilon_i^{cr}$, in the global x, y and z coordinates can be obtained by transforming the local crack strain increment Δe_i^{cr} as follows:

$$\Delta\varepsilon_i^{cr} = N_i \Delta e_i^{cr} \tag{3.7}$$

$$\Delta e_i^{cr} = \begin{Bmatrix} \Delta e_{nn}^{cr} \\ \Delta\gamma_{ns}^{cr} \\ \Delta\gamma_{nt}^{cr} \end{Bmatrix}_i \tag{3.8}$$

The local coordinate system (n, s, t) is crack-aligned as shown in Figure 3.3, where n refers to the direction normal to a crack and s, t refer to the directions tangential to a crack.

In equation (3.8), Δe_{nn}^{cr} is the mode I local crack normal strain increment and $\Delta\gamma_{ns}^{cr}$, $\Delta\gamma_{nt}^{cr}$ are the mode II and III local crack shear strain increments respectively. N_i is a transformation matrix between the global and local coordinates at the crack (i).

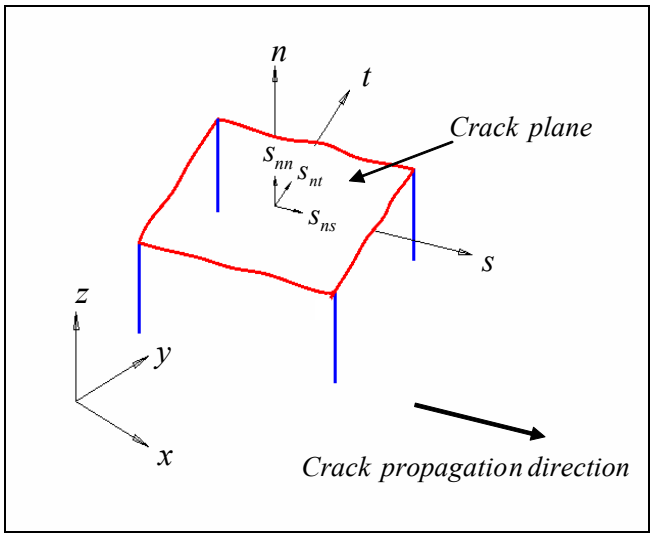

Figure 3.3 - Coordinate system and traction vectors across a crack for 3-D application

For a 3-D configuration, N_i has the following format:

$$N_i = \begin{bmatrix} l_1^2 & l_1 l_2 & l_3 l_1 \\ m_1^2 & m_1 m_2 & m_3 m_1 \\ n_1^2 & n_1 n_2 & n_3 n_1 \\ 2l_1 m_1 & l_1 m_2 + l_2 m_1 & l_3 m_1 + l_1 m_3 \\ 2m_1 n_1 & m_1 n_2 + m_2 n_1 & m_3 n_1 + m_1 n_3 \\ 2n_1 l_1 & n_1 l_2 + n_2 l_1 & n_3 l_1 + n_1 l_3 \end{bmatrix}_i \tag{3.9}$$

Where l_1, l_2, l_3, m_1, m_2, m_3, n_1, n_2, n_3 are the direction cosines of the axes defined in Tables 3.1 and 3.2 (refer to Figures 3.1 and 3.3):

TABLE 3.1 - Direction cosines of local axes in global axis

	x	y	z	Global coordinate
n	l_1	m_1	n_1	
s	l_2	m_2	n_2	
t	l_3	m_3	n_3	
Local coordinate				

For a 2-D application (plane stress or plane strain), Table 3.1 becomes the following Table 3.2.

TABLE 3.2 - Direction cosines of local axes in global axis (2-D)

Local coordinate	x	y	z	Global coordinate
n	$l_1 = cos\theta$	$m_1 = sin\theta$	$n_1 = 0$	
s	$l_2 = -sin\theta$	$m_2 = cos\theta$	$n_2 = 0$	
t	$l_3 = 0$	$m_3 = 0$	$n_3 = 1$	

Where θ is the angle between the normal of a crack and the global x-axis shown in Figure 3.1.

For equation (3.7), it is convenient to assemble the individual crack vectors and matrices into a general form as follows.

$$\Delta\varepsilon^{cr} = N\,\Delta e^{cr} \tag{3.10}$$

Where $N = [N_1\ N_2 \cdots]$ is a transformation matrix which combines all the individual crack transformation matrices, and $\Delta e^{cr} = [\Delta e_1^{cr}\ \Delta e_2^{cr} \cdots]^T$ is the local crack strain increment which is composed of the contributions of multiple cracks.

The local stress increment ΔS^{cr} can be derived by transforming the global stress increment $\Delta\sigma$ as follows:

$$\Delta S^{cr} = N^T\,\Delta\sigma \tag{3.11}$$

Where $\Delta S^{cr} = [\Delta S_1^{cr}\ \Delta S_2^{cr} \cdots]^T$ is composed of the contributions of multiple cracks.

For an individual crack (*i*), the local crack stress increment vector ΔS_i^{cr} is defined as:

$$\Delta S_i^{cr} = \begin{Bmatrix} \Delta S_{nn}^{cr} \\ \Delta S_{ns}^{cr} \\ \Delta S_{nt}^{cr} \end{Bmatrix}_i \tag{3.12}$$

Where ΔS_{nn}^{cr} is the mode I normal stress increment and $\Delta S_{ns}^{cr}, \Delta S_{nt}^{cr}$ are the mode II and III shear stress increments respectively.

The constitutive relationships of the concrete between the cracks and the local cracks are as follows:

$$\Delta\sigma = D^{co}\,\Delta\varepsilon^{co} \tag{3.13}$$

$$\Delta S^{cr} = D^{cr}\,\Delta e^{cr} \tag{3.14}$$

Where

D^{co} is the constitutive matrix of the 'intact' concrete between the cracks as follows:

$$D^{co} = \frac{E}{(1+\nu)(1-2\nu)} \begin{bmatrix} 1-\nu & \nu & \nu & 0 & 0 & 0 \\ \nu & 1-\nu & \nu & 0 & 0 & 0 \\ \nu & \nu & 1-\nu & 0 & 0 & 0 \\ 0 & 0 & 0 & \frac{1-2\nu}{2} & 0 & 0 \\ 0 & 0 & 0 & 0 & \frac{1-2\nu}{2} & 0 \\ 0 & 0 & 0 & 0 & 0 & \frac{1-2\nu}{2} \end{bmatrix} \tag{3.15}$$

and

D^{cr} is the constitutive matrix of the local cracks as follows:

$$D^{cr} = \begin{bmatrix} D_1^{cr} & 0 & \cdots \\ 0 & D_2^{cr} & \cdots \\ \cdots & \cdots & \cdots \end{bmatrix} \tag{3.16}$$

Where the size (columns and rows) of D^{cr} depends on the number of cracks at the Gauss point. Zero off-diagonal terms implies that the coupling effects between different cracks are ignored.

For a crack (i): $D_i^{cr} = \begin{bmatrix} D_i^I & 0 & 0 \\ 0 & D_i^{II} & 0 \\ 0 & 0 & D_i^{III} \end{bmatrix}$ in which D_i^I is the mode I stiffness modulus, $D_i^{II} = \frac{\beta}{1-\beta} G$ is the mode II shear stiffness modulus and D_i^{III} is the mode III stiffness modulus. β is the shear retention factor to be defined in Section 3.5. $G = \frac{E}{2(1+\nu)}$ is the elastic shear modulus. Again, no coupling is considered between the shear and normal strains on the crack plane.

From equations (3.11), (3.13), (3.5) and (3.10), we have:

$$\Delta S^{cr} = N^T \Delta\sigma = N^T D^{co} \Delta\varepsilon^{co} = N^T D^{co} (\Delta\varepsilon - N\Delta e^{cr}) \tag{3.17}$$

From equations (3.17) and (3.14), we have:

$$D^{cr} \Delta e^{cr} = N^T D^{co} (\Delta\varepsilon - N\Delta e^{cr}) \tag{3.18}$$

From equation (3.18), we have:

$$(D^{cr} + N^T D^{co} N)\Delta e^{cr} = N^T D^{co} \Delta\varepsilon \tag{3.19}$$

From equation (3.19), we have:

$$\Delta e^{cr} = \left[D^{cr} + N^T D^{co} N\right]^{-1} N^T D^{co} \Delta\varepsilon \tag{3.20}$$

From equations (3.20) and (3.13), (3.5) and (3.10), we have:

$$\Delta\sigma = D^{co}\left\{\Delta\varepsilon - N\left[D^{cr} + N^T D^{co} N\right]^{-1} N^T D^{co} \Delta\varepsilon\right\} \tag{3.21}$$

The overall relationship between global stress and strain is obtained from the above equation (3.21):

$$\Delta\sigma = \left\{D^{co} - D^{co} N\left[D^{cr} + N^T D^{co} N\right]^{-1} N^T D^{co}\right\}\Delta\varepsilon \tag{3.22}$$

3.3.1 Plane stress application used in this research

For the plane stress analysis in equation (3.22), we have:

$$D^{co} = \begin{bmatrix} \dfrac{E}{1-\nu^2} & \dfrac{\nu E}{1-\nu^2} & 0 \\ \dfrac{\nu E}{1-\nu^2} & \dfrac{E}{1-\nu^2} & 0 \\ 0 & 0 & \dfrac{E}{2(1+\nu)} \end{bmatrix} \tag{3.23}$$

$$D^{cr} = \begin{bmatrix} D_1^{cr} & 0 & \cdots \\ 0 & D_2^{cr} & \cdots \\ \cdots & \cdots & \cdots \end{bmatrix} \tag{3.24}$$

$$\Delta S_i^{cr} = D_i^{cr}\,\Delta e_i^{cr} \quad \Longrightarrow \quad \begin{Bmatrix} \Delta S_{nn}^{cr} \\ \Delta S_{ns}^{cr} \end{Bmatrix}_i = \begin{bmatrix} D_i^{I} & 0 \\ 0 & D_i^{II} \end{bmatrix} \begin{Bmatrix} \Delta e_{nn}^{cr} \\ \Delta \gamma_{ns}^{cr} \end{Bmatrix}_i \tag{3.25}$$

Where D_i^I is the mode I stiffness, which will be discussed in the next section, Section 3.4.

$D_i^{II} = \dfrac{\beta}{1-\beta} G$ is the mode II stiffness, which will be discussed in the Section 3.5.

$N = \left[N_1 \, N_2 \cdots \right]$ is the overall transformation matrix composed of all the transformation matrices (equation 3.26) of each individual crack at a point.

The transformation matrix of an individual crack (i) reduces to a 3 x 2 matrix from equation (3.9) as follows:

$$N_i = \begin{bmatrix} l_1^2 & l_1 l_2 \\ m_1^2 & m_1 m_2 \\ 2l_1 m_1 & l_1 m_2 + l_2 m_1 \end{bmatrix}_i = \begin{bmatrix} \cos^2\theta_i & -\cos\theta_i \sin\theta_i \\ \sin^2\theta_i & \cos\theta_i \sin\theta_i \\ 2\cos\theta_i \sin\theta_i & \cos^2\theta_i - \sin^2\theta_i \end{bmatrix} \tag{3.26}$$

Where θ_i is the angle between the normal of a crack (i) and the global x-axis shown in Figure 3.1.

3.3.2 Plane strain application used in this research

For the plane strain analysis in equation (3.22), we have:

$$D^{co} = \frac{E}{(1+\nu)(1-2\nu)} \begin{bmatrix} 1-\nu & \nu & 0 & 0 \\ \nu & 1-\nu & 0 & 0 \\ \nu & \nu & 0 & 0 \\ 0 & 0 & 0 & \frac{1-2\nu}{2} \end{bmatrix} \tag{3.27}$$

$$D^{cr} = \begin{bmatrix} D_1^{cr} & 0 & \cdots \\ 0 & D_2^{cr} & \cdots \\ \cdots & \cdots & \cdots \end{bmatrix} \tag{3.28}$$

$$\Delta S_i^{cr} = D_i^{cr} \, \Delta e_i^{cr} \quad \Longrightarrow \quad \begin{Bmatrix} \Delta S_{nn}^{cr} \\ \Delta S_{ns}^{cr} \end{Bmatrix}_i = \begin{bmatrix} D_i^{I} & 0 \\ 0 & D_i^{II} \end{bmatrix} \begin{Bmatrix} \Delta e_{nn}^{cr} \\ \Delta \gamma_{ns}^{cr} \end{Bmatrix}_i \tag{3.29}$$

Where D_i^I is the mode I stiffness, which will be discussed in the next section, Section 3.4.

$D_i^{II} = \dfrac{\beta}{1-\beta} G$ is the mode II stiffness, which will be discussed in Section 3.5.

Equation (3.28) is the same as equation (3.24), and equation (3.29) is the same as equation (3.25).

$N = \left[N_1 \, N_2 \cdots \right]$ is the transformation matrix composed of all the transformation matrices (equation 3.30) of each individual crack at a point.

The transformation matrix of an individual crack (i) reduces to a 4 x 2 matrix from equation (3.9) as follows:

$$N_i = \begin{bmatrix} l_1^2 & l_1 l_2 \\ m_1^2 & m_1 m_2 \\ n_1^2 & n_1 n_2 \\ 2l_1 m_1 & l_1 m_2 + l_2 m_1 \end{bmatrix}_i = \begin{bmatrix} \cos^2\theta_i & -\cos\theta_i \sin\theta_i \\ \sin^2\theta_i & \cos\theta_i \sin\theta_i \\ 0 & 0 \\ 2\cos\theta_i \sin\theta_i & \cos^2\theta_i - \sin^2\theta_i \end{bmatrix} \tag{3.30}$$

3.4 Mode I tensile softening

In equation (3.22), the constitutive matrix of the local crack at a Gauss point is composed of all the individual cracks at that point. For any one crack (i) at that point, the mode I stiffness of the crack, D_i^I, is dependent on the fracture energy G_f of the material, which is defined as the energy dissipation for a unit area of a mode I (tension) crack plane propagation, the shape of the tensile softening diagram, the direct tensile strength f_t and the crack blunt width h_c. The fracture energy G_f and the direct tensile strength f_t are taken as fixed material properties for a specific concrete. The crack blunt width h_c will be discussed later in Section 3.7. The shape of the crack softening diagram for mode I fracturing of concrete would significantly change the values of the mode I softening modulus and is still a much-debated matter. The mode I softening diagram could take

various forms. Linear, bilinear and non-linear curves have been adopted in past and current analyses of the cracking of concrete structures (refer to Figure 3.4).

Linear strain softening (see for example Figure 3.5) has been widely adopted in the fracture analysis of concrete structures, in particular for concrete dams. The mode I stiffness modulus of a local crack is defined as follows:

$$D_{i,l}^{I} = \frac{EE_s}{E - E_s} = -\frac{f_t^2 h_c}{2G_f} \tag{3.31}$$

Where E_s is the strain-softening modulus shown in Figure 3.5. In Figures 3.5 and 3.6, e_n is the normal strain of cracked concrete in a local coordinate system (sum of the normal strains of the concrete between cracks and of the cracks themselves). S_n^{cr} is the normal stress in the local crack. e_{nn}^{cr} is the normal strain in the local crack. e_n^f is the ultimate normal crack strain, after which tensile stress vanishes.

Various experimental studies have revealed that concrete actually fractures in a non-linear softening format, where an exponential softening curve best fits the experimental data as done by Cornelissen, Hordijk & Reinhardt (1986). However, since a non-linear softening curve is normally difficult to implement in the analysis, it is not considered justified at this stage for practising engineers to use this non-linear softening approach. A bilinear softening strategy is adopted in this research to approximate the real softening curve by adjusting the values of the two shape parameters α_1 and α_2 (refer to Figure 3.6), while maintaining simplicity of implementation.

For the purpose of this research, the following bilinear strain-softening equations were developed:

$$G_f = -\frac{h_c}{2}\left[\frac{(\alpha_1 f_t + f_t)(1-\alpha_1) f_t}{D_{i,bl}^{I}} + \frac{\alpha_1^2 f_t^2}{\alpha_2 D_{i,bl}^{I}}\right] = -\frac{f_t^2 h_c}{2}\left[\frac{\alpha_2 + (1-\alpha_2)\alpha_1^2}{\alpha_2 D_{i,bl}^{I}}\right] \tag{3.32}$$

$$D_{i,bl}^{I} = \frac{\alpha_2 + (1-\alpha_2)\alpha_1^2}{\alpha_2}\left(-\frac{f_t^2 h_c}{2G_f}\right) = \frac{\alpha_2 + (1-\alpha_2)\alpha_1^2}{\alpha_2} D_{i,l}^{I} \tag{3.33}$$

Where α_1 and α_2 are bilinear softening shape parameters. α_1 is defined as the portion of the tensile strength below which the strain softening becomes flattened (the mode I softening modulus uses the second slope line of softening). α_2 is defined as the ratio of the second softening modulus to the first softening modulus.

$D_{i,bl}^{I}$ is the first mode I softening modulus in the bilinear softening diagram (refer to Figure 3.6), which is controlled by the shape parameters of the softening diagram (α_1 and α_2), the fracture energy G_f, the direct tensile strength f_t and the crack blunt width of the finite elements h_c.

When $\alpha_1 = 0$, $D_{i,bl}^{I} = D_{i,l}^{I}$, the strain softening becomes linear

When $\alpha_2 = 1$, $D_{i,bl}^{I} = D_{i,l}^{I}$, the strain softening becomes linear.

Figure 3.7 shows how the shapes of the bilinear diagram are changed and their relationship with the linear mode I softening modulus $D_{i,l}^{I}$ if α_1 is fixed at 1/3 while α_2 is taken as 0.1, 0.2 and 0.3 respectively.

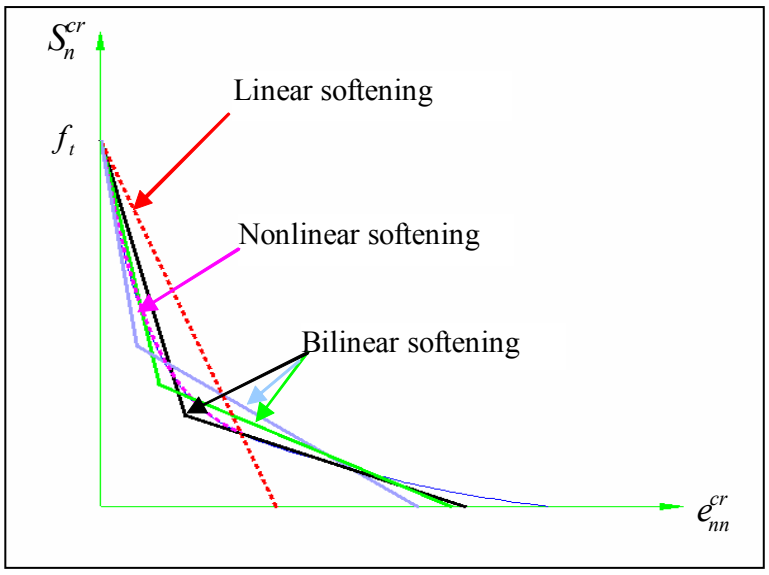

Figure 3.4 - Linear, bilinear and curved mode I strain-softening diagram of "crack"

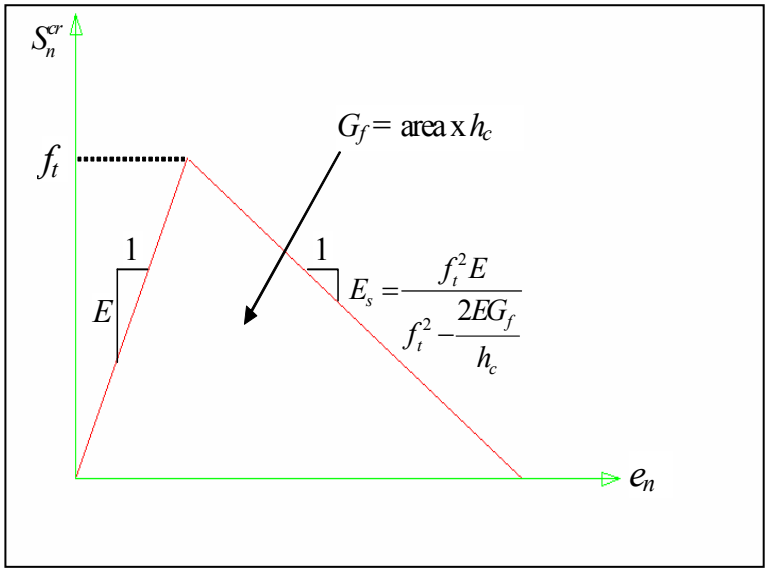

Figure 3.5 - Linear elastic – mode I strain-softening diagram of cracked concrete

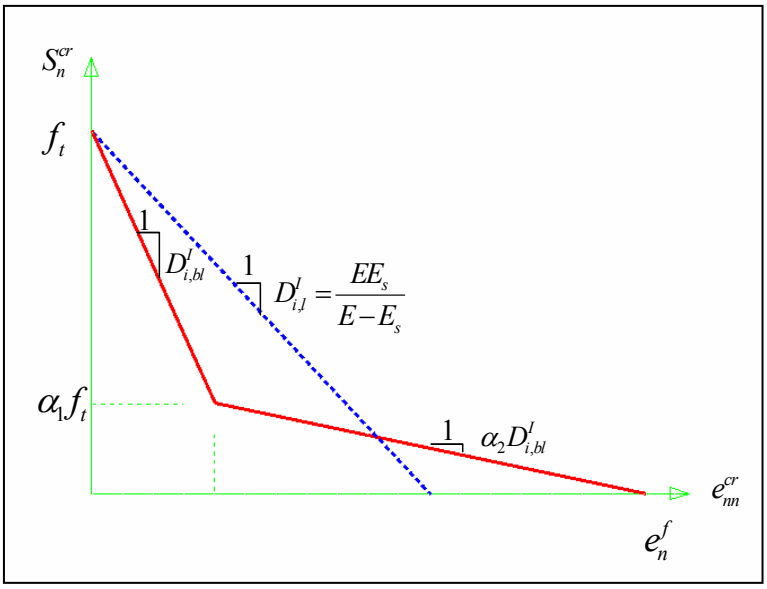

Figure 3.6 - Definition of bilinear mode I strain-softening diagram of “crack”

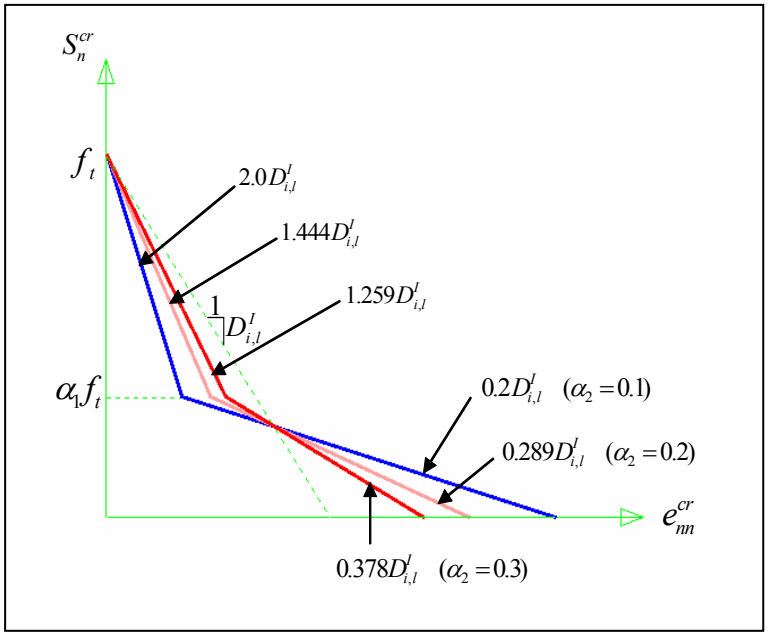

Figure 3.7 - Bilinear mode I strain-softening diagrams for α_1 = 1/3; α_2 = 0.1, 0.2 and 0.3 (local coordinate)

3.5 Mode II shear softening

Due to aggregate interlock in plain concrete, the shear modulus does not reduce to zero immediately after cracking. Therefore, shear stress can be developed on the plane of a crack at subsequent loading. In the past, a simple non-zero shear retention factor β was adopted to represent shear softening in modelling concrete cracking (Bhattacharjee & Leger 1993; Lotfi & Espandar 2004). However, this method ignores the shear dilation and the dependence of crack shear on the crack opening displacement. This also results in a constant cracking shear modulus that cannot take into account the fact that the shear strain varies with the normal crack strain, as observed in experimental studies. For this research, the shear stiffness of a crack is defined as a decreasing function of the crack normal strain in the following formula (equation 3.34), which is similar to that used by Rots & Blaauwendraad (1989), except for a maximum shear retention factor β_{max} defined here to limit the maximum shear allowed in a crack. The value of β_{max} usually varies from 0 to 0.5. A high shear retention value (β close to 0.5) could cause extensive cracking in certain applications, while zero retention (β = 0) could result in numerical instabilities (Lotfi & Espandar 2004).

$$\beta = \beta_{\max} (1 - \frac{e_{nn}^{cr}}{e_n^f})^p \tag{3.34}$$

Where e_{nn}^{cr} and e_n^f have been defined previously and p is a constant defining the shear-softening shape. As shown in Figure 3.8, if p=0, $\beta = \beta_{\max}$ (constant); if p=1, shear softening is in a descending linear format; if p=2, shear softening is in a descending non-linear format.

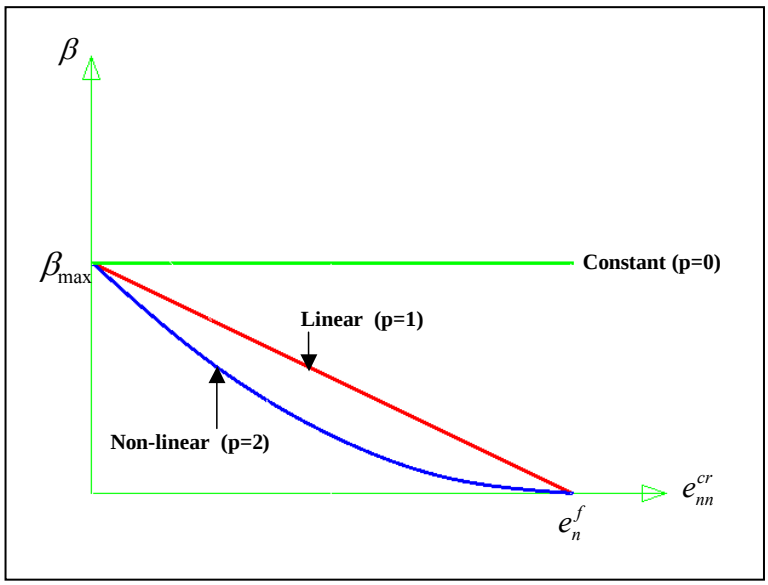

Figure 3.8 - Relationship between shear retention factor and "crack" strain (local coordinate)

3.6 Fixed/rotating, unloading/reloading and closing/reopening of cracks

As stated previously, the direction of cracking is generally aligned perpendicular to the principal stress direction and is fixed after the crack has been initiated in the fixed non-orthogonal crack model. Each fixed crack is "remembered" with its own direction and is kept unaltered for the rest of analysis. This permanent "memory" of crack directions increases the cost of computation.

After cracking, the shear stresses would cause the principal stress axes to rotate, which could increase the tensile principal stresses well above the concrete tensile strength. In this

research, a new crack is initiated whenever the angle between the normal to the crack plane of the last crack and the current principal stress direction exceeds a pre-defined threshold angle or whenever the inclined tensile principal stress σ_1 violates the crack onset criterion. The reason why the above new crack initiation criterion is adopted will now be explained.

If only the stress criterion applies (i.e. if the maximum tensile principal stress exceeds the material's tensile strength), then the total number of cracks cannot be limited. For example, if high shear stress remains in a crack, a new crack could be initiated with almost every loading increment, which would render the analysis inefficient. On the other hand, the threshold angle condition (i.e. when the angle between the principal stress and the last existing crack exceeds a threshold angle) does not control the maximum tensile stress. A tensile principal stress three times higher than the tensile strength could occur without violating the threshold angle condition (Rots & Blaauwendraad 1989). Only if these two conditions are combined can a reasonable new crack initiation criterion be established.

Depending on the magnitude of the pre-defined threshold angle, many cracks could occur at a Gauss point. For the purpose of limiting the computing memory required and making the multi-directional crack model more robust, a maximum of six cracks are allowed to form at a Gauss point. The effect of each additional crack on the results becomes progressively and significantly less as the number of cracks at a point increases.

Concrete structures are normally subjected to both tension and shear stress conditions. The mixed-mode fracturing behaviour leads to the rotation of the axes of principal stress after a crack is formed. Consequently, the fixed crack axes no longer represent the axes of principal stress. The fixed, multi-directional, non-orthogonal crack model adopted here is able partially to reduce the misalignment between the crack orientation and the principal direction.

Alternatively, a rotating approach can be used in which the normal axis to the crack plane is allowed to co-rotate with the principal stress axis. A rotating crack concept, in which the axes of a crack co-rotate with the orientation of the principal stress, has been proposed

in the past to eliminate the discrepancy between and the misalignment of the crack directions and principal directions.

Rots & Blaauwendraad (1989) proposed a rotating crack model by simply vanishing the threshold angle and making all previous cracks inactive, erasing them from memory. In this way, the crack orientation changes continuously to align with the direction of principal stress. The following three conditions were set for the rotating model by Rots & Blaauwendraad (1989):

- The orientation of subsequent cracks is only controlled by setting the threshold angle to zero.
- Only the current crack is allowed to remain active, by erasing all previous cracks at the Gauss point.
- The influence of previous cracks is accounted for and the mode II shear-softening modulus D^{II} in the following equation (3.36) is used to ensure coaxiality.

In order to enforce coaxiality between the principal stress and strain, the softening shear modulus for a 2-D analysis should be calculated as follows:

$$\beta G = \frac{\sigma_1 - \sigma_2}{2(\varepsilon_1 - \varepsilon_2)} \tag{3.35}$$

$$\frac{1}{\beta G} = \frac{1}{G} + \frac{1}{D^{II}} \quad \Rightarrow \quad D^{II} = \frac{\sigma_1 - \sigma_2}{2(\varepsilon_1 - \varepsilon_2)G - (\sigma_1 - \sigma_2)} \tag{3.36}$$

The proposed fixed, multi-directional, non-orthogonal crack model can be converted into a rotating model by applying the above-mentioned conditions for the rotating crack approach.

The post-fracturing behaviour forms an important part of the crack constitutive model. The unloading/reloading and closing/reopening strategy used is shown in Figures 3.9 and 3.10. A secant unloading approach is adopted in this study, which implies that the crack stress-strain relationship follows a path back to the origin upon a strain reduction. This

strategy is often used by researchers since it yields a closer approximation to the real unloading behaviour of concrete for application in smeared based crack models than the elastic unloading approach used in the past, in which the crack closes immediately during a strain reduction (Calayir & Karaton 2005; Rots 2002; Cervera *et al*. 1990).

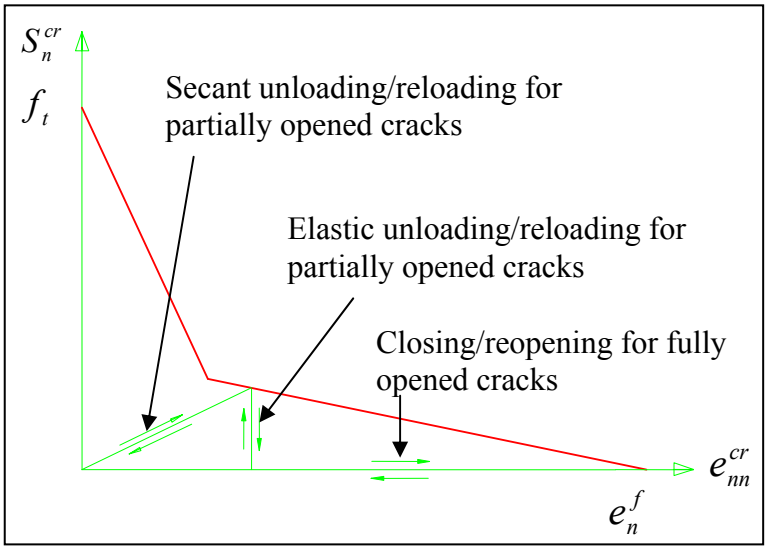

Figure 3.9 - Diagram of unloading/reloading and closing/reopening (in crack strain)

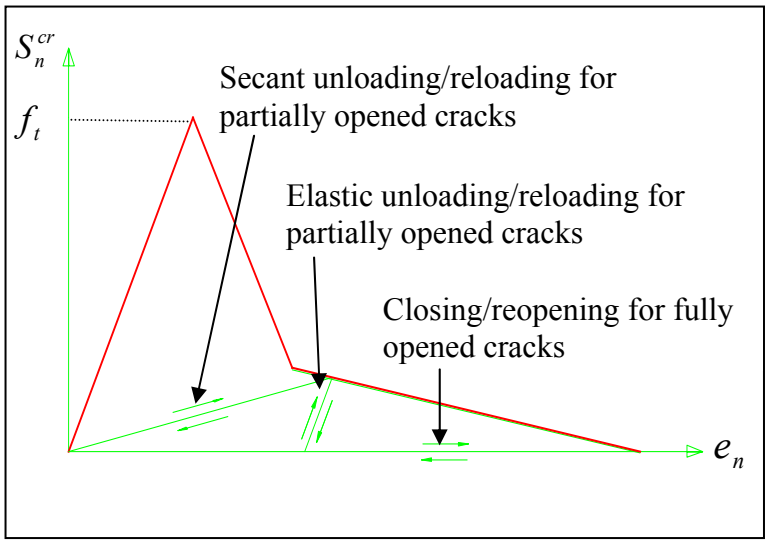

Figure 3.10 - Diagram of unloading/reloading and closing/reopening (in total strain)

3.7 Width of crack blunt front and mesh objectivity

In the smeared crack approach, a crack in an element is formed and propagated over an area related to the size of the element. The characteristic length of the crack band in smeared modelling must be defined in order to obtain mesh objectivity. The fracture process is assumed to occur in bands of micro-defects over a so-called *crack band width*. Gajer & Dux (1990) treated the width of the crack band as a material property, which should be three to ten times the maximum aggregate size.

Bhattacharjee & Leger (1992) distinguished between the characteristic length h_c in non-linear fracture mechanics models and the width of the crack band w_c in the crack band model (Bažant & Oh 1983). Unlike the crack band width w_c, the characteristic dimension h_c is a geometric property of the cracking element (refer to Figures 2.6 and 2.7 in Chapter II for illustrations of w_c and h_c).

The introduction of a characteristic length h_c into the determination of the mode I softening modulus is a step towards a non-local softening model for mesh objectivity.

The following definition of the crack characteristic length h_c has been proposed by researchers in the past:

- $h_c = \sqrt{Area\ of\ element}$; i.e. square root of the area of the cracking element for a 2-D application (Bhattacharjee & Leger 1992) or
- h_c = size of the cracking element, across the direction of crack propagation (Bhattacharjee & Leger 1992).
- h_c is taken as the side of an equivalent cube having the same volume as the tributary volume at the cracked point of a solid isoparametric element for a 3-D application (Lotfi & Espandar 2004).
- $h_c = \sqrt{2} \times size\ of\ the\ cracking\ element$ (Rots & Blaauwendraad 1989).

A more rigorous description of h_c, which is dependent on the mesh size, crack direction and spatial position, can be found in the paper by Oliver (1989).

In this research, the response quantities of elements were computed at each integration point of the elements. Thus, the size adjustment of the strain-softening modulus E_s (refer to Figure 3.5) and the fracture energy dissipation are determined on the basis of local response quantities. The crack characteristic length h_c is defined as the size of the element across the crack direction if the finite element mesh is oriented to be parallel to the crack band (Figure 3.11(a)). If a crack is propagating obliquely through an element, as shown in Figure 3.11(b), then h_c is defined as the square root of the element area.

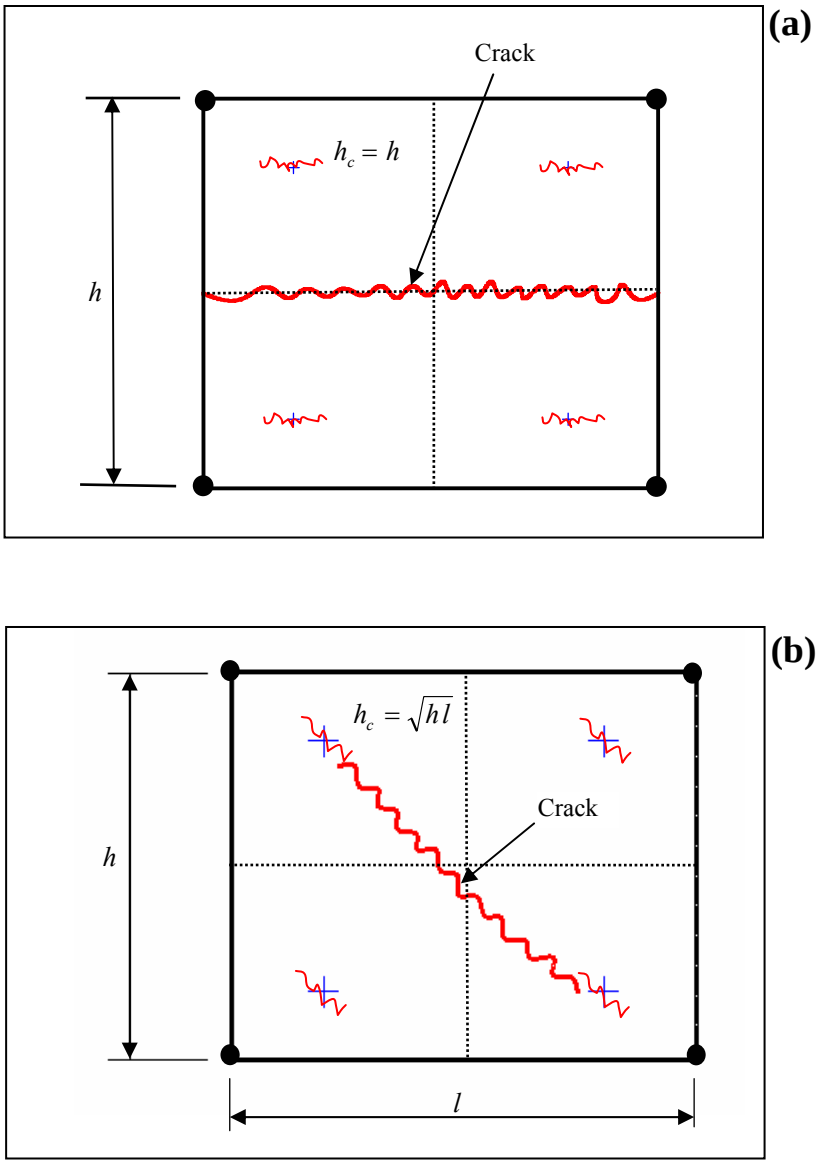

Figure 3.11 - Crack characteristic length h_c of a quadrilateral element (first order with full integration)

3.8 Element selection for crack analysis

The application of reduced integration is less reliable than the normal integration element. It could induce a spurious hour-glass mode, which could easily cause divergence of the iterative procedure. Dodds, Darwin, Smith & Leibengood (1982) investigated the hour-glassing problems and suggested that reduced integration elements should not be used. In this research, first-order elements with full integration have been selected for the analysis of concrete cracking, as used by many researchers in the past (Bhattacharjee & Leger 1993; Bhattacharjee & Leger 1994; Rots & Blaauwendraad 1989). Second-order elements can also be used for the proposed smeared crack model if needed.

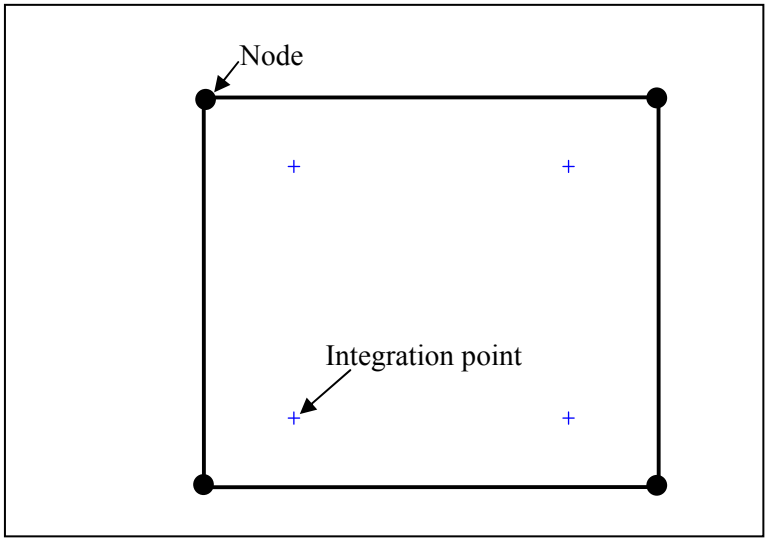

Figure 3.12 - Quadrilateral element of first order with full integration used in the research

3.9 Concluding remarks

The constitutive crack model adopted for the smeared crack analysis of concrete structures in this research has been presented. The crack initiation criterion and direction were described first. An enhanced mode I and II strain-softening strategy has been developed for this research. The conditions for subsequent new crack(s) to occur after the initial cracking have been established. Fixed or rotating cracks, a definition of crack closing and reopening, the crack mechanism for unloading and reloading, etc. have also been described. A bilinear mode I strain-softening formula has been given. The crack characteristic length h_c and the element type selected for this research have been defined.

The constitutive crack model proposed in this chapter will be fully implemented in an FE program in Chapter IV.

CHAPTER IV - NUMERICAL TECHNIQUE AND PROGRAM FOR FINITE ELEMENT CONSTITUTIVE CRACKING ANALYSIS

The main purpose of this chapter is to develop a sub-program which is to be incorporated into the commercial general-purpose finite element (FE) program – MSC.Marc – and to test the sub-program using elementary, simple specimens of both plane stress and plane strain elements. The sub-program should have the capacity to simulate the cracking process in concrete, using the adopted constitutive relationships of crack softening outlined in Chapter III.

Very few general-purpose commercial FE packages can accommodate the non-linear cracking analysis of concrete structures. MSC.Marc is an FE program which can model concrete cracking with linear post-peak strain softening and a constant shear retention factor β. Bilinear or non-linear strain softening, and arbitrary crack-opening-dependent reduced shear modulus in the constitutive modelling of concrete cracking are not available in this program. However, MSC.Marc allows users to develop and substitute their own sub-programs in the package. This feature provides users with a powerful way of solving non-standard problems, such as crack simulation in concrete. The program was available for the author to use for this research.

The FE method basically has six steps. The success of any FE program depends partly on how the program implements these steps. A description of the FE method (including the following six steps) and the algorithm used in MSC.Marc is given in the Annexure.

Step 1: Choose shape functions
Step 2: Establish material relationship
Step 3: Compile element matrices
Step 4: Assemble to form the overall structural stiffness matrix
Step 5: Solve equations
Step 6: Recover the stresses and strains.

4.1 Program framework for the cracking analysis of concrete

4.1.1 Framework for the implementation of the constitutive model in the FE analysis of concrete structures

The flow chart shown in Figure 4.1 illustrates the general FE procedure for the crack analysis of concrete structures.

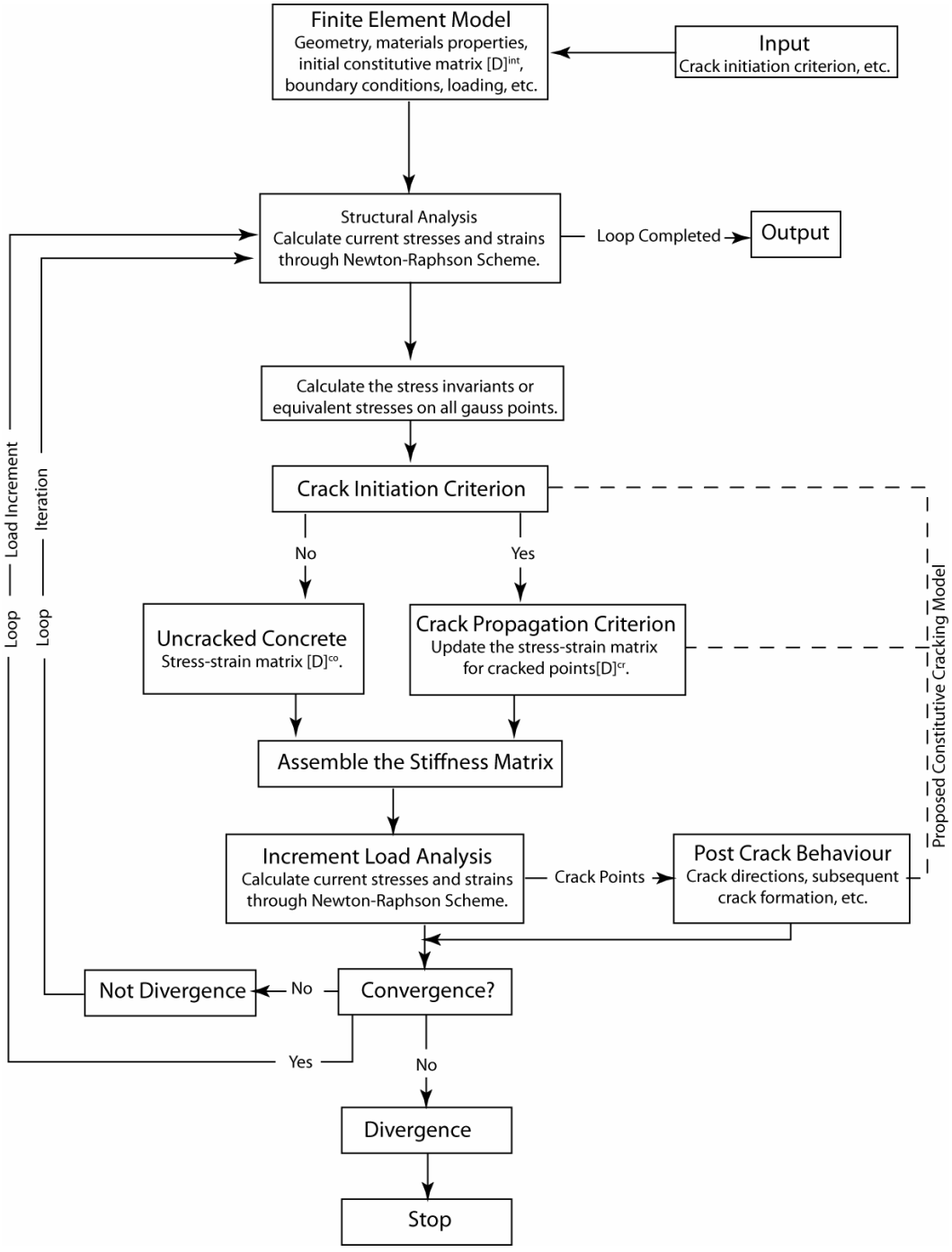

Figure 4.1 - General FE crack analysis procedure for concrete structures

4.1.2 Sub-program coded in MSC.Marc to implement the crack constitutive model

Modelling bilinear or non-linear mode I and II softening requires the development and programming of a subroutine in MSC.Marc. The lack of advanced fracture-modelling capacity in this FE package (and in other generally available FE packages) requires a considerable programming effort to implement crack modelling.

A subprogram called HYPELA, incorporated into MSC.Marc, was specially and independently developed for this research on the FE modelling of the cracking behaviour of concrete structures. The subroutine has the capacity to simulate the cracking process in concrete, using the adopted constitutive relationships of crack softening outlined in Chapter III.

The cracking analysis starts with the linear elastic stress-strain law. In the subprogram HYPELA, the following steps are performed (refer to Figure 4.2 for the flowchart of these steps):

Step 1: Material properties and parameters related to concrete strain softening, such as the fracture energy G_f, Young's modulus E, Poisson's ratio v, tensile strength f_t, mode I softening parameters (α_1 / α_2), maximum mode II shear reduced factor β_{max}, etc. are input for a specific crack analysis application.

Step 2: The utility routine ELMVAR is called to retrieve element data (e.g. stresses σ_{ij}, strains ε_{ij}) from the MSC.Marc program's internal data storage. ELMVAR is provided with the following information: element post code (icode); element number (m); integration point number (nn); layer number (kc) and requested variables (var).

Step 3: A further subroutine – STRM –was specially coded for this research to be called in the subprogram HYPELA in order to calculate the principal stresses and their direction cosines from the stress tensor $\sigma_{ij} = \begin{bmatrix} \sigma_{11} & \sigma_{12} & \sigma_{13} \\ \sigma_{21} & \sigma_{22} & \sigma_{23} \\ \sigma_{31} & \sigma_{32} & \sigma_{33} \end{bmatrix}$ retrieved by ELMVAR at any Gauss point.

In the subroutine STRM, the principal stresses and direction cosines at a Gauss point are calculated as follows (refer to Chen 1982):

- Calculate the first invariant of the stress tensor: $I_1 = \sigma_{11} + \sigma_{22} + \sigma_{33}$ (4.1)

- Calculate the mean normal stress: $\sigma_m = \frac{1}{3} I_1$ (4.2)

- Obtain the stress deviator tensor $S_{ij} = \begin{bmatrix} \sigma_{11} - \sigma_m & \sigma_{12} & \sigma_{13} \\ \sigma_{21} & \sigma_{22} - \sigma_m & \sigma_{23} \\ \sigma_{31} & \sigma_{32} & \sigma_{33} - \sigma_m \end{bmatrix}$ (4.3)

- Calculate the second invariant of the stress tensor:

$$J_2 = \frac{1}{2} S_{ij} S_{ij} = \frac{1}{2}(S_{11}^2 + S_{22}^2 + S_{33}^2) + S_{12}^2 + S_{23}^2 + S_{31}^2 \quad (4.4)$$

- Calculate the third invariant of the stress tensor:

$$J_3 = \frac{1}{3} S_{ij} S_{jk} S_{ki} = S_{11} S_{22} S_{33} + 2 S_{12} S_{23} S_{31} - S_{11} S_{23}^2 - S_{22} S_{13}^2 - S_{33} S_{12}^2 \quad (4.5)$$

- Calculate $\cos 3\theta = \frac{3\sqrt{3}}{2} \frac{J_3}{\sqrt{J_2^3}}$ (4.6)

  where θ is the angle of similarity.

- Calculate the principal stresses:

$$\begin{bmatrix} \sigma_1 \\ \sigma_2 \\ \sigma_3 \end{bmatrix} = \begin{bmatrix} S_1 \\ S_2 \\ S_3 \end{bmatrix} + \sigma_m \begin{bmatrix} 1 \\ 1 \\ 1 \end{bmatrix} = \frac{2\sqrt{J_2}}{\sqrt{3}} \begin{bmatrix} \cos\theta \\ \cos(\theta - \frac{2}{3}\pi) \\ \cos(\theta + \frac{2}{3}\pi) \end{bmatrix} + \frac{I_1}{3} \begin{bmatrix} 1 \\ 1 \\ 1 \end{bmatrix} \quad (4.7)$$

- Set $\sigma = \sigma_1$, solve $\begin{bmatrix} \sigma_{11}-\sigma_1 & \sigma_{12} & \sigma_{13} \\ \sigma_{21} & \sigma_{22}-\sigma_1 & \sigma_{23} \\ \sigma_{31} & \sigma_{32} & \sigma_{33}-\sigma_1 \end{bmatrix} \begin{bmatrix} l_1 \\ m_1 \\ n_1 \end{bmatrix} = \begin{bmatrix} 0 \\ 0 \\ 0 \end{bmatrix}$ (4.8)

  and $l_1^2 + m_1^2 + n_1^2 = 1$; (4.9)

  The Cramer method in matrix algebra is adopted to obtain the direction cosines of the first principal stress to the global coordinates l_1, m_1 and n_1.

- Similarly, set $\sigma = \sigma_2$ and $\sigma = \sigma_3$ to obtain the direction cosines of the second and third principal stresses to the global coordinates l_2, m_2, n_2 and l_3, m_3, n_3 respectively.

Step 4: Check the crack initiation criterion ($\sigma_1 \geq f_t$) for a Gauss point which has not cracked before. Also check new crack conditions for an existing crack at a Gauss point ($\sigma_1 \geq f_t$, or whether the angle between the previous crack and the present crack at a Gauss point is greater than the threshold angle). For a Gauss point that has not cracked before, if the crack initiation criterion is met, then the point is assumed to be cracking. Otherwise, the point remains linear elastic. For an existing crack point, if either of the conditions is met, then a new additional crack is assumed at that point, at an angle to the previous crack.

Step 5: For the cracking points, using the direction cosines calculated from STRM, form the transformation matrix $N = [N_1\ N_2 \cdots]$ (see equations 3.9, 3.26 and 3.30 in Chapter III for 3-D, plane stress and plane strain application respectively) and transform the strains from global coordinates to local coordinates.

Step 6: Check the status of stress and strain at the cracking points to see if the crack is still opening, or unloading/reloading, or closing (see Figures 3.9 and 3.10).

Step 7: According to the different crack statuses, define the mode I stiffness modulus D_i^I for crack opening, or crack unloading/reloading, or crack closing accordingly in

$D_i^{cr} = \begin{bmatrix} D_i^I & 0 & 0 \\ 0 & D_i^{II} & 0 \\ 0 & 0 & D_i^{III} \end{bmatrix}$ for the constitutive matrix D^{cr} (refer to equation 3.16 and Figures 3.9 and 3.10 in Chapter III). After that, form the constitutive relationship of equation 3.22**.**

Step 8: Transform the stresses and the stiffness matrix from local coordinates to global coordinates.

In the subprogram, the transformation of stresses, strains and the stiffness matrix between the global and local coordinate systems is carried out using the following equations (4.13 to 14.15):

Transformation matrix R, in which l_1, l_2, l_3, m_1, m_2, m_3, n_1, n_2, n_3 are the direction cosines of the axes defined in Tables 3-1 and 3-2 in Chapter III, is as follows:

For 3-D analysis:

$$[R]=\begin{bmatrix} l_1^2 & m_1^2 & n_1^2 & l_1m_1 & m_1n_1 & n_1l_1 \\ l_2^2 & m_2^2 & n_2^2 & l_2m_2 & m_2n_2 & n_2l_2 \\ l_3^2 & m_3^2 & n_3^2 & l_3m_3 & m_3n_3 & n_3l_3 \\ 2l_1l_2 & 2m_1m_2 & 2n_1n_2 & l_1m_2+l_2m_1 & m_1n_2+m_2n_1 & n_1l_2+n_2l_1 \\ 2l_2l_3 & 2m_2m_3 & 2n_2n_3 & l_2m_3+l_3m_2 & m_2n_3+m_3n_2 & n_2l_3+n_3l_2 \\ 2l_3l_1 & 2m_3m_1 & 2n_3n_1 & l_3m_1+l_1m_3 & m_3n_1+m_1n_3 & n_3l_1+n_1l_3 \end{bmatrix} \quad (4.10)$$

For 2-D plane stress analysis:

$$[R]=\begin{bmatrix} l_1^2 & m_1^2 & l_1m_1 \\ l_2^2 & m_2^2 & l_2m_2 \\ 2l_1l_2 & 2m_1m_2 & l_1m_2+l_2m_1 \end{bmatrix}=\begin{bmatrix} \cos^2\theta & \sin^2\theta & \cos\theta\sin\theta \\ \sin^2\theta & \cos^2\theta & -\cos\theta\sin\theta \\ -2\cos\theta\sin\theta & 2\cos\theta\sin\theta & \cos^2\theta-\sin^2\theta \end{bmatrix} \quad (4.11)$$

For 2-D plane strain analysis:

$$[R]=\begin{bmatrix} l_1^2 & m_1^2 & n_1^2 & l_1m_1 \\ l_2^2 & m_2^2 & n_2^2 & l_2m_2 \\ l_3^2 & m_3^2 & n_3^2 & l_3m_3 \\ 2l_1l_2 & 2m_1m_2 & 2n_1n_2 & l_1m_2+l_2m_1 \end{bmatrix}=\begin{bmatrix} \cos^2\theta & \sin^2\theta & 0 & \cos\theta\sin\theta \\ \sin^2\theta & \cos^2\theta & 0 & -\cos\theta\sin\theta \\ 0 & 0 & 1 & 0 \\ -2\cos\theta\sin\theta & 2\cos\theta\sin\theta & 0 & \cos^2\theta-\sin^2\theta \end{bmatrix} \quad (4.12)$$

$$\{\varepsilon'\}=[R]\{\varepsilon\}; \qquad \{\varepsilon\}=[R]^{-1}\{\varepsilon'\} \quad (4.13)$$

$$\{\sigma'\}=[R]^{-T}\{\sigma\}; \qquad \{\sigma\}=[R]^{T}\{\sigma'\} \quad (4.14)$$

$$[K']=[R]^{-T}[K][R]^{-1}; \quad [K]=[R]^{T}[K'][R] \quad (4.15)$$

Where $\{\varepsilon'\}$is the local strain vector; $\{\varepsilon\}$is the global strain vector

$\{\sigma'\}$is the local stress vector; $\{\sigma\}$is the global stress vector

$[K']$is the local constitutive matrix; $[K]$is the global constitutive matrix.

Step 9: Return to the main program – MSC.Marc.

The HYPELA subprogram developed has the overall organization for the coding process as shown in Figure 4.2.

4.1.3 Possible numerical implementation problems

In the implementation of the constitutive model, concrete fracture modelling problems could be encountered, such as snap-back, non-convergence or hour-glass modes.

'Snap-back' behaviour (in which the deflection response decreases after peak-point loading) could occur in the strain-softening analysis of concrete structures (Rots & de Borst 1987). Normal direct displacement control, installed in general FE programs, was demonstrated as being inadequate in modelling this "dramatic" behaviour to get a fully converged solution after peak load (de Borst 1986). An indirect displacement control technique, developed by de Borst (1986) for snap-back behaviour, has proved to be successful. However, this technique could not be implemented in MSC.Marc due to the

limitations of the package. In general, the limitations of FE packages require a special solution strategy to solve snap-back problems. The implementation of such a solution strategy is demonstrated in verification case 2 in Chapter V.

Non-convergence is a problem frequently encountered in highly non-linear analyses. The computation process is terminated at the stage where numerical difficulties, which can be caused by many factors (such as an ill-conditioned stiffness matrix or unstable crack propagation) cannot be overcome.

A further potential problem in modelling the cracking of concrete is 'hour-glass' modes, which have been reported by several researchers (de Borst 1986; Rots & de Borst 1987). These are spurious zero-energy modes that could cause non-convergence by developing a singular, or nearly singular, global stiffness matrix. They are often encountered when using reduced integration, although full-integration elements are not free from this phenomenon. Mixed-mode softening (normal and shear softening) and multiple crack simulation are potential factors that could trigger hour-glass modes.

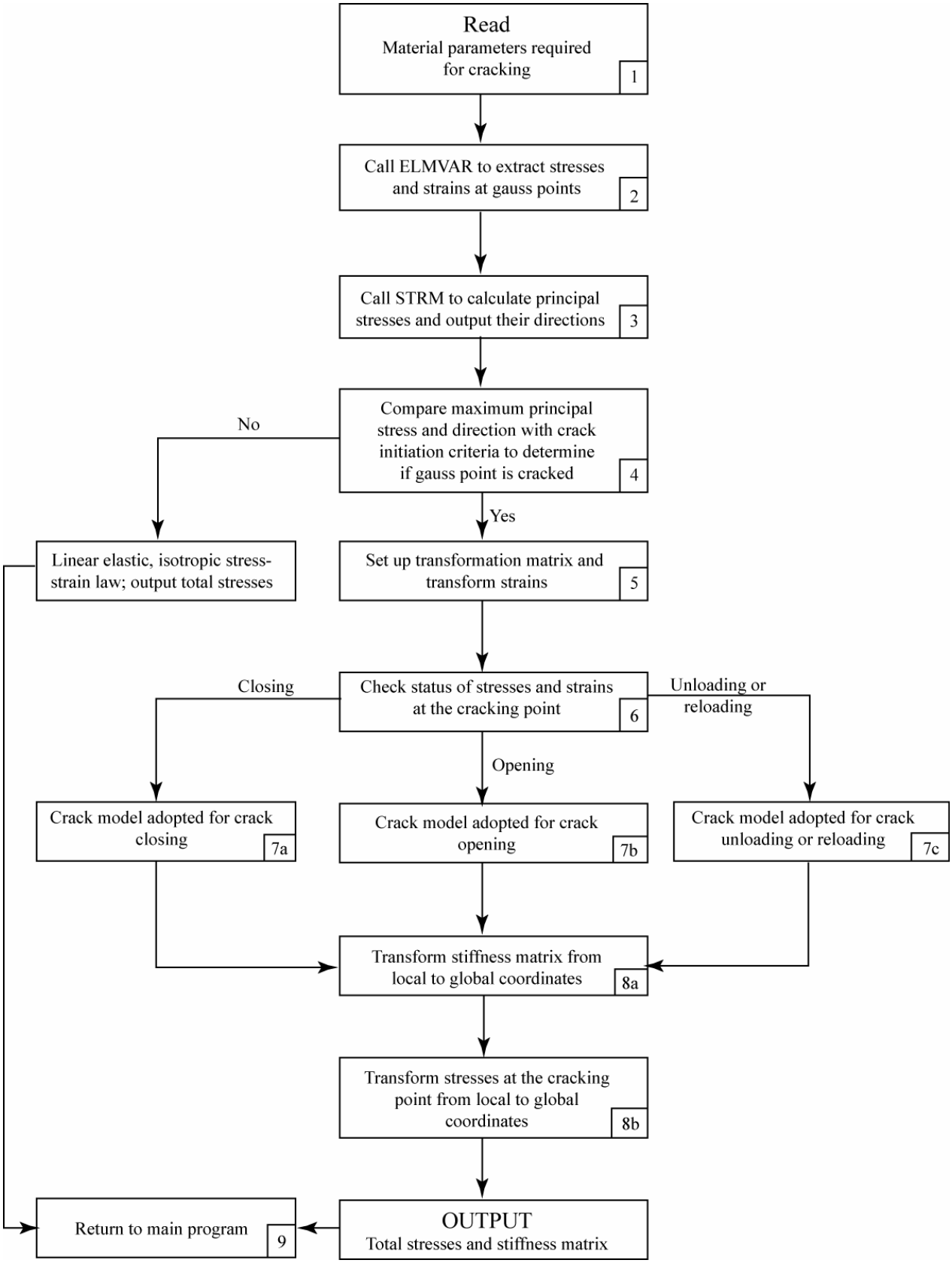

Figure 4.2 - Flow chart of the overall organization for coding the sub-program HYPELA

To save computer time, two groups of elements could be defined in the FE model: (1) elements that are not allowed to crack for the region where cracking under the given loadings is unlikely; and (2) elements which could possibly crack. The elements that could crack are called by the subprogram HYPELA, developed as explained above. The elements that are defined as not cracking are run as normal in MSC.Marc. The flow diagram in Figure 4.3 illustrates the implementation position of the subprogram HYPELA in the FE process of MSC.Marc.

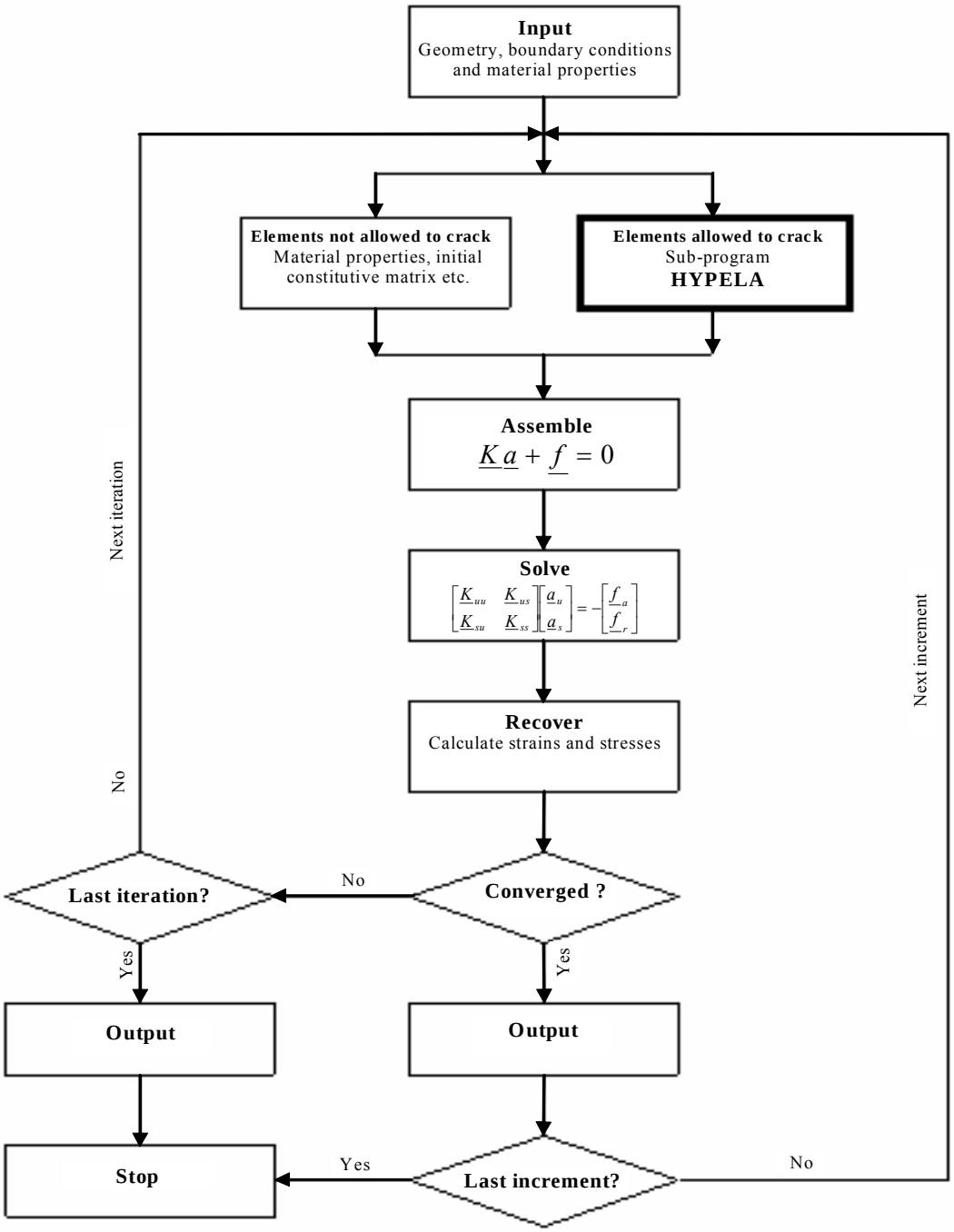

Figure 4.3 - Flow diagram for finite element analysis process in MSC.Marc

4.2 Verification study with MSC.Marc and other specimens investigated in the past

For the purpose of verifying the general application of the subroutine developed, it is logical to test the subroutine thoroughly on specimens that are fracture-sensitive.

Prior to cracking, concrete is assumed to be linear elastic and isotropic until the maximum principal stress exceeds the material's tensile strength. When this strength-based crack-initiating criterion is violated, cracks form in the direction perpendicular to the maximum principal stress. The strain-softening process starts at those Gauss points by moderating the isotropic, linear elastic stress-strain stiffness matrix to the adopted cracking stress-strain laws that have been selected for this testing purpose.

Four cases – called specimens 1, 2, 3 and 4 using plane stress elements, are verified in this section.

4.2.1 Built-in crack model in MSC.Marc for specimens 1 and 2 (with reference to MSC.Marc *Volume A: Theory and User Information*)

MSC.Marc has a built-in cracking model that can be used to handle concrete and other low-tension material. The model can predict crack initiation and simulate tension softening, plastic yielding and crushing. The cracking model is built on the uniaxial stress-strain diagram shown in Figure 4.4.

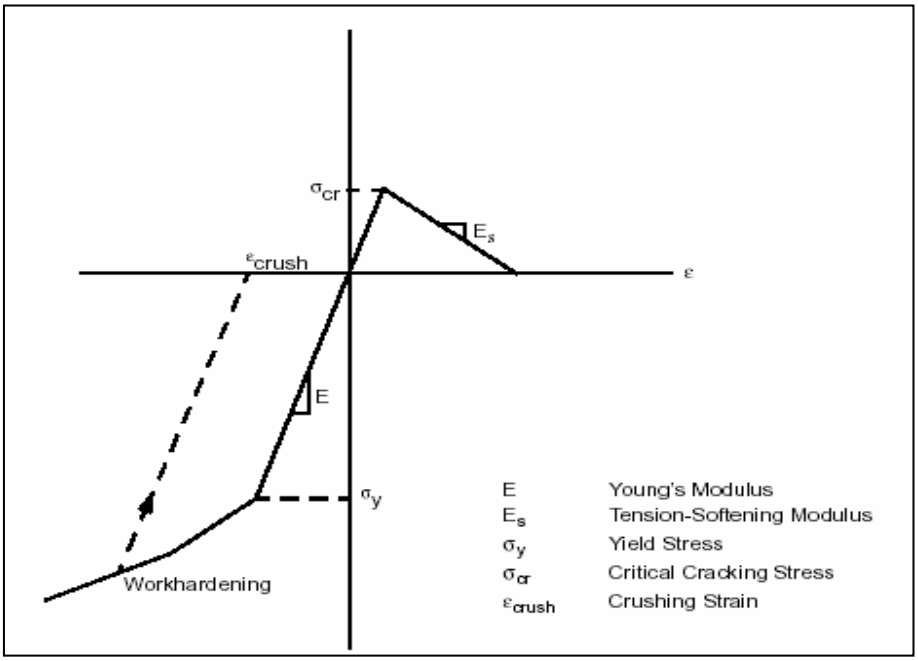

Figure 4.4 - Uniaxial stress-strain diagram

In this model, a crack develops in a material perpendicular to the direction of the maximum principal stress if the maximum principal stress σ_1 in the material exceeds a certain value σ_{cr} (see Figure 4.4 and Figure 3.1 in Chapter III). Linear tension softening, characterized by a descending branch as shown Figure 4.4, is then adopted. The shear modulus across the crack is reduced by a constant shear retention factor. This model is by nature an orthotropic model, similar to the mode I and II improved Rashid model (smeared model 3 in Chapter II). At a material point, a second crack can only form perpendicular to the first crack.

An opened crack can close again if the loading is reversed. If crack closing occurs, it is assumed that the crack has the capability to carry full compressive stress.

4.2.2 The smeared model adopted for specimens 1 and 2

In Chapter II, all the major crack models are reviewed and elaborated on. The crack model adopted for this verification purpose is briefly as follows:

Verification crack model (refer to smeared model 3 in Chapter II for a description of the mode). This model is used for verification purposes mainly for two reasons:

1. It is similar to the built-in crack model in MSC.Marc and can be used to validate the subprogram by comparing the results from the two methods.

2. It has the general capacity to model mode I and II fracturing in concrete.

4.2.3 The smeared crack model adopted for specimens 3 and 4

The non-orthogonal, multi-directional crack models outlined in Chapter III that are implemented in the subprogram HYPELA are used to verify specimens 3 and 4 in this section.

4.2.4 FE models benchmarked

Four test specimens are designed or selected for the verification exercise. Due to the fact that the built-in crack model in MSC.Marc can only handle linear mode I softening and a constant shear retention factor β to account for the loss of shear modulus after cracks, only the elementary simple-tension specimens (specimens 1 and 2) are believed to be adequate for the verification of the subprogram in the application of basic NLFM analysis. The results obtained from the subprogram are compared with the related results from either the built-in elastic, linear softening crack model in MSC.Marc or those from past investigations.

Description of the element type and solution method used for the verification

For this verification, a four-node quadrilateral isoparametric element with bilinear interpolation is adopted. A full 2 x 2 Gauss integration (four integration points) rule is used for the computation of the element stiffness matrix (see Figure 4.5). All the specimens used for verification purposes in this section are modelled as plane stress elements.

Each node in the element has two degrees of freedom (U_x, U_y), which results in a total of eight degrees of freedom in one single element.

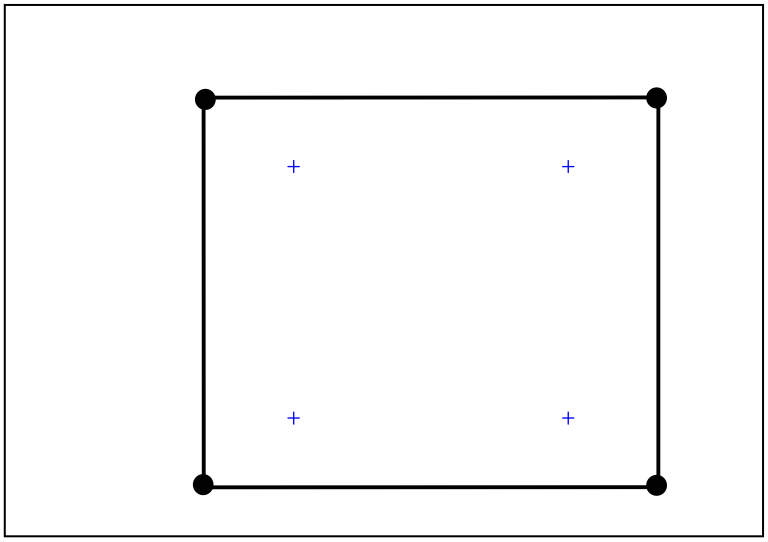

Figure 4.5 - First-order plane stress element with full integration

The element is formed by mapping from the x-y plane to the ξ, η plane. Both the mapping and the assumed displacement function take the form:

$$x = a_0 + a_1 \xi + a_2 \eta + a_3 \xi \eta \tag{4.16}$$

$$y = b_0 + b_1 \xi + b_2 \eta + b_3 \xi \eta \tag{4.17}$$

Either the coordinate or the displacement function can be expressed in terms of the nodal quantities by the interpolation functions.

$$x = \sum_{i=1}^{4} x_i \phi_i \tag{4.18}$$

Where

$$\phi_1 = \frac{1}{4}(1-\xi)(1-\eta)$$

$$\phi_2 = \frac{1}{4}(1+\xi)(1-\eta)$$

$$\phi_3 = \frac{1}{4}(1+\xi)(1+\eta)$$

$$\phi_4 = \frac{1}{4}(1-\xi)(1+\eta)$$

The full Newton-Raphson method is adopted for the solution of the stiffness formulation.

An adapted stepping procedure is adopted to automatically adjust the step time in the increment.

Convergence: the relative residual criterion is used with the default tolerance Tol = 0.01 (see equation A.15)

Description of the test specimens used for the verification

Un-reinforced concrete structures are the most fracture-sensitive. Plain concrete uniaxial tension specimens are probably more sensitive to fracture than any other type. For this reason, the following four plain concrete specimens are believed to provide a good test for the fracture sensitivity of the FE crack models.

1). Specimen 1 (tension specimen with one side fixed and node displacements applied at the other end – Figure 4.6). This model is considered for the purpose of checking the accuracy of the stress-update procedure in the subprogram.

The crack directions are fixed after the cracks have formed. Three mode I linear softening moduli E_s of 2 000, 20 000 and 50 000 MPa are adopted to test the sensitivity of the subprogram to the mode I softening parameters. An arbitrary non-zero shear retention factor β is selected to stabilize the numerical solution as the β value will not influence the response of this pure tensile fracture mode I analysis. The built-in crack model in MSC.Marc is also run for the same crack parameters for this verification purpose.

The material properties and crack softening parameters are shown in Figure 4.6.

An increase in node displacements is applied gradually up to the maximum value and then gradually released to zero as shown in Figure 4.7.

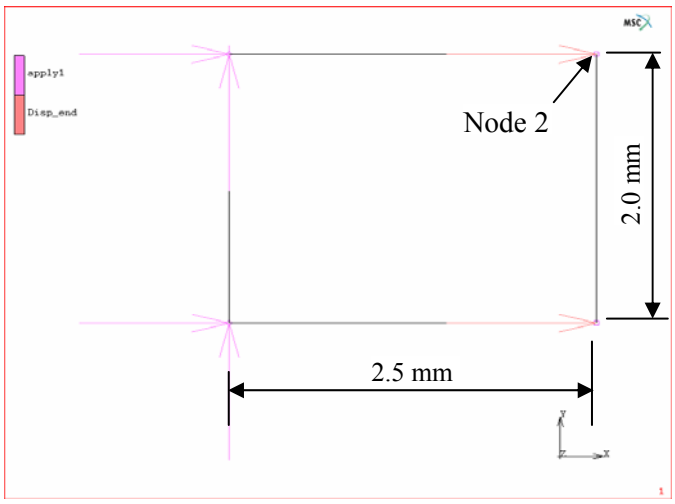

Young's modulus E = 20 000 MPa

Poisson's ratio υ = 0

Tensile strength f_t = 1.2 MPa

Shear retention factor β = 0.2 (arbitrary)

Applied node displacement = 0.0008 mm

Figure 4.6 - FE model and model input (specimen 1)

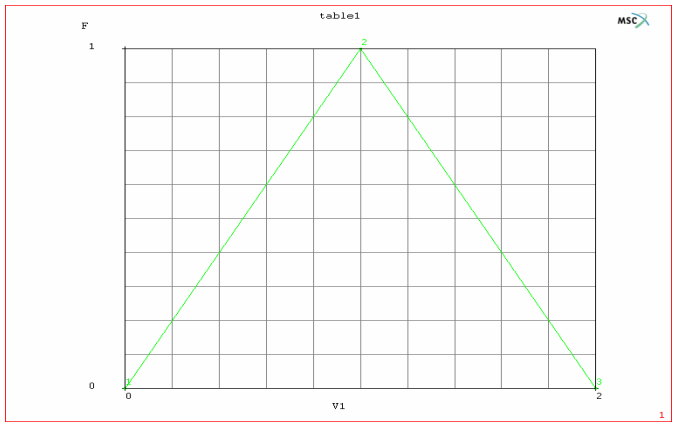

Figure 4.7 - Applied displacement load vs. time (specimen 1)

2). Specimen 2 (tension specimen of four elements fixed at one end and node displacements applied at the other end – Figure 4.8). This model was designed to further test the subprogram developed for correct stress-strain interaction between the cracked element and neighbouring uncracked elements. Only one element adjacent to the fixed boundary is allowed to soften, as shown in Figure 4.9.

Similar to specimen 1, the crack directions are fixed after the cracks have formed. Three mode I linear softening moduli E_s of 2 000, 5 000 and 20 000 MPa are adopted to test the sensitivity and correctness of the program to the mode I softening parameters. Again, an arbitrary non-zero shear retention factor β is selected only to stabilize the numerical solution as the β value will not influence the response of this pure tensile fracture mode I

analysis. The built-in crack model in MSC.Marc is also run for the same crack parameters for this verification purpose.

The material properties and crack softening parameters are shown in Figure 4.8.

An increase in node displacements is applied gradually up to the maximum value and then gradually released to zero, as shown in Figure 4.10.

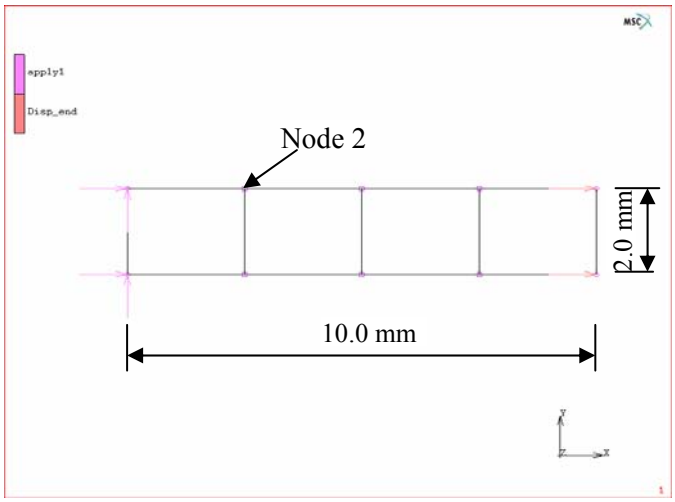

Young's modulus E = 20 000 MPa
Poisson's ratio υ = 0
Tensile strength f_t = 1.2 MPa
Shear retention factor β = 0.2 (arbitrary)
Applied node displacement = 0.0021 mm

Figure 4.8 - FE model – beam of four elements (specimen 2)

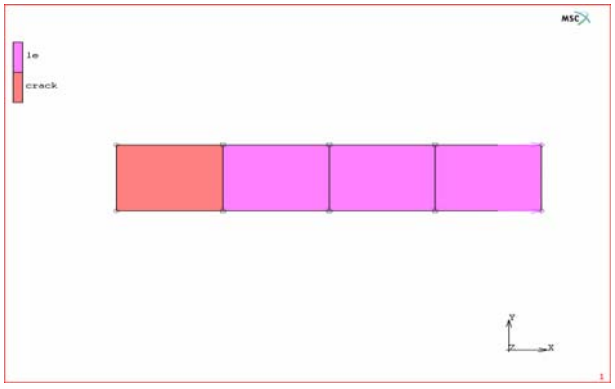

Figure 4.9 - Only one element softening (specimen 2)

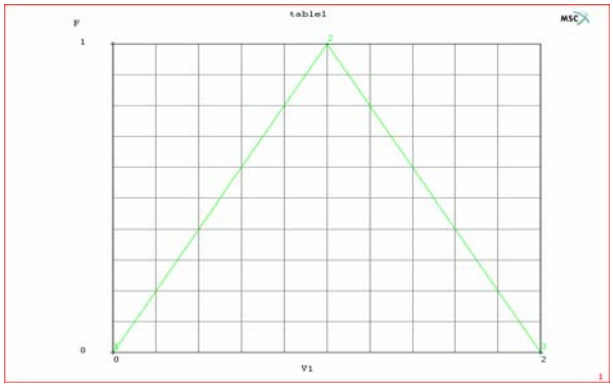

Figure 4.10 - Applied load vs. time (specimen 2)

3). Specimen 3 (tension specimen fixed at one end and pulled by node displacements at the other end). This specimen has the same model size (2 mm x 10 mm), the same material properties and the same boundary conditions as **Specimen 2**. As widely reported (de Borst

1986), local softening constitutive modelling of concrete could cause mesh-dependent results and even snap-back behaviour if the FE mesh is discretized differently for the same model. This non-objectivity regarding the mesh size could be eliminated if the non-local formulation, or the fracture energy based NLFM by adjusting the slope of the softening branch according to the magnitude of the fracture energy, is introduced into the constitutive model. This specimen is used to demonstrate that the phenomenon reported previously by de Borst (1986) can be modelled by the subprogram developed if the constitutive law is not adjusted according to the element size or other factors. The analysis of this specimen is designed to test the post-peak mesh-dependent problem existing in material fracture. The strain-softening constitutive relationship is shown in Figure 4.11. The ultimate strain ε_n^u is assumed to be four times the strain ε_n^e at the tensile strength. The shear retention factor β is arbitrarily assumed to be 0.2 as its value would not affect the results of this pure-tension specimen. The various subdivisions of the specimen are shown in Figures 4.13 to 4.17. In each case only the element on the left adjacent to the fixed boundary is allowed to crack.

The loading of node displacements is applied gradually up to the maximum value, as shown in Figure 4.12.

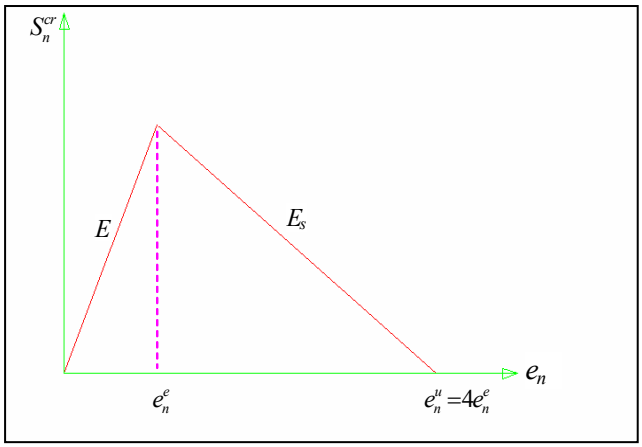

Young's modulus E = 20 000 MPa
Poisson's ratio υ = 0
Tensile strength f_t = 1.2 MPa
Shear retention factor β = 0.2 (arbitrary)
Applied node displacement = 0.0021 mm
Softening modulus E_s = -6 666.67 MPa

Figure 4.11 - Strain-softening diagram (specimen 3)

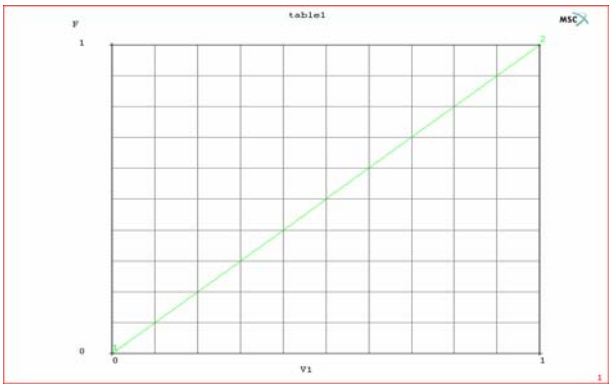

Figure 4.12 - Applied load vs. time (specimen 3)

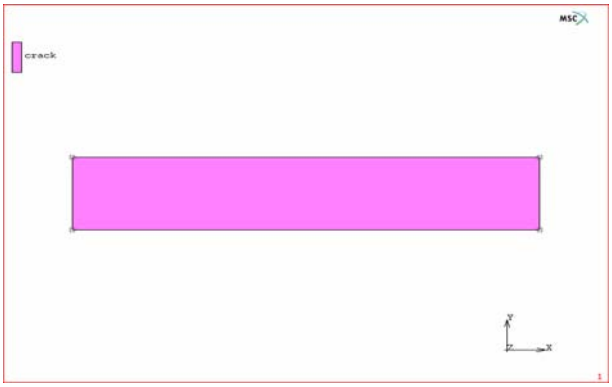

Figure 4.13 - Scenario 1: One element

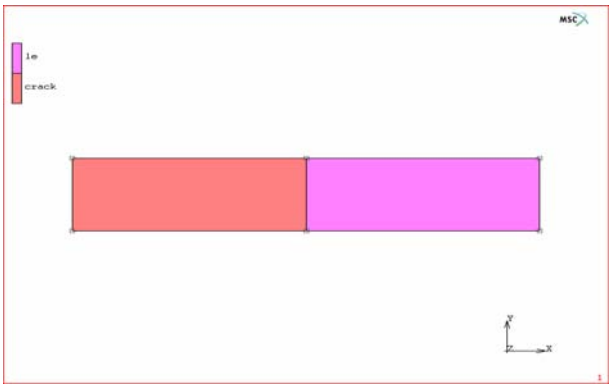

Figure 4.14 - Scenario 2: Two elements

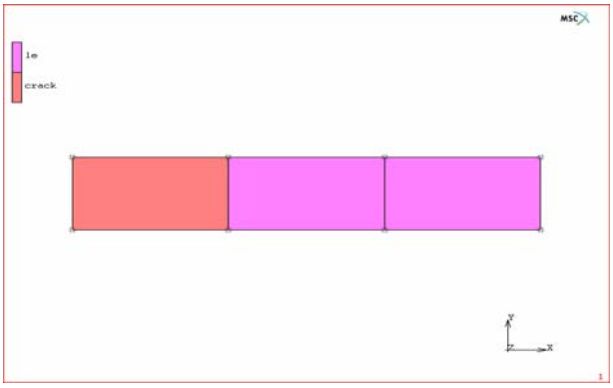

Figure 4.15 - Scenario 3: Three elements

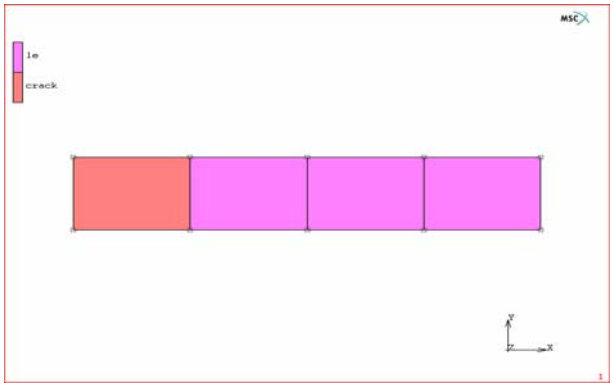

Figure 4.16 - Scenario 4: Four elements

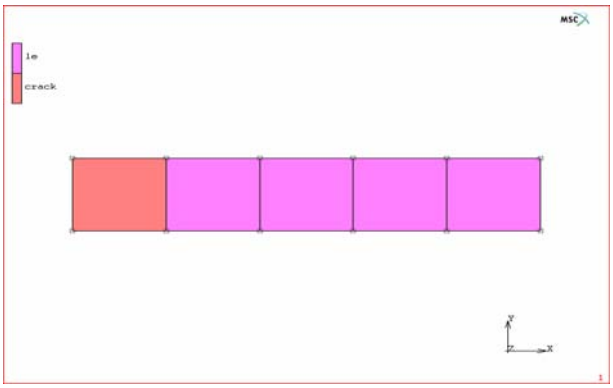

Figure 4.17 - Scenario 5: Five elements

4). Specimen 4 (A simple pure-tension specimen subjected to a constant stress field). A specimen (supported at one end, pulled at the other end – see Figure 4.18) of the unit thickness analyzed previously by Bhattacharjee & Leger (1993) is adopted to validate the

numerical implementation of the cracking model. This simple case is useful to confirm that the stress-strain response corresponds exactly to that of the material model. The FE model and the material properties are taken as the same as in the analysis of Bhattacharjee & Leger (1993) and are shown in Figure 4.18. For comparison purposes, a linear strain softening (see Figure 4.19) is selected and only the two elements at the fixed boundary are allowed to crack (see Figure 4.21). An arbitrary non-zero shear retention factor β is selected to stabilize the numerical solution since the β value will not influence the response of this mode I fracture analysis.

The loading of node displacements is applied gradually up to the maximum value, as shown in Figure 4.20.

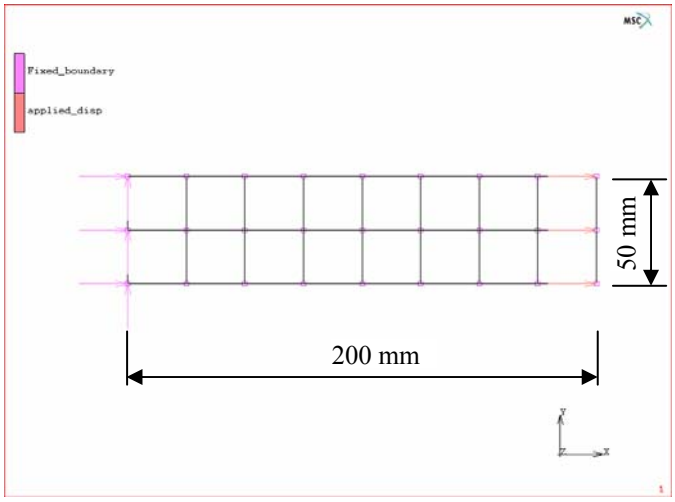

Young's modulus E = 20 000 MPa
Poisson's ratio υ = 0
Tensile strength f_t = 2.0 MPa
Fracture energy G_f = 0.04 N/mm
Softening modulus E_s = -1 333.33 MPa
Thickness = 1.0 mm
Applied node displacement = 0.04 mm

Figure 4.18 - FE model – beam of 16 elements (specimen 4)

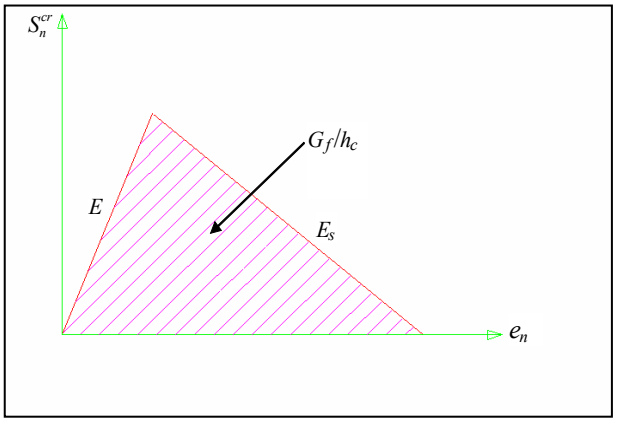

Figure 4.19 - Strain-softening diagram (specimen 4)

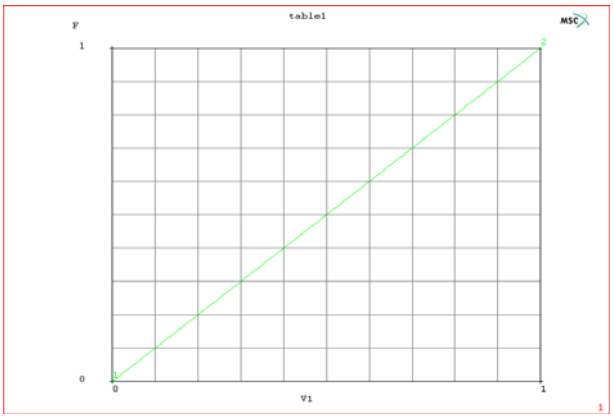

Figure 4.20 - Applied load vs. time (specimen 4)

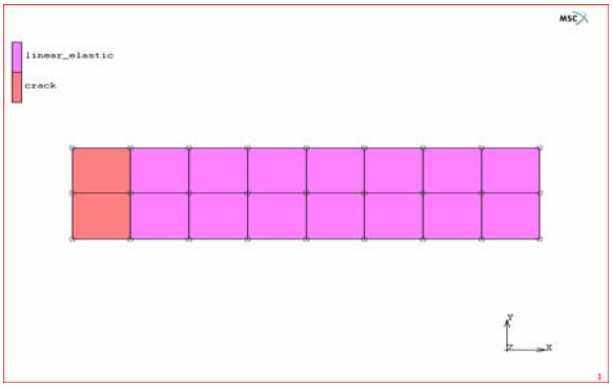

Figure 4.21 - Only the elements adjacent to rigid boundary softening (specimen 4)

4.2.5 Discussion of results of the verification

The results from the four specimens analyzed are shown and discussed in this section.

Specimen 1. As seen from the following plots (Figures 4.22 to 4.24) of different softening moduli of 2 000, 20 000 and 50 000 MPa, the results from HYPELA are in very good agreement with those from the built-in crack model in MSC.Marc. This preliminary study shows that the subprogram HYPELA is capable of simulating cracking in this very simple one-element model.

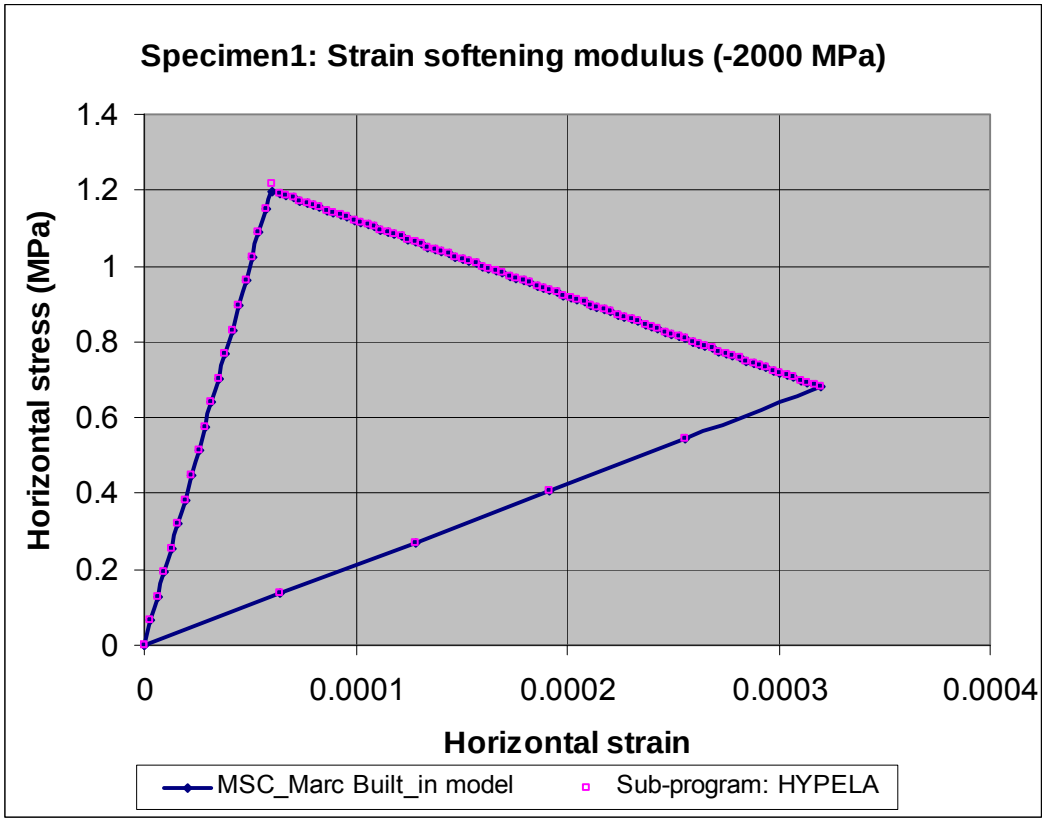

Figure 4.22 - Stress-strain plots for softening modulus E_s = -2 000 MPa (specimen 1)

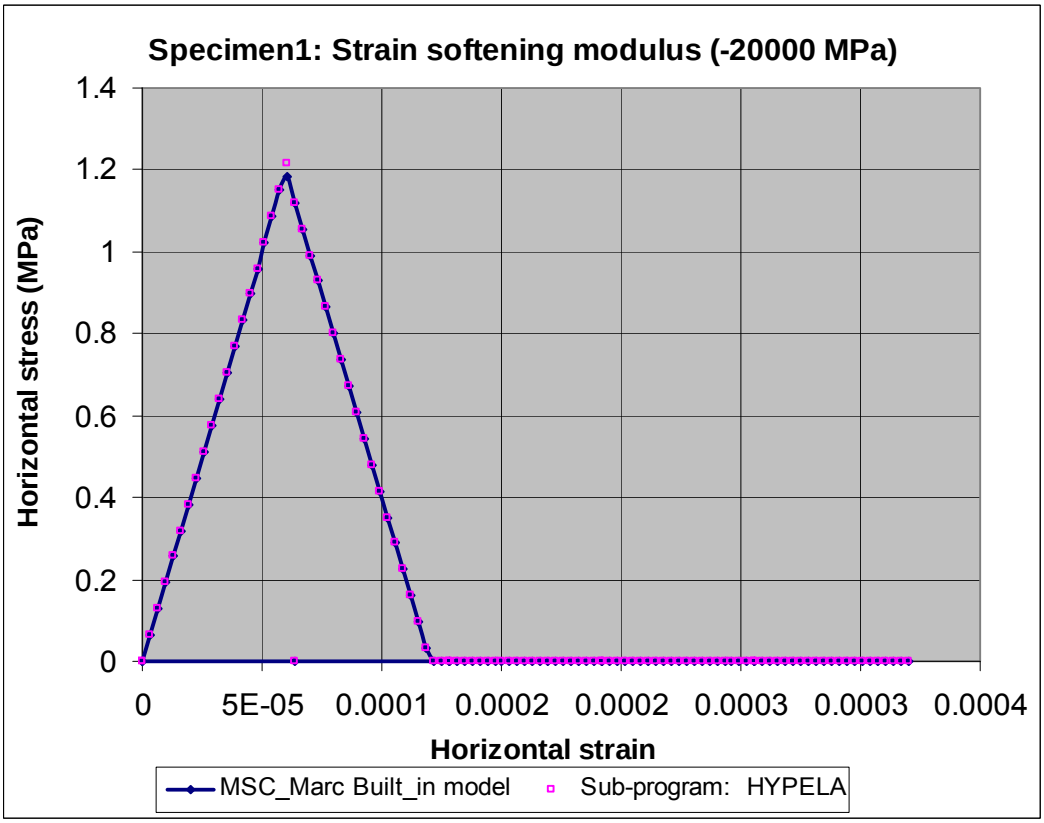

Figure 4.23 - Stress-strain plots for softening modulus E_s = -20 000 MPa (specimen 1)

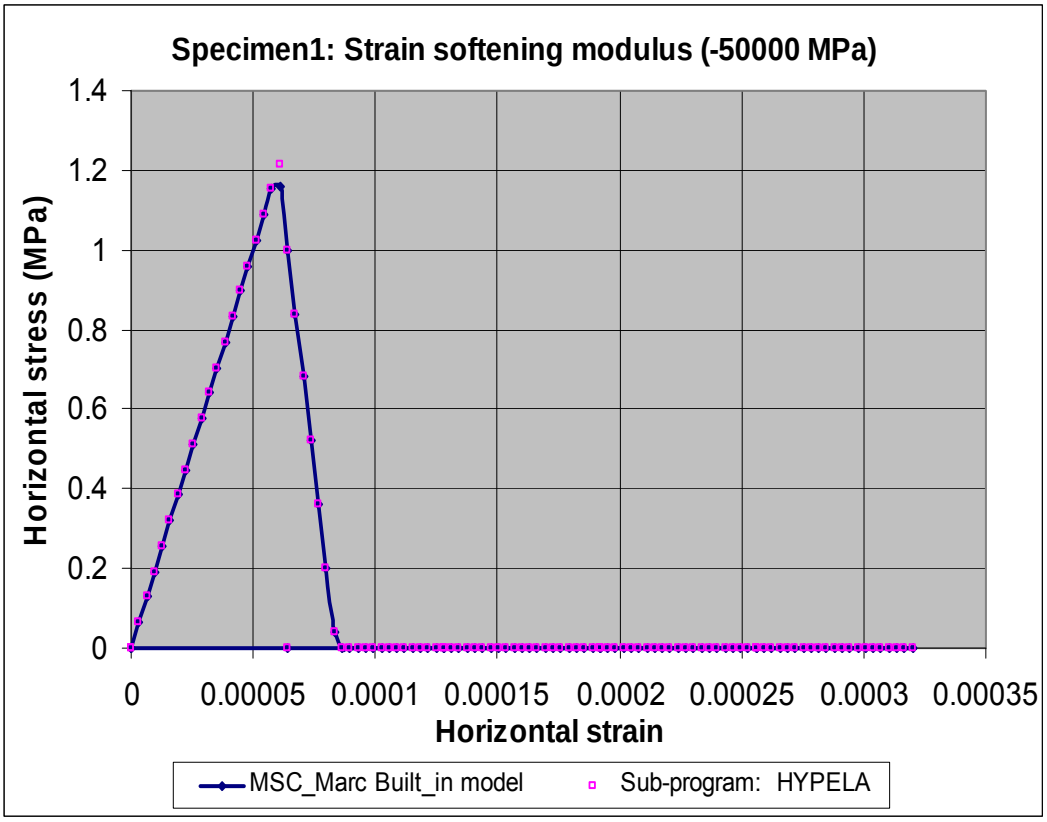

Figure 4.24 - Stress-strain plots for softening modulus E_s = -50 000 MPa (specimen 1)

Specimen 2. The following stress-strain plots (Figures 4.25 to 4.27) of node 2 (shown in Figure 4.8) for different softening moduli of 2 000, 5 000 and 20 000 MPa show that the results from HYPELA are in excellent agreement with those from the built-in crack model in MSC.Marc. This again shows that the subprogram HYPELA is capable of simulating cracking in this four-element model.

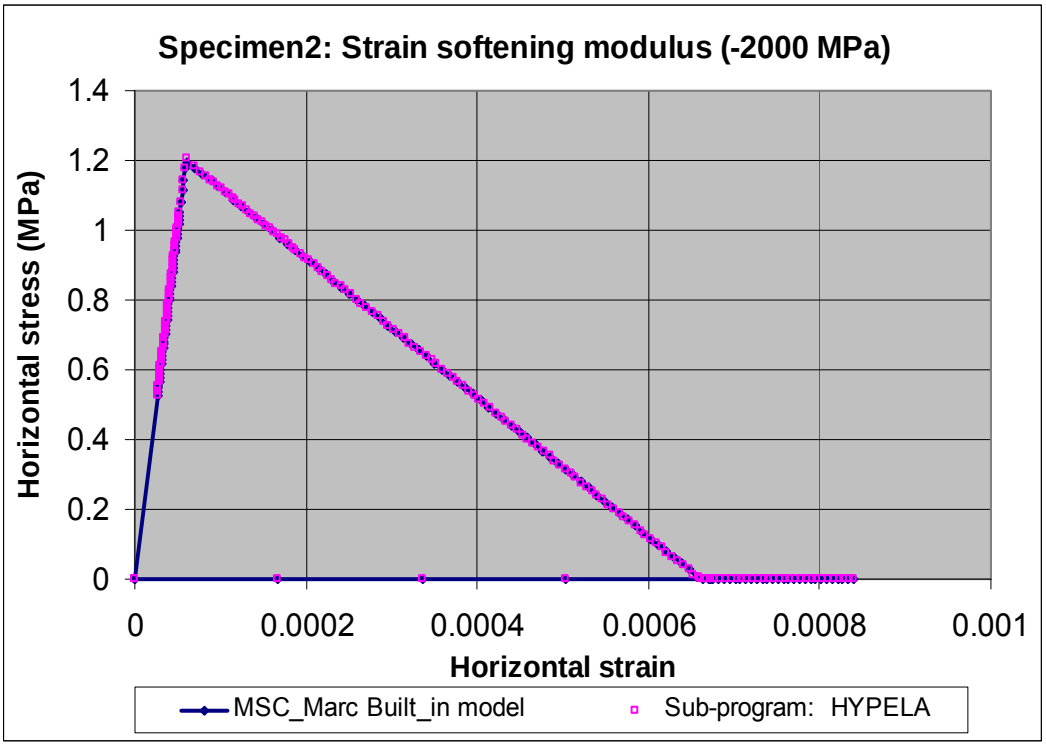

Figure 4.25 - Stress-strain plots (softening modulus E_s = -2 000 MPa) (specimen 2)

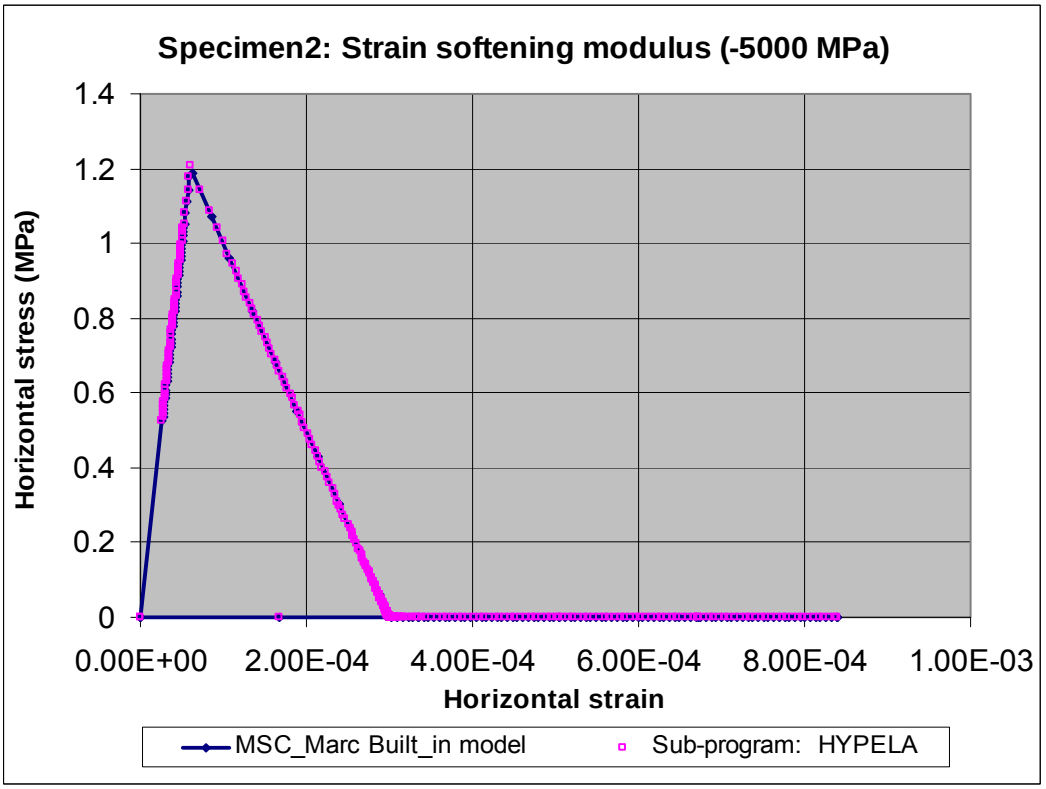

Figure 4.26 - Stress-strain plots (softening modulus E_s = -5 000 MPa) (specimen 2)

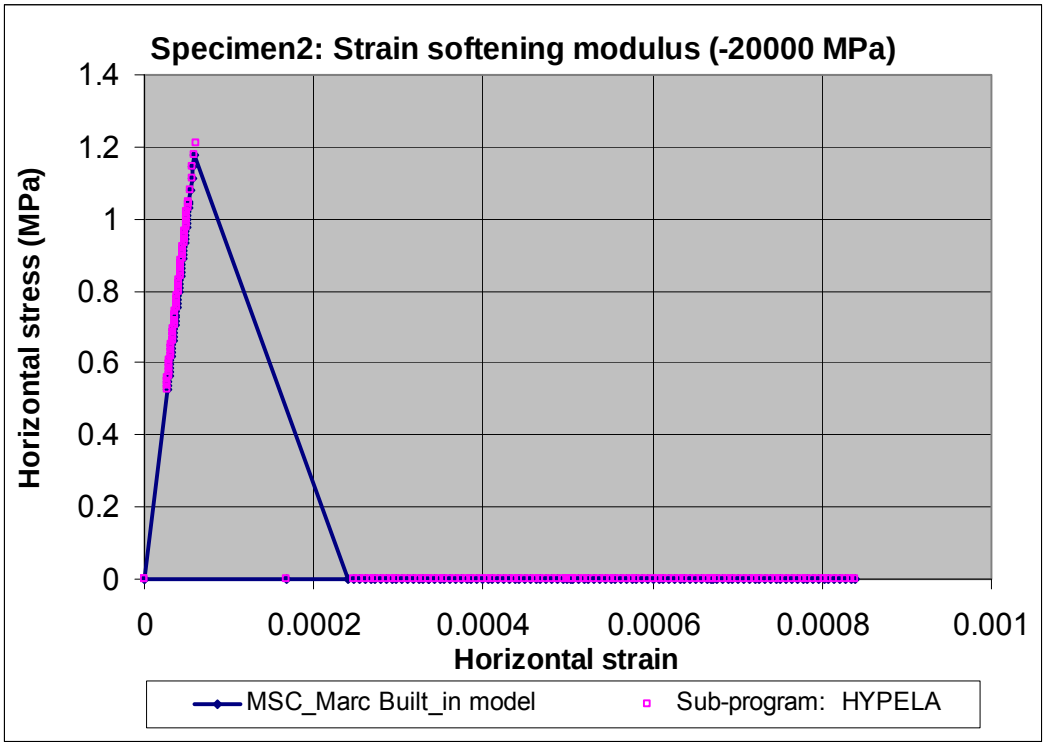

Figure 4.27 - Stress-strain plots (softening modulus E_s = -20 000 MPa) (specimen 2)

Specimen 3. The model shows that when one element is cracking, the other elements are unloading correctly. Figure 4.28 shows that after the assumed tensile strength f_t = 1.2 MPa has been reached, as the FE model is meshed with an increasing number of elements, the averaged horizontal strain of the model decreases until a value of zero averaged strain increment is obtained when the model is meshed with four elements. This four-element model of zero averaged strain increment corresponds to the linear strain-softening modulus chosen, which has an ultimate strain ε_n^u four times the strain at the tensile strength (refer to Figure 4.11). If the number of elements in the model is greater than four, the snap-back phenomenon appears. In other words, as the model is discretized with more and more elements (up to five elements), the averaged strain of the model is gradually decreased and even snapped back as indicated by de Borst (1986).

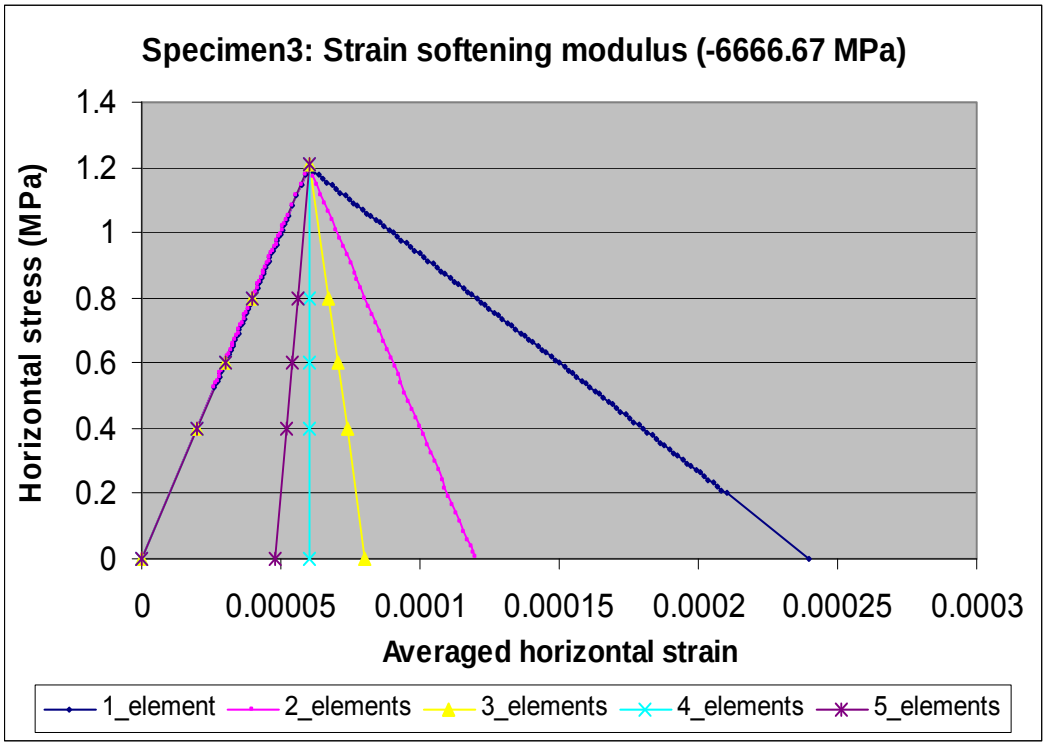

Figure 4.28 - Averaged strain for different numbers of elements in the model (specimen 3)

Specimen 4. This simple, pure-tension beam was designed for the verification of mode I (opening) concrete fracture, which is widely regarded to be the dominant mode for most concrete structures. The calculated force-displacement response is shown in Figure 4.29 demonstrating very close agreement with the results of Bhattacharjee & Leger (1993) and further validating the numerical implementation of HYPELA for the crack models adopted.

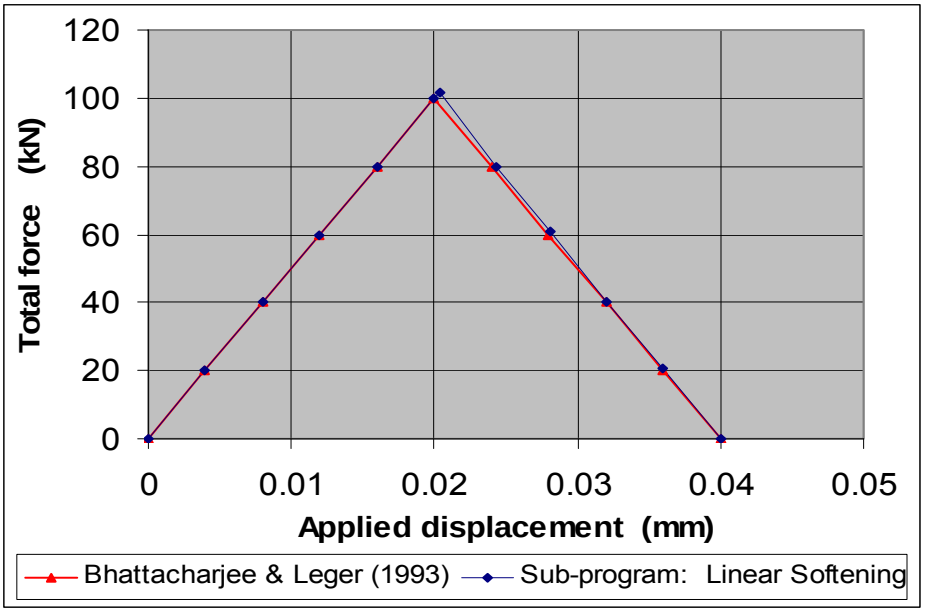

Figure 4.29 - Force-displacement response (specimen 4)

4.3 Verification study with DIANA

The commercial general-purpose FE program DIANA (DIANA 1998) is a well-known code for non-linear crack analysis. Three cracking-verification cases in DIANA are selected to further benchmark the subprogram HYPELA.

Second-order plane strain elements with four integration points are used in this verification study (Figure 4.30).

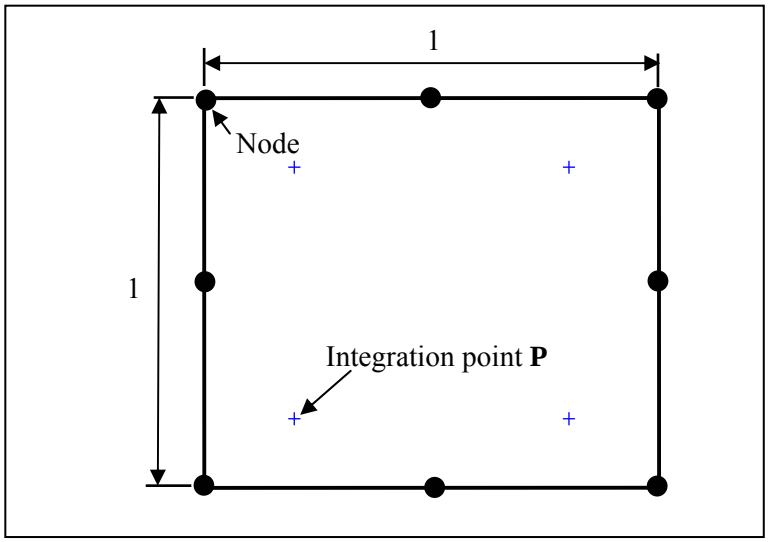

Figure 4.30 - Second-order plane strain element

The specimens are fixed on one side and pulled at the other side by a horizontal deformation δx = 1.0E-4, which is multiplied by a factor of f, as shown in Figure 4.31.

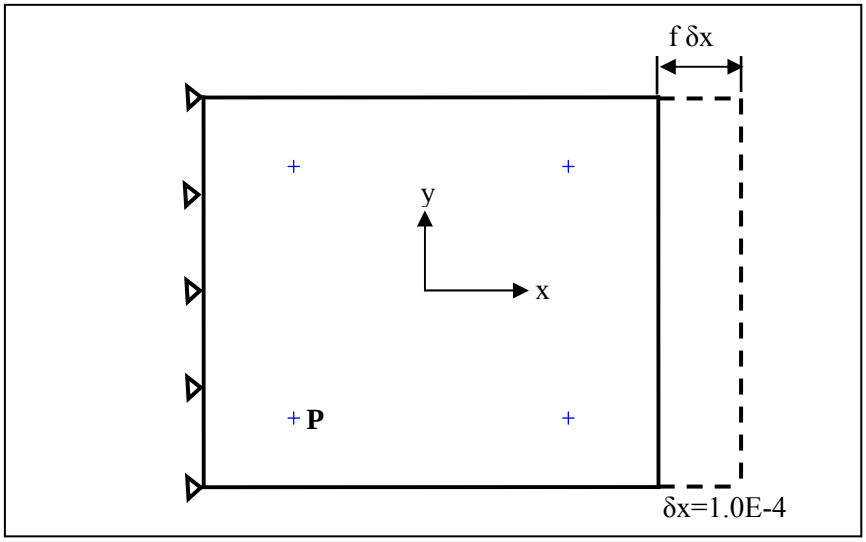

Figure 4.31 - Boundary and loading

The purpose of these case verifications is to check the consistency of the crack status, crack strain and total stress for the integration point P after each loading step.

4.3.1 Cracking with linear tensile softening – plane strain (called PET1CR in DIANA)

Smeared cracking with linear tension softening and full shear retention are applied. The loading is deformation, applied in six steps up to f = 41,1. The results shown in Figure 4.32 indicate that the proposed smeared crack model coded in the subprogram HYPELA produces the same results as those from DIANA.

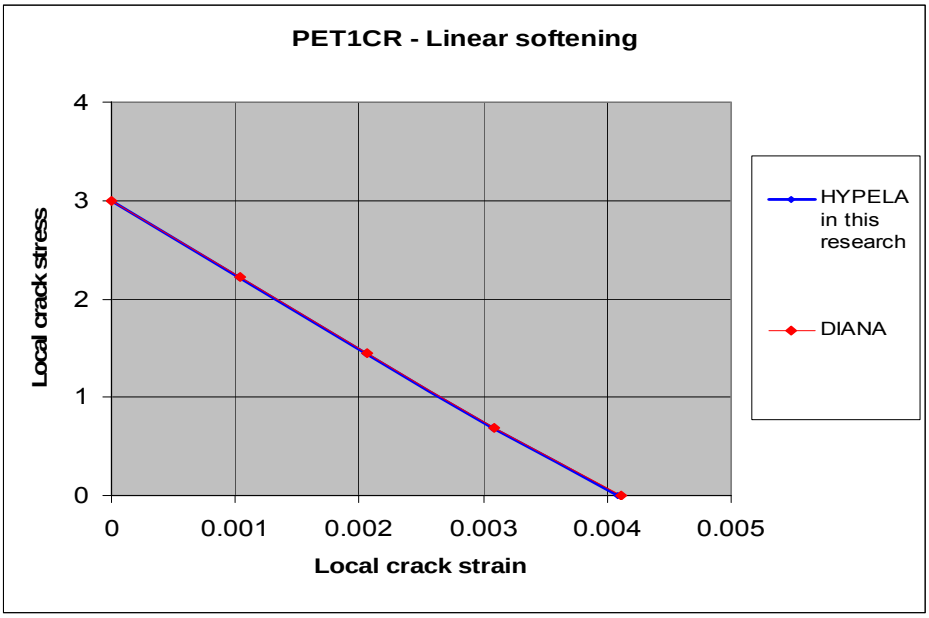

Figure 4.32 - Crack stress and crack strain response (PET1CR)

4.3.2 Cracking with bilinear tensile softening – plane strain (PET2CR)

Smeared cracking with bilinear tension softening and full shear retention are applied. The loading is deformation, applied in six steps up to f = 41,1. The results in Figure 4.33 show that the HYPELA subprogram produces the same results as those from DIANA.

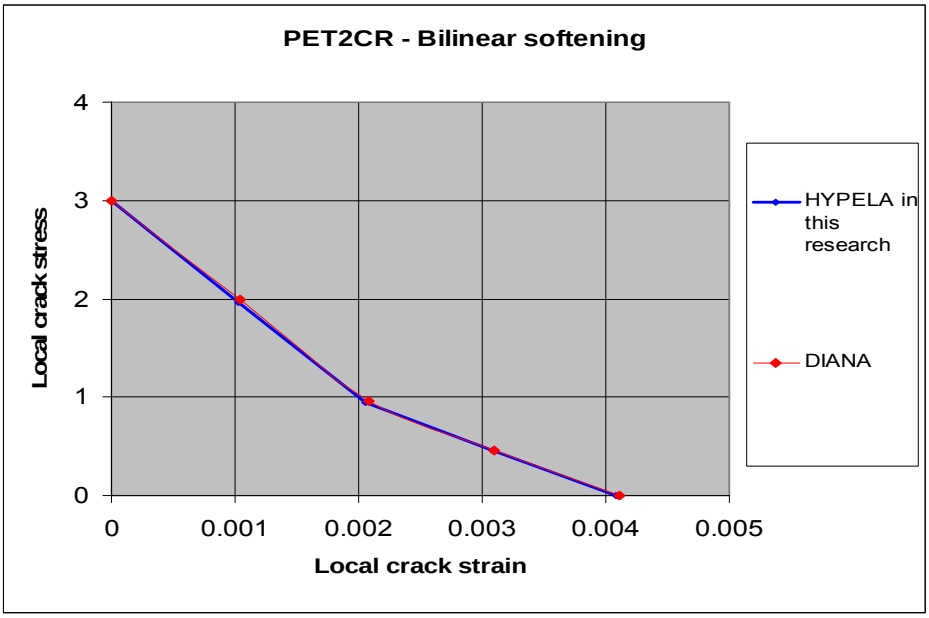

Figure 4.33 - Crack stress and crack strain response (PET2CR)

4.3.3 Cracking with alternating loading – plane strain (PECLOP)

Smeared cracking with linear tension softening and full shear retention are applied. The loading is deformation, applied in ten alternating steps, as shown in Figure 4.34. The crack closes and reopens due to the alternating loading. The results shown in Figure 4.35 indicate that the HYPELA subprogram developed in this chapter can correctly model crack closing and reopening.

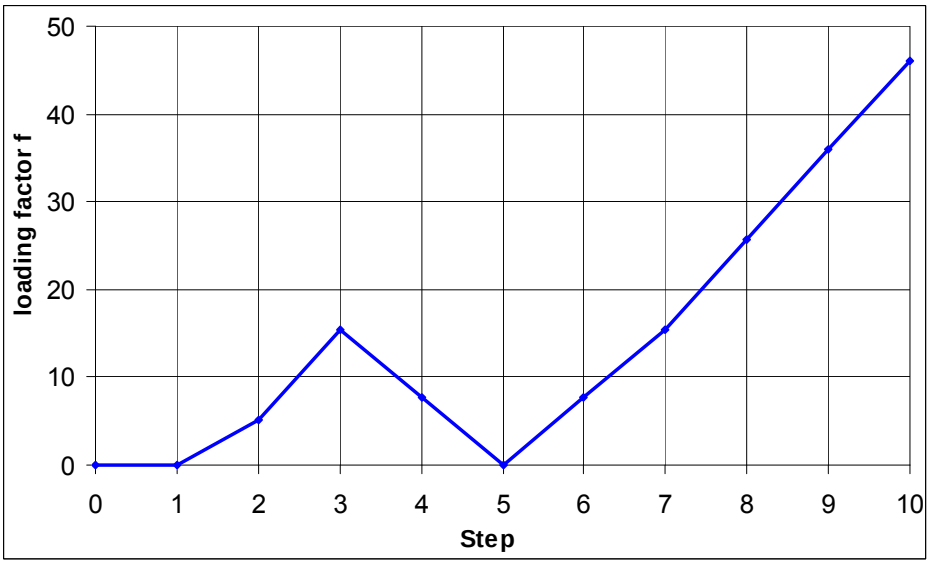

Figure 4.34 - Loading factor f at steps (PECLOP)

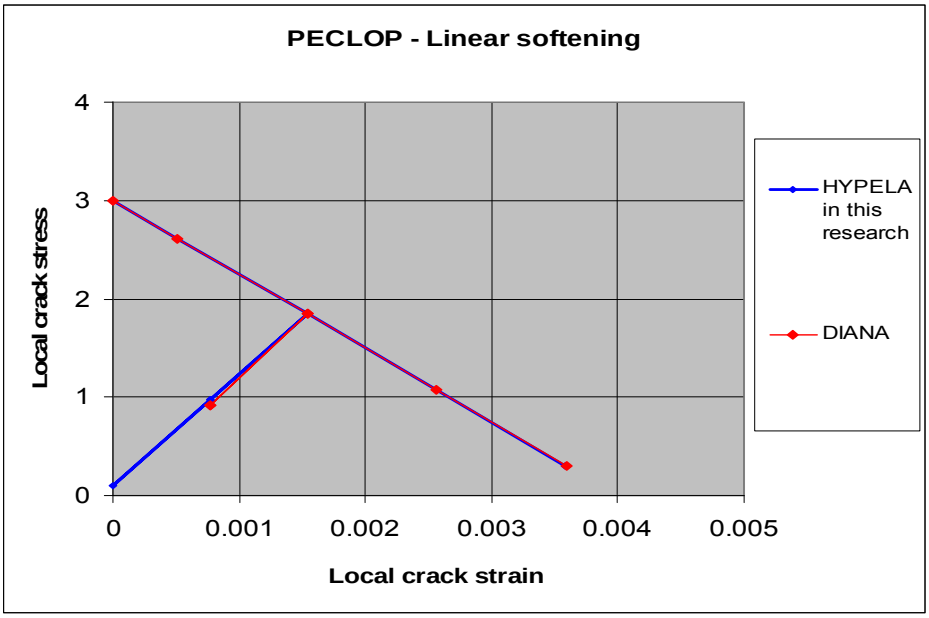

Figure 4.35 - Crack stress and crack strain response (PECLOP)

4.4 Concluding remarks

Incorporated into the commercial general-purpose FE program MSC.Marc, a subprogram called HYPELA has been coded to model the non-linear cracking process in concrete, using the smeared crack models developed previously for constitutive stiffness adjustment. For the plane stress elements, the subprogram was thoroughly benchmarked and verified in the four chosen FE models (mode I), either specially designed for this verification purpose or previously numerically tested. The HYPELA subprogram was further verified using plane strain elements, which showed good correlation with DIANA.

Based on this first-stage benchmark exercise, which was intended to test the implementation procedure on elementary, simple specimens, the subprogram developed for this research can be used with confidence for further validation on more complicated concrete cracking structures, including concrete gravity dams, and eventually for the constitutive cracking analysis of a real concrete dam.

The crack model outlined in Chapter III will also be used to benchmark and validate the crack models and the numerical implementation procedure in the analysis of mode I and mixed-mode concrete beams in Chapter V and in the analysis of concrete gravity dams in Chapter VI. The benchmark studies in Chapters V and VI are more detailed and

complicated for the purpose of thoroughly testing the versatility of the coded subprogram. Eventually, the crack models and numerical techniques that have been developed will be applied in the cracking analysis of a real gravity dam in South Africa and in the evaluation of the safety of the dam.

CHAPTER V - STATIC FRACTURE ANALYSIS OF CONCRETE STRUCTURES

5.1 Introduction

In Chapter IV, the implementation of the crack model (subprogram) on simple pure-tension specimens was preliminarily validated. These pure-tension members are only subject to the mode I fracture response and the directions of crack propagation are fixed and *a priori* known. Thus a fixed, single-crack model can be accurately employed to simulate the fracture behaviour. The validation exercise is extended in this chapter to mode I and mixed-mode fracture simulation of more complicated concrete structures, such as a three-point, single-notched, centrally loaded beam and a four-point, single-notched shear beam.

A three-point, single-notched, centrally loaded beam is first adopted to benchmark the proposed bilinear mode I tensile softening diagram and the related numerical implementation. The specimen is mode I dominant because no shear fracture deformation would occur in this specimen due to the symmetry of the geometry and the loading conditions. Therefore, a fixed, single-crack model is sufficient to simulate the fracture process in such a specimen.

A well-investigated, single-notched shear beam under four-point, mixed-mode static loading conditions is further used to validate the crack model adopted with study of the fracture parameters.

Mesh objectivity is definitely both a requirement and a necessity for any crack model proposed for finite element (FE) fracture analysis in any sensible fracture evaluation of concrete structures. For this reason, three differently meshed FE models of the same geometry were considered to test the objectivity regarding the mesh discretization of the crack model adopted and the numerical technique developed.

All the models of the following three verification problems employ plane stress, and are four-noded and four-Gauss point isoparametric elements, with the exception of the second-order, eight-noded nine-Gauss point isoparametric elements used in case 3 for the

validation of the crack models and the implementation on second-order elements. A modified Newton-Raphson solution procedure is adopted.

5.2 Case 1: three-point, centre-loaded, single-notched beam

A symmetrical centre-notched concrete beam under three-point bending (two supports and a midpoint load) is used to validate the implementation of the cracking model with a parametric study. The beam has a length of 838 mm, a span of 788 mm and a cross-section of 102 mm x 102 mm. The notch:depth ratio (a/d) is 0.5. Malvar & Fourney (1990) carried out 12 experimental tests and also a numerical simulation on the beam.

The beam is symmetrical along its centreline so that only half the beam (as modeled by Malvar & Fourney 1990) needs to be modelled in the FE analysis, as shown in Figure 5.1. The material properties used are as follows:

Young's modulus E = 21 700 MPa; Tensile strength f_t = 3.1 MPa
Poisson's ratio υ = 0.2; Fracture energy G_f = 0.0763 N/mm
Crack characteristic length h_c = 10 mm (width of element at the crack)

Linear, bilinear and non-linear exponential strain-softening branches are used to investigate the cracking behaviour of the beam, as shown in Figure 5.2. This symmetrical specimen is not sensitive to shear softening since the crack propagates along the centre of the beam. No shear deformation would occur in the crack formation zone. Numerical studies are compared with the experimental results from Malvar & Fourney (1990), as shown in Figure 5.3.

Cornelissen *et al.* (1986) conducted a series of tests to determine the crack-softening characteristics of normal-weight concrete and proposed an empirical formula obtained by curve fitting the test data:

$$\frac{\sigma}{f_t} = \left[1 + (C_1 \frac{\delta}{\delta_0})^3\right] e^{(-C_2 \frac{\delta}{\delta_0})} - \frac{\delta}{\delta_0}(1 + C_1^3) e^{(-C_2)} \qquad (5.1)$$

Where $C_1 = 3$, $C_2 = 6.93$, δ is the crack opening and δ_0 is the crack opening at which the crack stress can no longer be transferred. This stress-crack opening relationship in equation (5.1) is transformed into a crack stress-strain law for this study, as shown in Figure 5.2.

As shown in Figure 5.3, the calculated linear softening response (labelled as LS) yields the highest peak loading of all the softening relationships. This indicates that if linear softening is assumed when concrete fracture is modelled, then the resistance of the structure will be overestimated. The calculated non-linear softening response based on the experimental softening relationship derived by Cornelissen *et al.* (1986) (labelled as CS), yields the closest load-displacement relationship to the experimental results.

The bilinear softening models (labelled as BLS) improve the response significantly when compared with the linear softening model. Therefore, the bilinear softening model is able to provide a reasonably accurate prediction of the cracking response, while remaining relatively simple to implement. The investigation demonstrates the importance of adopting bilinear softening analysis in concrete structures, instead of the general application of linear softening in concrete cracking analysis used in the past. Although Cornelissen *et al.*'s exponential non-linear softening relationship remains the most accurate, it requires greater effort to implement in an FE analysis compared with the simpler bilinear softening model.

A series of constitutive parameters for bilinear softening curves was investigated for the purpose of calibrating the correct range of shape parameters α_1 and α_2 for concrete structures.

A parameter study was conducted to determine the bilinear softening model parameters α_1 and α_2 that best fit the experimental response. The results of the parameter study are shown in Figures 5.2 to 5.7, in which it can be seen that by setting the bilinear shape parameters α_1 to between 1/3 and 0.44 and α_2 to 0.1 respectively, good agreement with the experimental results can be obtained.

By selecting α_2 as constant and equal to 0.1, and setting α_1 to 0.25, 1/3 and 0.44, it can be seen that the first part of the bilinear softening modulus becomes steeper as α_1 increases (see Figure 5.2), while the predicted response improves when compared with the experimental results (Figure 5.3).

From Figures 5.5 and 5.7, in which α_1 is fixed at 0.25 and 1/3 respectively (see Figures 5.4 and 5.6), while α_2 is varied from 0.1 to 0.3, it can be seen that as α_2 decreases from 0.3 to 0.1, the first part of the bilinear softening modulus becomes steeper and the second part of the bilinear softening branch becomes flattener (see Figures 5.4 and 5.6), while the predicted response improves. It is concluded that the first part of the bilinear softening modulus is of greater importance than the second part, although it is the combination of the bilinear shape parameters α_1 and α_2 that determines the complete softening response. It is important to note that the particular values of α_1 and α_2 would depend on the concrete mix of the particular structure and need to be carefully determined experimentally.

Compared with the numerical investigation by Malvar & Fourney (1990), this study has produced a better simulation of the experiment results.

It is evident that the cracking model and the calculation procedure can accurately predict the cracking behaviour of concrete, provided a suitable softening response is adopted.

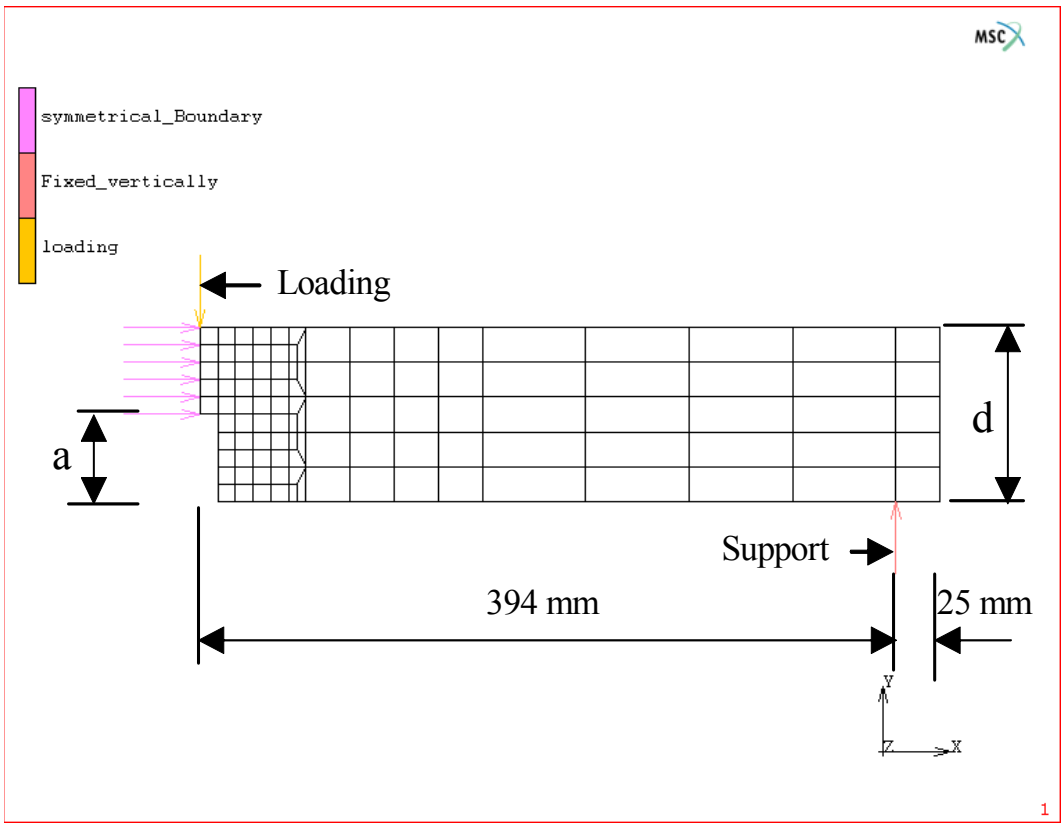

Figure 5.1 - Finite element model (Case 1)

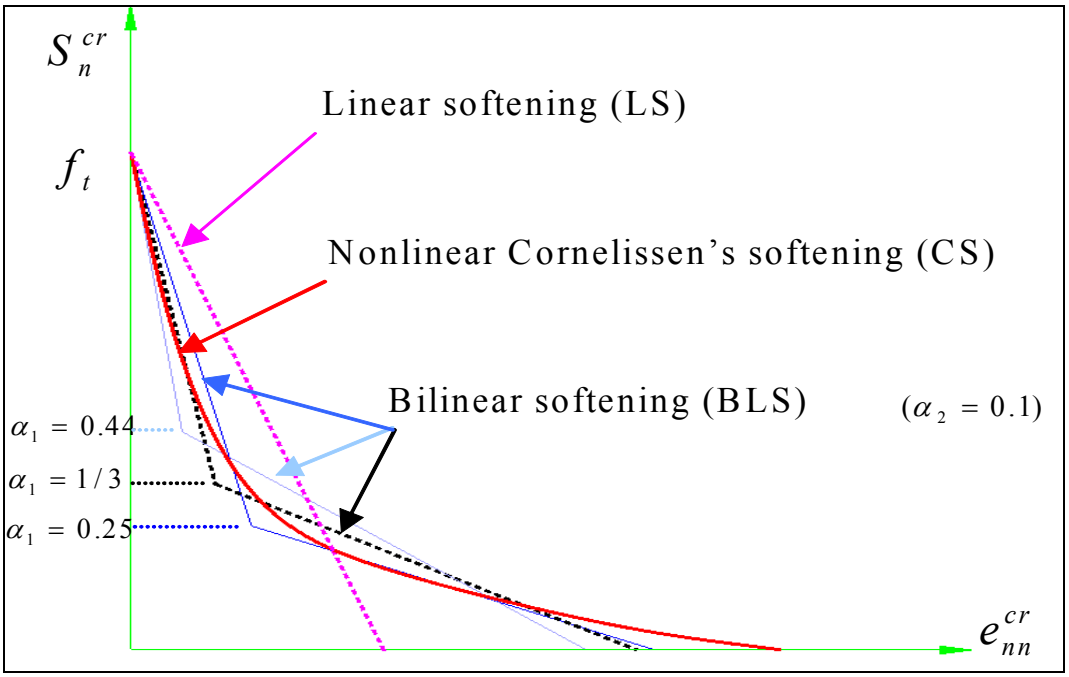

Figure 5.2 - Linear, bilinear and non-linear strain softening

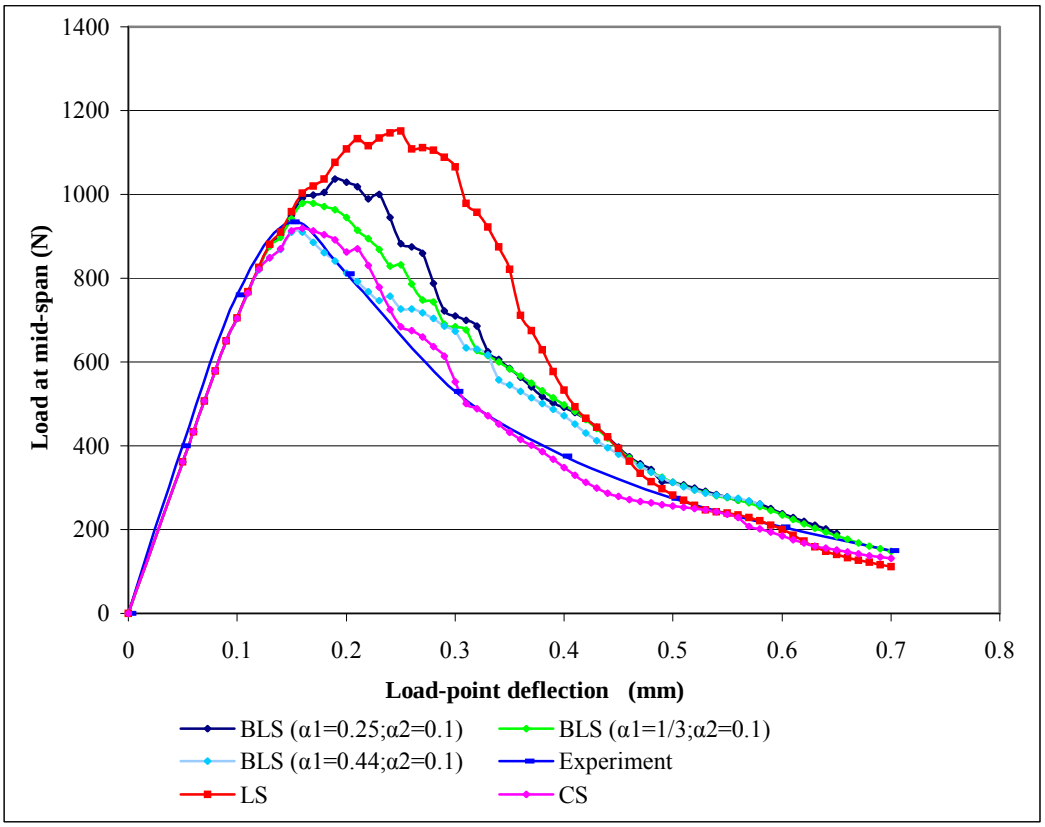

Figure 5.3 - Load-load point deflection for strain-softening branches in Figure 5.2

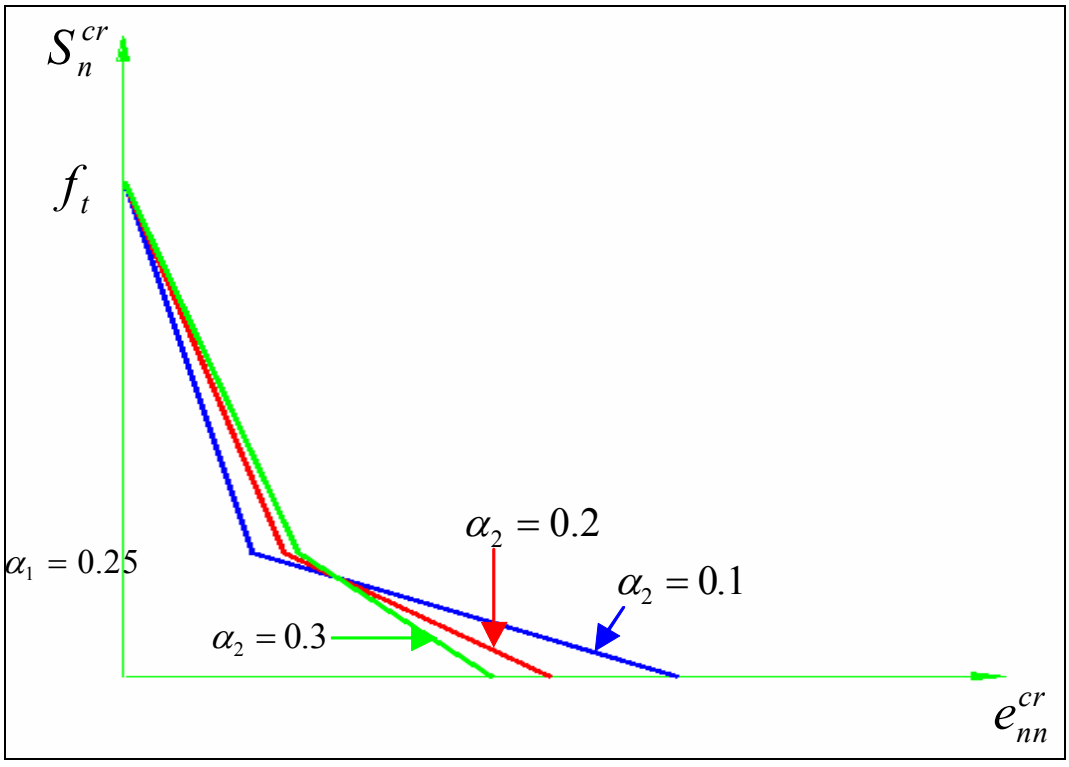

Figure 5.4 - Bilinear strain softening with $\alpha_1 = 0.25$ and $\alpha_2 = 0.1$, 0.2 and 0.3

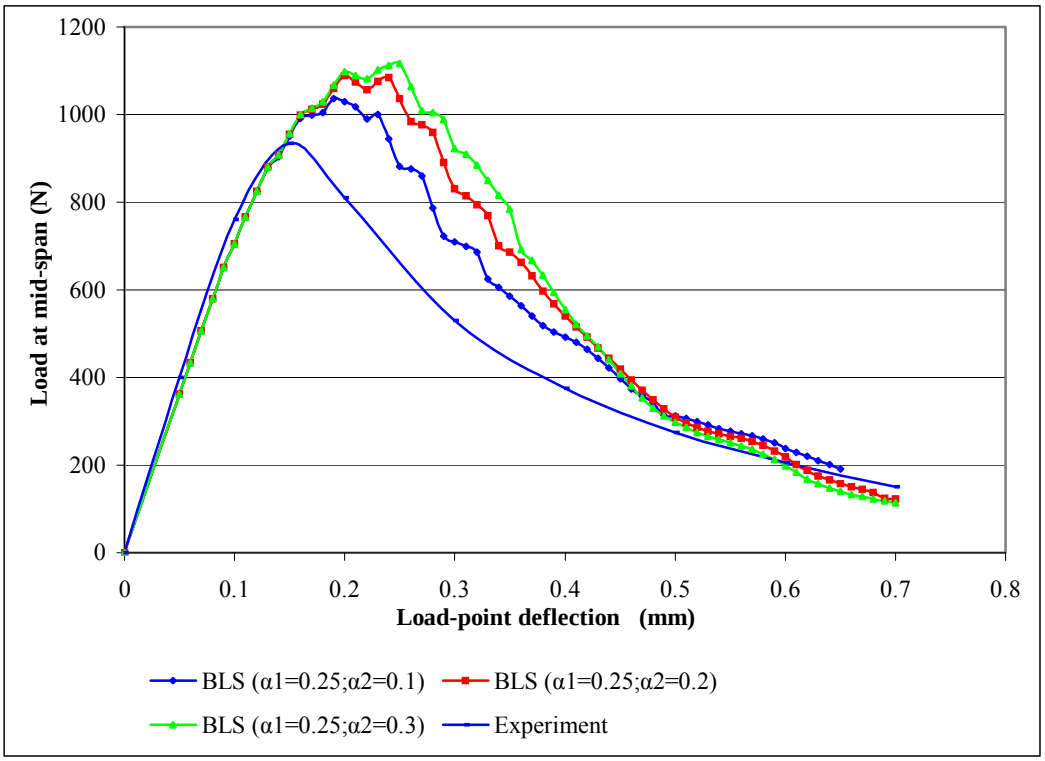

Figure 5.5 - Load-load point deflection for strain-softening branches in Figure 5.4

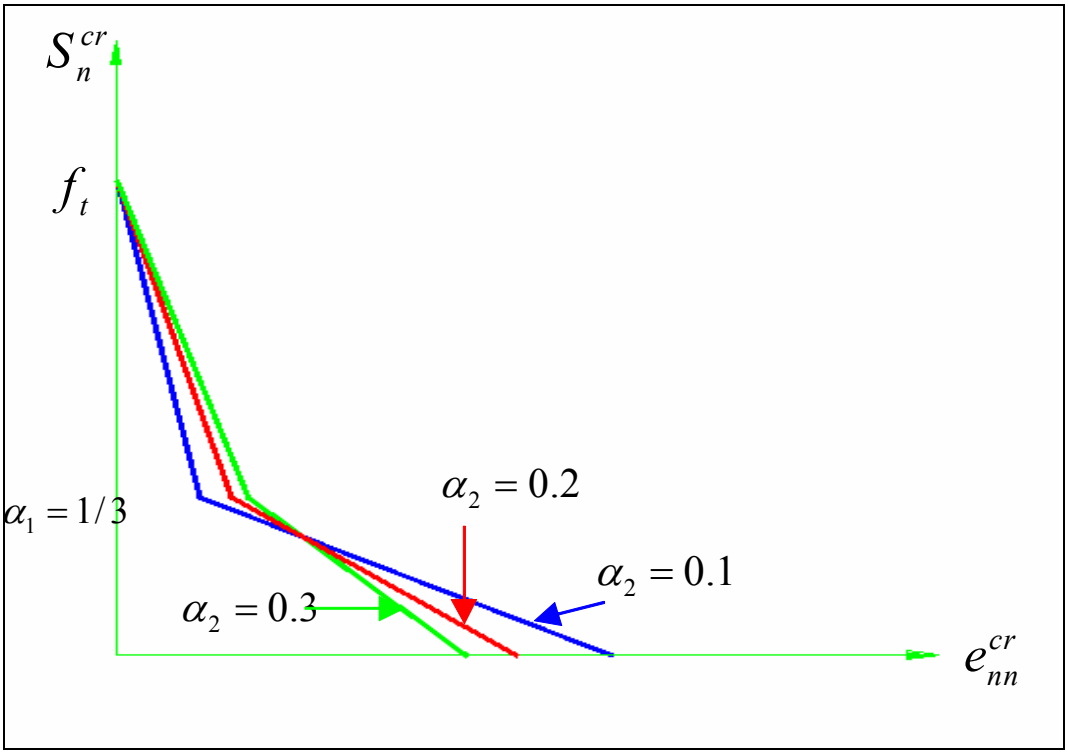

Figure 5.6 - Bilinear strain softening with $\alpha_1 = 1/3$ and $\alpha_2 = 0.1$, 0.2 and 0.3 respectively

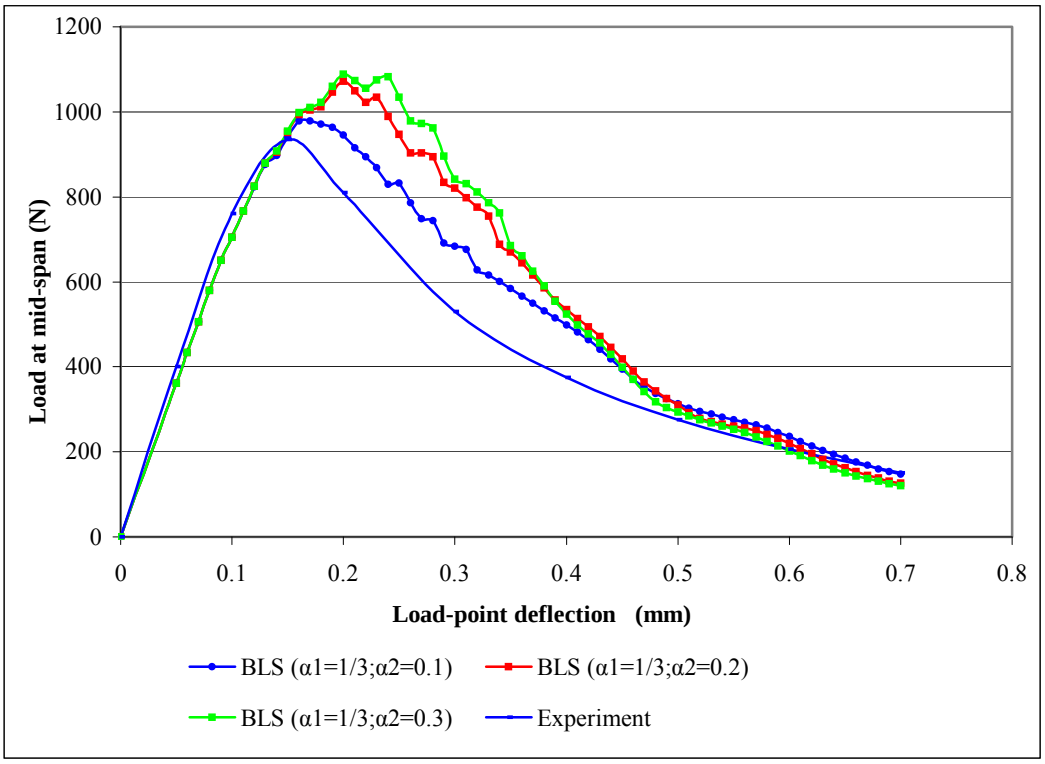

Figure 5.7 - Load-load point deflection for strain-softening branches in Figure 5.6

5.3 Case 2: single-notched shear beam

A single centre-notched shear beam, loaded at points A and B and supported at two points at the bottom, is shown in Figure 5.8. The generality and accuracy of the crack model and the code developed are to be investigated. The beam has been tested experimentally by Arrea & Ingraffea (1981) and is widely used as a benchmark for numerical fracture analysis models (Rots & de Borst 1987; Bhattacharjee & Leger 1994).

The FE model is shown in Figure 5.8 and the material properties and constitutive parameters are as follows.

Young's modulus E = 24 800 MPa; Tensile strength f_t = 2.8 MPa

Poisson's ratio υ = 0.18; Fracture energy G_f = 0.1 N/mm

Thickness of the beam = 156 mm Bilinear shape parameters α_1 = 1/3 and α_2 =0.2

Crack characteristic length h_c = 13.5 mm

During laboratory testing the load was applied to the specimen by means of a stiff steel beam, ACB. Since the steel beam is statically determinate, the ratio between its reactions at A and B (acting on the concrete beam) and the applied load can be easily determined. The load in this study was therefore applied directly to the concrete beam at A and B, using the same ratios as in the laboratory test. The crack opening is measured as a crack mouth sliding displacement (CMSD) and a crack mouth opening displacement (CMOD), as defined in Figure 5.13.

Snap-back behaviour has been modelled numerically by several researchers (Rots & Blaauwendraad 1989; Rots & de Borst 1987; Bhattacharjee & Leger 1994), using an indirect displacement control strategy with the CMSD as controlling parameter. Due to the limitations in the FE package, which lacks the mechanism for an indirect displacement control solution, the author had to resort to a manual solution procedure. A peak load was firstly obtained by identifying the load beyond which the beam experienced unstable cracking and the solution was unable to converge. Subsequently, manual unloading beyond the peak load is achieved by defining the unloading path. It should be noted that the CMSD response of the beam is sensitive to the unloading path, which explains why CMSD was adopted to control the applied load directly or indirectly in the experimental and numerical investigations carried out by other researchers.

Three solutions are presented: two linear softening models (labelled as LS) with $\beta = 0.05$ and 0.1 respectively, and one bilinear softening model with $\beta = 0.05$ (labelled as BLS). A comparison with the experimental results for the load – CMSD response is shown in Figure 5.9. In the post-peak regime, the results of the linear softening model with $\beta = 0.1$ fall outside the range of the experimental results, producing a less accurate post-peak response than the other two solutions. The results of the bilinear softening model are well within the experimental scattering range and show a significant improvement over the linear softening solutions. It is also observed that the CMSD response is very sensitive to the shear-softening parameters selected for this specimen due to the mixed-mode fracture. The numerical results agree well with the results of other researchers.

The load–crack mouth opening displacement (CMOD) response obtained in this study, together with the results from Rots & de Borst (1987) (labelled as R&D 1987), are shown

in Figure 5.11. It must be noted that a mode I fracture energy of 0.1 N/mm is used in this investigation (for the purpose of comparison with other investigations) whereas a fracture energy of 0.075 N/mm was adopted by Rots & de Borst (1987). Most past investigations have adopted a mode I fracture energy of 0.1 N/mm such as Bhattacharjee & Leger (1994) and Rots & Blaauwendraad (1989) and others. For comparison with the results from the more available past investigations (mainly to compare with the work done by Bhattacharjee & Leger 1994), a mode I fracture energy of 0.1 N/mm was also adopted in this research. This is the main reason for the post-peak CMOD response of this investigation being slightly higher than those from Rots & de Borst (1987). In general, however, good agreement has been achieved.

As pointed out by Rots & de Borst (1987), the beam responded in both mode I and II fracture propagations, with mode I being the main fracture mechanism in this application. This is confirmed by the ultimate CMOD response being approximately twice the corresponding CMSD response.

The load-vertical displacement response at point C obtained in this study for the three cases mentioned above, together with the results from Rots & Blaauwendraad (1989) (labelled as R&B 1989) and Bhattacharjee & Leger (1994) (labelled as B&L 1994), are shown in Figure 5.10. The deflection at point C is obtained from the deflections at points A and B by assuming that the steel beam ACB used in the experimental test was infinitely stiff. Good agreement with the results obtained by Rots & Blaauwendraad (1989) and Bhattacharjee & Leger (1994) is exhibited for the snap-back behaviour. A mode I fracture energy of 0.1 N/mm was selected in the latter two references (Rots & Blaauwendraad 1989; Bhattacharjee & Leger 1994).

The final crack zone and the deformed shape of the beam are shown in Figures 5.12 and 5.13. Figure 5.12 demonstrates that there is some discrepancy between the smeared cracks and the crack profile observed in the test. As shown in Figures 5.9 to 5.11, the post-peak structural resistance does not reduce to zero, indicating that stress-locking (which is inherent in smeared crack models) is present. This phenomenon was also observed in the other investigations using smeared crack models (Rots & Blaauwendraad 1989; Bhattacharjee & Leger 1994).

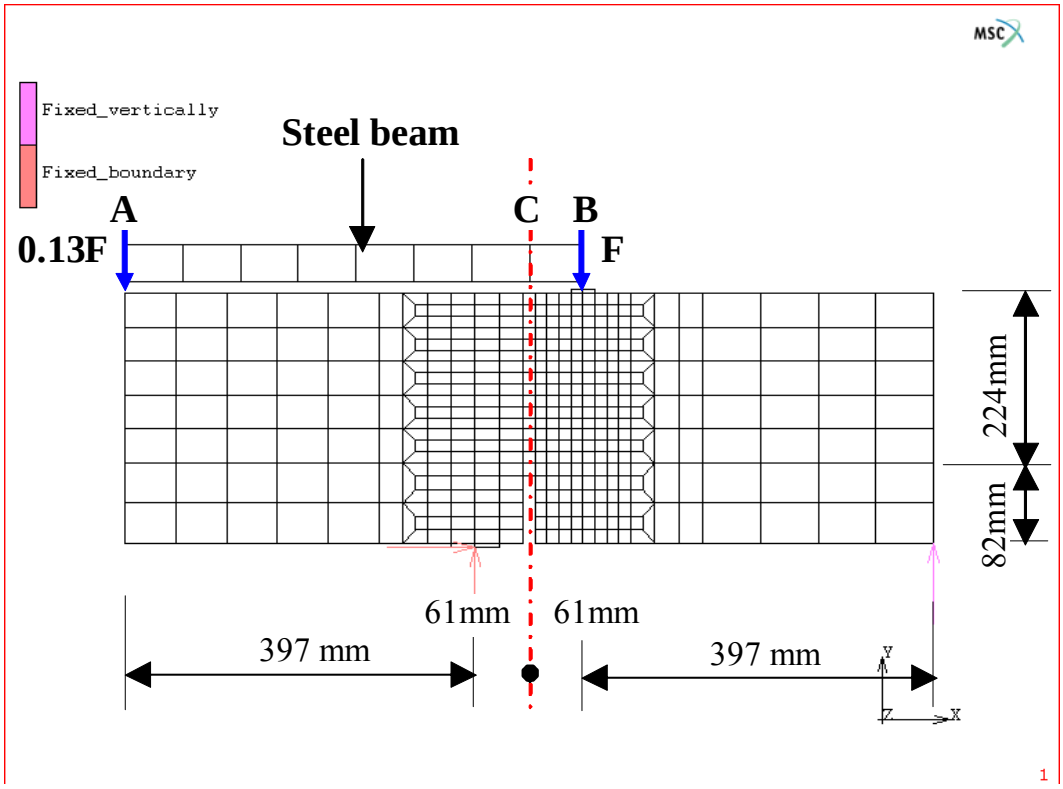

Figure 5.8 - Finite element model (Case 2)

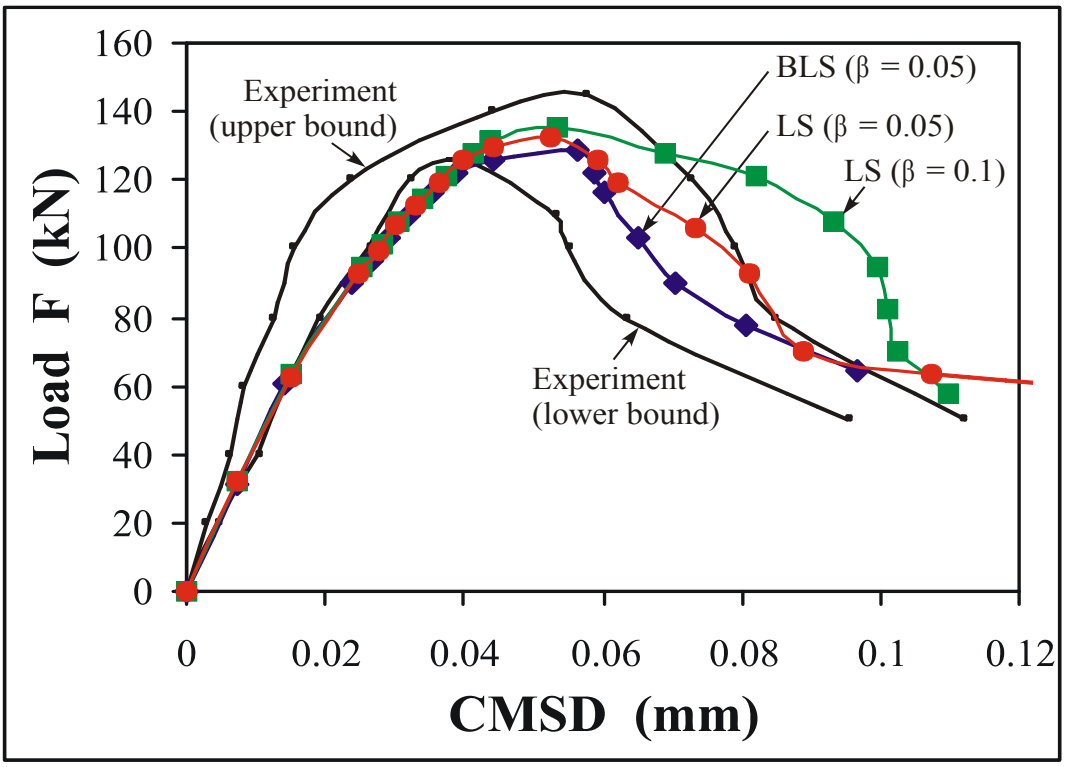

Figure 5.9 - Load – CMSD

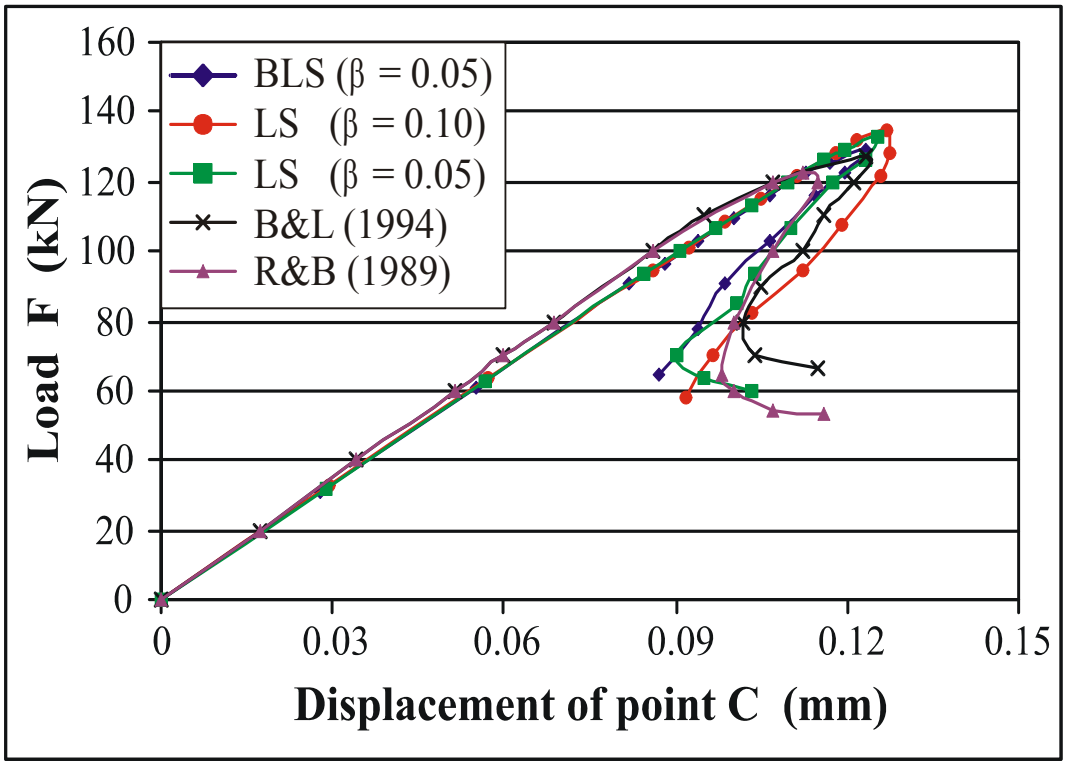

Figure 5.10 - Snap-back in load – deflection at point C

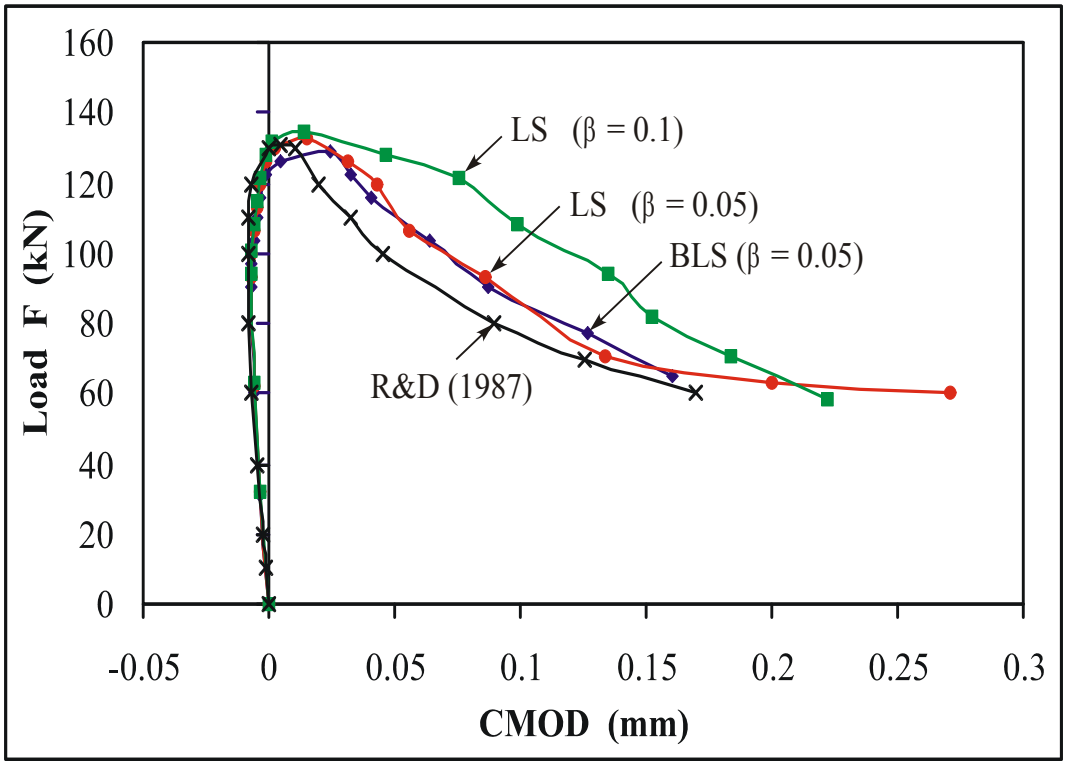

Figure 5.11 - Load – CMOD

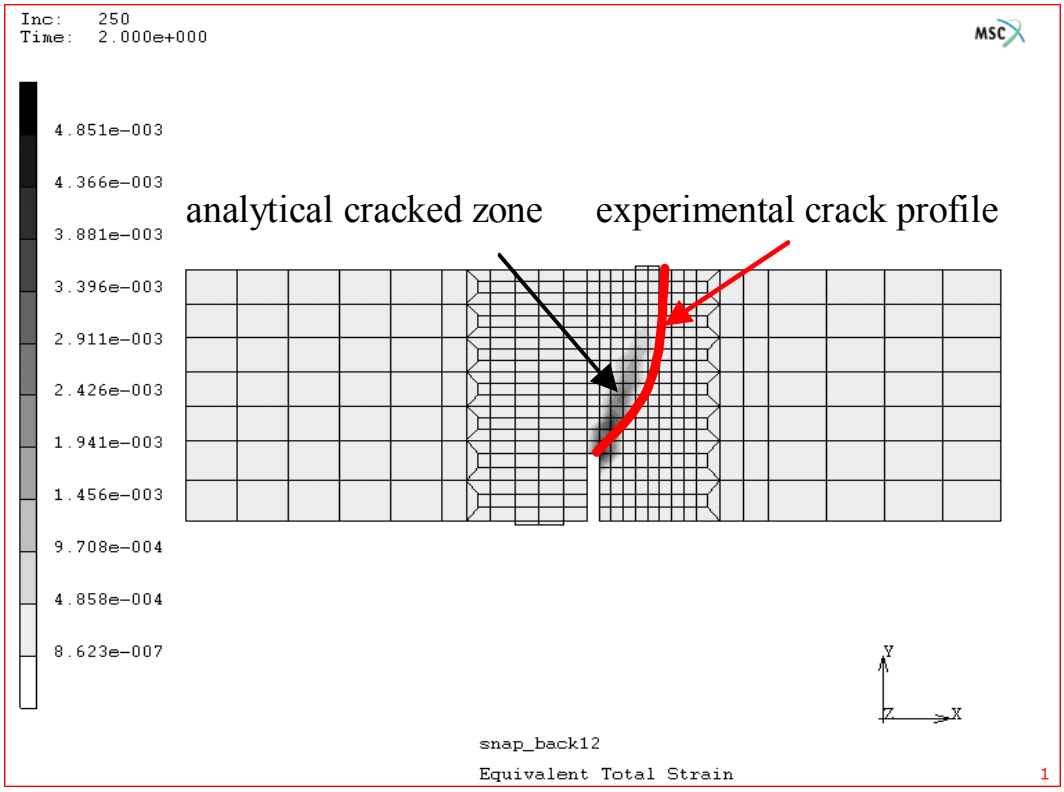

Figure 5.12 - Crack profiles

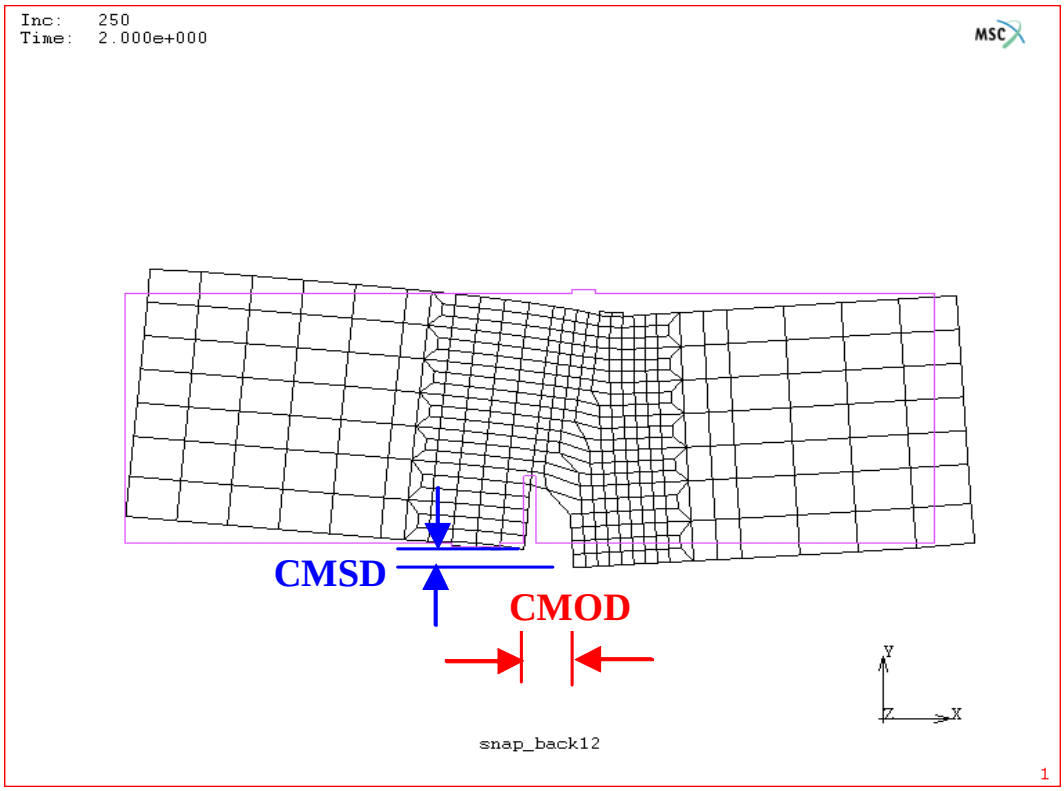

Figure 5.13 - Predicted deformation

5.4 Case 3: mesh objectivity and second-order elements validation

A single-notched, three-point loaded beam is used to validate the mesh objectivity of the FE analysis of concrete fracture and the use of second-order elements for the implementation of the cracking model. This specimen was tested experimentally by Bažant & Pfeiffer (1987) and numerically investigated by Bhattacharjee & Leger (1993).

The material properties are adopted from Bhattacharjee & Leger (1993) and are listed below. The specimen is shown in Figure 5.14. Linear strain softening is selected for comparison purposes. Shear softening does not influence the peak load in this specific application in which mode I fracture propagation is dominant.

Young's modulus E = 27 413 MPa;	Tensile strength f_t = 2.886 MPa
Poisson's ratio υ = 0.18;	Fracture energy G_f = 0.04029 N/mm
Thickness of beam = 38.1 mm;	Depth of beam d = 304.8 mm

The crack characteristic length h_c is dependent on the size of the elements at the crack in the different FE models used.

Three FE models with 6, 12 and 24 elements through the depth of the beam are created for the mesh objectivity study, as shown in Figures 5.15 to 5.17 (namely model 1). The three FE models in Figures 5.15 to 5.17 are also modelled by the eight-noded, second-order elements with full integration for the purpose of verifying the crack models implemented with high-order elements.

The loads P_0 required to cause a crack-tip tensile stress equal to the tensile strength f_t are determined using elastic bending theory and are given in Table 5.1 for the three FE models. The peak loading resistances P_u from the analyses for each of the three FE models are also shown in Table 5.1. Figure 5.18 compares the experimental results, the conventional elasto-brittle strength-based fracture analysis (labelled as SBM) and the numerical analysis done by Bhattacharjee and Leger (1993) (labelled as B&L 1993), by plotting the $\frac{P_u}{P_0}$ ratio versus the mesh fineness. Also shown in Figure 5.18 are the results

from this research (labelled as LS), which appear to be mesh objective since the fineness of the mesh has practically no influence on the predicted response, unlike the SBM analyses. The difference in results between the strain-softening models and the experimental findings, as explained by Bhattacharjee and Leger (1993), stems from the fact that the constitutive model parameters had to be assumed since they were not available from the experimental results.

The peak loading resistance P_u from the analyses of the three FE models of the second-order elements and the related $\frac{P_u}{P_0}$ ratio are shown in Table 5.2.

The results from the first-order element models and the second-order element models for the three different mesh finenesses in Figures 5.15 to 5.17 are compared in Figure 5.19. It is clear that the analyses based on the implemented crack models are objective with regard to the different order elements used.

TABLE 5.1 - Loads from elastic bending theory and FE analyses for different mesh finenesses – first-order elements

Mesh fineness (number of elements through the depth)	P_0 **(kN)**	P_u **(kN)**	$\frac{P_u}{P_0}$
Coarse mesh – 6 elements	6.65	7.304	1.098
Medium mesh – 12 elements	6.42	7.064	1.100
Fine mesh – 24 elements	6.31	6.936	1.099

TABLE 5.2 - Loads from elastic bending theory and FE analyses for different mesh finenesses – second-order elements

Mesh fineness (number of elements through the depth)	P_0 **(kN)**	P_u **(kN)**	$\frac{P_u}{P_0}$
Coarse mesh – 6 elements	6.65	7.330	1.102
Medium mesh – 12 elements	6.42	7.036	1.096
Fine mesh – 24 elements	6.31	6.860	1.087

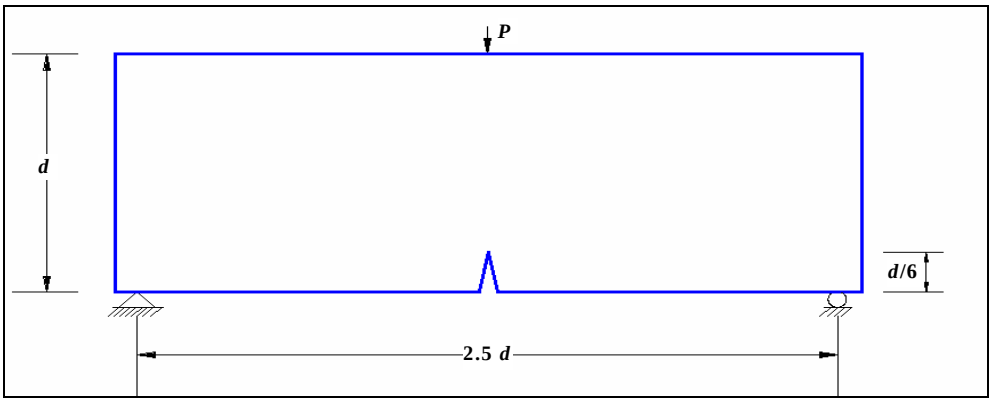

Figure 5.14 - Geometric configurations and boundary conditions

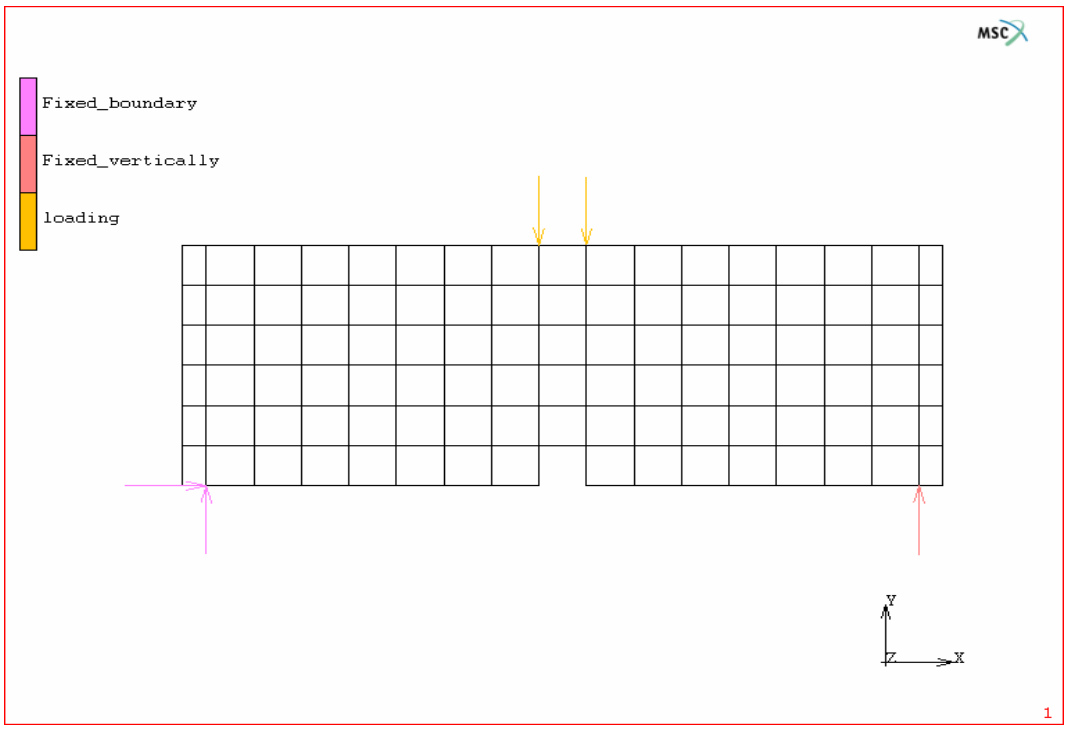

Figure 5.15 - Coarse model 1 – 6 elements in depth

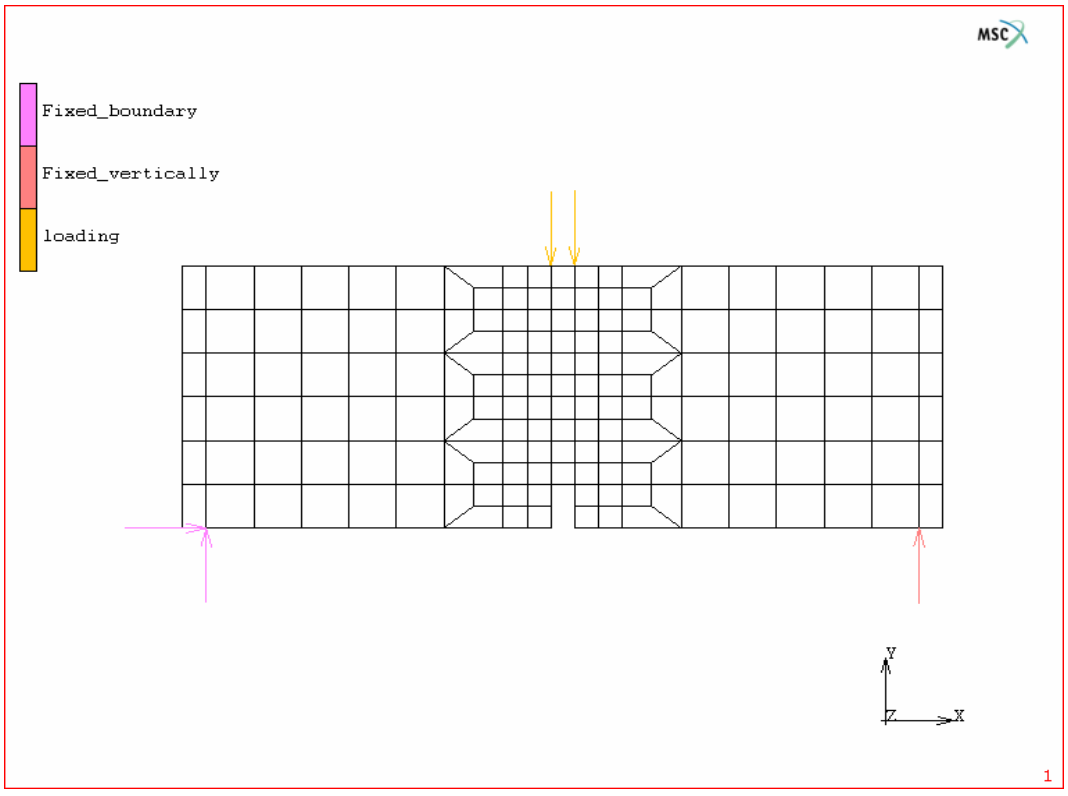

Figure 5.16 - Medium model 1 – 12 elements in depth

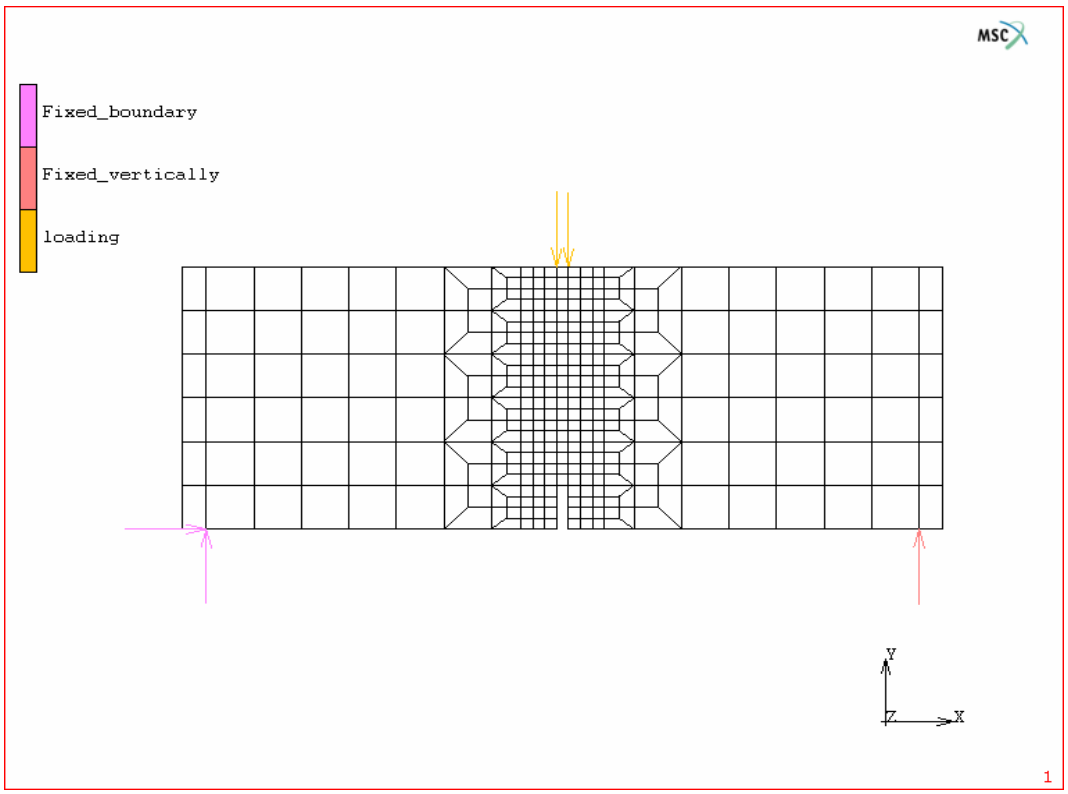

Figure 5.17 - Fine model 1 – 24 elements in depth

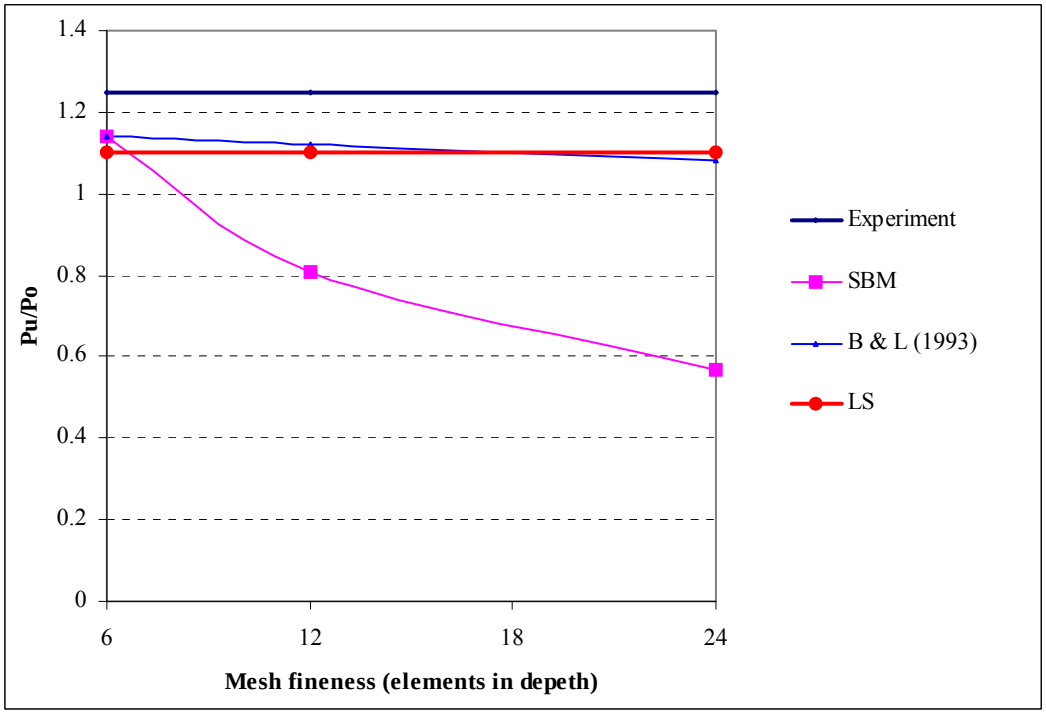

Figure 5.18 - Comparison of mesh objectivity (models 1)

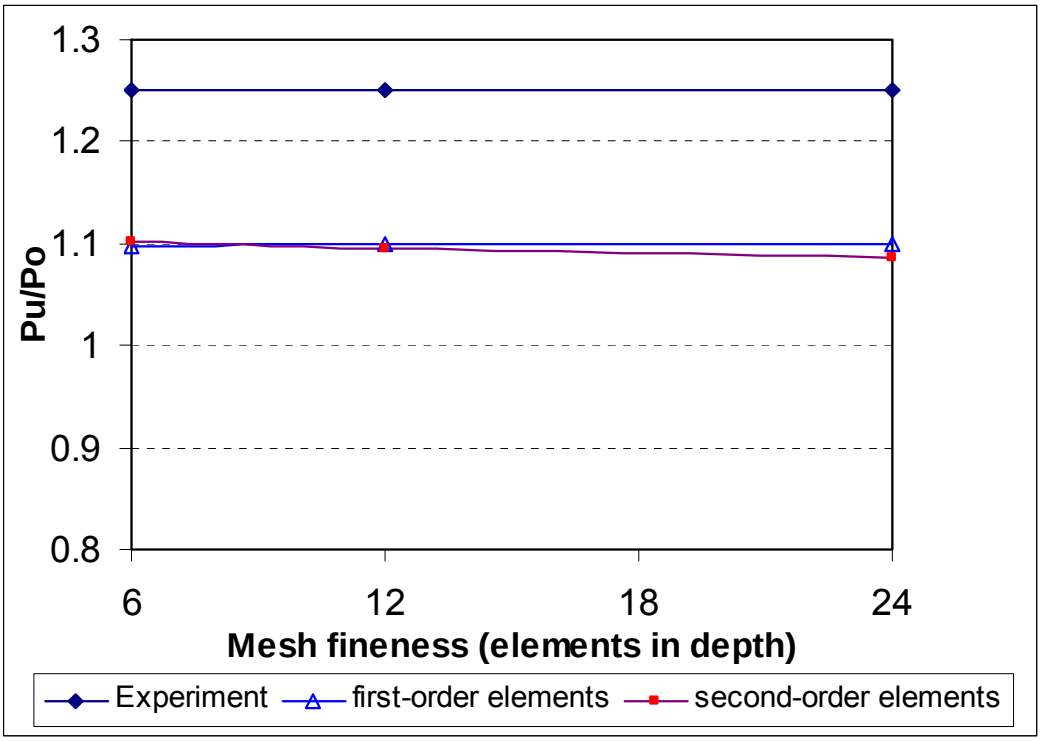

Figure 5.19 - Comparison of element objectivity (models 1)

The above mesh objectivity verification analyses have the following limitations:

- The width of the notch in the three meshes is not fixed but varies with the element size used in the mesh.
- The loadings in the three mesh models are not applied at the same distance to the centreline of the models, but vary with the element size used.

Therefore, a further mesh objectivity study was carried out to eliminate the above-mentioned limitations. The following three mesh models (namely model 2) (see Figures 5.20 to 5.22) are created in this study based on the same beam configurations. All the material properties and boundary conditions are the same as above. The only difference between these three mesh models (Figures 5.20 to 5.22) and those in the previous mesh objectivity study (Figures 5.15 to 5.17) is that the position of the loadings and the width of the notches are kept the same in order to achieve the aim of this mesh objectivity verification.

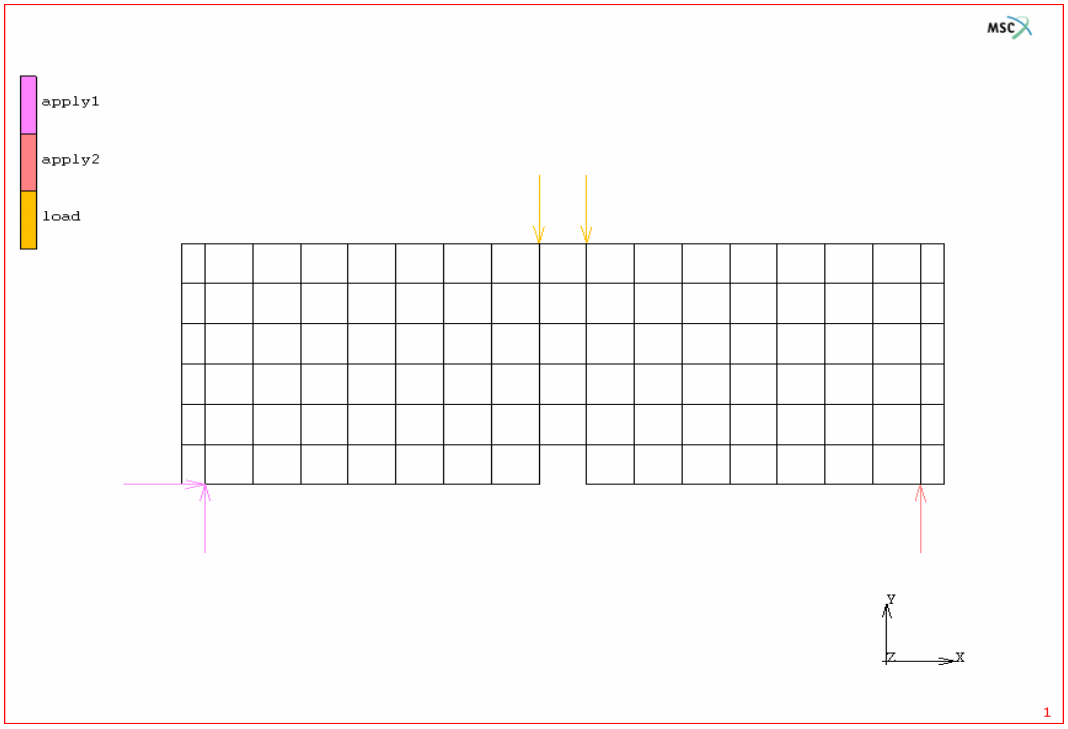

Figure 5.20 - Coarse model 2 – 6 elements in depth

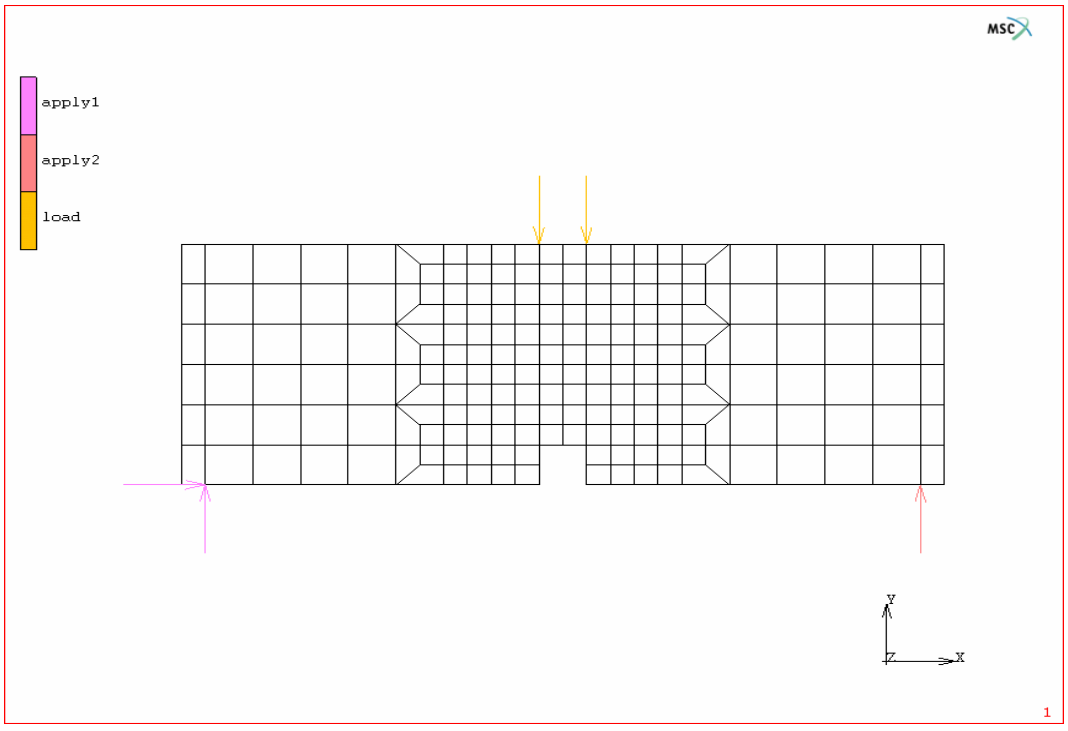

Figure 5.21 - Medium model 2 – 12 elements in depth

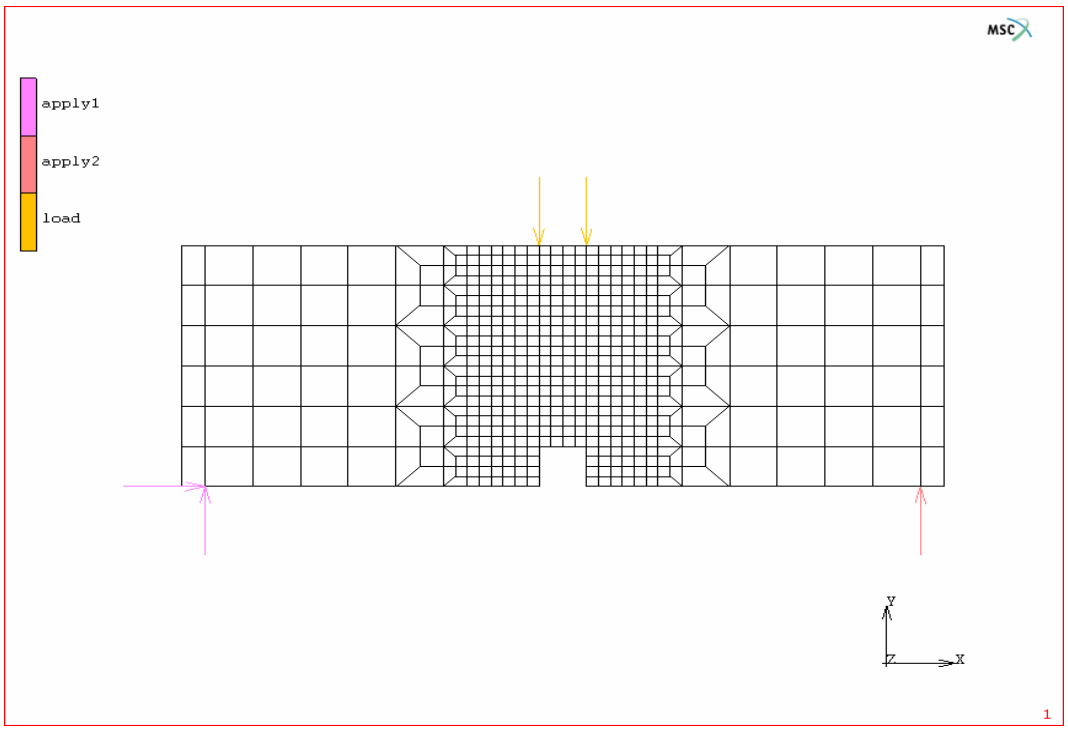

Figure 5.22 - Fine model 2 – 24 elements in depth

The results of the analyses are shown in Figure 5.23 in which it can be seen that the crack analysis method and procedures developed can be regarded as mesh objective. Different meshes only result in a maximum discrepancy of approximately 7% in the result of the $\frac{P_u}{P_0}$ ratio.

It can be concluded from the verification studies on mesh objectivity that the proposed crack model and the numerical technique developed achieve the goal of mesh objectivity.

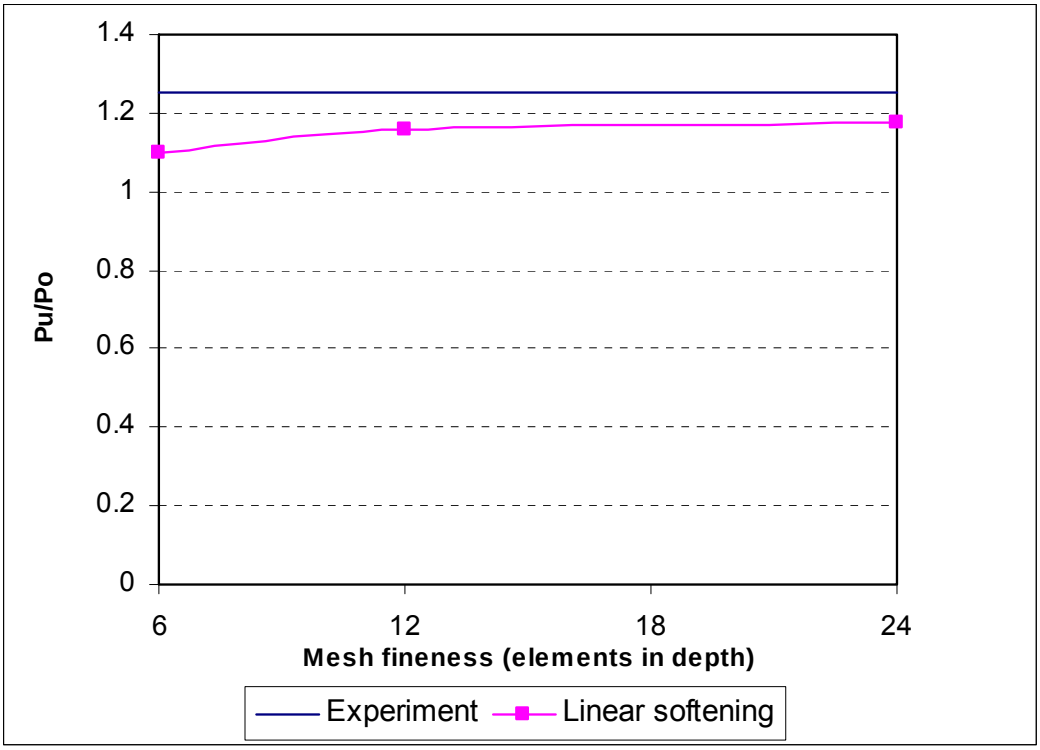

Figure 5.23 - Comparison of mesh objectivity (models 2)

5.5 Conclusion

In this chapter, a comprehensive study on the versatility and accuracy of implementation of the proposed smeared crack FE model, based on non-linear fracture mechanics for concrete structures, has been carried out for the purpose of eventually applying the constitutive model in predicting the crack behaviour of concrete dams and in evaluating dam safety.

A three-point, single-notched beam was considered for the comparative study on linear, bilinear and non-linear experimental curved softening, with experimental load-deflection relationships. The parametric bilinear shape study shows that if α_1 and α_2 are set in the vicinity of 1/3 and 0.1 respectively, which is a good approximation to the experimental non-linear softening curve of Cornelissen *et al*. (1986), very good numerical results are obtained compared with the results of the experiment. It can be concluded that a bilinear softening analysis yields significantly better results than the linear softening solutions mostly adopted in concrete cracking analysis, and that it can be applied with confidence in the fracture analysis of concrete structures.

Normal and shear stress field prevailingly exists in concrete structures. Therefore, it is very important to validate the adopted numerical procedure in mixed mode application. A mixed-mode fracturing beam were analysed with the results demonstrating that bilinear mode I softening is superior to the linear strain softening.

The mesh and element-order objectivity of the numerical method developed was observed in the analysis of a three-point, single-notched beam.

Based on these case studies, the following conclusions are drawn:

- The crack model is valid for both mode I and mixed-mode fracture analysis.
- The proposed bilinear softening model remains relatively simple to implement, but significantly improves the prediction of the softening response.
- The proposed method is mesh objective and could overcome problems such as non-convergence and snap-back.
- The proposed method is element-order objective.

CHAPTER VI - STATIC FRACTURE ANALYSIS OF CONCRETE GRAVITY DAMS

6.1 Introduction

In the preceding chapter, Chapter V, small-scale concrete structures of beams were analyzed under mode I or mixed-mode fracture loadings. It is necessary to verify the localized strain-softening constitutive models and the program developed on large-scale structures, such as concrete gravity dams, before the crack analysis method developed here is eventually applied for evaluating the safety of a real concrete gravity dam subjected to cracking.

Due to the low tensile resistance of concrete, cracking in concrete dams is a common phenomenon. Accurate prediction and evaluation of the crack propagation trajectory, and of the structural response due to rising water levels, are very important and necessary to establish safety of a dam. Concrete gravity dams are, in general, subjected to both flexure and shear loadings, which would induce mixed-mode fracturing. This co-existence of mode I tensile strain softening and mode II shear strain softening influences the prediction of the structure's fracture resistance.

The objective of this chapter is to investigate the applicability of the crack models to large concrete structures, such as concrete gravity dams, and to validate the results using past experimental and numerical investigations.

Firstly, a model of a concrete gravity dam scaled down to 1:40, tested and numerically analyzed by Carpinteri *et al*. (1992), Bhattacharjee & Leger (1994) and Ghrib & Tinawi (1995), is analyzed to determine its fracture-development response. Thereafter, analyses on full-scale gravity dams, an 80-m-high "benchmark" dam adopted by Network Integrity Assessment of Large Concrete Dams (NW-IALAD 2005) and the existing 103-m-high Koyna Dam, are carried out for the purpose of comparing the structural results and the crack profiles with those of other published research.

6.2 Model concrete dam

A scaled-down 1:40 model concrete gravity dam tested by Carpinteri *et al*. (1992) is considered to validate the crack model and implementation procedure. The model had a pre-assigned horizontal notch on the upstream face at 1/4 of the height and was subjected to a lateral loading which simulated the hydrostatic pressure (shown in Figure 6.1).

A plane stress finite element (FE) model with four-noded, full integration elements with a thickness of 30 cm (the same as used by Bhattacharjee & Leger 1994) has been adopted. A fixed boundary condition is applied along the bottom line of the model. Four concentrated loads, with different percentages of the total applied force, are applied directly to the upstream wall (shown in Figure 6.1) similar to the experiment.

The geometric dimensions, material properties and fracture parameters used in this verification are listed in Table 6.1.

TABLE 6.1 - Model parameters (model dam)

Dimensions of the model (m)		**Constitutive parameters**	
Dam height	2.55	Young's modulus E (MPa)	35 700
Crest width	0.248	Poisson's ratio v	0.1
Bottom width	2.0	Mass density (kg/m^3)	2 400
Notch/depth ratio	0.2	Tensile strength f_t (MPa)	3.6
Thickness of the model	0.3	Fracture energy G_f (N/m)	184
		Crack characteristic length h_c (mm)	80
		Maximum shear retention factor β_{max}	0.1
		Threshold angle	30^o

In the experiment, the crack mouth opening displacement (CMOD) was used as a control parameter to monitor and adjust the applied load. As stated in Section 5.3 in Chapter V, the main program – MSC.Marc cannot carry out the "indirect displacement control" scheme using CMOD as a control parameter. In Chapter V, a tedious manual procedure was adopted to obtain the peak load and the snap-back phenomenon, but this will not be repeated in this analysis of the model dam. Therefore, this model is loaded up to the peak

total applied force, of approximately 750 kN, as obtained in the experiment (Carpinteri *et al*. 1992) and other numerical investigations (Bhattacharjee & Leger 1994 and Ghrib & Tinawi 1995). After that, linear unloading is applied to the model. The strains and thus the crack propagation path are obtained, and are shown in Figure 6.2. The experimentally observed crack is also shown. The predicted crack profile appears to be propagating correctly, firstly in a horizontal direction and then bending downward (due to the high compressive stresses). The cracking could not propagate downward as deeply as observed in the experiment, most probably due to the presence of stress-locking in the smeared analysis. Since the self-weight of the model was not successfully simulated in the experiment (due to premature failure along the foundation interface; refer to Bhattacharjee & Leger 1994), the results obtained in this validation only demonstrate the capability of the proposed crack model and the developed subprogram in predicting crack propagation in a dam-shaped structure. Full-size dams with the gravity effect will have to be used to further validate the constitutive model and the implementation procedure.

A linear softening modulus was used to analyze the fracture response of the model dam numerically. An effort was made to obtain the maximum total applied force which is in agreement with the experimental and numerical results as shown in Figure 6.3. No attempt was made to obtain the unloading curve in relation to CMOD due to the lack of an "indirect displacement control" scheme in MSC.Marc, as stated before.

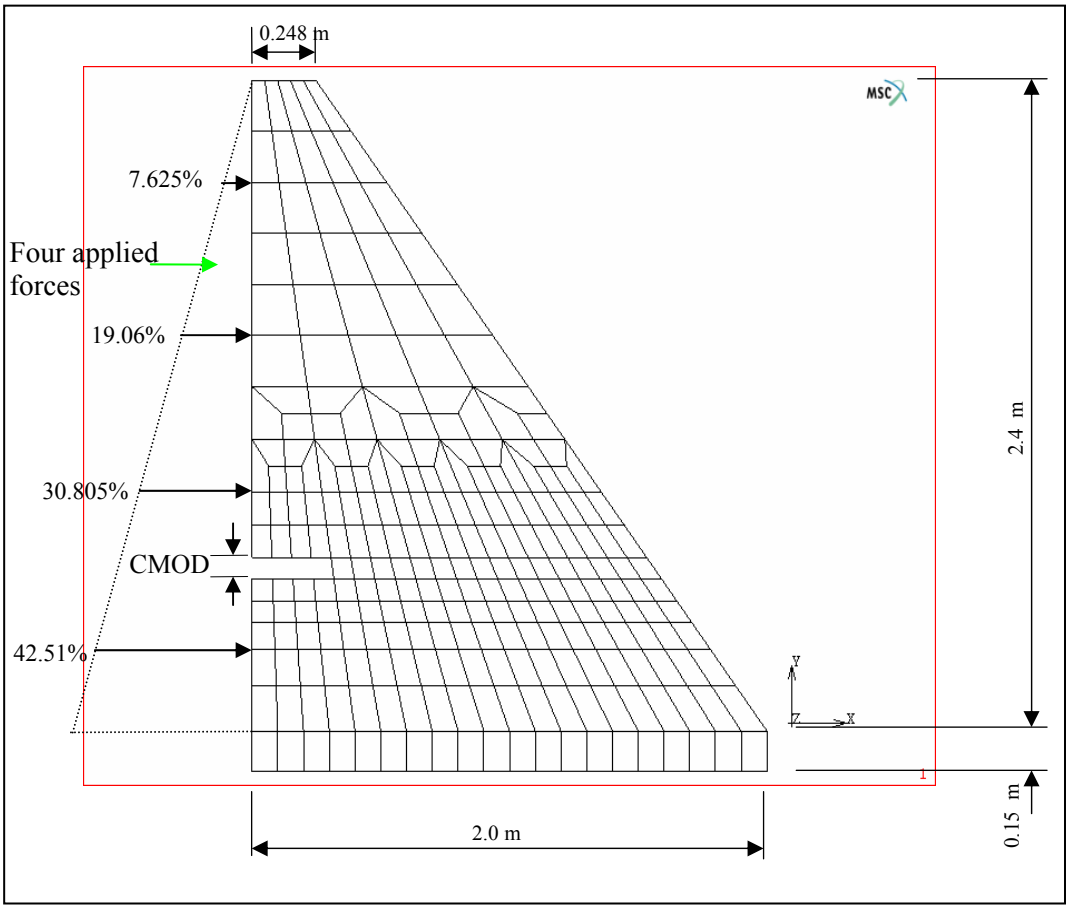

Figure 6.1 - Finite element model of concrete dam model and applied loads

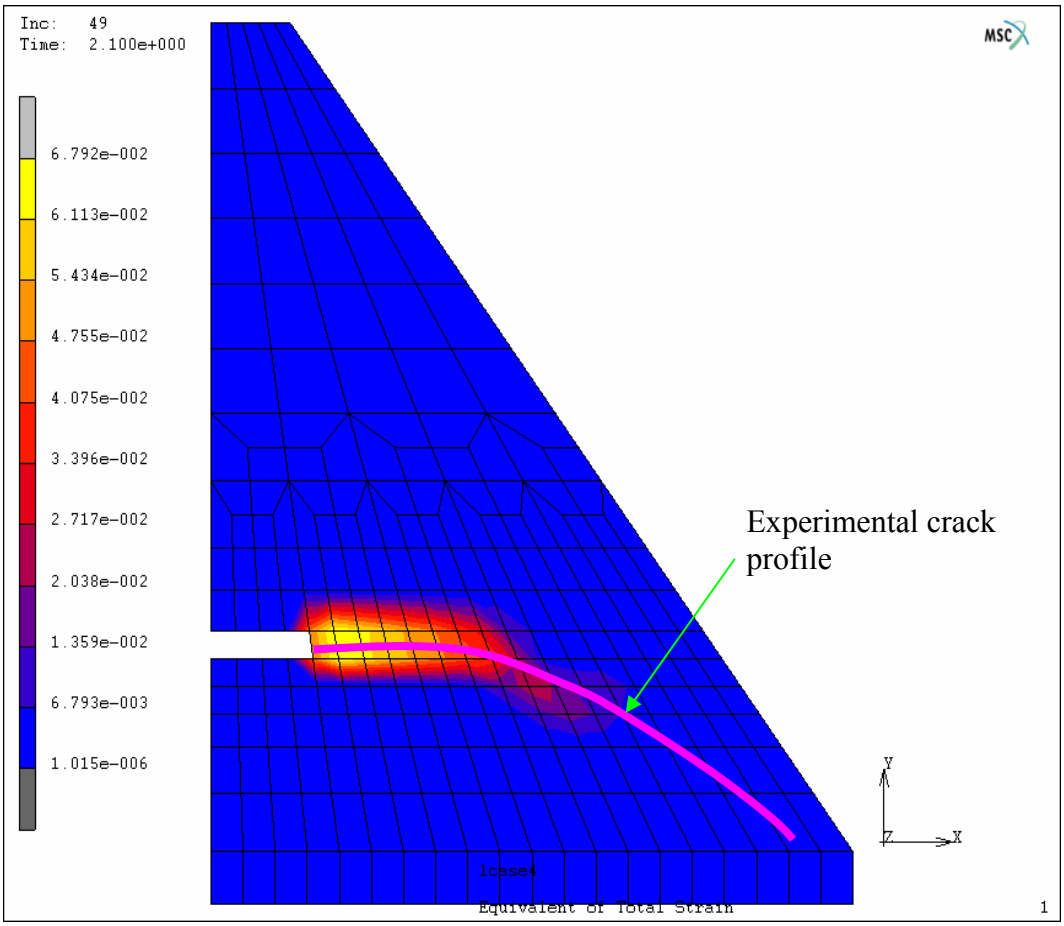

Figure 6.2 - Strains and crack profiles in the model dam

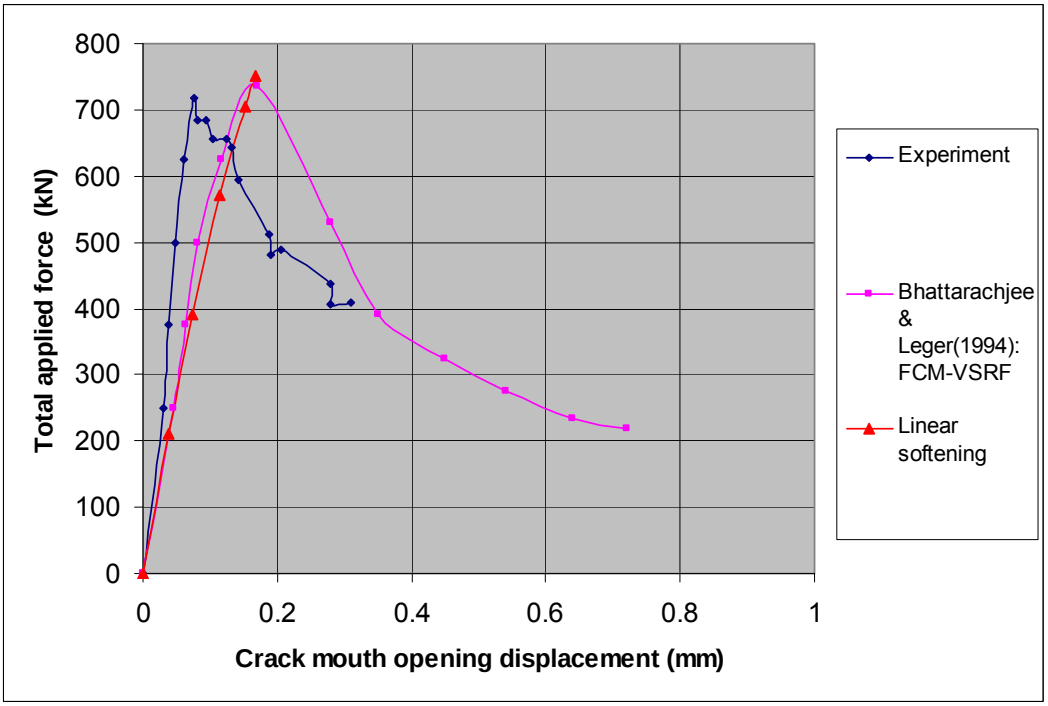

Figure 6.3 - Total force vs. CMOD response in the model dam

6.3 A concrete gravity dam adopted by NW-IALAD

An internet platform (http://nw-ialad.uibk.ac.at) was established by collaborating with researchers from across Europe to benchmark, amongst others, the fracture response of the chosen model of a concrete gravity dam using different FE analysis packages. The project was known as Network Integrity Assessment of Large Concrete Dams (NW-IALAD) and had a duration of three years from 01/05/2002 to 30/04/2005. The objective was the systematic comparison of the existing FE programs for the analysis of cracked concrete dams based on fracture/damage mechanics, which would help to identify their applicability to these problems and future developmental needs.

Three cases ('arrangements') were provided for the benchmark exercise to suit the capabilities of the different programs. Arrangement 2 in the benchmark exercise was selected for this verification purpose. The details of the arrangement are as follows.

The analysis was carried out for the self-weight of concrete and horizontal hydrostatic pressure, with the water level in the dam increasing gradually to the crest level (80 m) and then continuing to overflow to the maximum water level. Only the concrete wall was allowed to crack and no cracking was considered in the rock (Jefferson, Bennett & Hee 2005).

The model of the concrete gravity dam selected for the benchmark exercise is shown in Figure 6.4. The height of the dam was 80 m, with a crest width of 5 m and a base width of 60 m. The rock foundation was set at 120 m from each edge of the dam wall and 80 m deep below the base of the concrete dam. It was assumed that a perfect bond exists between the concrete wall and the rock foundation. The degrees of freedom on the foundation boundary were fully fixed (see Figure 6.5).

The above model was also analyzed by other researchers (Jefferson *et al.* 2005) using the FE programs LUSAS and DIANA. The same model parameters and loadings were assumed, except for the maximum hydrostatic overflow loading, which was set at 100 m and 90 m respectively for LUSAS and DIANA.

Linear and bilinear softening models were used to analyze the fracture response of the dam for the verification purpose. Uplift water pressure was not included in the analysis. The elements used are four-noded, full-integration quadrilateral plane strain elements. The analysis was carried out using a modified Newton-Raphson solution for the non-linear equations.

The fracture parameters used are as follows: bilinear shape parameters α_1 = 1/3 and $\alpha_2 = 0.1$; threshold angle = 60°; maximum shear retention factor β_{max} = 0.2; crack characteristic length h_c = 2 680 mm; concrete tensile strength f_t = 1.5 MPa and concrete fracture energy G_f = 150 N/m.

The material properties used in this verification are as given in Table 6.2.

TABLE 6.2 - Model parameters (NW-IALAD)

Constitutive parameters of concrete		**Constitutive parameters of rock**	
Young's modulus E (MPa)	24 000	Young's modulus E (MPa)	41 000
Poisson's ratio v	0.15	Poisson's ratio v	0.1
Mass density (kg/m^3)	2 400	Mass density (kg/m^3)	0

The crack profile of this analysis was plotted against the crack plot reported from LUSAS (Jefferson *et al.* 2005) and showed good agreement, although the crack for this analysis extended a little further and in a wider area (refer to Figure 6.6).

The results of the fracture analysis were compared with those from LUSAS and DIANA (Jefferson *et al.* 2005) in the relationship of the water level (overflow) vs. the crest displacement, as shown in Figure 6.7. The results for the displacement appear to be of the same order. The LUSAS results showed a bend, capturing the overall change in stiffness after cracking, while the DIANA results were still in a straight-line form. The results of linear softening in this research show less deformation than bilinear softening, which means that bilinear softening is more capable of simulating the loss of stiffness caused by fracture than linear softening. Nevertheless, both the linear and bilinear softening results of this analysis show a naturally bent curve, capturing the loss of stiffness in the cracked elements due to strain-softening behaviour and are in good agreement with the

displacement results from LUSAS and DIANA. In this research the analysis was terminated at a water level of approximately 92 m (only indication of the peak water level). This should not be regarded as the failure water level since no effort was made to increase the accuracy at failure by, for example, adjusting the convergence tolerance.

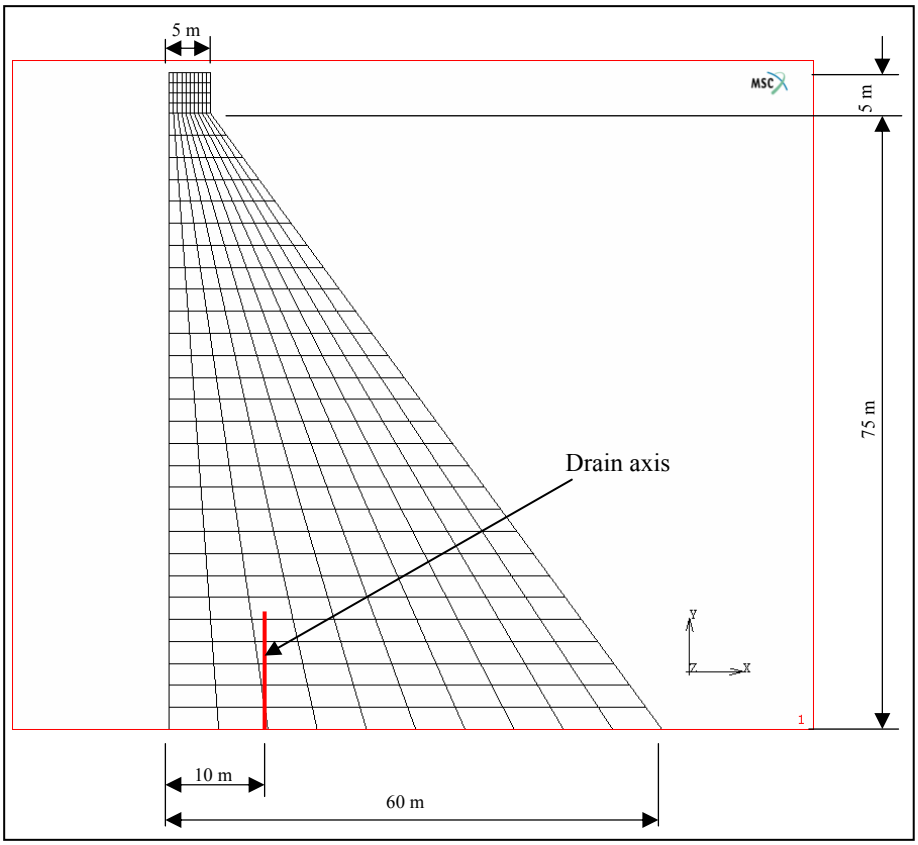

Figure 6.4 - Geometric configurations of concrete dam (NW-IALAD)

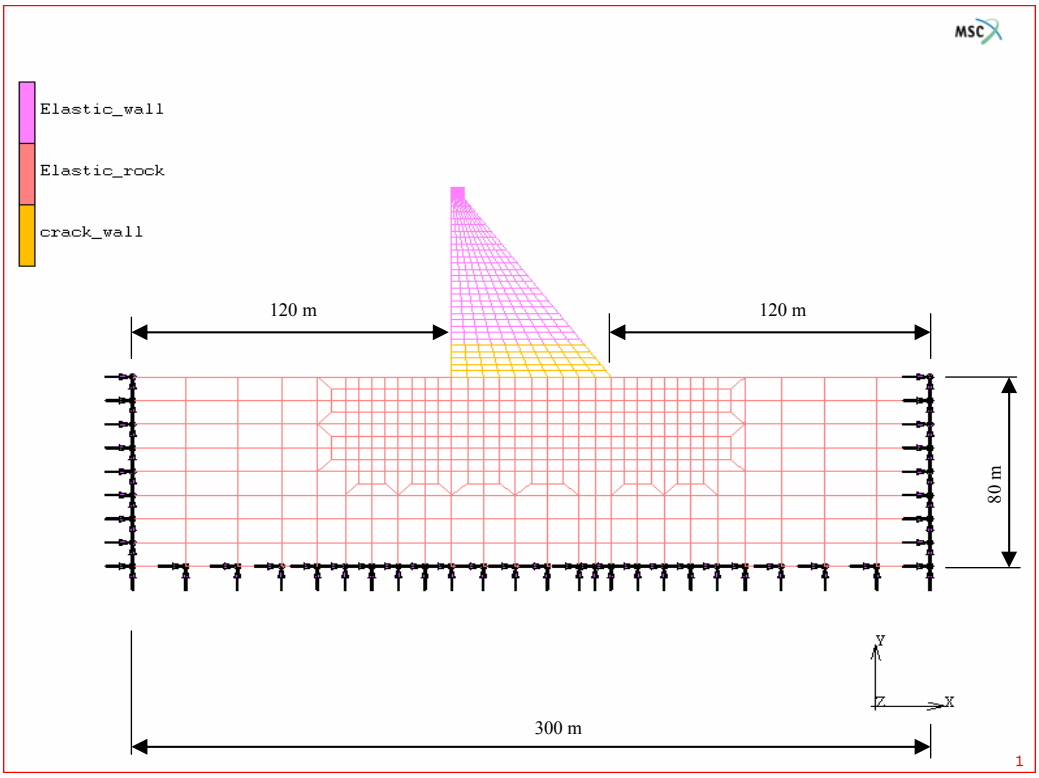

Figure 6.5 - Finite element model of concrete dam with rock foundation (NW-IALAD)

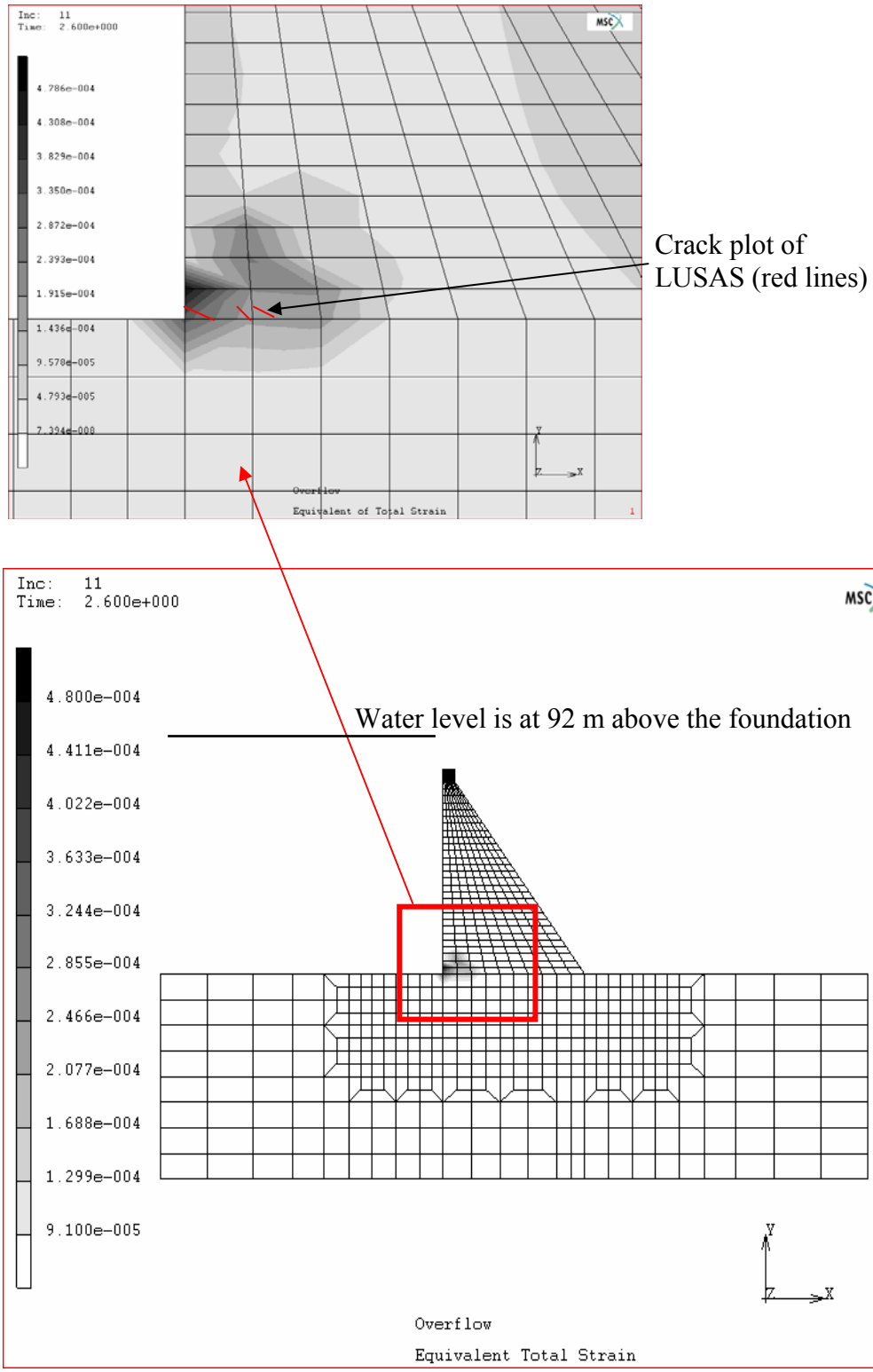

Figure 6.6 - Strain and crack plots for NW-IALAD dam

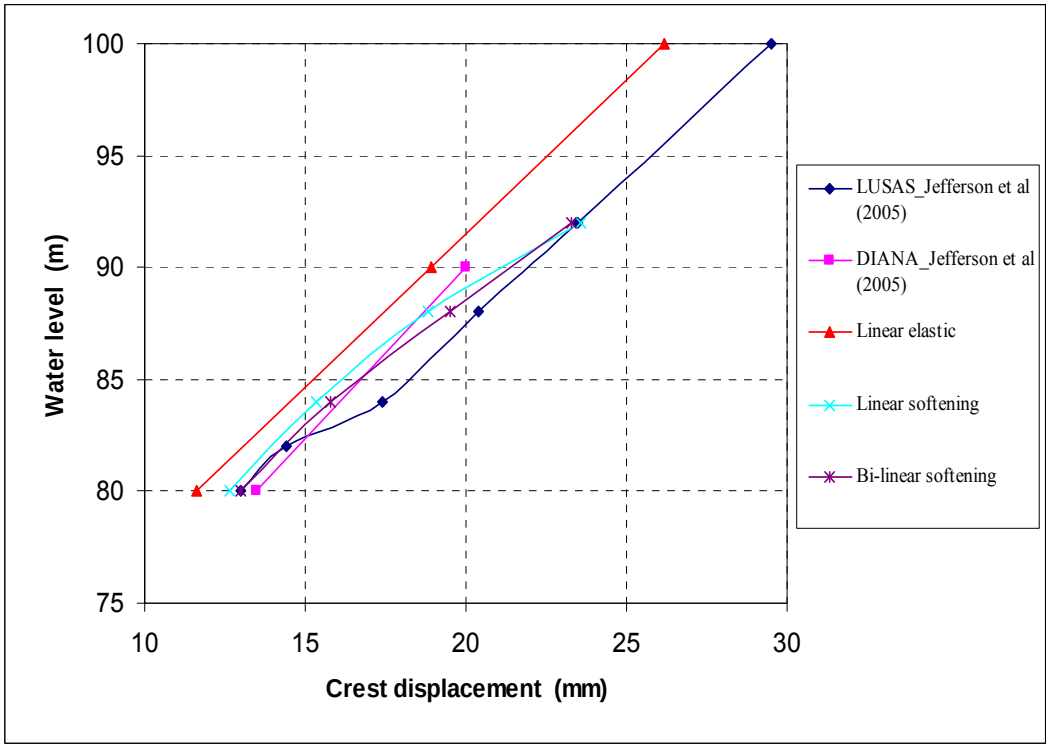

Figure 6.7 - Relationship of water level (overflow) vs. crest displacement (NW-IALAD)

6.4 Koyna Dam

Koyna Dam is a 103-m-high concrete gravity dam in India. This dam is widely used as a benchmark model in the literature for verifying the established concrete cracking models.

Gioia *et al.* (1992) analyzed this dam using a plasticity-based model and linear fracture mechanics under reservoir overflow. Three positions of a pre-set crack were studied and it was found that the crack located on the upstream side at the elevation of the slope change on the downstream face is the most critical position. Subsequently, Bhattacharjee & Leger (1994) and Ghrib & Tinawi (1995) analyzed this dam adopting this critical pre-existing crack position, using the smeared non-linear fracture mechanics and damage mechanics approaches respectively. In this study, the geometric configuration of the FE model is the same as in the FE model adopted by Bhattacharjee & Leger (1994) and Ghrib & Tinawi (1995), with a vertical upstream face as shown in Figure 6.8.

A plane stress model with four-noded, full-integration elements, subjected to gravity, hydrostatic pressure of full reservoir level and overflow loadings, is considered. No water pressure inside the cracks is considered in this study.

Table 6.3 gives the data used in the plane stress FE model and analysis.

TABLE 6.3 - Model parameters (Koyna Dam)

Dimensions of the model (m)		**Constitutive parameters**	
Dam height	103	Young's modulus E (MPa)	25 000
Crest width	14.8	Poisson's ratio v	0.2
Bottom width	70	Mass density (kg/m^3)	2 450
Width of dam at the level of initial notch h	19.3	Fracture energy G_f (N/m)	100 or 200
Depth of initial notch	0.1h	Tensile strength f_t (MPa)	1.0
		Crack characteristic length h_c (mm)	1 500

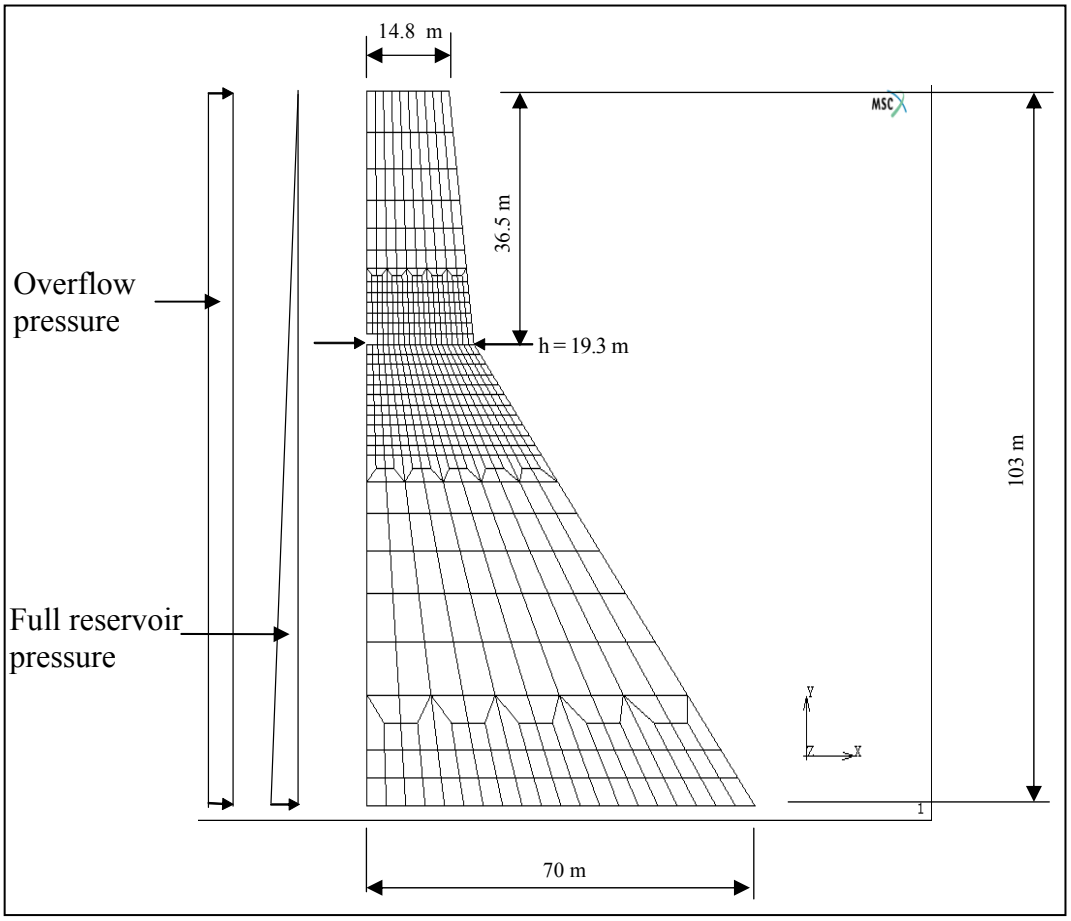

Figure 6.8 - Finite element model of Koyna Dam and applied loads

The purpose of the present analysis is to verify the implemented crack models on a full gravity dam under general gravity and hydrostatic pressure loads, and to undertake a sensitivity study on the following areas:

- Linear and bilinear strain-softening diagrams
- Fracture energy G_f
- Bilinear softening shape parameters (α_1 / α_2)
- Threshold angle
- Maximum shear retention factor β_{max}.

As shown in Figures 6.9 and 6.10, linear softening and bilinear softening (α_1 = 0.4; α_2 = 0.05) diagrams were used to predict the structural response in terms of crest displacement. The analyses were carried on two cases, with G_f = 100 and 200 N/m respectively. The fracture parameters used in the analyses were the threshold angle = 30^o and the maximum shear retention factor β_{max} = 0.1. It is clear that compared with the results from Bhattacharjee & Leger (1994), the bilinear softening diagram provides significantly better results than the linear softening diagram. The sudden drop over a short period predicted by Bhattacharjee & Leger (1994) could not be obtained in the present analysis due to the lack of an "indirect displacement control" scheme in the main program – MSC.Marc as stated previously in Chapter V.

The influence of the value of the fracture energy G_f on the predicted structural response was studied and is shown in Figures 6.11 and 6.12. The same constitutive fracture parameters were used as in the analyses shown in Figures 6.9 and 6.10. With the increase of the fracture energy G_f (from 100 to 200 N/m), the initial crack peak resistance of the dam structure is also increased. This initial stiffer response of the higher fracture energy (G_f = 200 N/m) following cracking, gradually becomes closer to the response of the lower fracture energy (G_f = 100 N/m) and eventually leads to a similar ultimate response for the two fracture energy G_f cases. Again, the bilinear softening solution is shown to provide a more accurate response than the linear softening solution.

The results of a study of the influence of the bilinear shape parameters α_1 and α_2 on the predicted structural response are shown in Figures 6.13 to 6.18. The fracture parameters used in the analyses are: fracture energy G_f = 100 N/m; threshold angle = 30^o and maximum shear retention factor β_{max} = 0.1. Figures 6.13 to 6.15 reveal that when α_1 is fixed at the values of 0.3, 0.4 and 0.44 respectively, while α_2 is increased from 0.1, 0.2 to 0.3, the structural responses are similar, with a slight increase in stiffness as α_2 increases.

In theory, when α_2 increases, the first softening modulus (absolute value) will decrease, while the second softening modulus (absolute value) will increase. This implies that the first softening modulus plays a more dominant role when the structure starts to crack. The fact that the smaller first softening modulus corresponds to the greater α_2 value means that localized softening provides a smaller and stiffer structural response. Gradually, the second softening modulus starts to influence the structural response, leading to a similar ultimate response for the different values of α_2.

When the value of α_2 is set to the values of 0.1, 0.2 and 0.3 respectively, while the values of α_1 increase from 0.3, 0.4 to 0.44, the predicted structural responses are similar, which means that α_1 does not have much influence on the structural response (refer to Figures 6.16 to 6.18).

The influences of threshold angle for the crack onset criterion and the maximum shear retention factor β_{max} on the predicted structural response were also studied and it was found that both values have a very limited influence on the overall structural response, as evidenced in Figures 6.19 and 6.20. The analyses were carried out with the fracture energy G_f = 100 N/m. The maximum shear retention factor β_{max} = 0.1 and the bilinear softening shape parameters α_1 = 0.4 and α_2 = 0.05 were used for the sensitivity study on the threshold angle. The threshold angle = 30^o and the bilinear softening shape parameters α_1 = 0.4 and α_2 = 0.05 were used for the sensitivity study on the maximum shear retention factor β_{max}. In theory, with an increase in the threshold angle, the crack numbers should decrease, leading to less loss of stiffness at the Gauss point and a stiffer response. If the maximum shear retention factor β_{max} becomes lower, the retained shear modulus

should become lower as well, and there is also less chance of the maximum principal stress exceeding the tensile strength, thus leading to lower crack numbers at the Gauss point and a stiffer response in the structure.

Since the threshold angle and the maximum shear retention factor β_{max} do not have much influence on the fracture response of the dam structure, their sensitivity to the crack profiles was not plotted. A bilinear softening study on the crack profiles was carried out for the reason that the bilinear softening modelling of crack behaviour is much better than the linear softening modelling for this structure.

Figures 6.21 and 6.22 indicate that the value of the fracture energy G_f does not have much influence on the crack profile. Due to a slightly softer response, the crack propagation path in the analysis with a fracture energy G_f = 100 N/m curves down a little more than the crack path in the analysis with a fracture energy G_f = 200 N/m.

Figures 6.22 to 6.26 are representative of the predicted crack profiles from the analyses based on the fracture energy G_f = 100 N/m, the threshold angle = 30^o and the maximum shear retention factor β_{max} = 0.1, with different combinations of the bilinear softening shape parameters α_1 and α_2.

As shown in Figures 6.21 to 6.26, the crack profiles predicted by introducing the different constitutive fracture parameters, such as the fracture energy G_f and the bilinear softening shape parameters (α_1/α_2), do not differ much and show good agreement with the crack profiles predicted by Bhattacharjee & Leger (1994). The crack profiles first stretch horizontally and then gradually bend downward owing to the existence of compressive stress on the downstream side.

It can be concluded from all the above sensitivity studies that the gravity force and hydrostatic pressure on the dam are so dominant that the localized fracturing influenced by the fracture energy G_f, the threshold angle, the maximum shear retention factor β_{max} and the softening shape parameters α_1 and α_2 does not affect the overall structural response significantly. In other words, as pointed out by Bhattacharjee & Leger (1994), the

structural response due to self-weight and hydrostatic pressure loads is much greater than that due to local material fracturing.

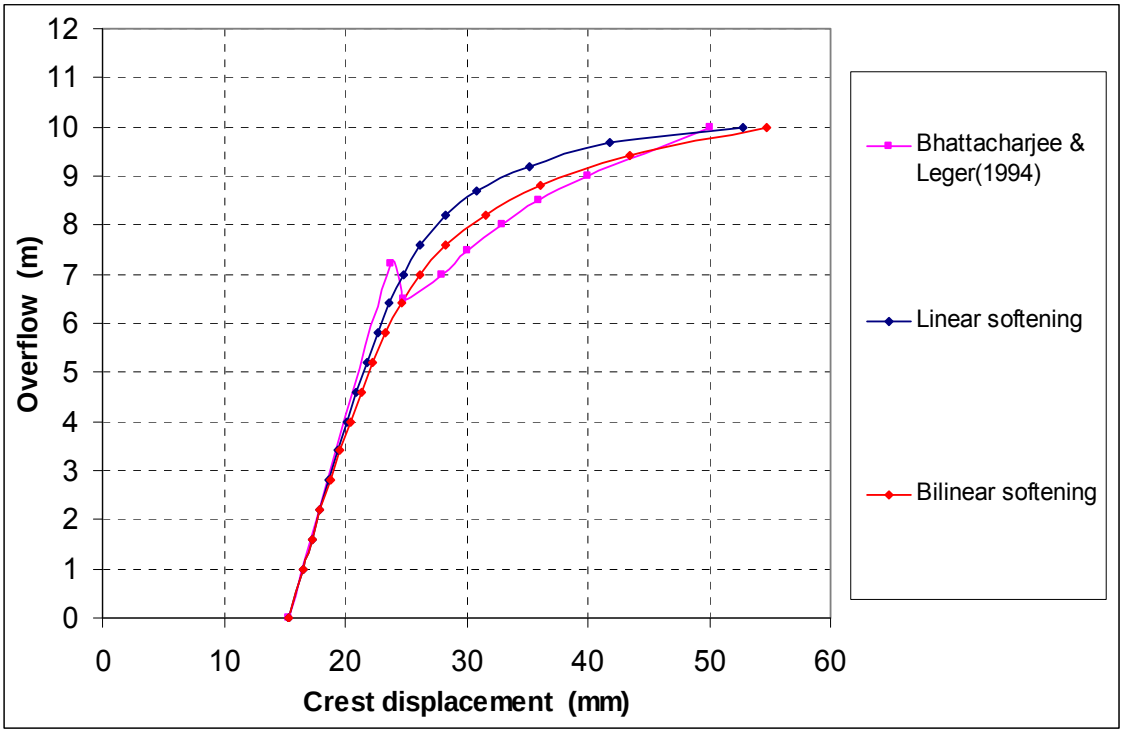

Figure 6.9 - Comparison of predicted responses to overflow load for different crack models (G_f = 100 N/m) (Koyna Dam)

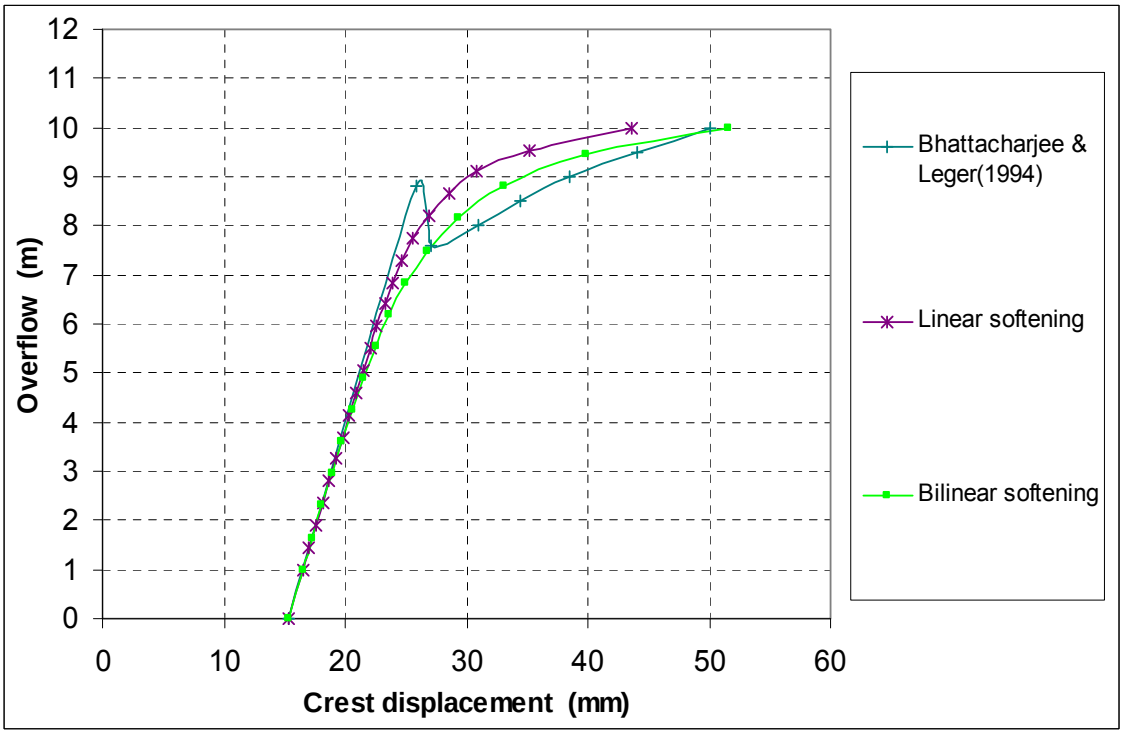

Figure 6.10 - Comparison of predicted responses to overflow load for different crack models (G_f = 200 N/m) (Koyna Dam)

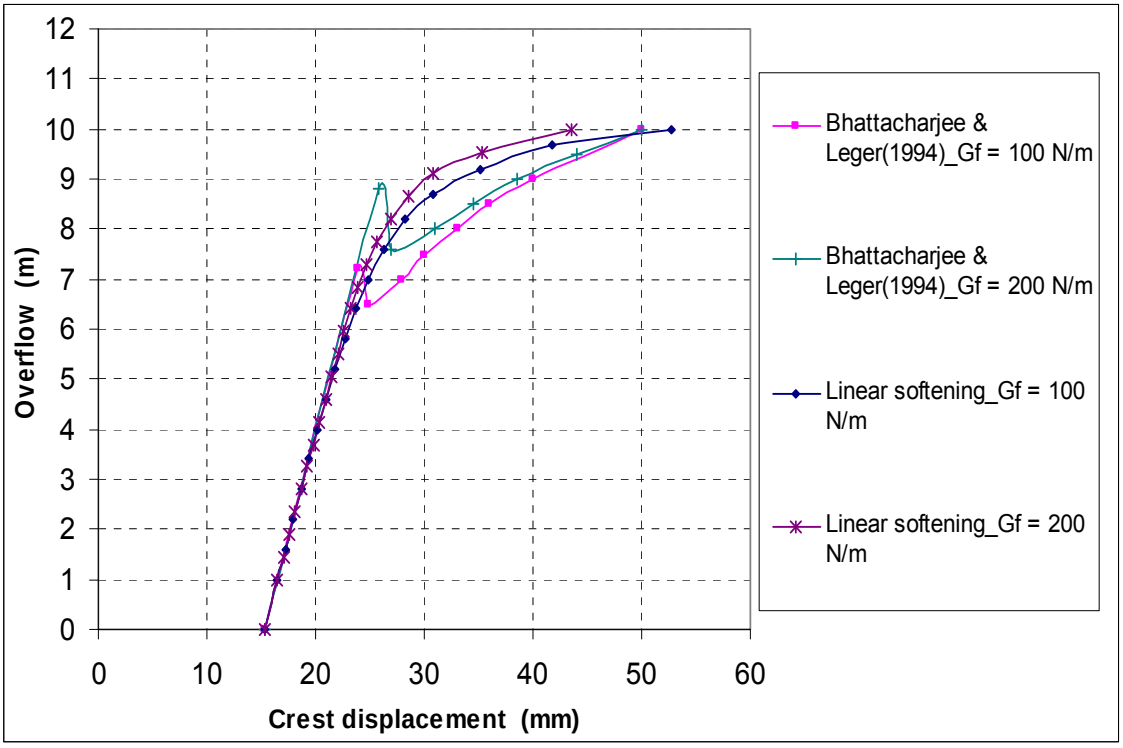

Figure 6.11 - Influence of fracture energy G_f on predicted structural response for linear softening models (Koyna Dam)

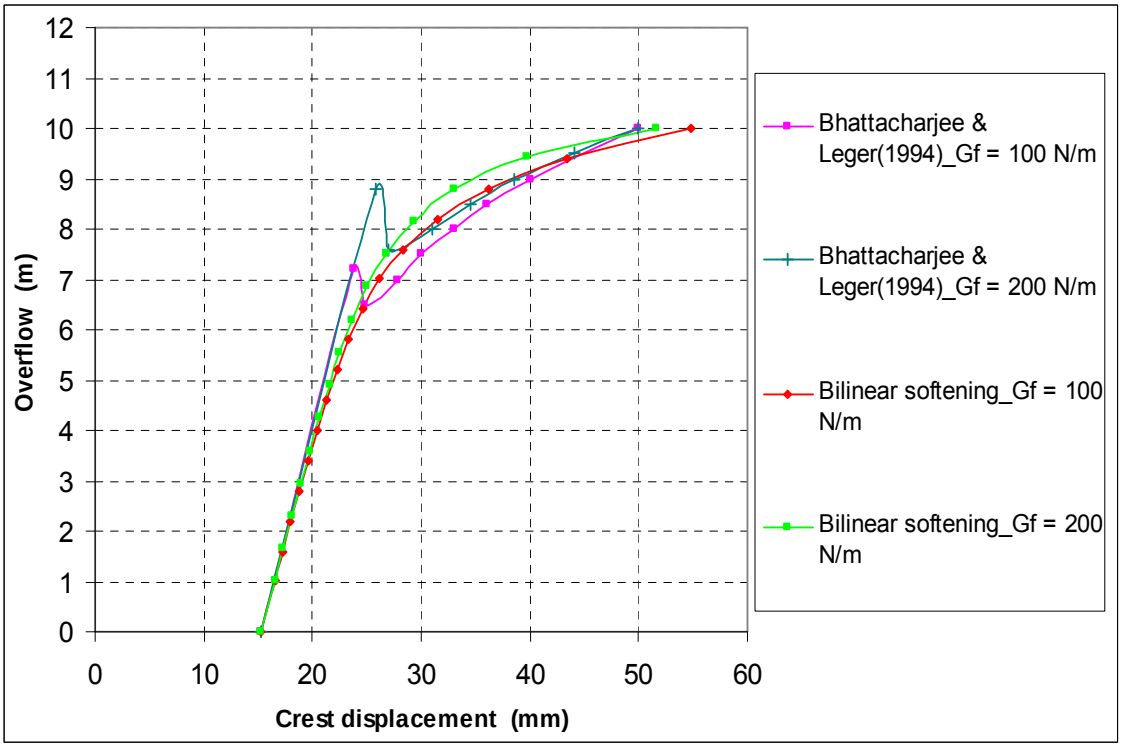

Figure 6.12 - Influence of fracture energy G_f on predicted structural response for bilinear softening models (Koyna Dam)

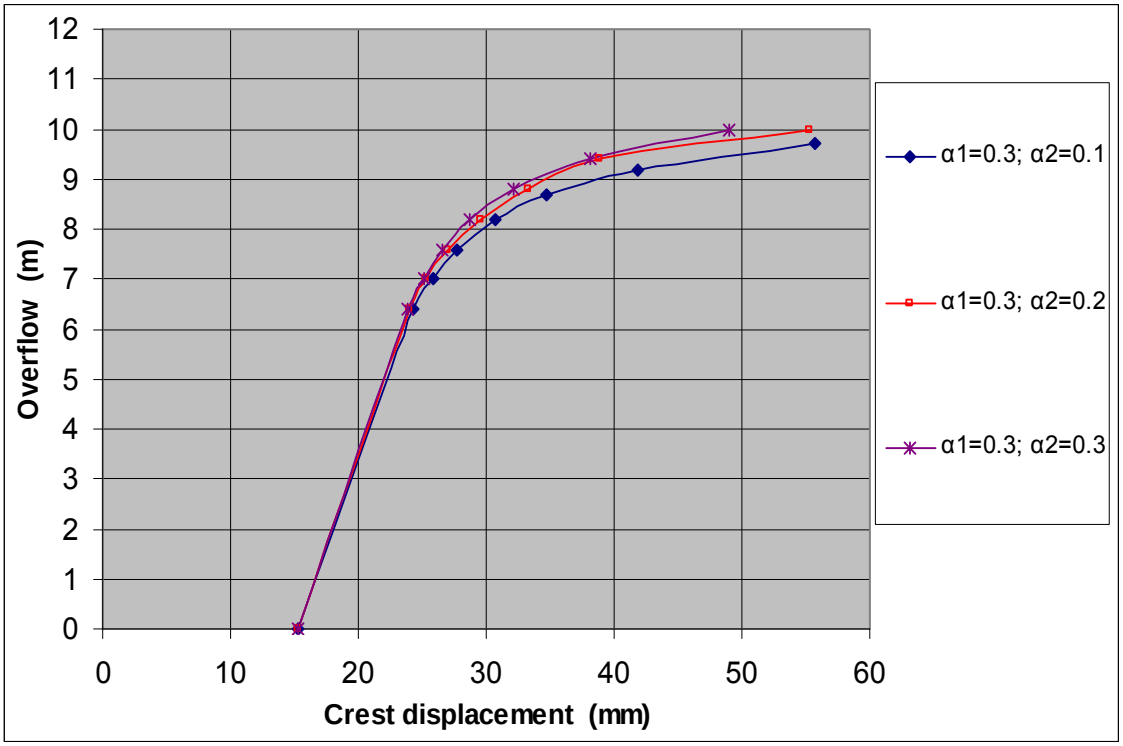

Figure 6.13 - Influence of bilinear softening parameters $\alpha_1 = 0.3$ and $\alpha_2 = 0.1$, 0.2 and 0.3 respectively on predicted structural response (Koyna Dam)

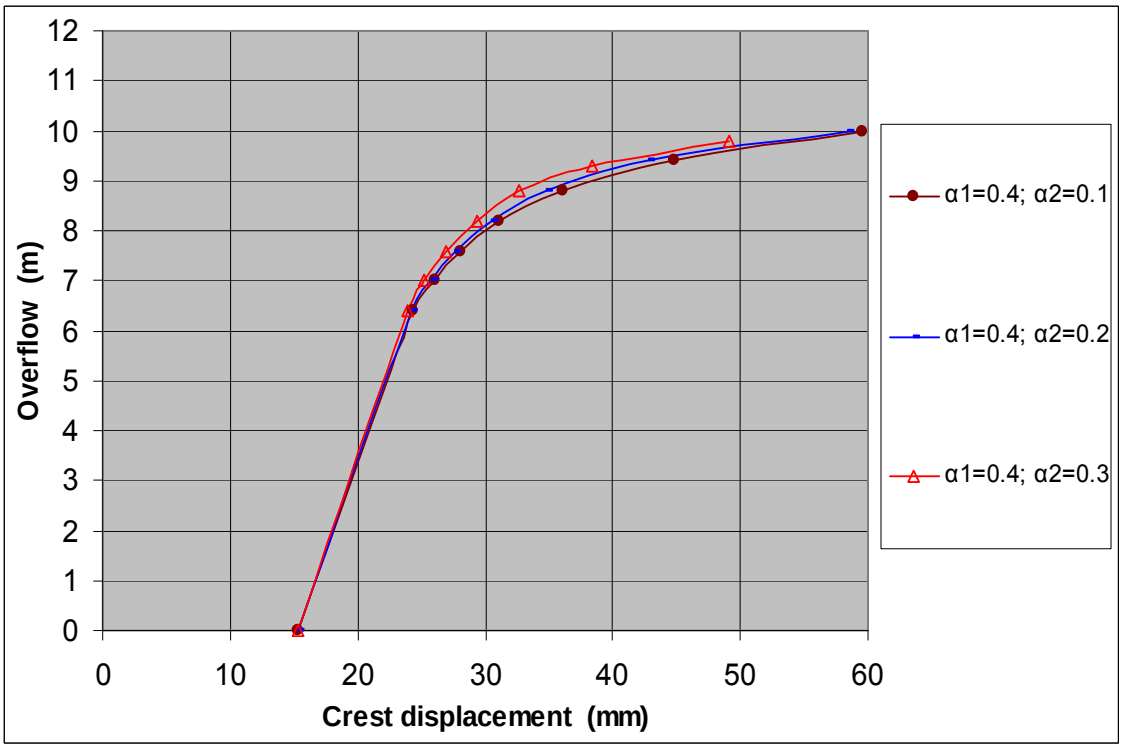

Figure 6.14 - Influence of bilinear softening parameters $\alpha_1 = 0.4$ and $\alpha_2 = 0.1$, 0.2 and 0.3 respectively on predicted structural response (Koyna Dam)

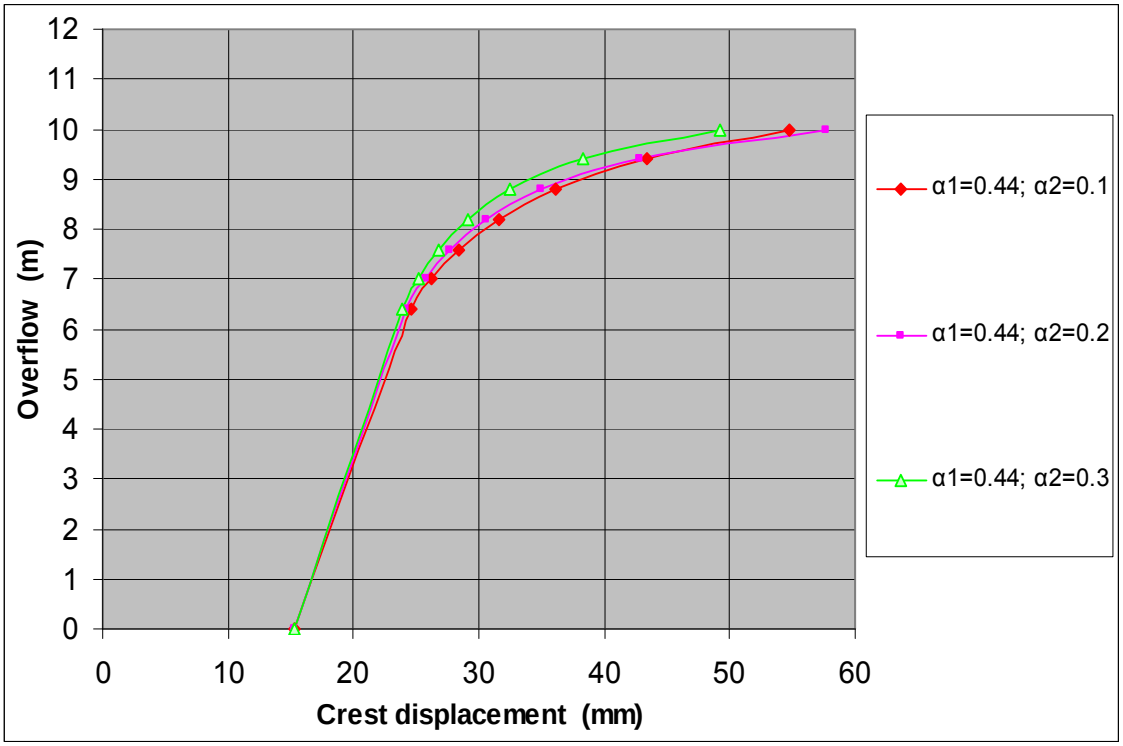

Figure 6.15 - Influence of bilinear softening parameters $\alpha_1 = 0.44$ and $\alpha_2 = 0.1$, 0.2 and 0.3 respectively on predicted structural response (Koyna Dam)

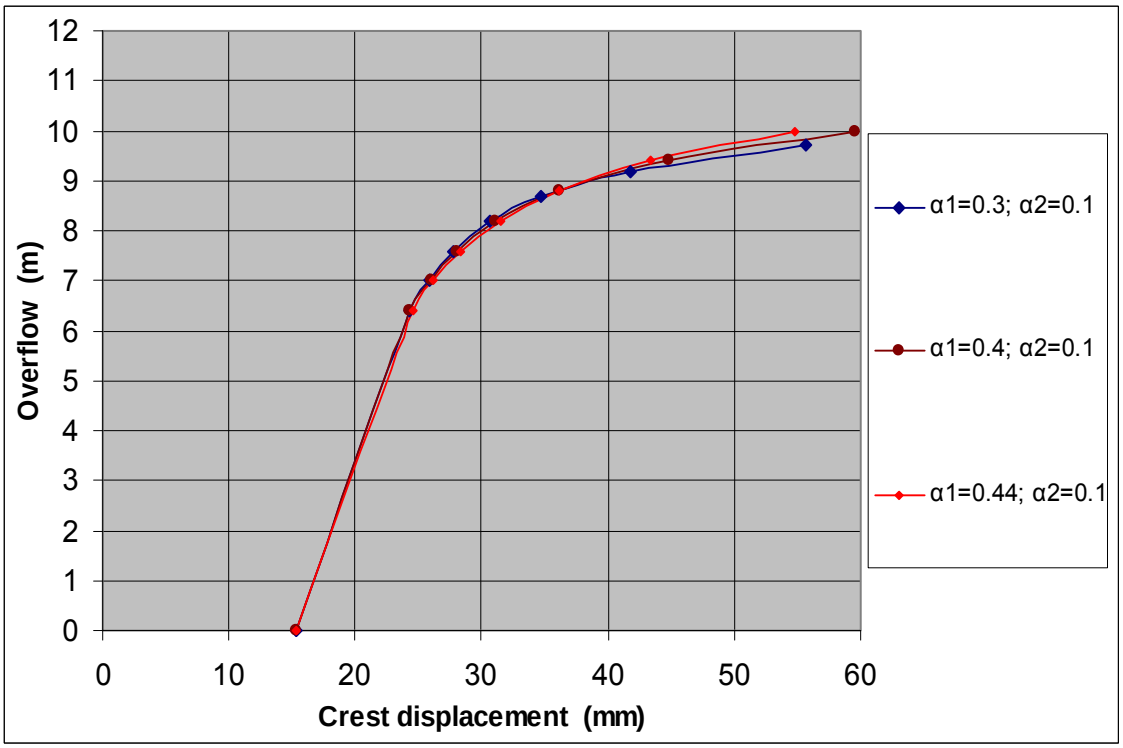

Figure 6.16 - Influence of bilinear softening parameters $\alpha_1 = 0.3$, 0.4 and 0.44, and $\alpha_2 = 0.1$ respectively on predicted structural response (Koyna Dam)

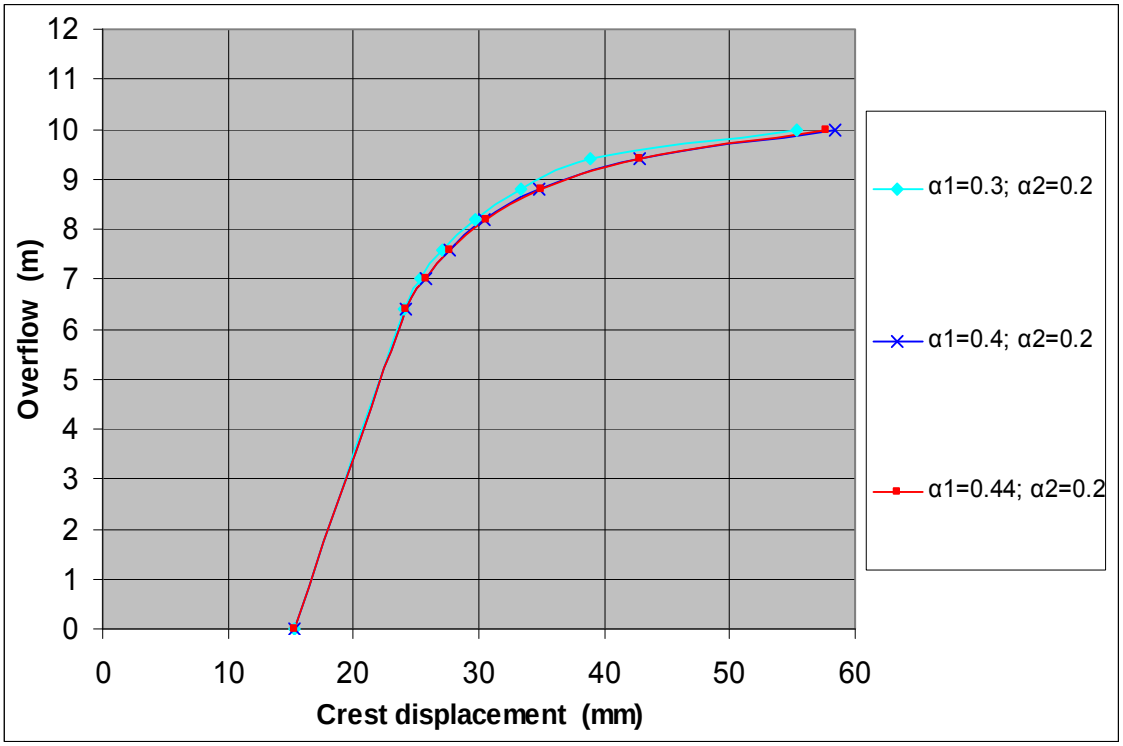

Figure 6.17 - Influence of bilinear softening parameters α_1 = 0.3, 0.4 and 0.44, and α_2 = 0.2 respectively on predicted structural response (Koyna Dam)

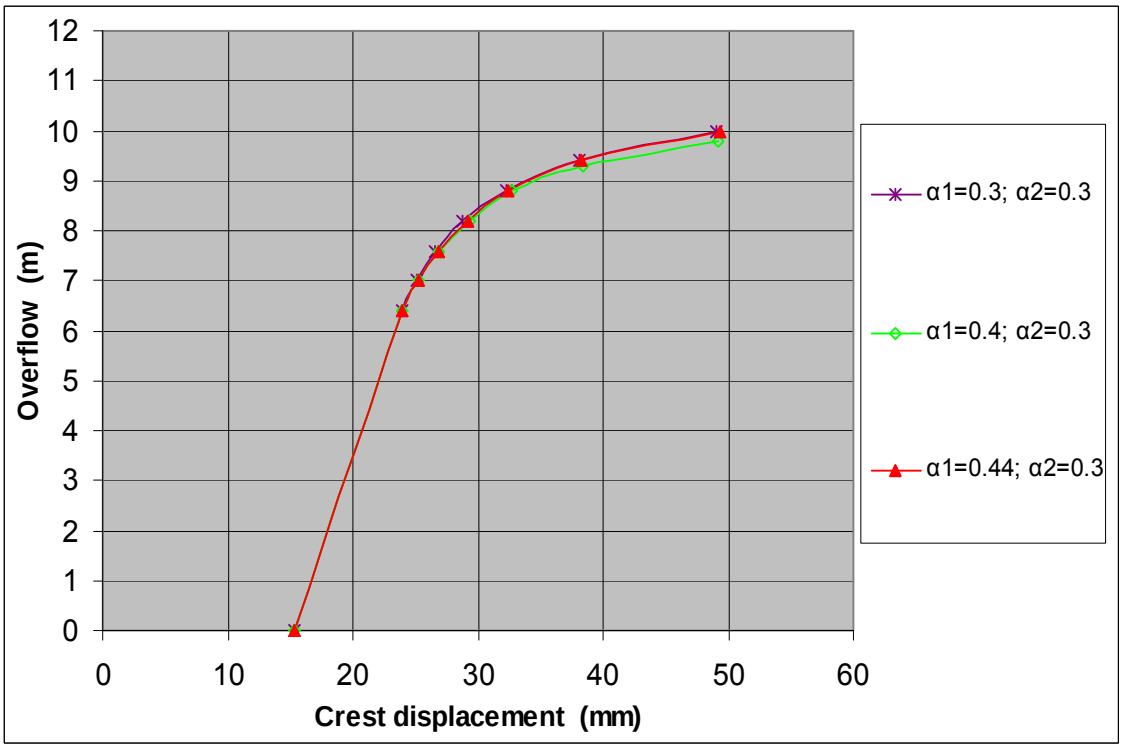

Figure 6.18 - Influence of bilinear softening parameters α_1 = 0.3, 0.4 and 0.44, and α_2 = 0.3 respectively on predicted structural response (Koyna Dam)

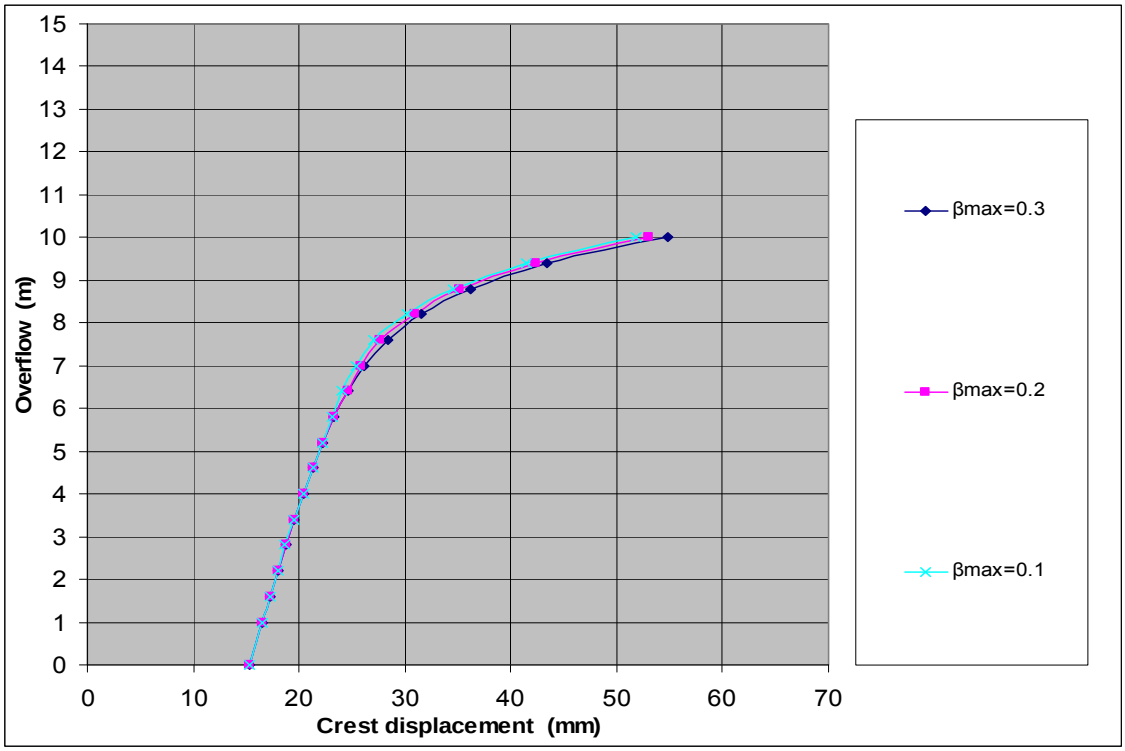

Figure 6.19 - Influence of maximum shear retention factor β_{max} on predicted structural response (Koyna Dam)

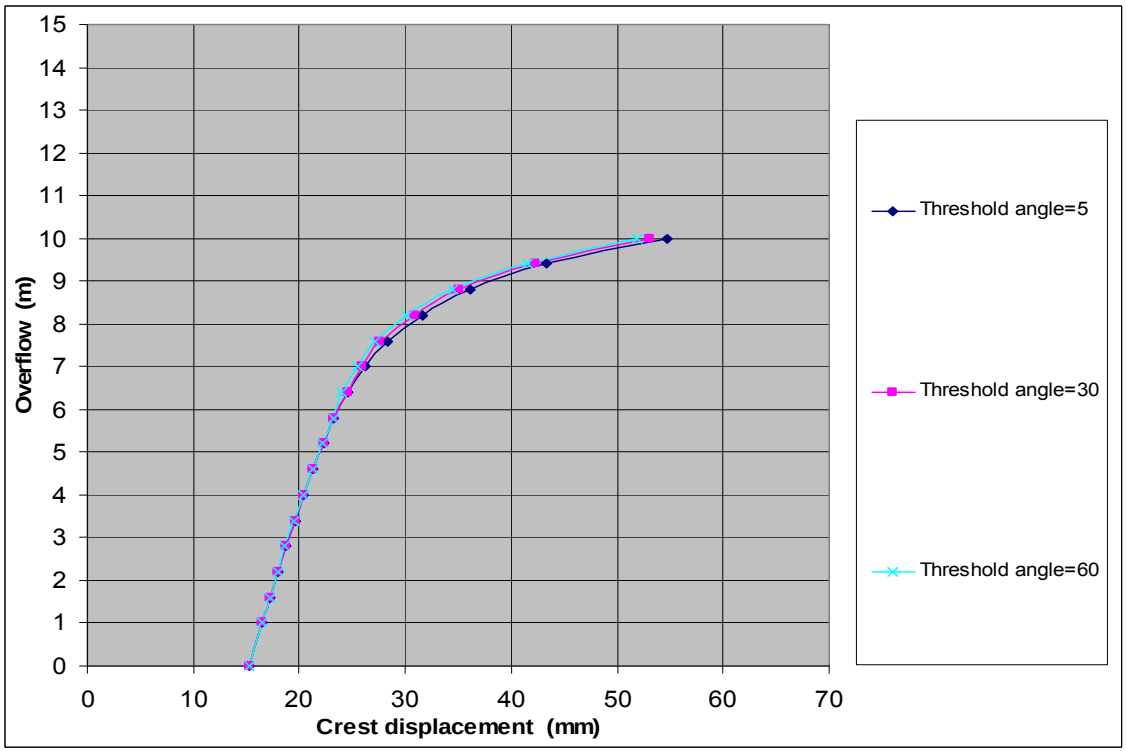

Figure 6.20 - Influence of threshold angle on predicted structural response (Koyna Dam)

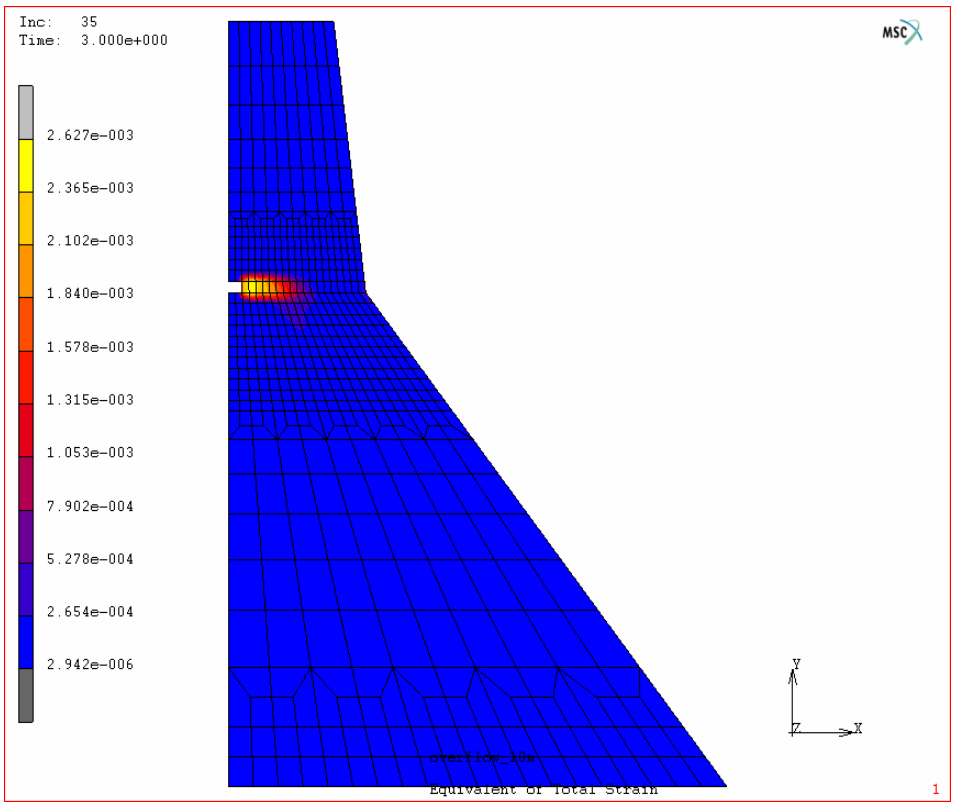

Figure 6.21 - Crack profile (bilinear softening, fracture energy G_f = 200 N/m) (Koyna Dam)

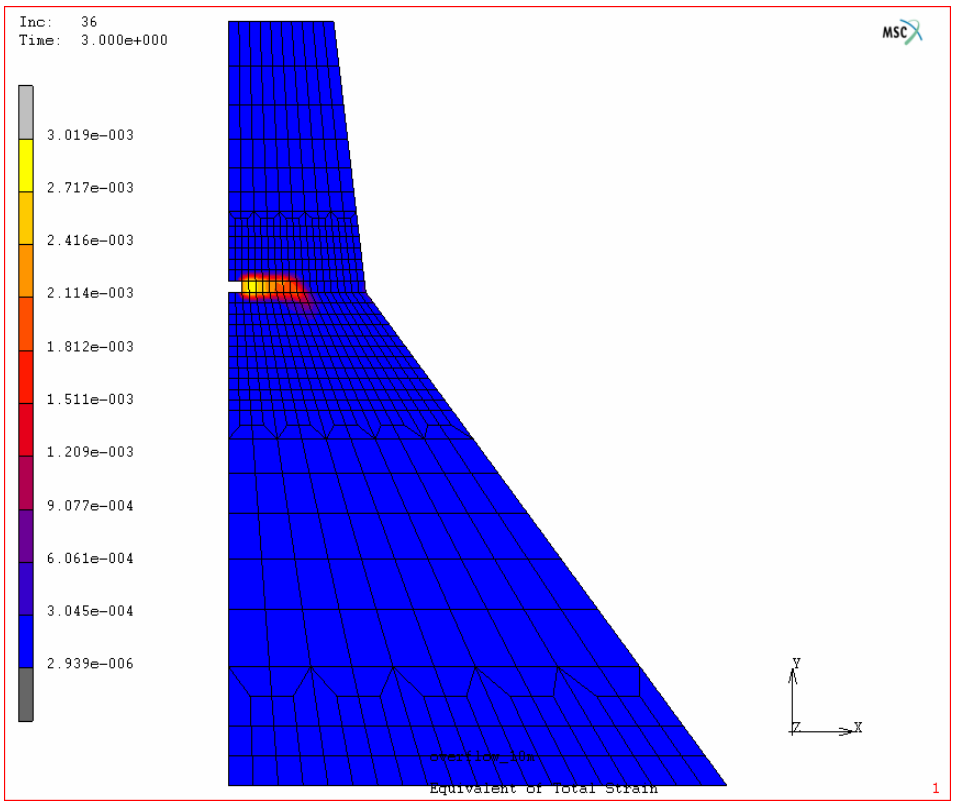

Figure 6.22 - Crack profile (bilinear softening α_1 = 0.3 and α_2 = 0.2, fracture energy G_f = 100 N/m) (Koyna Dam)

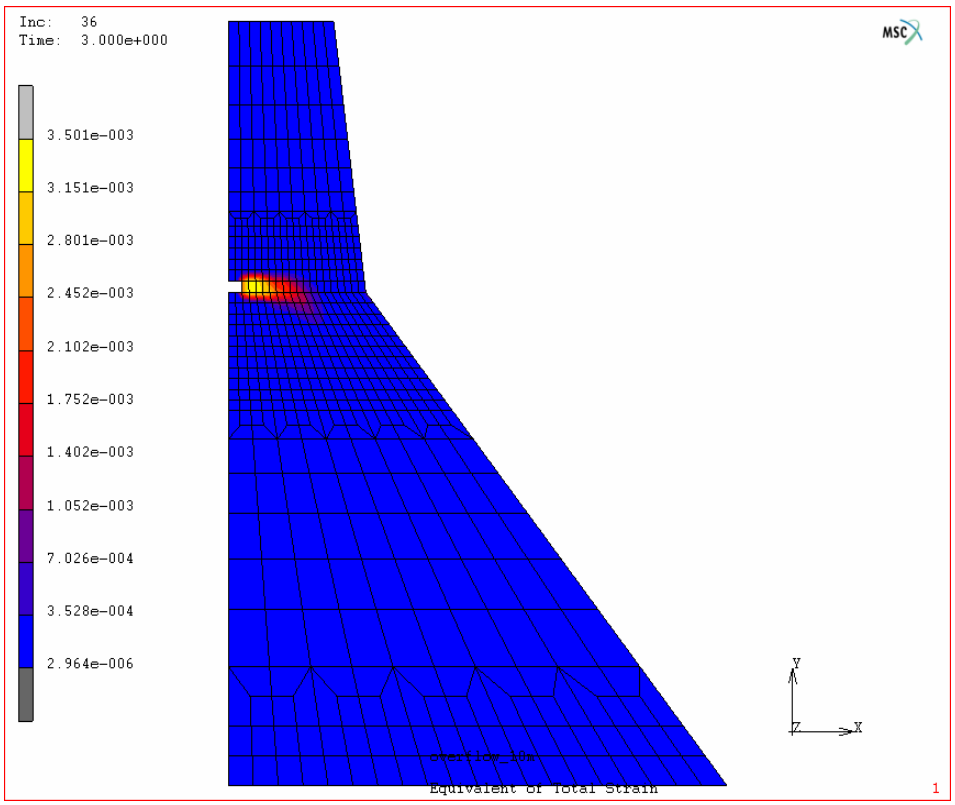

Figure 6.23 - Crack profile (bilinear softening $\alpha_1 = 0.4$ and $\alpha_2 = 0.1$) (Koyna Dam)

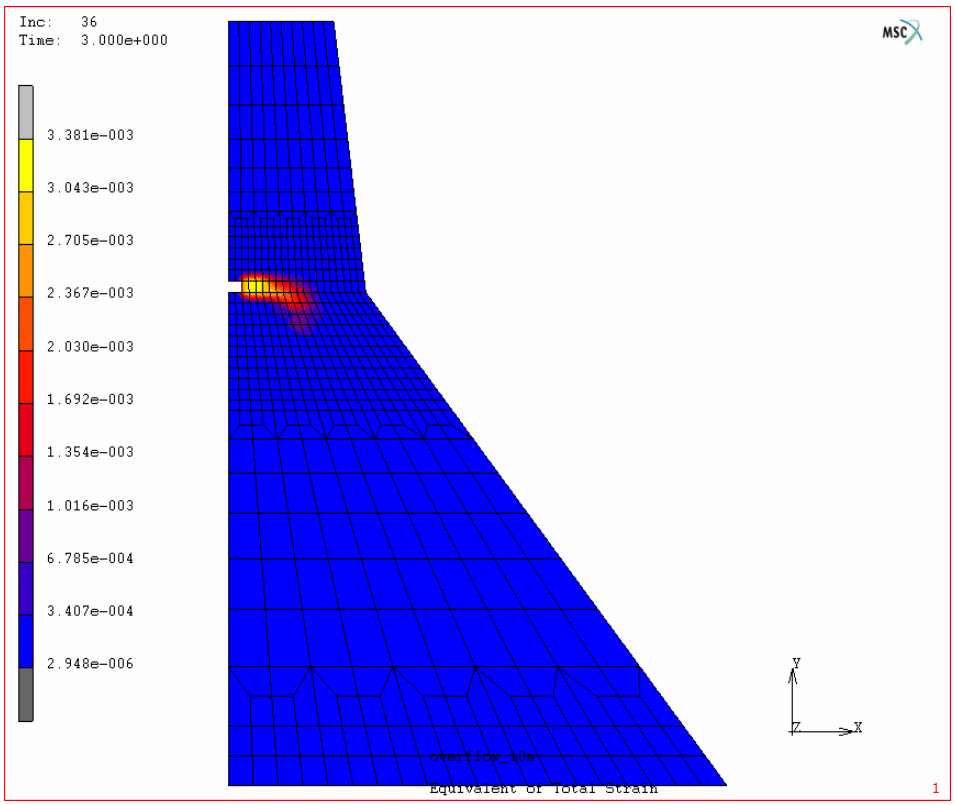

Figure 6.24 - Crack profile (bilinear softening $\alpha_1 = 0.4$ and $\alpha_2 = 0.2$) (Koyna Dam)

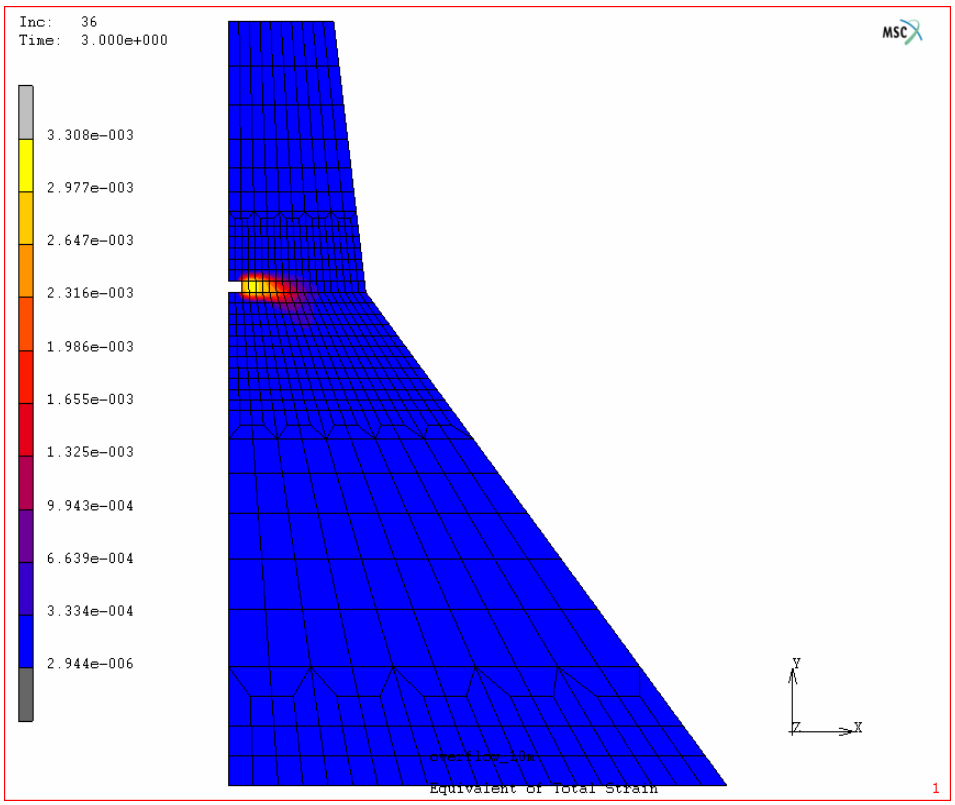

Figure 6.25 - Crack profile (bilinear softening $\alpha_1 = 0.44$ and $\alpha_2 = 0.2$) (Koyna Dam)

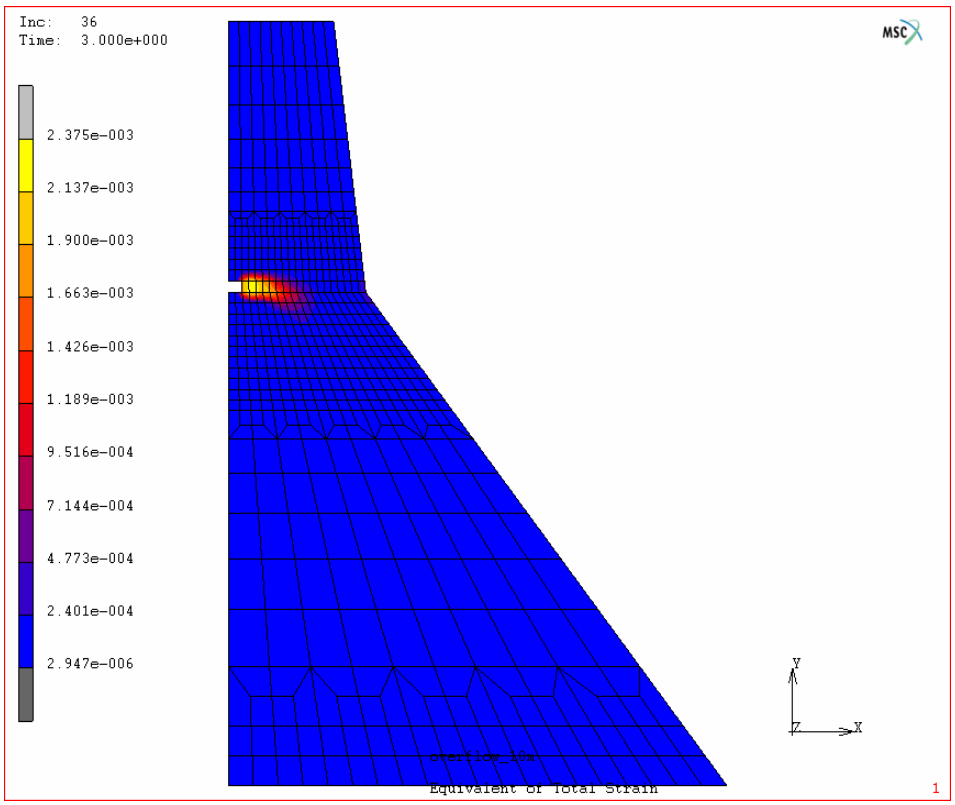

Figure 6.26 - Crack profile (bilinear softening $\alpha_1 = 0.44$ and $\alpha_2 = 0.3$) (Koyna Dam)

CHAPTER VII - SAFETY EVALUATION OF A CONCRETE GRAVITY DAM IN SOUTH AFRICA BASED ON FRACTURE ANALYSIS

7.1 Introduction

Evaluation of the safety of the existing dams in South Africa is carried out on a five-year basis. Cracking in concrete gravity dams could endanger the safety of the dams and needs to be accurately simulated and analyzed. In the preceding chapters, constitutive crack models have been adopted and a bilinear crack strain-softening law has been proposed. Implementation of the models and crack constitutive relationships has been undertaken by coding a subprogram. Verification and validation of the implemented crack models by means of fracture analyses of various concrete structures, including concrete gravity dams, have been carried out.

The objective of this chapter is to use the crack analysis method developed to predict crack propagation in an existing concrete gravity dam, namely the Van Ryneveld's Pass Dam in South Africa, and to evaluate the safety of the dam under the conditions of crack development in the dam.

7.2 Description of the gravity dam and finite element (FE) model (with reference to Seddon, Shelly, Moore & Forbes 1998)

The Van Ryneveld's Pass Dam is a 33-m-high concrete gravity dam completed in 1925 (see Figure 7.1). The dam is situated on the Sunday's River about one km north of Graaff-Reinet. The main function of the dam is to provide storage of over 47 million m^3 of water for the Graaff-Reinet Municipality and for irrigation.

The dam's foundation was not grouted and no drainage system was installed. The downstream face is made of large staggered, stepped blocks.

The main features of the dam are as follows:
(RL is the "reduced" or reference level)

Non-overspill crest level (walkway)	RL 790.35 m
Full supply level (FSL)	RL 787.60 m
Riverbed level	RL 757.00 m
Maximum height of concrete wall above riverbed	33.35 m
Maximum excavation depth	14.4 m
Crest thickness at NOC	3.05 m
Upstream slope	vertical
Downstream slope (RL 772.18 m to RL 787.60 m)	0.50: 1 (H:V)
Downstream slope (RL 755.40 m to RL 772.18 m)	0.65: 1 (H:V)
Downstream slope (below RL 755.40 m)	1: 1 (H:V)

Figure 7.1 - Van Ryneveld's Pass Dam (view from downstream)

The FE model is shown in Figures 7.2 and 7.3, assuming a conservative average critical level (RL 751.30 m, 5.7 m below the riverbed level) for the concrete/rock interface over the central high part of the dam (Seddon *et al*. 1998). Plane strain elements with first-order full integration are used in the analysis.

The boundary conditions are set as follows:

All the nodes at the outer edges of the area of the foundation being considered, shown in Figure 7.2, are fixed in both horizontal and vertical translation degrees of freedom, except for the nodes on the top face on which the base of the dam is situated.

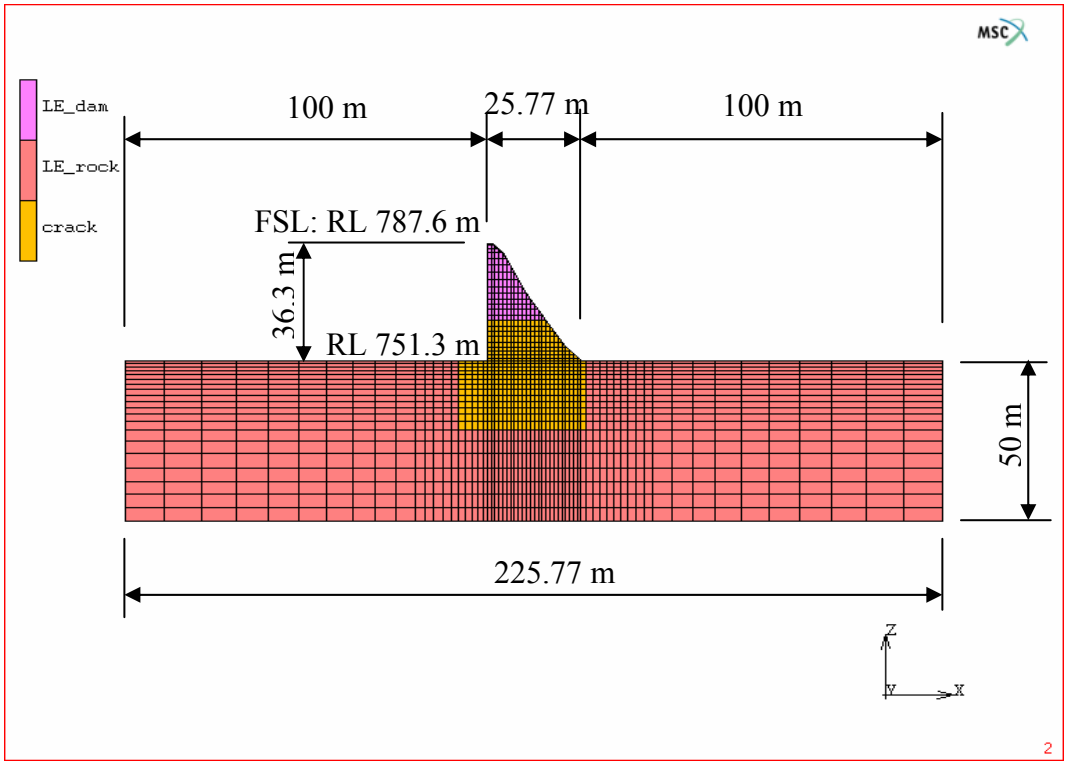

Figure 7.2 - Finite element model of Van Ryneveld's Pass Dam

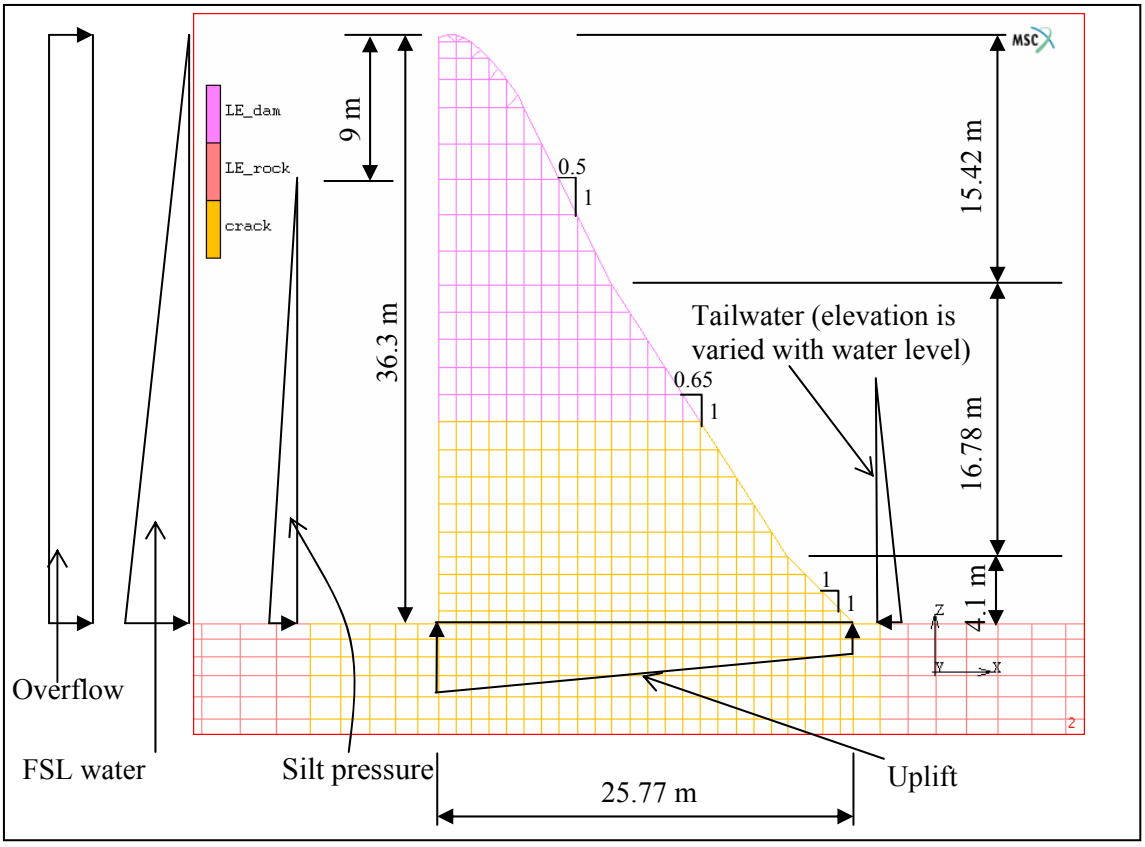

Figure 7.3 - Finite element model of Van Ryneveld's Pass Dam (close-up for dam wall) and hydrostatic and sediment loadings applied

7.3 Material properties and constitutive fracture parameters

The concrete used in the dam was tested from drilled cores and was fully reported by Van der Spuy (1992). The material properties of the concrete are given in Table 7.1, with reference to Van der Spuy (1992) and Seddon *et al*. (1998).

The rock foundation is reported to be sound dolerite bedrock. Schall (1988) conducted a visual inspection and laboratory tests on samples obtained by drilling through the dam's concrete wall and its rock foundation by means of five vertical holes. The tests on the rock samples showed that the rock is dolerite of excellent quality. Blake (1975) indicated that the uniaxial tensile strength of intact dolerite type of rock materials could be as high as 30 MPa. The intact shear strength of the dolerite varied in a range of 37.6 MPa to 63.3 MPa (Seddon *et al*. 1998). It is therefore reasonable to assume that the tensile strength of the fractured dolerite at the dam site to be 2.5 MPa.

The cohesion and frictional angle of the rock are matters of uncertainty because no laboratory test results are available. It is general practice for dam stability analysis in South Africa to assume that the tangent of the angle of internal friction of rock, $\tan\varphi$, is 0.8. The angle of internal friction of rock tested by the United States Bureau of Reclamation revealed that most rock samples have an angle of internal friction $\varphi \geq 45^0$ (Thomas 1976:170-171). Blake (1975:9-4–9-5) indicated $\tan\varphi$ = 1.1 for dolerite-type rock. In the present study, the angle of internal friction φ adopted is 39°. The cohesion of the rock is assumed to be 1 MPa to 10 MPa. Non-linear plasticity analyses have been carried out based on this value range of cohesion for dolerite rock. The material properties of rock are also presented in Table 7.1.

TABLE 7.1 - Material properties of concrete and rock

Concrete wall		**Rock foundation**	
Young's modulus E (MPa)	28 000	Young's modulus E (MPa)	30 000
Poisson's ratio v	0.2	Poisson's ratio v	0.22
Tensile strength f_t (MPa)	1.5	Tensile strength f_t (MPa)	2.5
Mass density (kg/m^3)	2 455	Mass density (kg/m^3)	0
Cohesion (MPa)	2.41	Cohesion (MPa)	1 ~ 10
Frictional angle φ	55°	Frictional angle φ	39°
Coefficient of thermal expansion	1.0E^{-5}/°C		

The constitutive fracture parameters of concrete and rock in the dam are also a matter of uncertainty. A sensitivity study on the fracture parameters is needed as part of a comprehensive fracture analysis of the dam for crack behaviour and safety evaluation.

7.4 Bilinear strain-softening shape parameters

As stated previously, concrete strain softening has been presented in the form of linear, bilinear and non-linear curve diagrams. A bilinear softening strategy provides a good approximation of the behaviour of the concrete material and has been accepted as a reasonable approximation of the softening curve for concrete. In the bilinear softening diagram, the first branch is steeper and represents large-scale debonding (fracture of

aggregates) and the second branch represents the frictional pull-out of aggregates which characterizes the behaviour of larger cracks (ICOLD report 2001).

The bilinear softening laws have been used in past investigations for the numerical analysis of concrete fracturing. High discrepancies in the values adopted for the shape parameters α_1 and α_2 have been reported since there is no agreement about the precise position of the kink point of concrete material. The kink position is also influenced by the type of concrete and the fracture energy G_f, etc.

The bilinear softening shape parameters α_1 = 1/3 and α_2 = 1/7 were selected by Li & Zimmerman (1998), Barpi & Valente (2001) and Yang & Proverbs (2003) in their analyses of fracturing in concrete structures such as a three-point bending beam, a dam model and a four-point shear beam.

The crack stress–crack opening relationships (see Figure 7.4) used in the above analyses had to be transformed into crack stress–strain softening laws (see Figure 7.5) for the present study. If constant strain is assumed in the crack blunt width, then the shape of the crack stress–crack opening can be viewed as the same as that of the crack stress–strain relationship. The following formula (equation 7.1) was derived for calculating α_2 from the given values of α_1, W_1 and W_2:

$$\alpha_2 = \frac{\alpha_1}{1-\alpha_1}\frac{W_1}{W_2 - W_1} = \frac{\alpha_1}{1-\alpha_1}\frac{\frac{W_1}{W_2}}{1-\frac{W_1}{W_2}} \qquad (7.1)$$

Shi *et al*. (2001) adopted a bilinear softening diagram in the analysis of a concrete tunnel. The bilinear softening shape parameters α_1= 1/4 and α_2= 1/17 were used, which are transformed by the formula in equation 7.1, from the original crack stress–crack opening relationship adopted in the analysis.

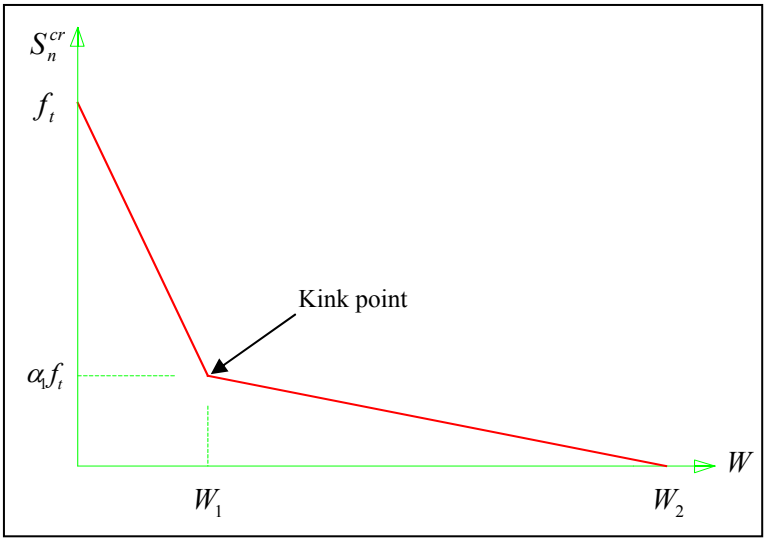

Figure 7.4 - Bilinear strain softening (tensile stress vs. crack opening displacement)

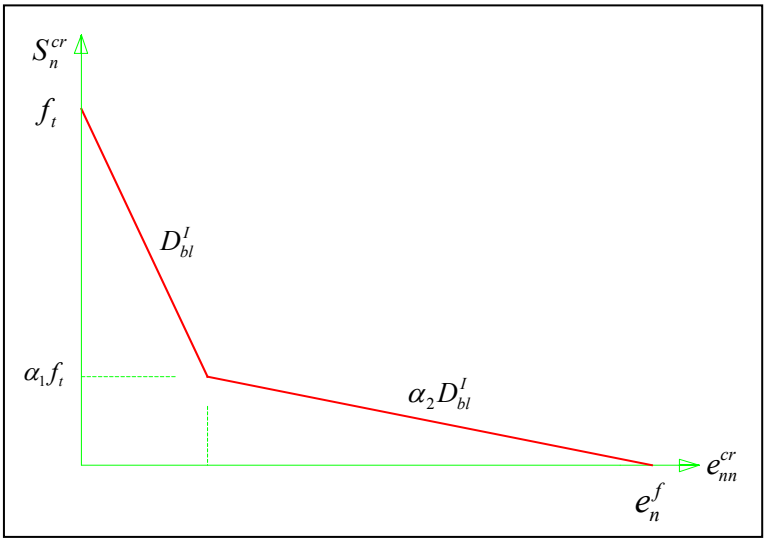

Figure 7.5 - Bilinear strain softening (tensile stress vs. local crack strain)

Gálvez *et al*. (2002) also adopted a bilinear strain-softening law in the analysis of cracking in concrete, but did not indicate the values for the bilinear softening shape parameters α_1 and α_2 in their paper.

Further, Hanson & Ingraffea (2003) adopted bilinear strain softening in the analysis of concrete fracturing. They undertook a comparative study on different combinations of the bilinear softening shape parameters α_1 and α_2. The range for α_1 was chosen as 0.1 ~ 0.5 and α_2 was selected from a very low value (1/171) to 1.0.

Bilinear strain softening has also been used in past investigations into the fracturing of concrete dams. Various researchers have proposed different values for the bilinear softening shape parameters α_1 and α_2. Petersson (1981) proposed the bilinear softening shape parameters $\alpha_1 = 0.3$ and $\alpha_2 = 0.107$ and Wittmann *et al*. (1988) proposed the bilinear softening shape parameters $\alpha_1 = 0.25$ and $\alpha_2 = 1/17$.

Feltrin, Wepf & Bachmann (1990) adopted a bilinear softening law in the seismic cracking analysis of concrete gravity dams, but gave no indication of the values of the bilinear softening shape parameters α_1 and α_2 used in their analysis.

Brühwiler & Wittmann (1990) conducted a series of wedge-splitting tests on the drilled cores from a concrete dam and presented bilinear strain-softening diagrams from the tests. According to the ICOLD report (2001) on the physical properties of hardened conventional concrete in dams, Brühwiler & Wittmann (1990) gave the bilinear softening shape parameters $\alpha_1 = 0.4$ and $\alpha_2 = 0.243$ for dam concrete.

Shi *et al*. (2003) also adopted a bilinear softening diagram in the analyses of concrete gravity dams. The bilinear softening shape parameters $\alpha_1 = 1/4$ and $\alpha_2 = 1/17$ were used, which are transformed by the formula in equation 7.1, from the original crack stress–crack opening relationship adopted in the analyses.

Espandar & Lotfi (2003) adopted bilinear softening diagram in the FE fracture analysis of a concrete arch dam. The bilinear softening shape parameters $\alpha_1 = 0.01$ and $\alpha_2 = 0.0001$ had been used in the analysis. Thus the bilinear softening is basically in the linear format. The very low value for α_2 was adopted mainly for avoiding zero stiffness in the crack normal direction.

Based on the past numerical and experimental investigations into the bilinear softening crack analysis of dam concrete, a good range for the bilinear softening shape parameters would be $\alpha_1 = 0.25 \sim 0.4$ and $\alpha_2 = 0.05 \sim 0.3$ to approximate dam concrete softening behaviour. A sensitivity study on the ranges of α_1 and α_2 should be carried out for analyzing the cracking behaviour of concrete in dams.

7.5 Fracture analysis and evaluation of the dam safety

A crack analysis is carried out, studying the sensitivity of the fracture parameters and comparing the results with the linear elastic and non-linear Mohr-Coulomb plasticity analyses. Evaluation of the dam's safety is based on the mode I and II crack analysis and the previous dam safety investigation (Seddon *et al*. 1998).

The dam is loaded by self-weight, hydrostatic pressure at full supply level (FSL), silt pressure, overflow of up to 20 m, uplift pressure, tailwater pressure and a seasonal temperature drop in the dam wall. This loading condition is shown in Figure 7.3. When overflow load is applied, a trapezoidal pressure distribution is acting on the upstream face by adding the FSL triangular pressure with the "overflow" rectangular pressure.

The hydrostatic loadings in the previous dam safety evaluation (Seddon *et al*. 1998) were set for three conditions, as follows:

- Water level at Full Supply Level (FSL - 36.3 m above the rock foundation).
- Water level at Recommended Design Flood (RDF - 4.61 m above the FSL).
- Water level at Safety Evaluation Flood (SEF - 9.99 m above the FSL).

The silt pressure is due to heavy siltation occurring in the dam reservoir which is assumed to be 9 m below the FSL. The density of the silt for the calculation of horizontal silt pressure acting on the upstream face of the dam is 3.53 kN/m^3 (Seddon *et al*. 1998).

The uplift pressure has been taken assuming the water level to be at FSL. For overflow conditions such as RDF and SEF, the same uplift pressure is adopted as for FSL, for the reason that higher pressure would not normally have time to develop due to the short duration of flash floods in South Africa.

The elevation of the tailwater is varied with the water level in the dam. When the water level is at FSL, the elevation of the tailwater is at 5.7 m above the foundation. When the water level is at RDF, the elevation of the tailwater is at 15.7 m above the foundation.

When the water level is at SEF, the elevation of the tailwater is at 25.7 m above the foundation.

Concrete dams are also subject to loading by seasonal changes in temperature. Normally, a temperature decrease inside a dam would cause tensile stresses at the upstream heel. Thus a drop in temperature is a loading scenario that must be included in the analysis regarding the safety of a concrete dam.

The drop in temperature for seasonal temperature fluctuations is determined from the standard formula (adopted in the DWAF, South Africa) used in previous arch dam analyses undertaken for South African climatic conditions. This is done due to the lack of more detailed information and the lack of a standard formula for gravity dams.

$$\Delta T = \frac{34}{2{,}4 + t} \tag{7.2}$$

Where t is the thickness (m) of the dam wall at a given level and ΔT is the temperature drop in degrees Celsius. The temperature distribution was assumed to be uniform through the horizontal section of the dam.

In fact, temperature drop loading makes cracking in this dam propagate even more when compared with the results of load cases without the influence of temperature.

7.5.1 Parametric study on the fracture energy of concrete and rock

The fracture energy G_f of the concrete used in dams was discussed and past investigations into it were presented in Section 2.6 of Chapter II. The fracture energy G_f of dam concrete can be set between 100 N/m and 300 N/m. In the present analysis of the dam, a sensitivity study on the concrete fracture energy G_f^c =100 ~ 300 N/m and the rock fracture energy G_f^r =200 ~ 400 N/m is carried out. Different combinations of the fracture energies of concrete and rock based on the above ranges are used in the crack analysis of

this dam. The other fracture parameters used for this sensitivity study are assumed to be as follows:

Bilinear shape parameters α_1 = 0.4 and α_2 = 0.05; crack onset threshold angle = 30°; maximum shear retention factor $\beta_{\max}$ = 0.1; and tensile strengths for concrete and rock = 1.5 and 2.5 MPa respectively.

Nine graphs of crest horizontal displacement in terms of overflow water level are shown in Figure 7.6. The fracture energy of rock G_f^r appears to have little influence on the crack response of the dam. As the fracture energy of rock increases from 200 N/m to 400 N/m with different values of the fracture energy of concrete G_f^c, the structural behaviours become nearly identical for the same fracture energy of concrete G_f^c. At low overflow water level, the lower fracture energy of concrete G_f^c (100 N/m) has a higher crest deformation. As the overflow water level increases to a higher level (approximately 17 m above), the crest deformation for a higher fracture energy of concrete G_f^c (300 N/m) becomes larger and increases at a faster rate.

It appears that the fracture energy of concrete and rock in general do not have much influence on the overall dam deformation. The fracture energy of concrete G_f^c, however, has a significant influence on the crack propagation paths in the dam structure, as shown in Figures 7.7 to 7.10. All these crack profiles are obtained at the same overflow water level of 20 m. As the fracture energy of concrete G_f^c increases, the crack will propagate from horizontal direction along the concrete/rock interface to bend more into the rock foundation. The fracture energies of concrete G_f^c = 300 N/m and rock G_f^r = 200 ~ 400 N/m will cause the highest deformation in the dam.

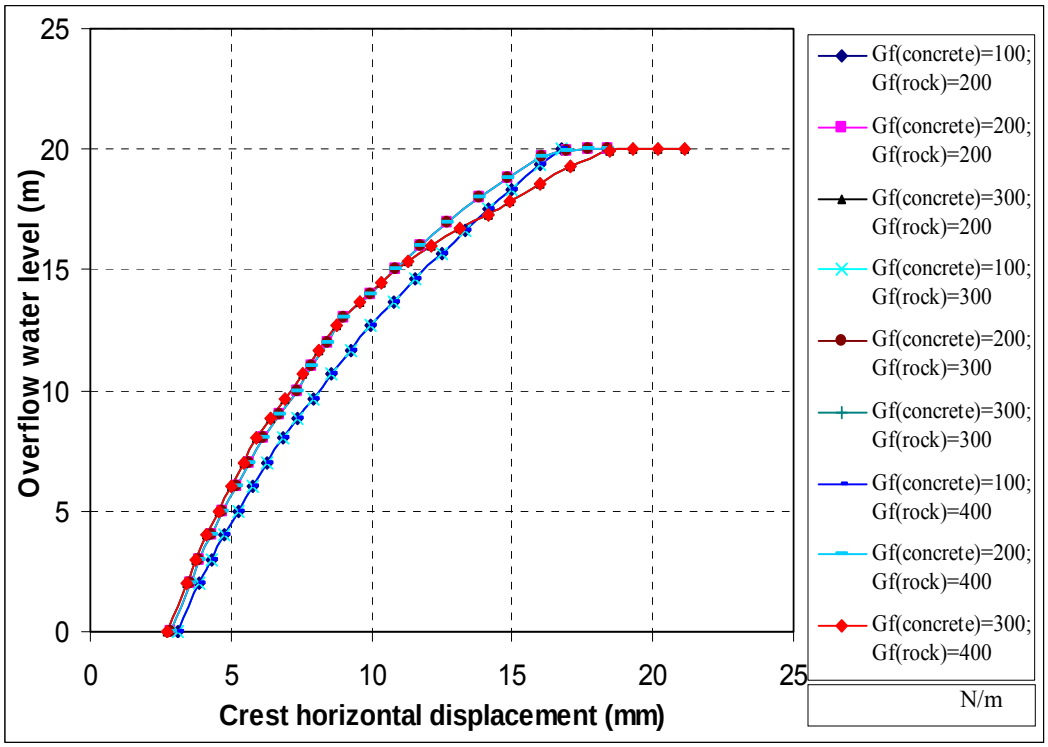

Figure 7.6 - Crest horizontal displacement vs. overflow for various values of fracture energy

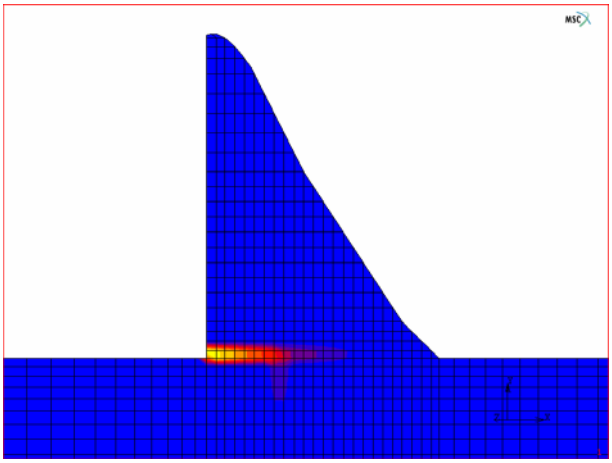

Figure 7.7 - Crack profile for G_f^c = 100 N/m and G_f^r = 400 N/m

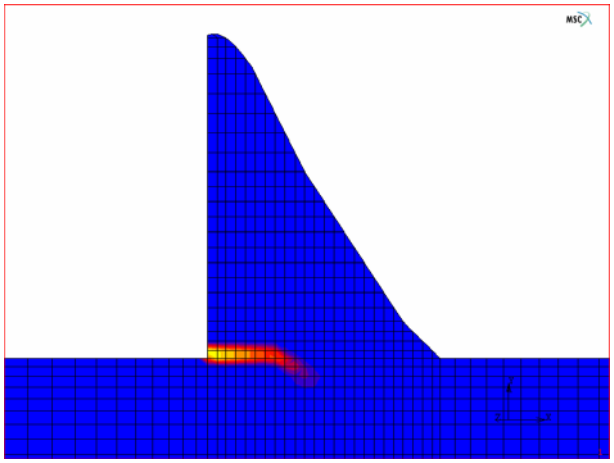

Figure 7.8 - Crack profile for G_f^c = 200 N/m and G_f^r = 400 N/m

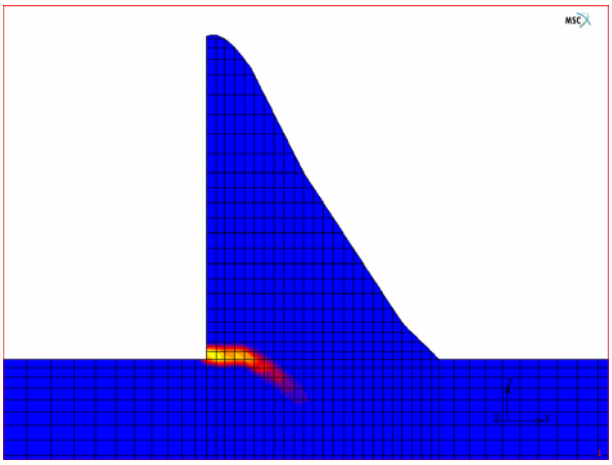

Figure 7.9 - Crack profile for G_f^c =300 N/m and G_f^r = 400 N/m

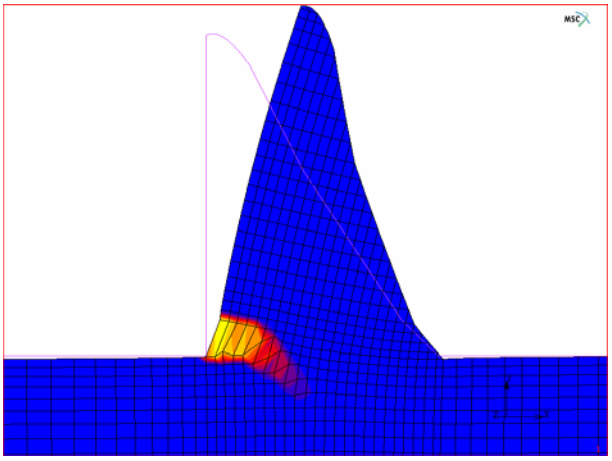

Figure 7.10 - Crack profile for G_f^c = 300 N/m and G_f^r = 400 N/m (deformed shape)

7.5.2 Parametric study on the bilinear shape parameters α_1 and α_2

In accordance with the discussion in Section 7.4 of the concrete used in the dam, the bilinear shape parameters α_1 and α_2 are studied for their influence on the dam's behaviour. The bilinear shape parameters α_1 and α_2 for the rock are assumed to be the same as those for the concrete. As stated previously, α_1 will be in the range of 0.25 ~ 0.4 and α_2 will be 0.05 ~ 0.3. The bilinear mode I strain-softening shapes for different values of α_1 and α_2 are shown in Figures 7.11 to 7.13.

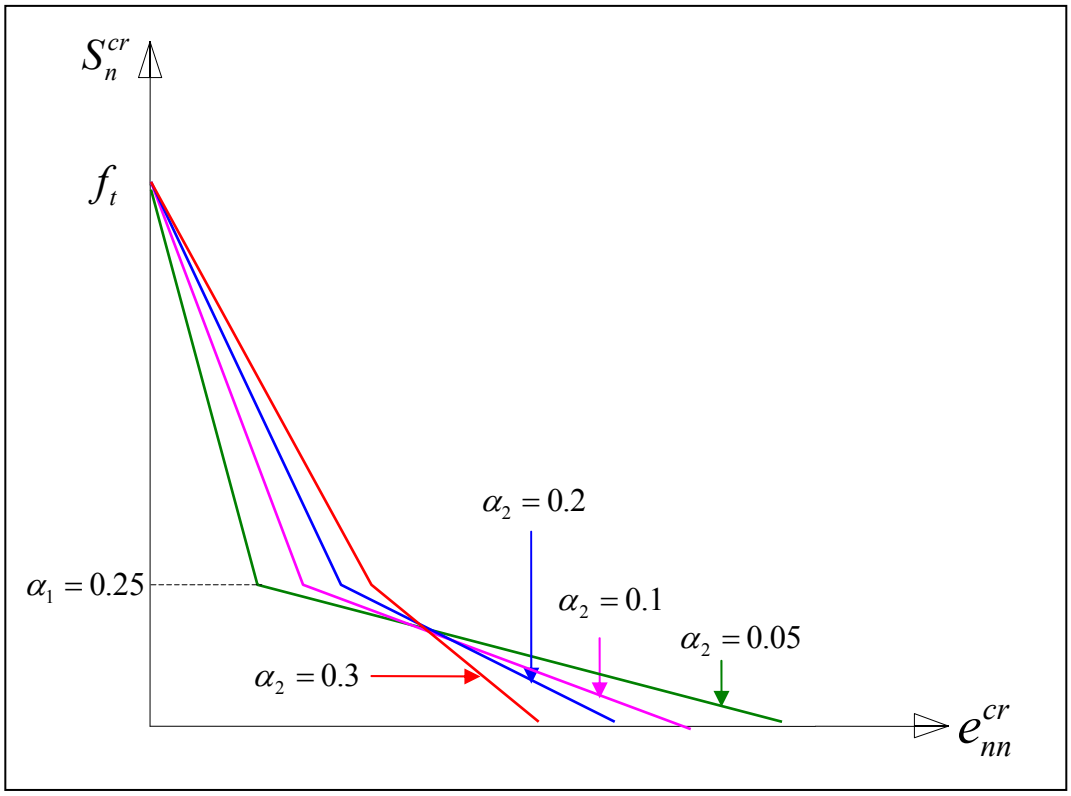

Figure 7.11 - Bilinear softening shapes with $\alpha_1 = 0.25$ and $\alpha_2 = 0.05$, 0.1, 0.2 and 0.3

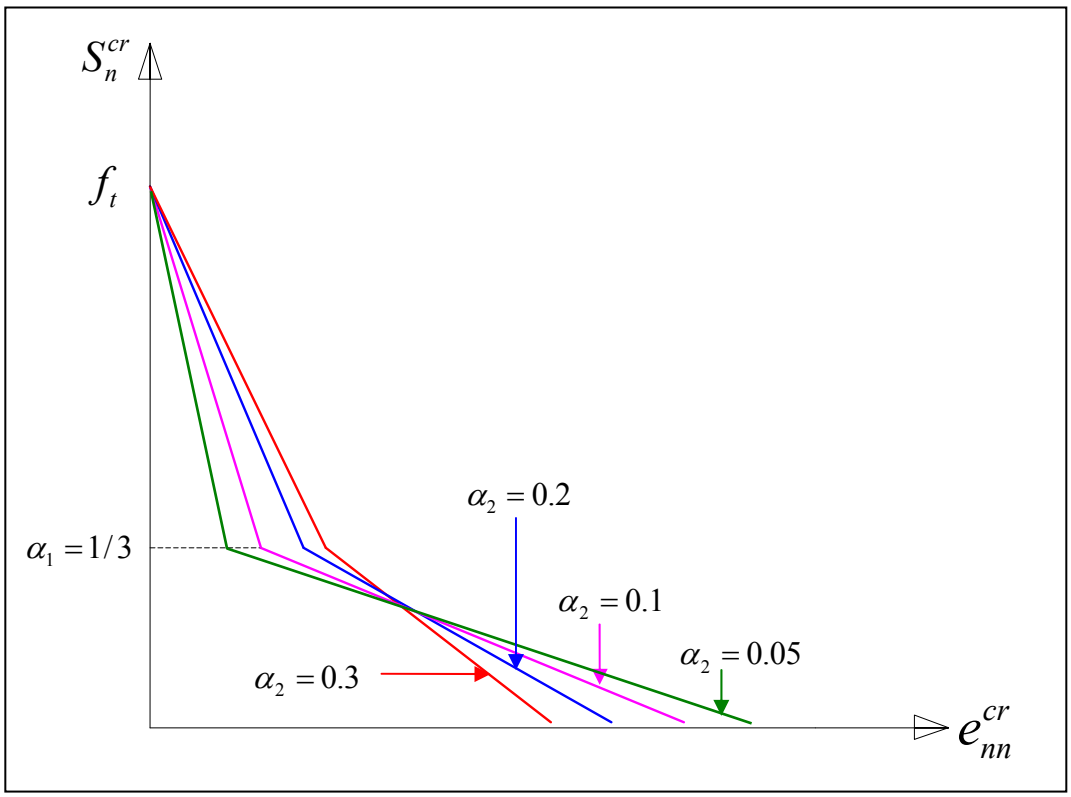

Figure 7.12 - Bilinear softening shapes with $\alpha_1 = 1/3$ and $\alpha_2 = 0.05$, 0.1, 0.2 and 0.3

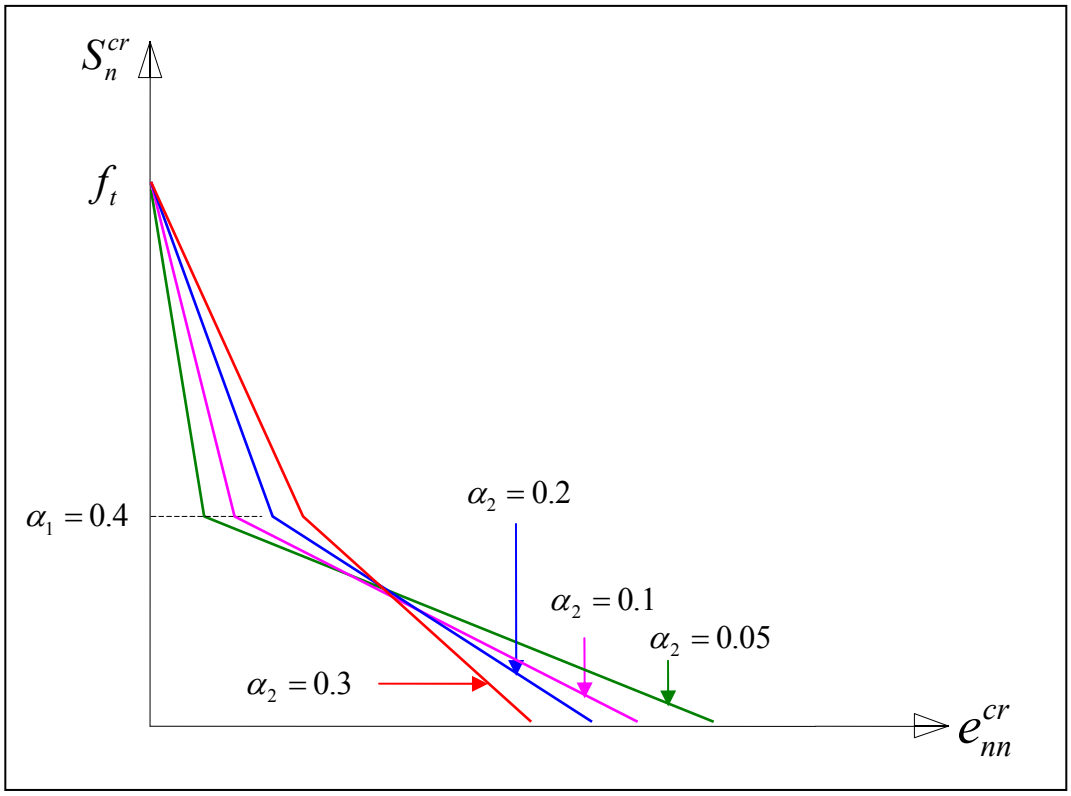

Figure 7.13 - Bilinear softening shapes with $\alpha_1 = 0.4$ and $\alpha_2 = 0.05$, 0.1, 0.2 and 0.3

The other fracture parameters used for this sensitivity study are assumed to be as follows:

Fracture energy G_f^c = 300 N/m and G_f^r = 400 N/m; threshold angle = 30°; maximum shear retention factor $\beta_{\max}$ = 0.1; and tensile strengths for concrete and rock = 1.5 and 2.5 MPa respectively.

As shown in Figures 7.14a to 7.14c, at the low overflow level, the crest deformation for all the combinations of α_1 and α_2 are similar. When the overflow water level exceeds approximately 7 m, the crest deformation curves of the cases α_1 = 1/3; α_2 = 0.05 and α_1 = 0.4; α_2 = 0.05 show significantly more deformation. The other combinations of α_1 and α_2 have similar crest deformations. The crack profiles (at the same overflow level) shown in Figures 7.15 to 7.26 for different values of α_1 and α_2 are much more sensitive than the crest deformation. Basically, when α_1 is fixed at 0.25 while α_2 ranges from 0.05 to 0.3 (see Figures 7.15 to 7.18), cracks in the dam propagate along the concrete/rock interface.

When α_1 increases to 1/3 and 0.4 with α_2 = 0.05, the crack will propagate by bending downward into the rock (see Figures 7.19 and 7.23). Analyses adopting α_1 = 1/3 ~ 0.4 and α_2 = 0.05 would cause the dam to deform more.

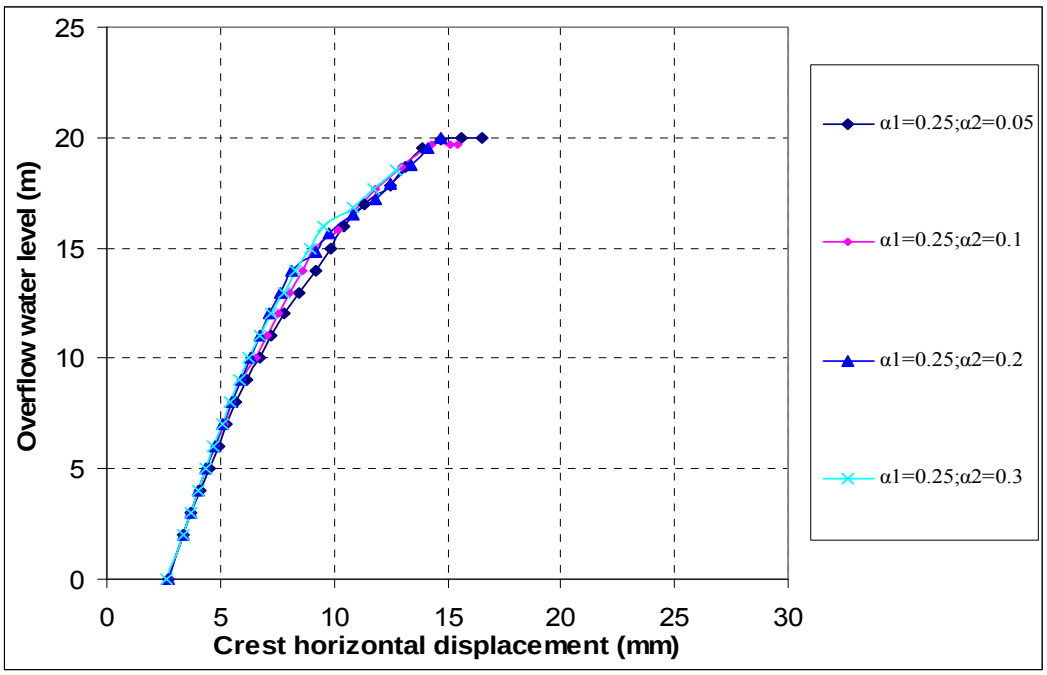

Figure 7.14a - Crest horizontal displacement vs. overflow level for strain-softening relationships with α_1 = 0.25 and α_2 = 0.05, 0.1, 0.2 and 0.3

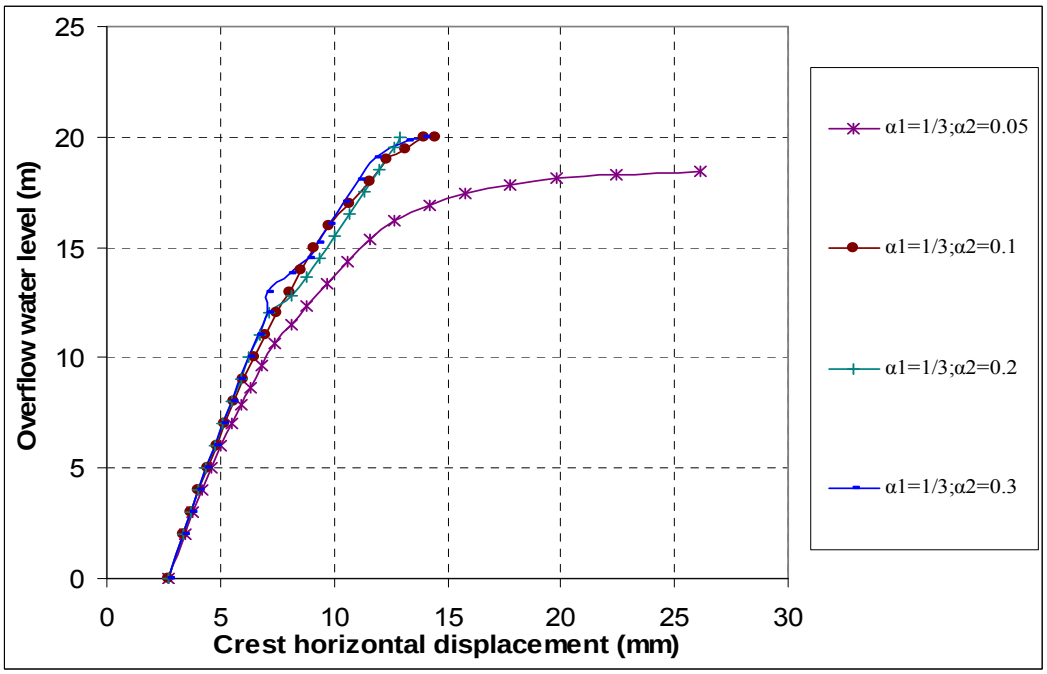

Figure 7.14b - Crest horizontal displacement vs. overflow level for strain-softening relationships with α_1 = 1/3 and α_2 = 0.05, 0.1, 0.2 and 0.3

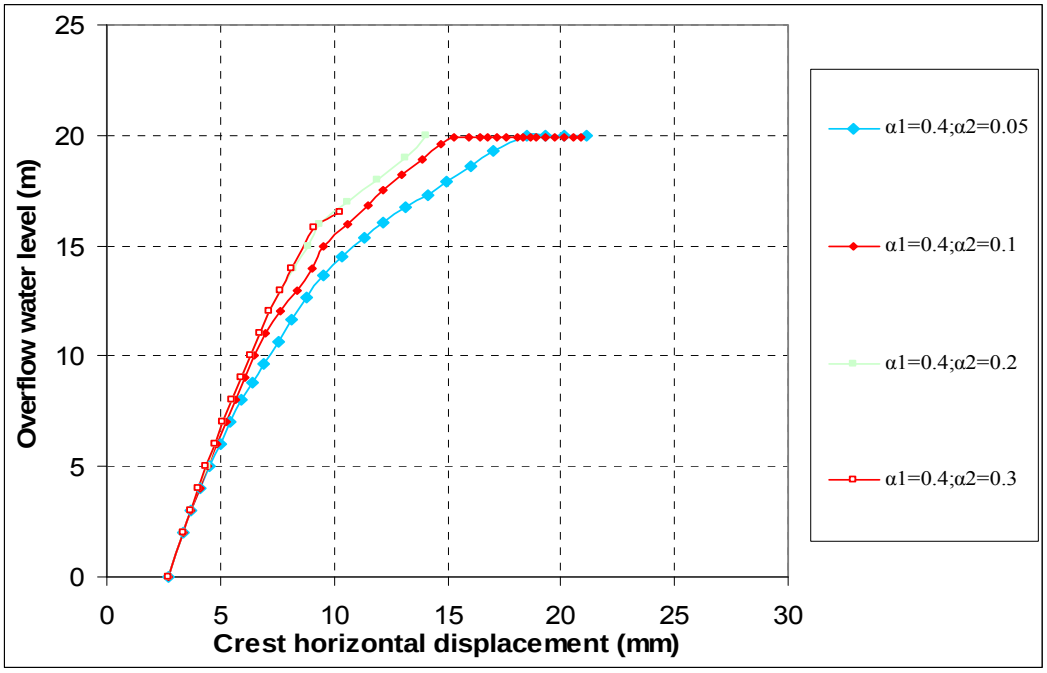

Figure 7.14c - Crest horizontal displacement vs. overflow level for strain-softening relationships with $\alpha_1 = 0.4$ and $\alpha_2 = 0.05$, 0.1, 0.2 and 0.3

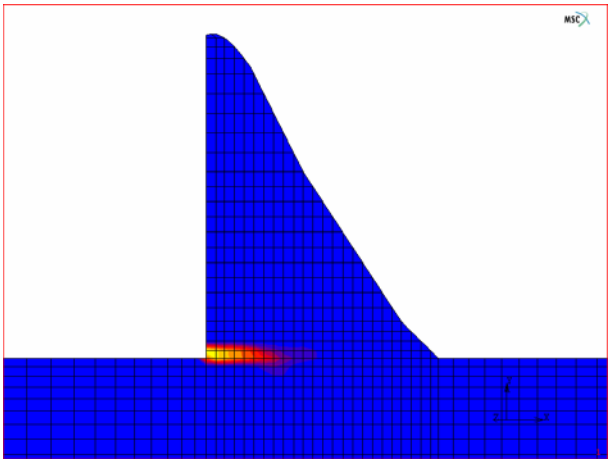

Figure 7.15 - Crack profile for $\alpha_1 = 0.25$ and $\alpha_2 = 0.05$

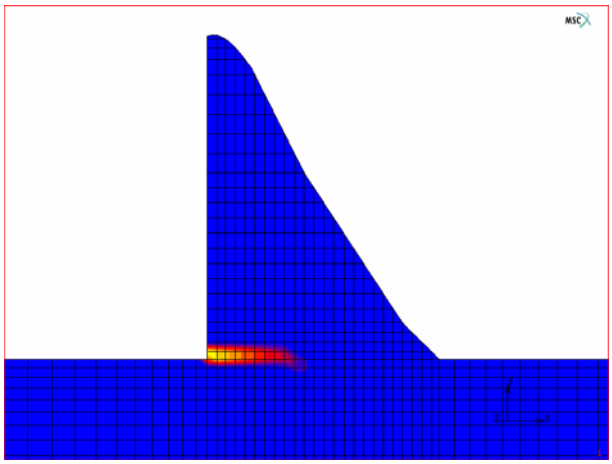

Figure 7.16 - Crack profile for $\alpha_1 = 0.25$ and $\alpha_2 = 0.1$

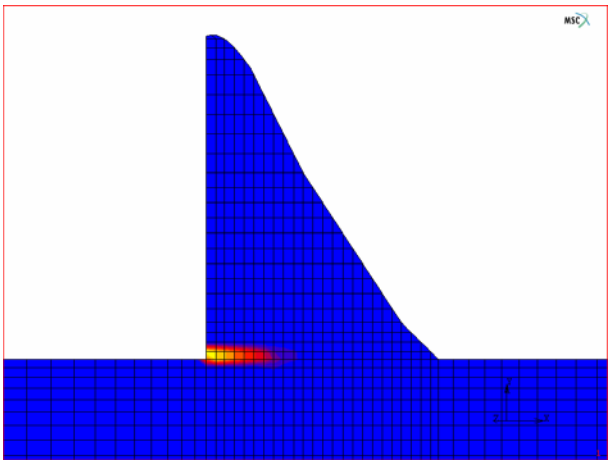

Figure 7.17 - Crack profile for $\alpha_1 = 0.25$ and $\alpha_2 = 0.2$

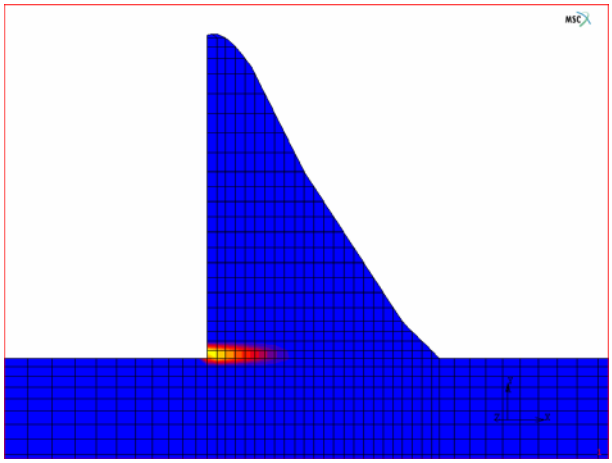

Figure 7.18 - Crack profile for $\alpha_1 = 0.25$ and $\alpha_2 = 0.3$

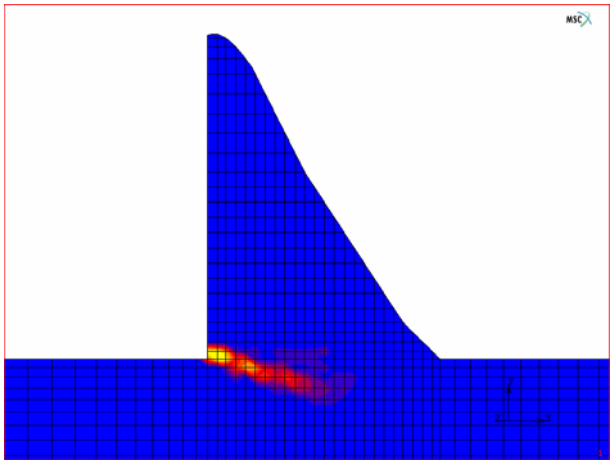

Figure 7.19 - Crack profile for $\alpha_1 = 1/3$ and $\alpha_2 = 0.05$

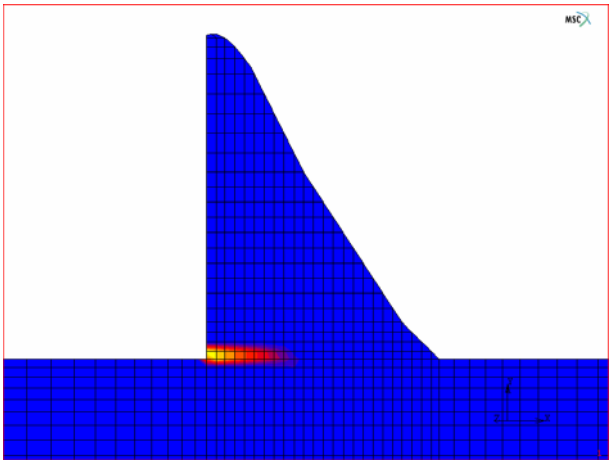

Figure 7.20 - Crack profile for $\alpha_1 = 1/3$ and $\alpha_2 = 0.1$

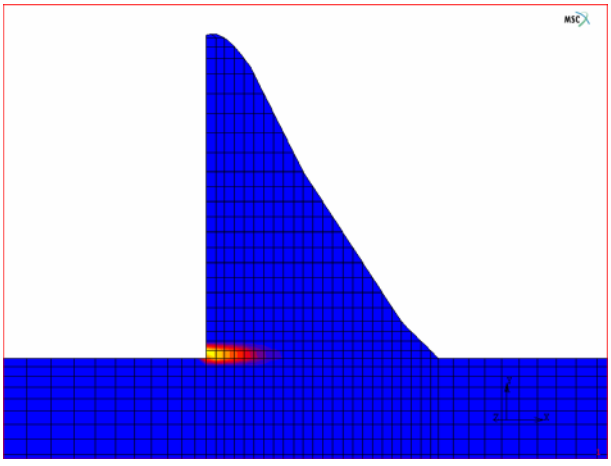

Figure 7.21 - Crack profile for $\alpha_1 = 1/3$ and $\alpha_2 = 0.2$

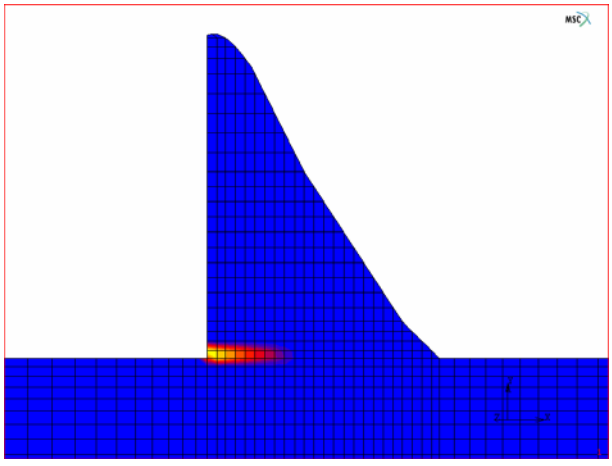

Figure 7.22 - Crack profile for $\alpha_1 = 1/3$ and $\alpha_2 = 0.3$

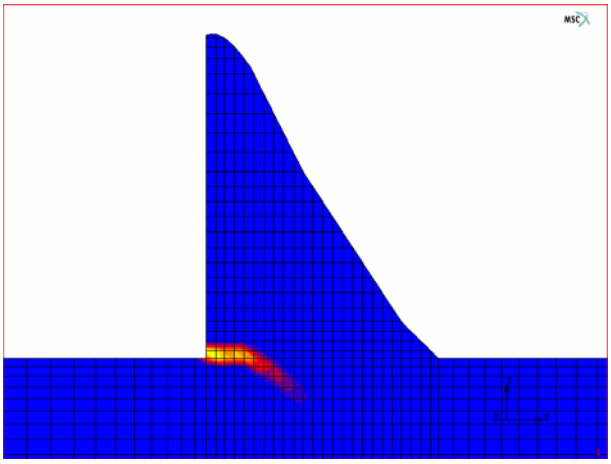

Figure 7.23 - Crack profile for $\alpha_1 = 0.4$ and $\alpha_2 = 0.05$

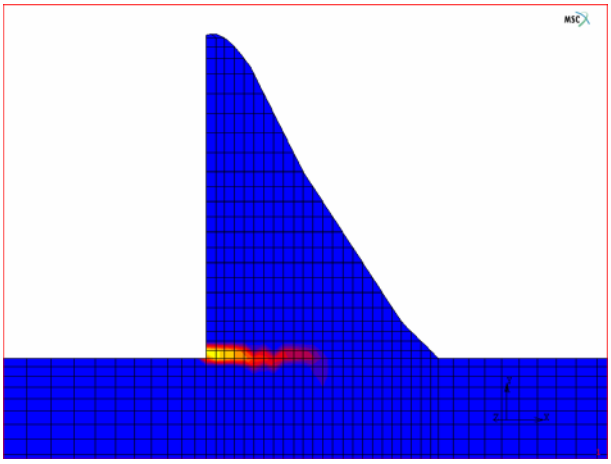

Figure 7.24 - Crack profile for $\alpha_1 = 0.4$ and $\alpha_2 = 0.1$

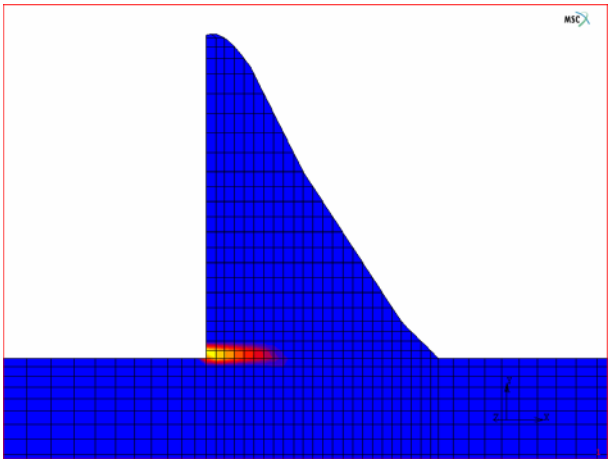

Figure 7.25 - Crack profile for $\alpha_1 = 0.4$ and $\alpha_2 = 0.2$

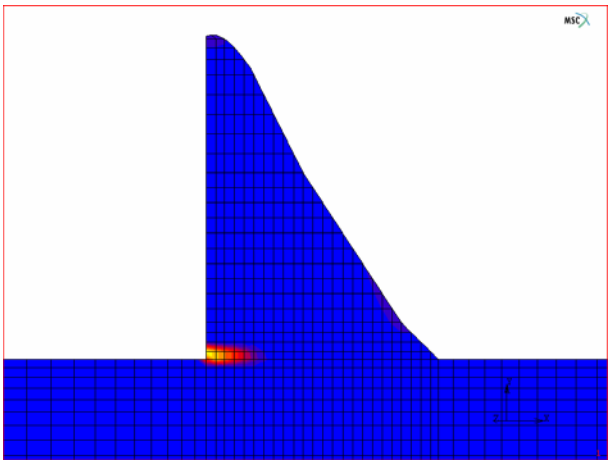

Figure 7.26 - Crack profile for $\alpha_1 = 0.4$ and $\alpha_2 = 0.3$

7.5.3 Parametric study on the tensile strength of concrete and rock

The tensile strengths of the wall concrete and the foundation rock for the crack onset criterion are varied to study their influence on the dam behaviour.

The tests on the drilled cores of the dam concrete revealed that the tensile strength of the concrete was 3.07 MPa and the tensile strength of the concrete for analysis can be taken as 1.5 MPa (Van der Spuy 1992). The influence of the tensile strength of the concrete on the crack response of the dam is studied by fixing the tensile strength of the rock f_t^r at

2.5 MPa, while the tensile strength of the concrete f_t^c ranges from 0.002 to 1.5 MPa. The other fracture parameters used for this sensitivity study are assumed to be as follows:

Bilinear shape parameters α_1 = 0.4 and α_2 = 0.05; threshold angle = 30°; maximum shear retention factor β_{max} = 0.1; and fracture energies for concrete and rock = 300 N/m and 400 N/m respectively.

If f_t^c is set equal 0.002 MPa (which represents no tensile strength at the concrete/rock interface as assumed by Seddon *et al*. 1998), the dam would crack through and fail even before water reached the FSL. Thus, the case of f_t^c = 0.002 MPa could not be shown in Figure 7.27. As seen in Figure 7.27, with an increase in the value of f_t^c, the dam has less deformation. Therefore, the crack response of the dam is obviously sensitive to the tensile strength of the concrete.

From Figures 7.28 to 7.31 it can be seen that with a higher value of f_t^c for the concrete, the cracks would bend more into the rock.

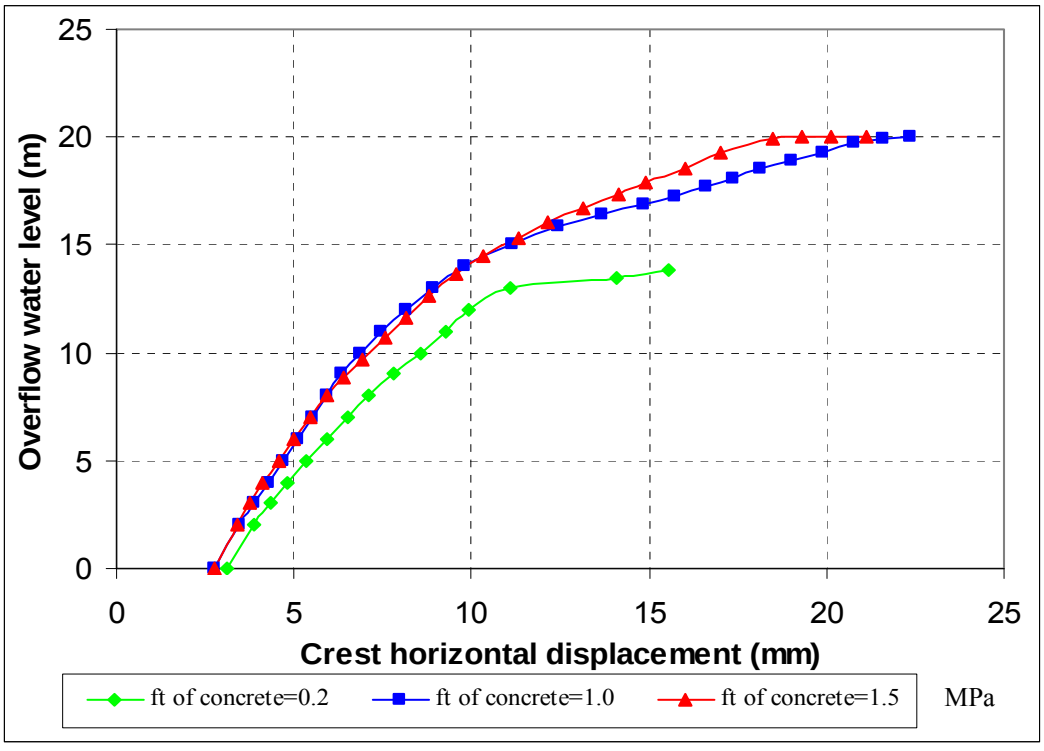

Figure 7.27 - Crest horizontal displacement vs. overflow level for various values of concrete tensile strength

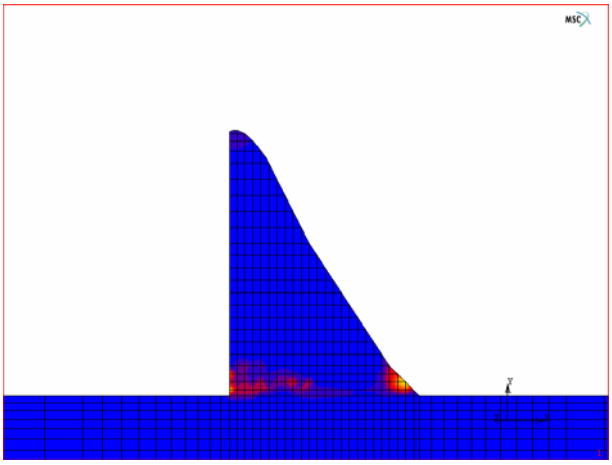

Figure 7.28 - Crack profile for f_t^c = 0.002 MPa and f_t^r = 2.5 MPa

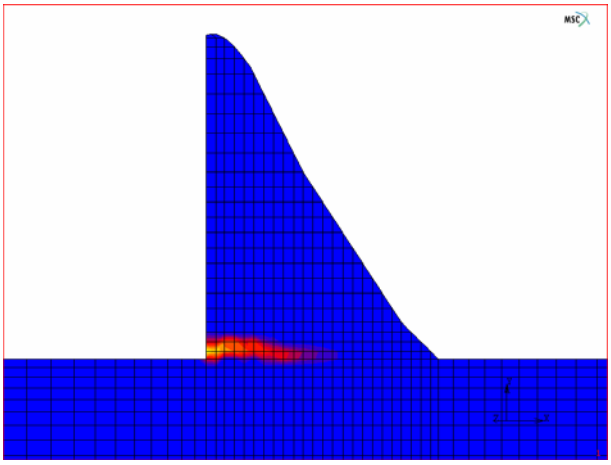

Figure 7.29 - Crack profile for f_t^c = 0.2 MPa and f_t^r = 2.5 MPa

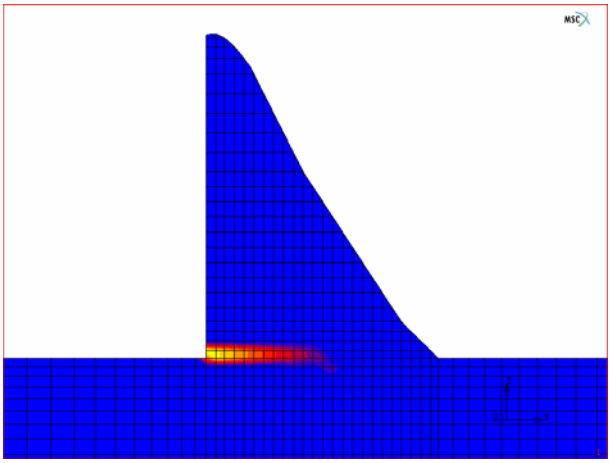

Figure 7.30 - Crack profile for f_t^c = 1.0 MPa and f_t^r = 2.5 MPa

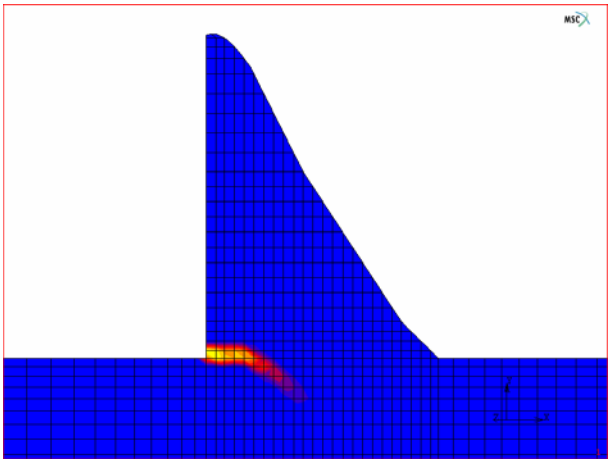

Figure 7.31- Crack profile for f_t^c = 1.5 MPa and f_t^r = 2.5 MPa

7.5.4 Parametric study on the crack onset threshold angle ϕ

Different threshold angles (ranging from 0.1° to 60°) for the crack onset criterion are studied. The threshold angle is discussed in Section 3.6 of Chapter III. The other fracture parameters used for this sensitivity study are assumed to be as follows:

Bilinear shape parameters α_1 = 0.4 and α_2 = 0.05; fracture energy of concrete and rock = 300 N/m and 400 N/m respectively; maximum shear retention factor $\beta_{\max}$ = 0.1; and tensile strengths for concrete and rock = 1.5 and 2.5 MPa respectively.

From Figure 7.32 it can be seen that there is no clear picture of the influence of the threshold angle on the crest displacement. The crack profiles for the same overflow level of 20 m shown in Figures 7.33 to 7.37 are very sensitive to the threshold angle. The cracks propagate in different directions (bifurcation) in the rock, which probably explains why the crest deformation is not sensitive to the values of the threshold angle.

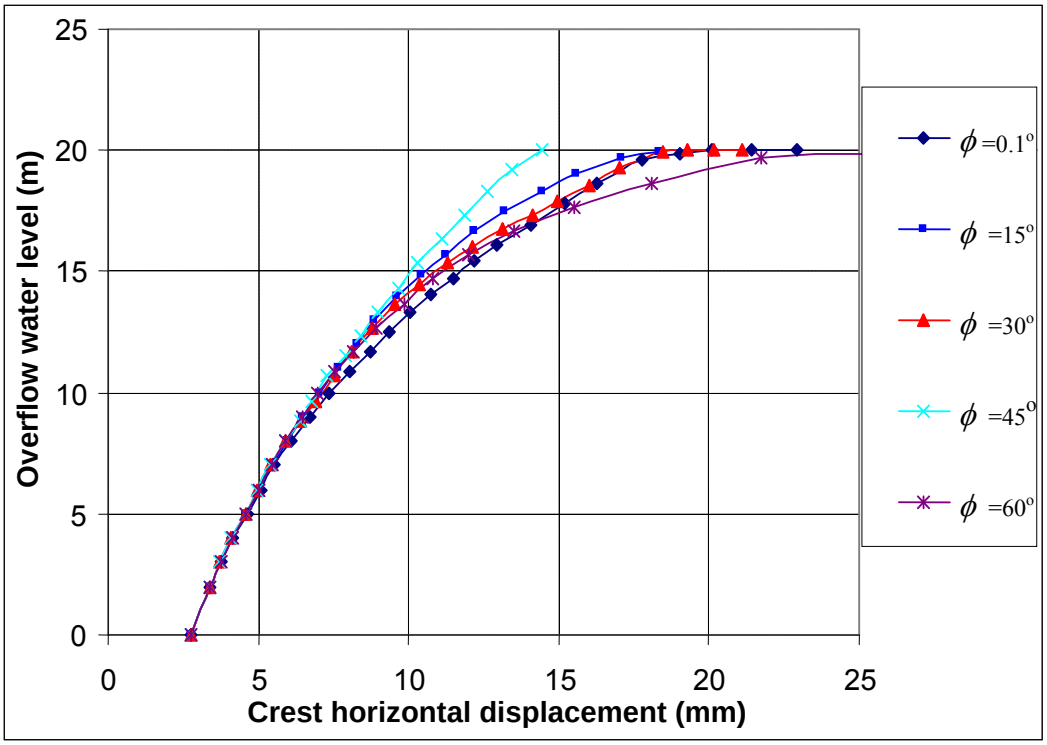

Figure 7.32 - Crest horizontal displacement vs. overflow level for various threshold angles

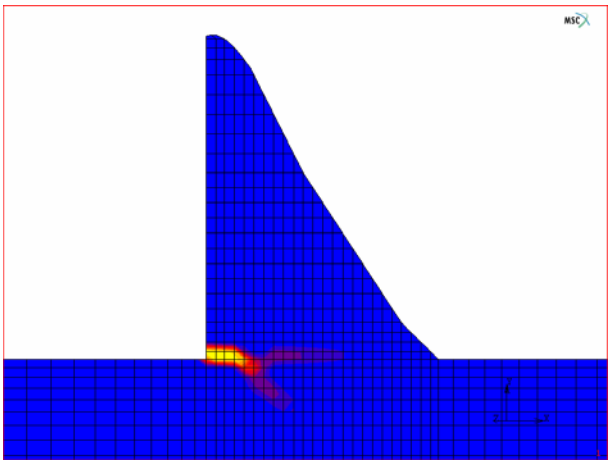

Figure 7.33 - Crack profile for threshold angle of 0.1°

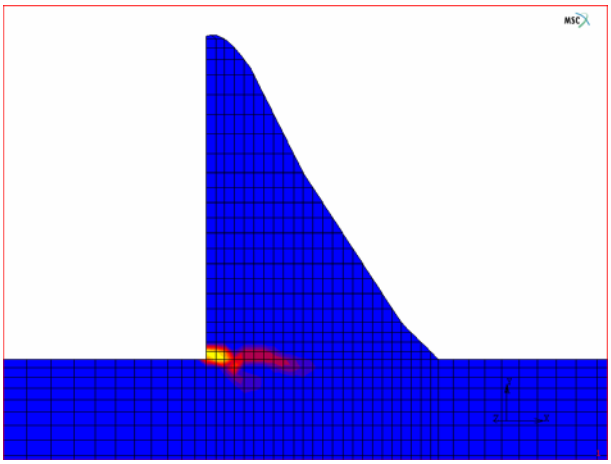

Figure 7.34 - Crack profile for threshold angle of 15°

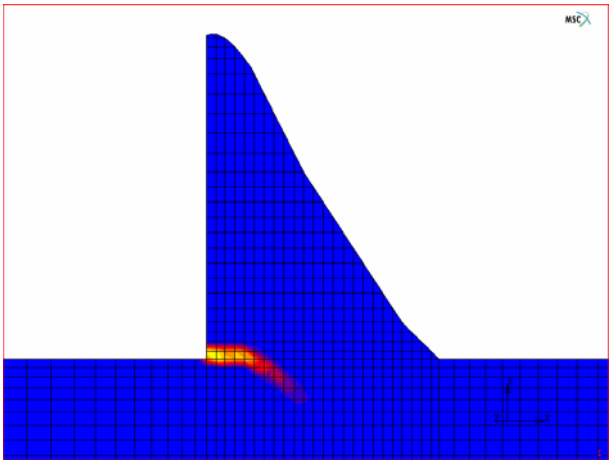

Figure 7.35 - Crack profile for threshold angle of 30^{o}

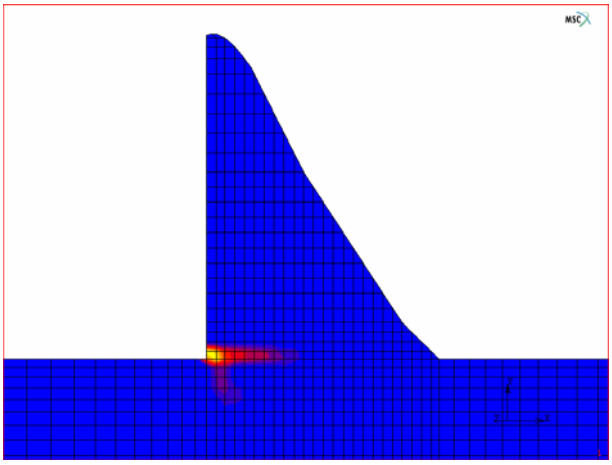

Figure 7.36 - Crack profile for threshold angle of 45^{o}

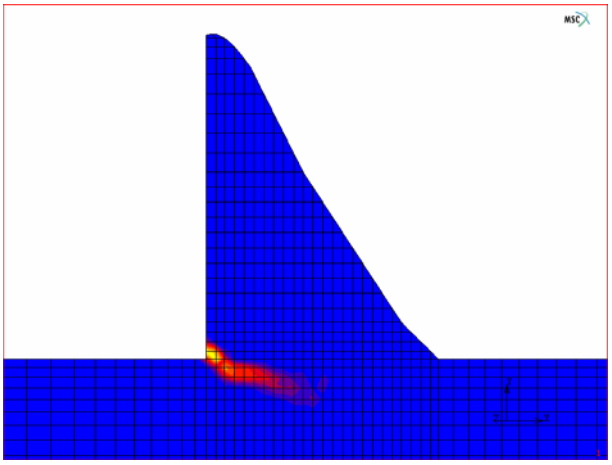

Figure 7.37 - Crack profile for threshold angle of 60^{o}

7.5.5 Parametric study on the maximum shear retention factor

The influence of the value of the maximum shear retention factor β_{max} on the structural behaviour of the dam are studied. The maximum shear retention factor is discussed in Section 3.5 of Chapter III. The other fracture parameters used for this sensitivity study are assumed to be as follows:

Bilinear shape parameters α_1 = 0.4 and α_2 = 0.05; threshold angle = 30^{o}; fracture energy of concrete and rock = 300 N/m and 400 N/m respectively; and tensile strengths for concrete and rock = 1.5 and 2.5 MPa respectively.

Figure 7.38 shows that with a decrease of β_{max}, the crest deformation becomes larger when the overflow level exceeds approximately 17 m. For higher values of β_{max} (0.2 and 0.3), the fracture analysis did not converge beyond overflow levels of 9 m and 15.7 m respectively. Figures 7.39 to 7.42 show that the smaller β_{max} is, the sooner and deeper the cracks kink into the rock.

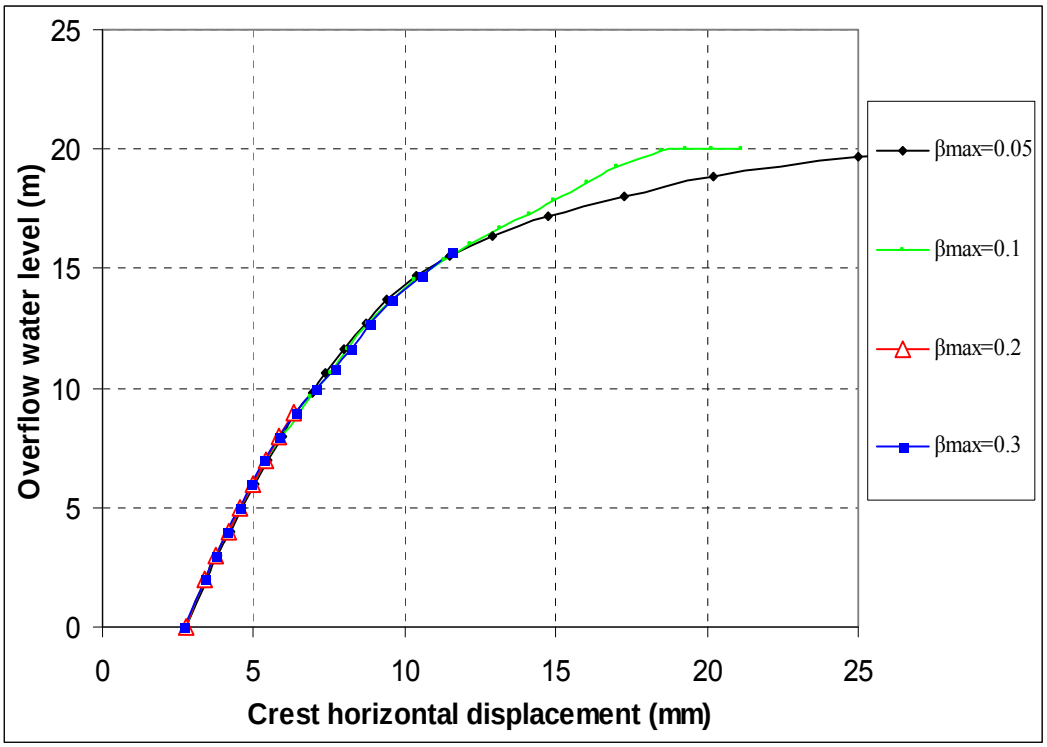

Figure 7.38 - Crest horizontal displacement vs. overflow level for various maximum shear retention factors

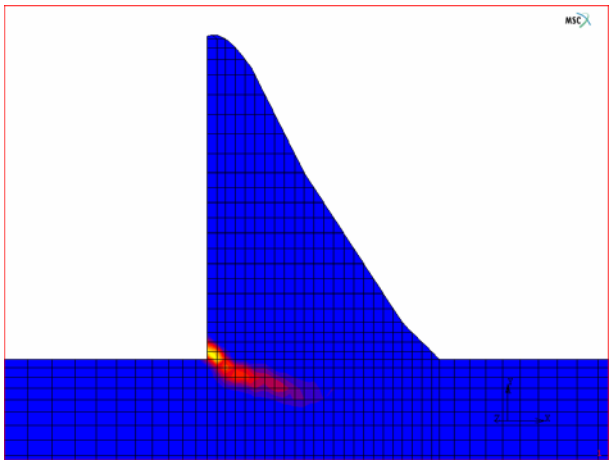

Figure 7.39 - Crack profile for $\beta_{max} = 0.05$

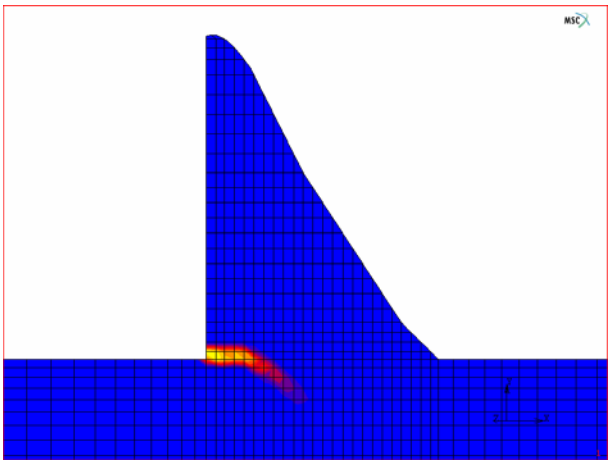

Figure 7.40 - Crack profile for $\beta_{max} = 0.1$

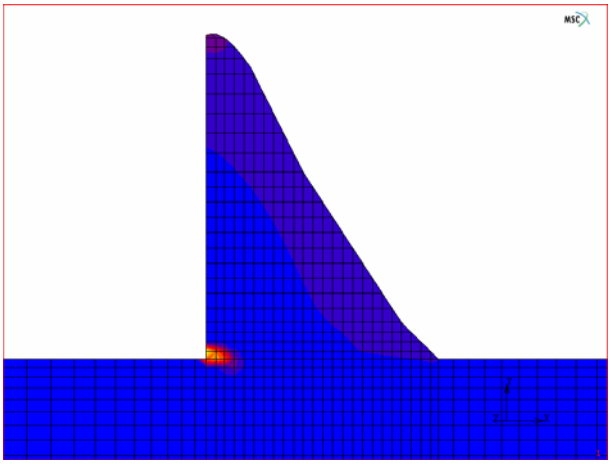

Figure 7.41 - Crack profile for $\beta_{max} = 0.2$

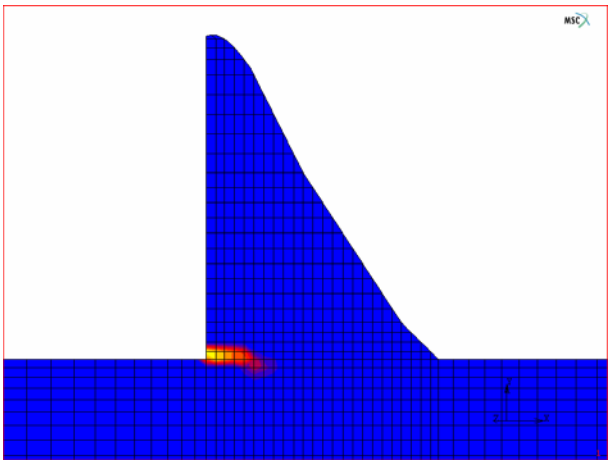

Figure 7.42 - Crack profile for $\beta_{max} = 0.3$

7.5.6 Comparison with linear elastic and plasticity analyses

A linear elastic analysis and a non-linear plasticity analysis based on the linear Mohr-Coulomb model are carried out and are compared with the results of various crack analyses. Figures 7.43a to 7.43c show a collection of previous graphs, as well as the results from the linear elastic and plasticity analyses. These graphs are representative of the previous sensitivity studies on fracture parameters. The Mohr-Coulomb yield criteria (refer to Chen & Saleeb 1982) require the cohesion C and the angle of friction φ of materials which are provided in Table 7.1.

In some study cases (such as case of G_f^c =100 N/m and G_f^r = 400 N/m) shown in Figure 7.43a, the cracking can be started as early as at FSL while in other cases, the dam starts to crack only after the water level is above FSL.

As can be seen in Figures 7.43a to 7.43c, for fracture analysis of the dam, the crest displacement starts to increase rapidly with an increase in the overflow water level above approximately 17 m over FSL. It appears that the dam is safe at RDF and SEF and can be regarded as unsafe when the overflow water level reaches approximately 17 m.

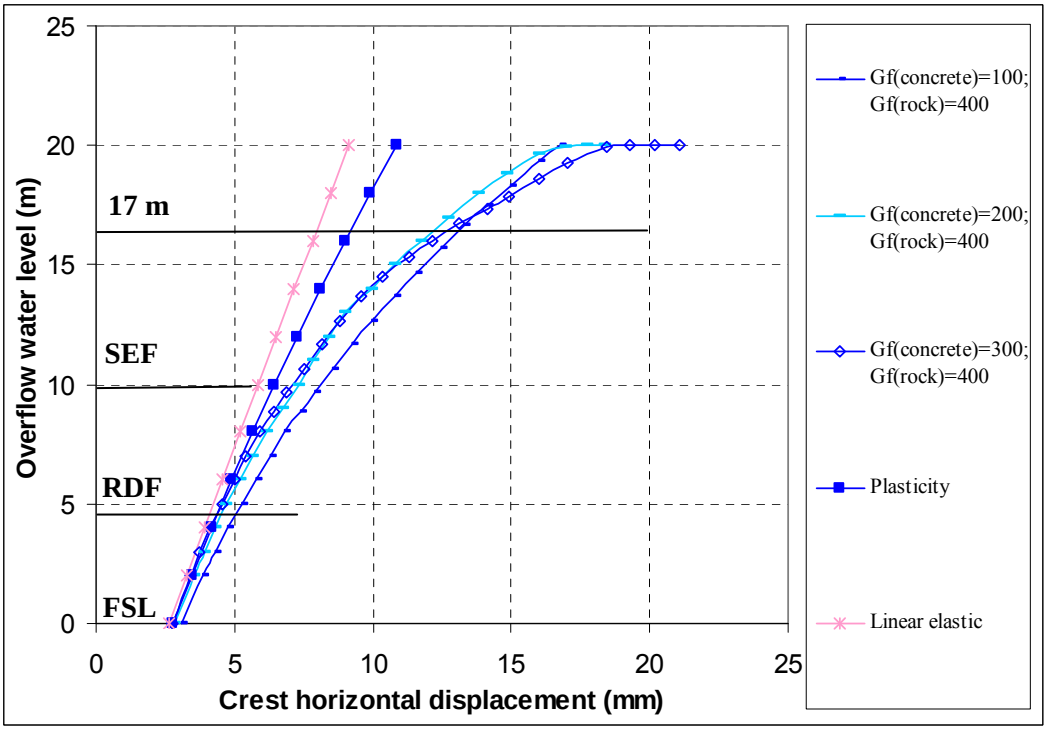

Figure 7.43a - Crest horizontal displacement vs. overflow level for various analysis methods

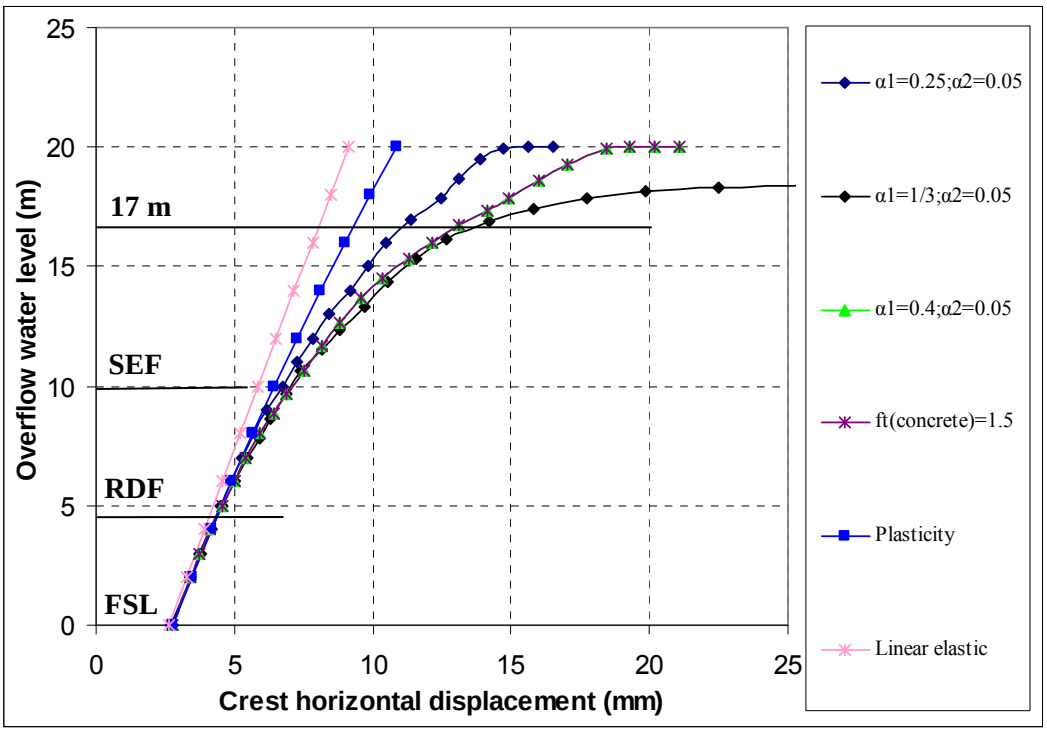

Figure 7.43b - Crest horizontal displacement vs. overflow level for various analysis methods

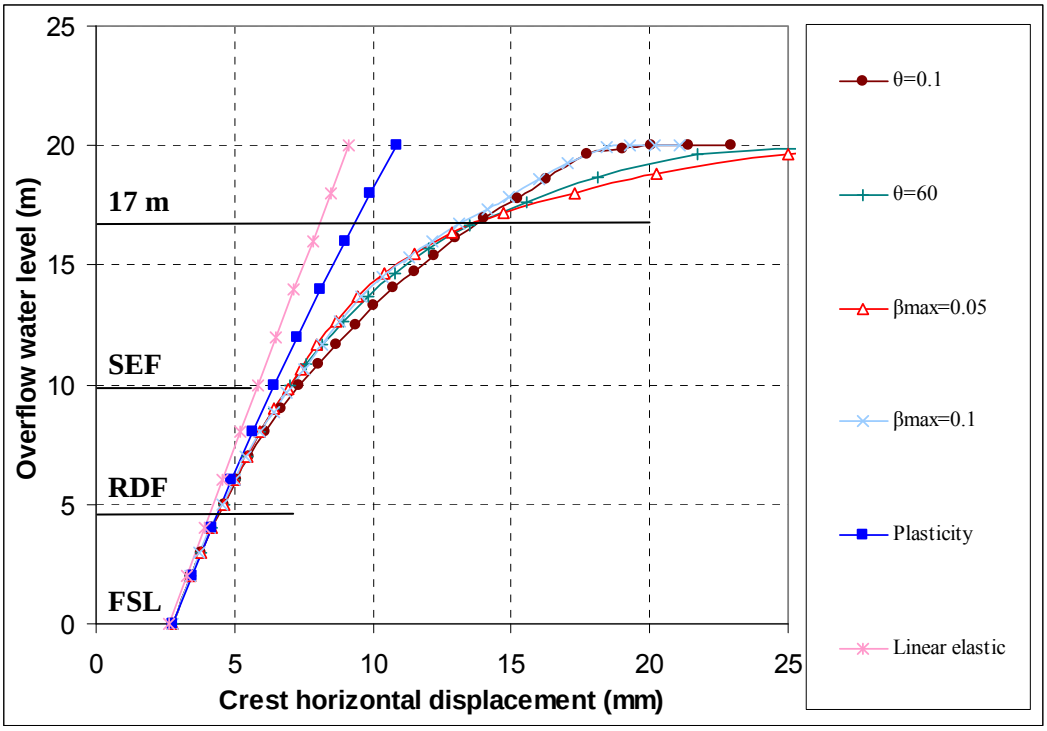

Figure 7.43c - Crest horizontal displacement vs. overflow level for various analysis methods

Subsequently, a new crack analysis is carried out based on the previous sensitivity studies on the fracture parameters (refer to Sections 7.5.1 to 7.5.5). The dam is loaded up to an overflow of 17 m, then unloaded. The constitutive fracture parameters used in this analysis are as follows:

Fracture energy G_f^c = 300 N/m and G_f^r = 400 N/m; bilinear shape parameters α_1 = 0.4 and α_2 = 0.05; threshold angle = 30°; maximum shear retention factor β_{max} = 0.05; and tensile strengths for concrete and rock = 1.5 and 2.5 MPa respectively.

The results are presented in Figures 7.44 to 7.46. Figure 7.44 clearly shows that the dam would crack continuously even under the unloading process (by reducing the overflow water level in the dam). The crest displacement continues to increase with unloading. It is clear that the cracking of the dam is in an unstable stage when the dam is loaded to an overflow of 17 m. Further loading, unloading and even keeping the same loading would make the cracking continue until reaching un-convergence in the analysis. This means that although the local elements may have "failed" due to cracking, the structure as a whole

would still be able to bear some further loading before it failed. This analysis further demonstrates that the dam can be regarded as unsafe when the overflow water level reaches approximately 17 m.

The crack profiles in the dam at the end of loading and unloading are shown in Figures 7.45 and 7.46 respectively. It is clear that the crack propagates further when the dam is in the process of unloading.

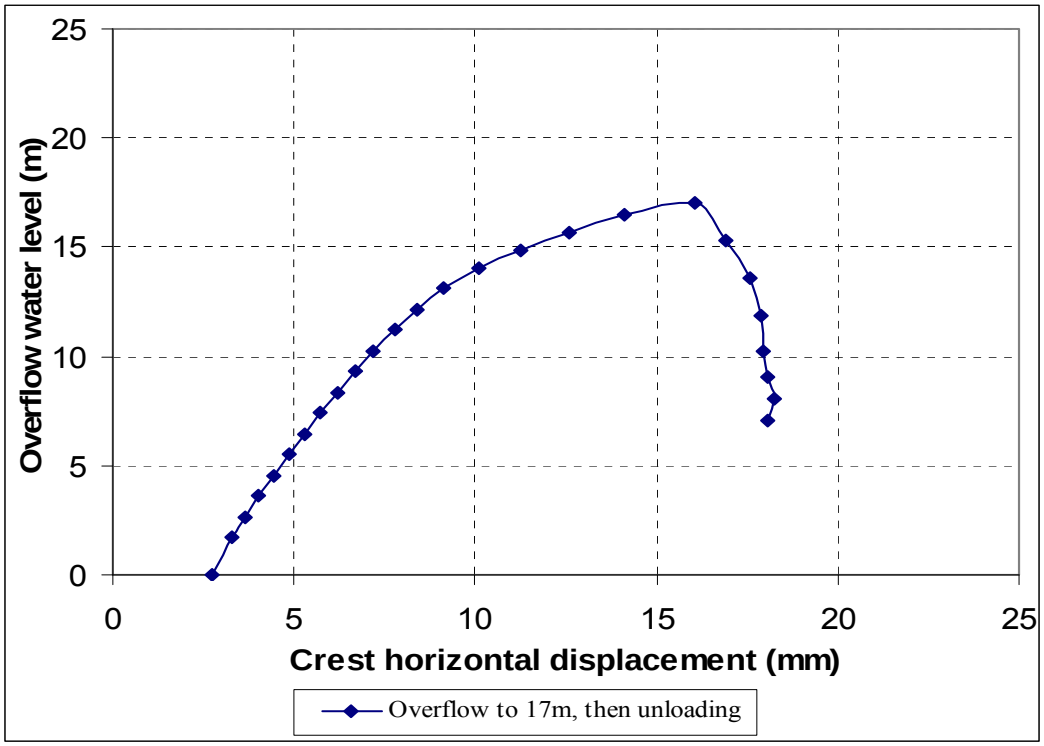

Figure 7.44 - Crest horizontal displacement vs. overflow

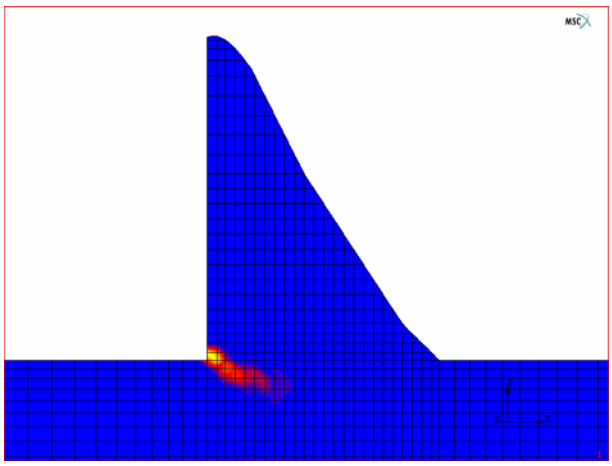

Figure 7.45 - Crack profile for overflow level at 17 m

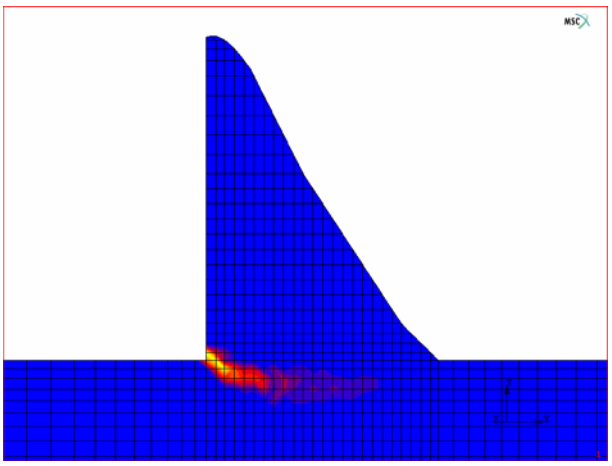

Figure 7.46 - Crack profile at the end of unloading

7.6 Evaluation of dam safety against sliding (shear)

As stated in Section 2.2 of Chapter II, the stability of a dam against sliding is of major concern to dam engineers. The classical equation (2.2) for the calculation of the factor of safety against sliding was used to evaluate the safety of this dam (Seddon *et al.,* 1998).

Due to the lack of an alternative method for evaluating the safety of a dam against sliding, in this chapter the horizontal uncracked length along the concrete/rock interface is compared with the calculated critical uncracked length, based on the classical method, to check the stability of the dam against sliding.

The calculated critical uncracked length for the abnormal load cases (20 m overflow, with a factor of safety that should be equal to or greater than 2.0) is 6.12 m, which means that if the uncracked length of the concrete/rock interface is greater than 6.12 m, then the dam is regarded as being safe against sliding (shear) under an overflow water level of 20 m.

Since all the previous sensitivity studies on the fracture parameters have uncracked lengths along the concrete/rock interface longer than the critical uncracked length of 6.12 m, the dam can be regarded as being safe against shear sliding with an overflow water level of up to 20 m.

7.7 Conclusions

The safety of the dam was evaluated by Seddon *et al*. (1998) using the traditional gravity method and cracked section analysis (rigid body equilibrium). The findings from their investigation are summarized as follows:

- The dam is stable and failure of the dam is considered very unlikely under FSL (Full Supply Level) condition (no overflow).
- The dam is unstable and the failure of the dam is considered probable under RDF (Recommended Design Flood) condition (overflow 4.6 m)

- The dam is unstable and the failure of the dam is considered possible under SEF (Safety Evaluation Flood) condition (overflow 10 m).

The crack analysis of the dam using the developed non-linear fracture mechanics (NLFM) method reveals that the dam is considered to be safe under FSL, RDF and SEF conditions. The maximum overflow that the dam can endure is found to be at approximately 17 m. Of course, this will leave the dam with no safety margin. Assuming the concrete strength has been taken as the characteristic value, if the overflow at 17 m is taken as a safety factor of 1 (total water level in the dam will be 17 + 36.3 = 53.3 m), then the SEF (9.99 + 36.3 = 46.29 m) will have a safety margin of 53.3/46.29 ≈ **1.15**, the RDF (4.61 + 36.3 = 40.91 m) will have a safety margin of 53.3/40.91 ≈ **1.3** and the FSL (36.3 m) will have a safety margin of 53.3/36.3 ≈ **1.47**.

The NLFM-based investigation into this dam yields a higher collapse load or Imminent Failure Flood (IFF) and provides higher safety factors than those predicted by classical rigid body equilibrium analysis.

The cracking, in general, would start along the concrete/rock interface. Then as the internal shear stresses rise in the rock, the cracking would kink downwards into the rock. This would leave a greater uncracked ligament length along the interface to resist shear sliding, thus giving the dam a higher safety margin.

To cover uncertainties about the material properties and fracture parameters of the concrete and rock, parametric analyses are undertaken for an appropriate structural evaluation concerning the safety of the dam. The influence of the fracture parameters on the cracking response of the dam in terms of crest deformation is summarized as follows:

- The fracture energy G_f normally does not have much influence on the dam's structural behaviour.
- The bilinear shape parameters α_1 and α_2 produce similar structural responses, except for α_1 = 1/3 ~ 0.4 and α_2 = 0.05, which would cause more deformation in the dam.

- The tensile strength f_t^c of the concrete has a significant effect on the crack response of the dam. The greater the f_t^c, the less crest deformation in the dam and the more cracking into the rock.
- The threshold angle does not have a significant influence on the dam's overall behaviour.
- The maximum shear retention factor β_{max} does not have much influence on the dam when the overflow is below approximately 17 m. When the overflow exceeds 17 m, however, the smaller β_{max} would cause the dam to deform more.

Nevertheless, the above fracture parameters, in general, do have a big influence on crack growth path, and therefore are sensitive to crack propagation in the dam structure.

It is worth pointing out that if no tensile strength is assumed at the concrete/rock interface, the dam would fail under FSL.

It is also worth pointing out that the water pressure that develops as cracks grow has not been taken into account in this research (or developed NLFM method). Therefore, the findings with regard to the safety of the dam should be taken as the maximum possible (upper boundary) safety limit that the dam can have.

CHAPTER VIII – CONCLUSIONS AND RECOMMENDATIONS

Developing a suitable constitutive material model and reliable computational procedure for analysing cracking processes in concrete has been a challenging and demanding task for many researchers worldwide. An analytical method (procedure) for the purpose of establishing a crack constitutive model and implementing the model for the fracture analysis of concrete structures, in particular massive concrete gravity dams under static loading conditions, has been developed, verified and applied in the safety evaluation of a concrete gravity dam subjected mixed-mode fracturing.

The constitutive material crack model, which permits non-orthogonal cracks (originally proposed by de Borst & Nauta 1985), is based on non-linear fracture mechanics (NLFM). A new bilinear tensile softening diagram has been proposed. A shear retention factor that depends on the crack normal strain is also included.

The constitutive material model has been implemented in a finite element (FE) analysis using a smeared crack approach. A sub-program has been specially coded for this research to be incorporated into a commercial, general-purpose FE package called MSC.Marc.

The influence on the cracking behaviour of modelling the strain softening as bilinear or non-linear has been investigated in this study. The concrete used in dams, which in general has a larger aggregate size (as large as 150 mm), a lower cement content and a lower water-cement ratio than normal structural concrete, would require careful investigation of the fracture parameters for the cracking analysis of full-scale concrete dams. The fracture energy G_f of dam concrete would be higher than that of normal concrete. Although the past investigations and experiments indicated huge discrepancies in the fracture energy of dam concrete, G_f = 100 ~ 300 N/m could be adopted for concrete in dams where no test results are available. The bilinear softening shape parameters α_1 and α_2 also need to be carefully determined for each particular concrete dam. In this research, α_1 = 0.25 ~ 0.4 and α_2 = 0.05 ~ 0.3 were studied for their sensitivity in the structural behaviour of concrete dams.

The validity of the proposed cracking model and the computational procedure developed for the purpose of analyzing the tensile fracture behaviour of concrete structures has been confirmed by verification on various concrete structures, including beams and gravity dams, subjected to either mode I or mixed-mode fracturing. All the verification specimens have been experimentally tested or/and numerically simulated before by other researchers.

The crack modelling technique developed has been successfully used in the FE analysis of an existing concrete gravity dam in South Africa and adequately predicted the cracking response of the dam structure under static loadings, including hydrostatic pressure due to overflowing, uplift pressure, silt pressure and seasonal temperature drops in the dam wall. The study has demonstrated the usefulness of NLFM in simulating the concrete cracking process and evaluating the stability of the observed cracks.

The strain-softening model proposed here for concrete could be extended to model other strain-softening materials such as rock, etc. Metallic materials, which normally exhibit a more ductile softening behaviour, could, under "brittle" fracture conditions, also be simulated by carefully calibrating the fracture parameters used in this research.

8.1 Conclusions

The following conclusions are drawn based on the comprehensive fracture modelling of varied concrete structures and the findings arising from the previous chapters:

- Both mode I fracture, which is dominant in the majority of concrete structures, and mode II fracture were modelled successfully.
- The linear softening model is popular because of its simplicity, but fails to predict the true fracture behaviour accurately. The proposed bilinear softening model remains relatively simple to implement, but significantly improves on predicting the softening response of "small-scale" concrete structures.
- For the bilinear softening diagram, the first softening modulus plays a more important (dominant) role when the structure starts to crack. The smaller first softening modulus will provide a stiffer structural response.

- Both plane stress and plane strain crack analyses have been considered and can be confidently adopted in two-dimensional applications.
- The proposed method is mesh objective and could overcome problems such as non-convergence and snap-back.
- The proposed method is element-order objective.
- The crack modelling method developed is able to predict correctly the crack propagation trajectory and the structural behaviour with regard to fracturing in concrete structures. It can therefore be confidently applied in concrete fracture analysis.
- If not considering shear stress concentration near the tip of a crack, constitutive crack analysis normally indicates a higher safety factor and a higher Imminent Failure Flood (IFF) than the classical methods in the analysis of concrete gravity dams for safety evaluation.

Regarding the sensitivity of constitutive fracture parameters to the predicted fracture response of concrete gravity dams, the following conclusions are drawn:

➢ In terms of the cracking propagation profile developed in the concrete dam structures, the following findings are obtained:

- The fracture energy of the concrete G_f has a greater influence on the crack propagation in the lower part of a dam (such as in the vicinity of the concrete/rock interface of Van Ryneveld's Pass Dam discussed in Chapter VII; the greater G_f is, the sooner and deeper the crack will bend into the rock), and less influence on the crack propagation in the upper part of the dam (such as with cracking in Koyna Dam discussed in Chapter VI).
- The influence of the bilinear shape parameters α_1 and α_2 is similar to the general findings for the fracture energy G_f. The value of α_1 does not seems to have much influence, but α_2 with a lower value will make the crack bend downwards into the rock.
- The tensile strength f_t of concrete has a significant effect on the crack trajectory path in a dam. The greater f_t is, the more the crack will bend into the rock.

- The threshold angle also has a large influence on the dam's crack propagation profile, although there no clear trend for this influence.
- The maximum shear retention factor $\beta_{\max}$ has a large influence on the crack profile in a dam. A smaller value of $\beta_{\max}$ will cause the crack to bend sooner into the rock foundation.

➢ In terms of the overall structural displacement on the crest of gravity dams, the following findings are obtained:

- The fracture energy G_f normally does not have much influence on the dam's ultimate deformation response.
- The bilinear shape parameters α_1 and α_2 are quite sensitive to the fracture response in normal "small-scale" concrete structures, such as beams, but have only some limited influence on the structural response of large-scale structures, such as concrete gravity dams.
- The tensile strength f_t of concrete has a significant effect on the crack response of a dam. The greater the value of f_t, the less crest deformation there will be in the dam.
- The threshold angle does not have a significant influence on the dam's ultimate deformation behaviour.
- The maximum shear retention factor $\beta_{\max}$ does not have much influence on the behaviour of a dam.

From all the above findings from the sensitivity study, it can be concluded that the influence of gravity and hydrostatic pressure on a dam are so dominant that the localized fracturing – influenced by the fracture energy G_f, the threshold angle, the maximum shear retention factor $\beta_{\max}$ and the softening shape parameters α_1 and α_2 – does not affect the structural response significantly. In other words, the effect on the structural response of a concrete dam due to loads, such as self-weight and hydrostatic pressure, etc., is much greater than the effect of the local material fracturing.

8.2 Recommendations

Based on this study, the following recommendations are made for future research on the cracking analysis of concrete structures:

- Water pressure inside cracks could reduce the concrete's resistance to fracturing. Water penetration and uplift pressure inside cracks should be considered.
- Three-dimensional crack analysis of dam structures, in particular of arch dams, is the preferred method of analysis.
- The tensile strength of the concrete and rock should be determined from the tests on the drilled samples taken in situ since the cracking path and the overall response in a dam are very sensitive to the magnitude of the tensile strength.
- The fracture energy of the concrete and foundation rock should also be determined from the tests on the drilled samples taken in situ.
- The bilinear softening parameters α_1 and α_2 should be determined from the data fitting of the experimental non-linear softening curve of the concrete.
- Further research on the influence of the parameters of mode II in the mixed-mode I/II fracture of concrete is recommended.
- A more rigorous definition of the crack blunt width h_c is needed.
- A study on the interaction of cracks with construction joints and foundation contacts could make the prediction of dam safety more accurate.
- The results from the numerical fracture analyses should be combined with field investigations, laboratory testing and common engineering sense to provide a clear overall picture for the evaluation of dam safety.
- The fracture analysis of a dam should be adopted as part of the routine dam safety evaluation by practising engineers for a better and more accurate evaluation of dam safety.
- Constitutive crack modelling is a powerful analysis technique which can be used to supplement the "classical" methods for dam safety analysis.
- In the case of the need for the rehabilitation of "apparently unsafe" dams predicted by classical methods, the fracture analysis method developed can be used to recheck the dam's structural behaviour and its safety, and could lead to a huge saving on unnecessary rehabilitation works.

8.3 Closure

The most challenging areas of this research have been the establishment of the smeared NLFM cracking analysis method and its numerical implementation into a finite element program for the crack safety evaluation of concrete dams. This research shows promise for establishing the ultimate strength of concrete dam structures.

ANNEXURE FINITE ELEMENT METHOD AND ALGORITHM IN MSC.Marc

MSC.Marc is a general-purpose finite element (FE) program for advanced engineering analysis, which can be used to perform a wide variety of structural, fluid and coupled analyses using the finite element method (FEM) (MSC.Marc 2005).

The purpose of this annexure is to review the FEM for a better understanding of how MSC.Marc works.

A.1 Finite element method

The FE method basically has the following six steps. The success of any FE program depends in part on how the program implements these steps.

Step 1: Choose Shape Functions: The FEM expresses the displacement field, $\underline{u}(\underline{x})$, in terms of the nodal point displacement, $\underline{a}^e$, by using the shape functions, $\underline{N}(\underline{x})$, over the domain of the element Ω^e, as:

$$\underline{u}(\underline{x}) = \underline{N}(\underline{x})\ \underline{a}^e \tag{A.1}$$

Step 2: Establish the Material Relationship: The FEM expresses the dependent fields, such as the strain and stress, in terms of the nodal point displacement as:

$$\underline{\varepsilon}(\underline{x}) = \underline{L}\left[\underline{u}(\underline{x})\right] = \underline{B}\,\underline{a}^e \ ; \quad \underline{\sigma} = \underline{\sigma}(\underline{\varepsilon}) = \underline{D}\,\underline{\varepsilon}(\underline{x}) = \underline{D}\,\underline{B}\,\underline{a}^e \tag{A.2}$$

where

$\underline{L}$	Differential operator
$\underline{B} = \underline{L}\underline{N}(\underline{x})$	Strain – displacement operator
$\underline{D}$	Constitutive matrix

Step 3: Element Matrices: The FEM equilibrates each element with its environment, which can be expressed as:

$$\underline{K}^e \, \underline{a}^e + \underline{f}^e = 0 \qquad \text{(A.3)}$$

where

$\underline{K}^e = \int_{\Omega^e} \underline{B}^T \, \underline{D} \, \underline{B} \, dV$ Represents physical properties such as stiffness

$-\underline{f}^e = \int_{\Omega^e} \underline{N}(\underline{x})^T \, \underline{b} \, dV + \int_{\Gamma^e} \underline{N}(\underline{x})^T \, \underline{t} \, dS + \underline{F}$ Represents loads experienced by the element.

These loads may be: body loads $\underline{b}$, such as weight or internal heat generation in volume Ω^e; surface loads $\underline{t}$, such as pressure on surface Γ^e; or concentrated loads $\underline{F}$.

Step 4: Assembly: The FEM assembles all the elements to form a complete structure in such a manner as to equilibrate the structure with its environment.

$$\underline{K} \, \underline{a} + \underline{f} = 0 \qquad \text{(A.4)}$$

where

$\underline{K} = \sum_e \underline{K}^e$ Overall structural stiffness matrix

$\underline{f} = \sum_e \underline{f}^e$ Overall structural load vector

$\underline{a}$ Overall nodal unknowns (such as displacement) vector

Step 5: Solve the Equations: The FEM specifies the boundary conditions, namely the nodal point values on the boundary, and the system equations are partitioned as:

$$\begin{bmatrix} \underline{K}_{uu} & \underline{K}_{us} \\ \underline{K}_{su} & \underline{K}_{ss} \end{bmatrix} \begin{bmatrix} \underline{a}_u \\ \underline{a}_s \end{bmatrix} = - \begin{bmatrix} \underline{f}_a \\ \underline{f}_r \end{bmatrix} \tag{A.5}$$

where: $\underline{a}_u$ are the unknown nodal values; $\underline{a}_s$ are the specified nodal values; $\underline{f}_a$ are the applied nodal loads; and $\underline{f}_r$ are the nodal point reactions. Hence the solution becomes:

$$\underline{a}_u = - \underline{K}_{uu}^{-1} (\underline{f}_a + \underline{K}_{us} \underline{a}_s) \tag{A.6}$$

$$\underline{f}_r = - (\underline{K}_{su} \underline{a}_u + \underline{K}_{ss} \underline{a}_s) \tag{A.7}$$

Step 6: Recover: The FEM recovers the stresses by substituting the unknown nodal values found in Step 5 back into Step 2 to find the dependent fields, such as strain and stress.

A.2 Non-linear FE analysis and iteration solution

For the solution step, the following equation must be solved:

$$[K]\{a\} = \{F\} \quad \text{or} \quad \underline{I} - \underline{F} = 0 \tag{A.8}$$

where

$[K]$ Overall structural stiffness matrix

$\{a\}$ Overall nodal unknowns vector

$\{F\}$ Overall structural load vector.

$$\underline{I} = [K]\{a\}$$

$$\underline{F} = \{F\}$$

For non-linear equations, both the stiffness and external forces may be functions of the nodal displacements:

$$\underline{I}(\underline{a})-\underline{F}(\underline{a})=0 \tag{A.9}$$

To solve a non-linear set of equations, MSC.Marc generally applies the following two solution methods:

a. Newton-Raphson (NR) method

This is an iterative method. The structural stiffness matrix is constantly updated at each iteration. Given a general non-linear equation $f(a) = 0$, and a known point a_i, a correction Δa_{i+1} can be calculated as follows:

$$\Delta a_{i+1}=\frac{f(a_i)}{f'(a_i)} \tag{A.10}$$

with

$$a_{i+1}=a_i+\Delta a_{i+1} \tag{A.11}$$

By defining the tangent stiffness:

$$f'(\underline{a}_i)\equiv \underline{K}_i^T(\underline{a}_i)=\frac{\partial}{\partial \underline{u}}(\underline{I}(\underline{a}_i)-\underline{F}(\underline{a}_i)) \tag{A.12}$$

and the residual:

$$f(\underline{a}_i)\equiv R(\underline{a}_i)=\underline{I}(\underline{a}_i)-\underline{F}(\underline{a}_i) \tag{A.13}$$

the Newton-Raphson method (equation A.10) can be rewritten in a more familiar form:

$$\underline{K}_i^T(\underline{a}_i)\Delta a_{i+1}=R(\underline{a}_i) \tag{A.14}$$

Gauss elimination techniques can be used to solve this set of equations for Δa_{i+1} .

With each iteration, the residual should decrease. If it does, the method converges to the correct solution.

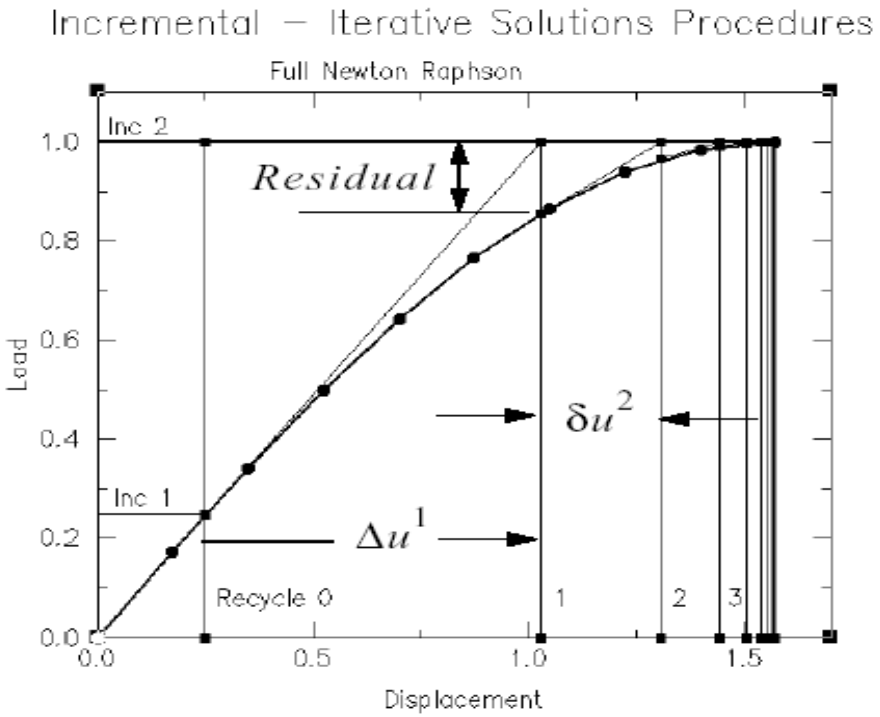

Figure A.1 - Full Newton-Raphson method (MSC.Marc 2005)

b. Modified Newton-Raphson (MNR) method

In this method, constant stiffness is applied within each load step and only updated at the beginning of the next load increment. There may be slow convergence behaviour.

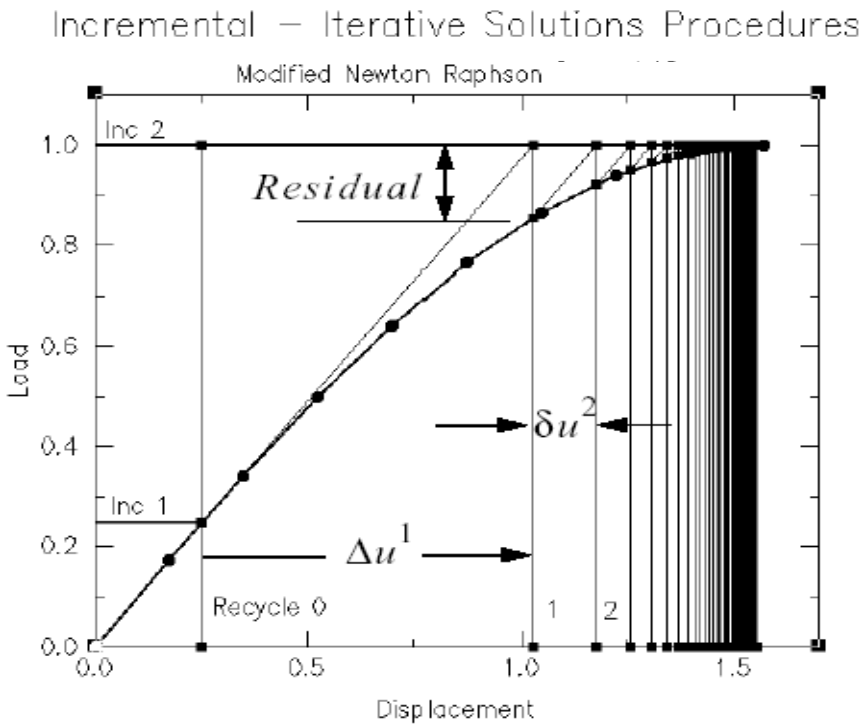

Figure A.2 - Modified Newton-Raphson method (MSC.Marc 2005)

A.3 Convergence checking

The iterative procedure is terminated when the convergence ratio is less than a criterion of tolerance.

a. Residual checking: Residuals and reactions

Relative: $$\frac{\|F_{residual}\|_{\max}}{\|F_{reaction}\|_{\max}} < Tol \qquad \text{(A.15)}$$

Absolute: $$\|F_{residual}\|_{\max} < Tol \qquad \text{(A.16)}$$

where

$\|F_{residual}\|_{\max}$ = maximum residual force

$\|F_{reaction}\|_{\max}$ = maximum reaction force

Tol = tolerance (default $Tol = 0.1$)

The residuals are the difference between the external forces and the internal forces at each node, namely:

$$\underline{F}_{residual} = \underline{F}_{external} - \int_{\Omega^e} \underline{B}^T \underline{D}\, \underline{B}\, dV \tag{A.17}$$

The nodal reactions are from the system equations, namely equation (A.7):

$$\underline{F}_{reaction} = \underline{f}_r = -(\underline{K}_{su}\, \underline{a}_u + \underline{K}_{ss}\, \underline{a}_s) \tag{A.18}$$

The maximum residuals and reactions occur at different degrees of freedom (dof) that have the largest magnitude, namely:

$$\left\|F_{residual}\right\|_{\max} = \text{Max}(F^i_{residual})\ ;\ \text{i} = 1, \text{maxdof} \tag{A.19}$$

and

$$\left\|F_{reaction}\right\|_{\max} = \text{Max}(F^i_{reaction})\ ;\ \text{i} = 1, \text{maxdof} \tag{A.20}$$

b. Displacement checking: Maximum displacement change and maximum displacement increment

Relative: $$\frac{\left\|\delta u\right\|_{\max}}{\left\|du\right\|_{\max}} = \frac{\left\|\Delta u^{i+1} - \Delta u^i\right\|_{\max}}{\left\|\Delta u^i\right\|_{\max}} < Tol \tag{A.21}$$

Absolute: $$\left\|\delta u\right\|_{\max} < Tol \tag{A.22}$$

where

$\left\|\delta u\right\|_{\max}$ = maximum displacement change

$\left\|du\right\|_{\max}$ = maximum displacement increment

Tol = tolerance (default $Tol = 0.1$)

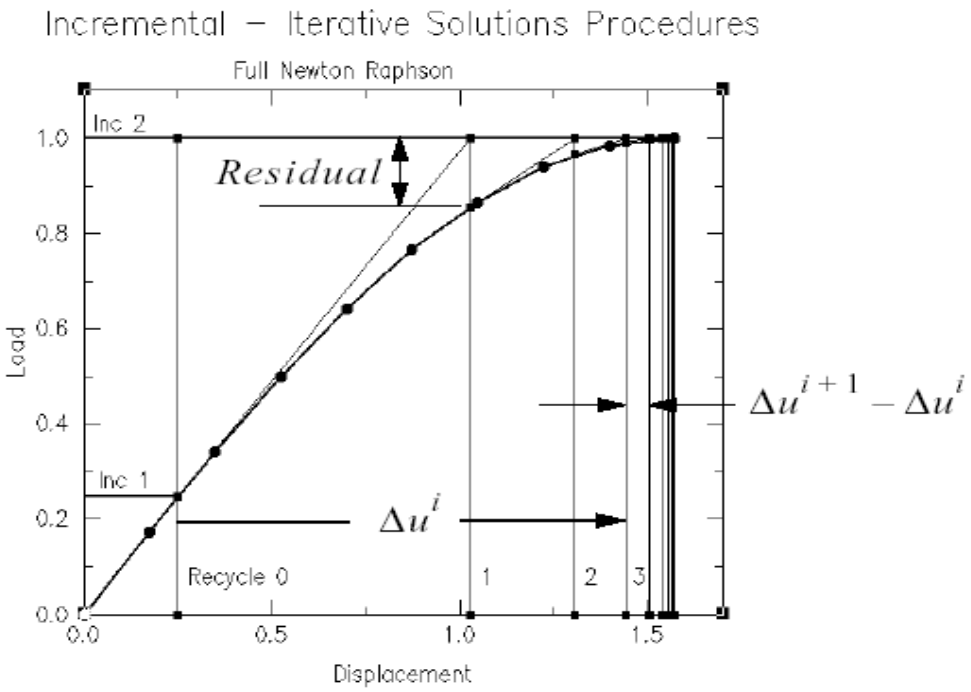

Figure A.3 - Convergence checking (MSC.Marc 2005)

REFERENCES/BIBLIOGRAPHY

ACI committee report. 1997. Finite element analysis of fracture in concrete structures: State-of-the-art. *ACI 446.3R-97*, 446.3R, 1-33.

AHMADI, M.T., Izadinia, M. & Bachmann, H. 2001. A discrete crack joint model for nonlinear dynamic analysis of concrete arch dam. *Computers & Structures*, 79:403-420.

ARAÚJO, J.M. & Awruch, A.M. 1996. An objective cracking criterion for the analysis of concrete dams. *Computers & Structures*, 59(4):751-756.

ARAÚJO, J.M. & Awruch, A.M. 1998. Cracking safety evaluation on gravity concrete dams during the construction phase. *Computers & Structures*, 66(1):93-104.

ARREA, M. and Ingraffea, A.R. 1981. *Mixed-mode crack propagation in mortar and concrete*. Report No. 81-13, Department of Structural Engineering, Cornell University, Ithaca, N.Y.

AYARI, M.L. 1988. *Static and dynamic fracture mechanics of concrete gravity dams*. PhD thesis, Department of Civil, Environmental and Architectural Engineering, University of Colorado.

BALAKRISHNAN, S. & Murray, D.W. 1988. Concrete constitutive model for NLFE analysis of structures. *Journal of Structural Engineering (New York)*, 114(7):1449-1466.

BALLARINI, R. 1990. A semi-empirical analysis of micro-cracking in concrete. *Engineering Fracture Mechanics*, 35(1-3):55-66.

BARPI, F & Valente, S. 2001. Time-dependent fracture of concrete dam models with fuzzy parameters. *Fourth International Conference,* edited by D.M. Dubois, American Institute of Physics, 325-337.

BAUSTADTER, K. & Widmann, R. 1985. The behaviour of the Kolnbrein arch dam. *COMMISSION INTERNATIONALE DES GRANDS BARRAGES, Lausanne, Switzerland*, 57(37):633-651.

BAŽANT, Z.P. 1976. Instability, ductility and size effect in strain-softening concrete. *Journal of the Engineering Mechanics Division Proceedings, ASCE (NY)*, 102(2):331-344.

BAŽANT, Z.P. 1983. Comment on orthotropic models for concrete and geomaterials. *ASCE Journal of Engineering Mechanics*, 109(3):849-865.

BAŽANT, Z.P. 1984. Size effect in blunt fracture: Concrete, rock, metal. *Journal of Engineering Mechanics (NY)*, 110(4):518-538.

BAŽANT, Z.P. 1990. A critical appraisal of 'no-tension' dam design: A fracture mechanics viewpoint. *Dam Engineering*, 1(4):237-247.

BAŽANT, Z.P. 1996. Is no-tension design of concrete or rock structures always safe? – Fracture analysis. *Journal of Structural Engineering*, 122(1):2-10.

BAŽANT, Z.P. & Cedolin, L. 1979. Blunt crack band propagation in finite element analysis. *Journal of the Engineering Mechanics Division Proceedings, ASCE (NY)*, 105(2):297-315.

BAŽANT, Z.P. & Cedolin, L. 1980. Fracture mechanics of reinforced concrete. *Journal of the Engineering Mechanics Division Proceedings, ASCE (NY)*, 106(6):1287-1306.

BAŽANT, Z.P. & Cedolin, L. 1983. Finite element modeling of crack band propagation. *Journal of Structural Engineering (NY)*, 109(1):69-92.

BAŽANT, Z.P. & Gambarova, P.G. 1980. Rough cracks in reinforced concrete. *ASCE Journal of the Structural Division*, 106(ST4):819-842.

BAŽANT, Z.P. & Gambarova, P.G. 1984. Crack shear in concrete: crack band microplane model. *ASCE Journal of Structural Engineering*, 10(9):2015-2035.

BAŽANT, Z.P. & Kazemi, M.T. 1990. Determination of fracture energy, process zone length and brittleness number from size effect, with application to rock and concrete. *International Journal of Fracture*, 44:111-131.

BAŽANT, Z.P. & Kim, S. 1979. Plastic-fracturing theory for concrete. *Journal of the Engineering Mechanics Division, Proceedings of ASCE (NY)*, 105(3):407-428.

BAŽANT, Z.P., Kim, J.K. & Pfeiffer, P.A. 1986. Nonlinear fracture properties from size effect test. *Journal of Structural Engineering, ASCE*, 112(2):289-307.

BAŽANT, Z.P. & Lin, F.B. 1988. Nonlocal smeared cracking model for concrete fracture. *Journal of Structural Engineering (New York)*, 114(11):2493-2510.

BAŽANT, Z.P. & Mazars, J. 1990. France-US workshop on strain localization and size effect due to cracking and damage. *Journal of Engineering Mechanics*, 116(6):1412-1424.

BAŽANT, Z.P. & Oh, B.H. 1983. Crack band theory for fracture of concrete. *Materials and Structures*, 16(93):155-177.

BAŽANT, Z.P. & Oh, B.H. 1985. Microplane model for progressive fracture of concrete and rock. *Journal of Engineering Mechanics(NY)*, 111(4):559-582.

BAŽANT, Z.P. & Ozbolt, J. 1990. Nonlocal microplane model for fracture, damage, and size effect in structures. *Journal of Engineering Mechanics(NY)*, 116(11):2485-2504.

BAŽANT, Z.P. & Pfeiffer, P.A. 1987. Determination of fracture energy from size effect and brittleness number. *ACI Materials Journal*, November-December:463-480.

BAŽANT, Z.P. & Prat, P.C. 1988a. Microplane model for brittle-plastic material: I. Theory *Journal of Engineering Mechanics(NY)*, 114(10):1672-1688.

BAŽANT, Z.P. & Prat, P.C. 1988b. Microplane model for brittle-plastic material: II. Verification *Journal of Engineering Mechanics(NY)*, 114(10):1689-1702.

BAŽANT, Z.P. & Swartz, S.E. 1990. Fracture mechanics of concrete: concepts, models and determination of material properties. *ACI 446. IR-XX, Concrete International Design and Construction*, 12(12):67-70.

BAŽANT, Z. P. & Tsubaki, T. 1980. Total strain theory and path-dependence of concrete. *Journal of the Engineering Mechanics Division Proceedings, ASCE (NY)*, 106(6):1151-1173.

BAŽANT, Z.P. & Xiang, Y. 1997a. Size effect in compression fracture: Splitting crack band propagation. *Journal of Engineering Mechanics*, 123(2):162-172.

BAŽANT, Z.P. & Xiang, Y. 1997b. Crack growth and lifetime of concrete under long time loading. *Journal of Engineering Mechanics*, 123(4):350-358.

BEEBY, A.W. 1979. The prediction of crack widths in hardened concrete. *Structural Engineer (London)*, 57A(1):9-17.

BHATTACHARJEE, S.S. 1993. *Smeared fracture analysis of concrete gravity dams for static and seismic loads*. PhD thesis, Dept of Civil Engineering and Applied Mechanics, McGill Univ., Canada.

BHATTACHARJEE, S.S. & Leger, P. 1992. Concrete constitutive models for nonlinear seismic analysis of gravity dams - state - of - the art. *Canadian Journal of Civil Engineering*, 19(3):492-509.

BHATTACHARJEE, S.S. & Leger, P. 1993. Finite element modelling of the tensile strain softening behaviour of plain concrete structures. *Engineering Computations*, 10(3):205-221.

BHATTACHARJEE, S.S. & Leger, P. 1994. Application of NLFM models to predict cracking in concrete gravity dams. *Journal of Structural Engineering (New York)*, 120(4):1255-1271.

BHATTACHARJEE, S.S. & Leger, P. 1995. Fracture response of gravity dams due to rise of reservoir elevation. *Journal of Structural Engineering (New York)*, 121(9):1298-1305.

BHATTACHARJEE, S.S. & Linsbauer, H.N. 2000. Uplift pressure effects on the sliding resistance of concrete gravity dams. *Dam Engineering*, XI(3):143-169.

BICANIC, N. & Zienkiewicz, O.C. 1983. Constitutive model for concrete under dynamic loading. *International Journal of Earthquake Engineering and Structural Dynamics (London UK)*, 11(5):689-710.

BLAKE, L.S. 1975. Civil Engineer's Reference Book. 3rd edition. London: *Newnes-Butterworths*.

BOCCA, P., Carpinteri, A. & Valente, S. 1990. Size effects in the mixed mode crack propagation: Softening and snap-back analysis. *Engineering Fracture Mechanics*, 35(1-3):159-170.

BOONE, T.J., Wawrzynek, P.A. & Ingraffea, A.R. 1986. Simulation of the fracture process in rock with application to hydrofracturing. *Int. Journal of Rock Mechanics and Mining Sciences and Geomechanics Abstracts (Elmsford NY)*, 23(3):255-265.

BRÜHWILER, E. 1988. *Fracture mechanics of dam concrete subjected to quasi-static and seismic loading conditions*. PhD thesis, Laboratory for Building Materials, Swiss Federal Institute of Technology. Lausanne, Switzerland.

BRÜHWILER, E. 1990. Fracture of mass concrete under simulated seismic action. *Dam Engineering*, 1(3):153-176.

BRÜHWILER, E. & Wittmann, F.H. 1990. Failure of concrete subjected to seismic loading conditions. *Engineering Fracture Mechanics*, 35 (1/2/3):565-571.

CAI, Q., Robberts, J.M. & van Rensburg, B.W.J. (2004). Constitutive models for cracking in concrete dams – A literature review. *Proc. Second International Conference on Structural Engineering, Mechanics and Computation (SEMC 2004)*, editor A. Zingoni. Cape Town: South Africa.

CAI, Q, Robberts, J M & van Rensburg, B W J 2006. Cracking in concrete using smeared cracking finite element modelling. *South African Journal of Science*, 102(11/12):548-556.

CAI, Q, Robberts, J M & van Rensburg, B W J 2006. Finite element fracture modelling of concrete gravity dams. *Submitted for publication in the Journal of the South African Institution of Civil Engineering*.

CAI, Q. & Oosthuizen C. (2006). Dam safety evaluation of concrete dams – A nonlinear fracture mechanics approach. *Proc. Hydropower 2006 International Conference*, Kunming, China.

CALAYIR, Y. & Karaton, M. 2005. Seismic fracture analysis of concrete gravity dams including dam-reservoir interaction. *Computer & Structures*, 83(2005):1595-1606.

CARPINTERI, A., Valente, S., Ferrara, G. & Imperato, L. 1992. Experimental and numerical fracture modeling of a gravity dam. In: *Fracture Mechanics of Concrete Structures*, editor Z.P. Bažant, The Netherlands, Elsevier Applied Science. pp 351-360.

CARPINTERI, A., Chiaia, B. & Bocca, P. 1997. Size dependence of strength and fracture properties of brick masonry walls. *Journal of Structural Engineering*, 123(8):816-882.

CERVERA, M., Oliver, J. & Herrero, E. 1990. A computational model for progressive cracking in large dams due to the swelling of concrete. *Engineering Fracture Mechanics*, 35(1-3):573-585.

CERVERA, M., Oliver, J. & Galindo, M. 1992. Numerical analysis of dams with extensive cracking resulting from concrete hydration: Simulation of a real case. *Dam Engineering*, 3(1):1-22.

CHANG, K.J. & Yang, T.W. 1982. A constitutive model for the mechanical properties of rock. *Int. Journal of Rock Mechanics and Mining Sciences and Geomechanics Abstracts (Elmsford NY)*. 19(3):123-133.

CHAPPELL, J.F. & Ingraffea, A.R. 1981. *A fracture mechanics investigation of the cracking of Fontana dam*. Dept of Structural Engineering Report 81-7, School of Civil and Environmental Engineering, Cornell University, Ithaca, New York.

CHEMALY, A.G. 1995. Gravity dams and fracture mechanics. MEng (Structural Engineering) thesis, University of Pretoria, Pretoria, RSA.

CHEN, E.S. & Buyukozturk, O. 1985. Constitutive model for concrete in cyclic compression. *Journal of Engineering Mechanics (NY)*. 111(6):797-814.

CHEN, W.F. 1982. *Plasticity in Reinforced Concrete*, 2nd ed. New York: McGraw-Hill.

CHEN, W.F. & Saleeb, A.F. 1982. *Constitutive equations for engineering materials*. London: Wiley, New York: Chapman and Hall.

CHOPRE, A.K. & Chakrabarti, P. 1972. The earthquake experience at Koyna dam and stresses in concrete gravity dams. *Earthquake Engineering & Structural Dynamics*, 1:151-164.

CORNELISSEN, H.A.W., Hordijk, D.A. & Reinhardt, H.W. 1986. Experimental determination of crack softening characteristics of normalweight and lightweight concrete. *HERON*, 31(2):145-156.

CURBACH, M. & Eibl, J. 1990. Crack velocity in concrete. *Engineering Fracture Mechanics*, 35(1-3):321-326.

DAHLBLOM, O. & Ottosen, N.S. 1990. Smeared crack analysis using generalized fictitious crack model. *Journal of Engineering Mechanics (New York)*, 116(1):55-76.

DE BORST, R. 1986. *Non-linear analysis of frictional materials*. PhD thesis, Delft Univ. of Technology, Delft, The Netherlands.

DE BORST, R. 1987a. Computation of post-bifurcation and post-failure behaviour of strain-softening solids. *Computers & Structure*, 25(2):211-224.

DE BORST, R. 1987b. Smeared cracking, plasticity creep and thermal loading – A unified approach. *Computer Methods in Applied Mechanics and Engineering*, North-Holland, 62:89-100.

DE BORST, R. & Nauta, P. 1985. Non-orthogonal cracks in a smeared finite element model. *Engineering Computations*, 2:36-46.

DE BORST, R., Remmers, J.J.C. & Needleman, A. 2006. Mesh-independent discrete numerical representations of cohesive-zone models. *Engineering Fracture Mechanics*, 73(2006):160-177.

DEMMER, W. & Ludescher, H. 1985. Measures taken to reduce uplift and seepage at Kolnbrein dam. *COMMISSION INTERNATIONALE DES GRANDS BARRAGES, Lausanne, Switzerland*, 58(81):1373-1393.

DEWEY, R.R., Reich, R.W. & Saouma, V. 1994. Uplift modelling for fracture mechanics analysis of concrete dams. *Journal of Structural Engineering*, 120(10):3026-3044.

DE WITTE, F.C. & Kikstra, W-P. 2003. DIANA finite element user's manual: Analysis procedures *(release 8.1, 2nd ED.), TNO DIANA b.v.*

DIANA (1998), *DIANA-7 Verification Report*.

DIVAKAR, M.P., Fafitis, A. & Shah, S.P. 1987. Constitutive model for shear transfer in cracked concrete. *Journal of Structural Engineering (New York)*, 113(5):1046-1062.

DIVAKAR, M.P. & Fafitis, A. 1992. Micromechanics-based constitutive model for interface shear. *Journal of Engineering Mechanics (New York)*, 118(7):1317-1337.

DODDS, R.H., Darwin, D., Smith, J.L. and Leibengood, L.D. 1982. *Grid size effects with smeared cracking in finite element analysis of reinforced concrete*. SM report No. 6., Univ. of Kansas, Lawrence, KANS., 118 pp.

DU, J.J., Kobayashi, A.S. & Hawkins, N.M. 1990. An experimental-numerical analysis of fracture process zone in concrete fracture specimens. *Engineering Fracture Mechanics*, 35(1-3):15-27.

DUNGAR, R., Saouma, V.E. & Wittmann, F.H. 1991. The application of fracture mechanics in dam engineering. Report on a workshop held in Locarno, Switzerland. *Dam Engineering*, 2(1):3-20.

EL-AIDI, B. & Hall, J.F. 1989a. Non-linear earthquake response of concrete gravity dams Part 1 Modelling. *Earthquake Engineering and Structural Dynamics*, 18:837-851.

EL-AIDI, B. & Hall, J.F. 1989b. Non-linear earthquake response of concrete gravity dams Part 2 Behaviour. *Earthquake Engineering and Structural Dynamics*, 18:853-865.

ESPANDAR, R. & Lotfi, V. 2000. Application of the fixed smeared crack model in earthquake analysis of arch dams. *Dam Engineering*, 10(4):219-248.

ESPANDAR, R. & Lotfi, V. 2003. Comparison of non-orthogonal smeared crack and plasticity models for dynamic analysis of concrete arch dams. *Computers & Structures*, 81:1461-1474.

FANELLI, M., Ferrara, A. & Giuseppetti, G. 1985. The fracture mechanics researches applied to concrete co-ordinated by ENEL to study the dam fracture problem. *COMMISSION INTERNATIONALE DES GRANDS BARRAGES, Lausanne, Switzerland*, 57(39):671-691.

FAFITIS, A. & Shah, S.P. 1986. Constitutive model for biaxial cyclic loading of concrete. *Journal of Engineering Mechanics (NY)*. 112(8):760-775.

FEENSTRA, P.H. 1993. *Computational aspects of biaxial stress in plain and reinforced concrete*. PhD thesis, Delft Univ. of Technology, Delft, The Netherlands.

FEENSTRA, P.H., de Borst R. & Rots, J.G. 1991a. Numerical study on crack dilatancy I: Models and stability analysis. *ASCE Journal of Engineering Mechanics*, 117(4):733-753.

FEENSTRA, P.H., de Borst R. & Rots, J.G. 1991b. Numerical study on crack dilatancy II: Applications. *ASCE Journal of Engineering Mechanics*, 117(4):754-769.

FEENSTRA, P.H., Rots, J.G., Arnesen, A., Teigen, J.G. & Hoiseth, K.V. 1998. A 3D constitutive model for concrete based on a co-rotational concept. *Computational modeling of concrete structures, Proceedings, EURO-C1998*, editor R. de Borst *et al*., 13-22. Rotterdam: Balkema.

FELTRIN, G., Wepf, D. & Bachmann, H. 1990. Seismic cracking of concrete gravity dams. *Dam Engineering*, 1(4):279-289.

FENG, L.M., Pekau, O.A. & Zhang, C.H. 1996. Cracking analysis of arch dams by 3D boundary element method. *Journal of Structural Engineering (New York)*, 122(6):691-699.

FOSTER, S.J., Budiono, B. & Gilbert, R.I. 1996. Rotating crack finite element model for reinforced concrete structures. *Computers & Structures*, 58(1):43-50.

GAJER, G. & Dux, P.F. 1990. Crack band based model for finite element method analysis of concrete structures. *ASCE Journal of Structural Engineering*, 116(6):1696-1713.

GALVEZ, J., LLorca, J. & Elices, M. 1996. Fracture mechanics analysis of crack stability in concrete gravity dams. *Dam Engineering*, 7(1):35-63.

GALVEZ, J.C., Cervenka, J., Cendon, D.A. & Saouma, V. 2002. A discrete crack approach to normal/shear cracking of concrete. *Cement and Concrete Research*, 32:1567-1585.

GEERS, M.G.D., de Borst, R. & Peerlings, R.H.J. 2000. Damage and crack modeling in single-edge and double-edge notched concrete beams. *Engineering Fracture Mechanics*, 65:247-261.

GERSTLE, W.H. & Xie, M. 1992. FEM modelling of fictitious crack propagation in concrete. *Journal of Engineering Mechanics, ASCE*, 118(2):416-434.

GHRIB, F. & Tinawi, R. 1995. Nonlinear behavior of concrete dams using damage mechanics. *Journal of Engineering Mechanics*, 121(4):513-527.

GHOBARAH, A. & Ghaemian, M. 1998. Experimental study of small scale dam models. *Journal of Engineering Mechanics*, 124(11):1241-1248.

GIOIA, G., Bažant, Z. & Pohl, B.P. 1992. Is no-tension dam design always safe? – A numerical study. *Dam Engineering*, 3(1):23-34.

GRAVES, R.H. & Derucher, K.H. 1987. Interface smeared crack model analysis of concrete dams in earthquakes. *Journal of Engineering Mechanics (New York)*, 113(11):1678-1693.

HANSON, J.H. & Ingraffea, A.R. 2003. Using numerical simulations to compare the fracture toughness values for concrete from the size-effect, two-parameter and fictitious crack models. *Engineering Fracture Mechanics*, 70:1015-1027.

HASSANZADEH, M. 1991. Determination of mixed mode properties of concrete. *Fracture Processes in Concrete, Rock and Ceramics*, editors J.G.M. van Mier, J.G. Rots & A. Bakker. London: E.& F.N. Spon.

HE, S., Plesha, M.E., Rowlands, R.E. & Bažant, Z,P. 1992. Fracture energy tests of dam concrete with rate and size effects. *Dam Engineering*, 3(2):139-159.

HILLERBORG, A., Modeer, M. & Petersson, P.E. 1976. Analysis of a crack formation and crack growth in concrete by means of fracture mechanics and finite element. *Cement and Concrete Research*, 6:773-782.

HOLLINGWORTH, F. & Geringer, J.J. 1992. Cracking and leakage in RCC dams. *International Water Power and Dam Construction*, 44(2):34-36.

HORII, H. & Chen, S.C. 2003. Computational fracture analysis of concrete gravity dams by crack-embedded elements - Toward an engineering evaluation of seismic safety. *Engineering Fracture Mechanics*, 70:1029-1045.

ICOLD report. 2001. Physical properties of hardened conventional concrete in dams. *Committee on Concrete for Dams*.

INGRAFFEA, A.R. & Manu, C. 1980. Stress-intensity factor computation in three dimensions with quarter-point elements. *International Journal of Numerical Methods in Engineering*, 15(10):1427-1445.

INGRAFFEA, A.R. 1990. Case studies of simulation of fracture in concrete dams. *Engineering Fracture Mechanics*, 35(1-3):553-564.

JEFFERSON, A D 2003. Preliminary report on comparison of codes using various benchmark problems. NW-IALAD. Task Group 2.4, NW-IALAD [online]. Available: http://nw-ialad.uibk.ac.at/ [2005, March 15]

JEFFERSON, A D, Bennett, T & Hee, S C 2005. Fracture mechanics based problems for the analysis of dam concrete. Final Technical Report, Task Group 2.4, NW-IALAD [online]. Available: http://nw-ialad.uibk.ac.at/ [2005, March 15]

JENQ, Y.S. & Shah, S.P. 1985. A two parameter fracture model for concrete. *Journal of Engineering Mechanics*, 111(4):1227-1241.

JIN, C., Soltani, M. & An, X. 2005. Experimental and numerical study of cracking behavior of openings in concrete dams. *Computers & Structures*, 83:525-535.

JIRÁSEK, M. & Zimmermann, T. 1998. Rotating crack model with transition to scalar damage. *Journal of Engineering Mechanics*, 124(3):277-284.

JIRÁSEK, M. & Zimmermann, T. 1998. Analysis of rotating crack model. *Journal of Engineering Mechanics*, 124(8):842-851.

JIRÁSEK, M. & Bažant, Z. 2002. *Inelastic analysis of structures*. John Wiley & Sons, Ltd, England.

KAPLAN, M.F. 1961. Crack propagation and the fracture of concrete. *ACI Journal, Proceedings*, 58(5):591-610.

KARIHALOO, B.L. & Nallathambi, B.L. 1989. An improved effective crack model for the determination of fracture toughness of concrete. *Cement and Concrete Research*, 19:603-610.

KARIHALOO, B.L. 1995. *Fracture mechanics and structural concrete*. Harlow: Longman.

KASPERKIEWICZ, K. 1986. Fracture and crack propagation energy in plain concrete. *Heron*, 31(2):5-14.

KOTSOVOS, M.D. & Pavlovic, M.N. 1995. *Structural Concrete: Finite-Element Analysis for Limit-State Design*. Thomas Telford, London.

KOTSOVOS, M.D. & Pavlovic, M.N. 1997. Size effects in structural concrete: A numerical experiment. *Computers & Structures*, 64(1-4):285-295.

KOTSOVOS, M.D. & Spiliopoulos, K.V. 1998. Modelling of crack closure for finite-element analysis of structural concrete. *Computers & Structures*, 69:383-398.

KUO, J. 1982. *Joint opening nonlinear mechanism: Interface smeared crack model*. Report No. UBC/EERC82/10 Earthquake Engineering, Research Center, Berkeley, CA.

KROON, J. 2002. *Concrete dams*. Short course on design and rehabilitation of dams, University of Stellenbosch, Cape Town, RSA.

KUMAR, R. & Nayak, G.C. 1994. Numerical modelling of tensile crack propagation in concrete dams. *Journal of Structural Engineering (New York)*, 120(4):1053-1074.

LANDIS, E.N., Nagy, E.N. & Keane, D.T. 2003. Microstructure and fracture in three dimensions. *Engineering Fracture Mechanics*, 70:911-925.

LECLERC, M., Leger, P. & Tinawi, R. 2003. Computer aided stability analysis of gravity dam – CADAM. *Advances in Engineering Software*, 34:403-420.

LEMAÎTRE, J. 1986. Local approach of fracture. *Engineering Fracture Mechanics*, 25(5/6):523-537.

LI, Y.J. & Zimmerman, Th. 1998. Numerical evaluation of the rotating crack model. *Computers & Structures*, 69:487-497.

LIAW, B.M., Jeang, F.L., Du, J.J., Hawkins, N.M. & Kobayashi, A.S. 1990. Improved nonlinear model for concrete fracture. *Journal of Engineering Mechanics*, 116(2):429-445.

LINSBAUER, H.N. 1985. Fracture mechanics models for characterizing crack behaviour in concrete gravity dams. *COMMISSION INTERNATIONALE DES GRANDS BARRAGES, Lausanne, Switzerland*, 57(16):279-291.

LINSBAUER, H.N. 1990. Application of the methods of fracture mechanics for the analysis of cracking in concrete dams. *Engineering Fracture Mechanics*, 35(1-3):541-551.

LINSBAUER, H.N. 1991. Fracture mechanics material parameters of mass concrete based on drilling core tests – Review and discussion. *Fracture Processes in Concrete, Rock and Ceramics*, editors J.G.M. van Mier, J.G. Rots & A. Bakker. London: E.& F.N. Spon.

LINSBAUER, H.N., Bockhoff, N. & Camguilhem, J.M. 2000. Three-dimensional stress intensity factor evaluation routine for the investigation of cracking in dams – Special features. *Dam Engineering*, XI(1):3-17.

LINSBAUER, H.N., Ingraffea, A.R., Rossmanith, H.P. & Wawrzynek, P.A. 1989a. Simulation of cracking in large arch dam: Part 1. *Journal of Structural Engineering (New York)*, 115(7):1599-1615.

LINSBAUER, H.N., Ingraffea, A.R., Rossmanith, H.P. & Wawrzynek, P.A. 1989b. Simulation of cracking in large arch dam: Part 2. *Journal of Structural Engineering (New York)*, 115(7):1616-1630.

LOTFI, V. 1996. Comparison of discrete crack and elasto-plastic models in nonlinear dynamic analysis of arch dams. *Dam Engineering*, 107(1):65-110.

LOTFI, V. & Espandar, R. 2004. Seismic analysis of concrete arch dams by combined discrete crack and non-orthogonal smeared crack technique. *Engineering Structures*, 26:27-37.

LOU, J., Bhalerao, K., Soboyejo, A.B.O. & Soboyejo, W.O. 2003. An investigation of fracture initiation and resistance-curve behavior in concrete. *Cement & Concrete Composites*, 25:599-605.

LOURENCO, P. 1996. *Computational strategies for masonry structures*. PhD thesis, Delft Univ. of Technology, Delft, The Netherlands.

LUSAS, 2004, *LUSAS user and theory manuals*, Version 13.5, FEA Ltd.

MARTHA, L.F., Llorca, J., Ingraffea, A.R. & Elices, M. 1991. Numerical simulation of crack Initiation and propagation in an arch dam. *Dam Engineering*, 2(3):193-213.

MALVAR, L.J. & Fourney, M.E. 1990. A three dimensional application of the smeared crack approach. *Engineering Fracture Mechanics*, 35(1-3):251-260.

MSC.Marc, 2005. *Documentation and Manual*. MSC.Software Corporation, USA.

NGO, D. & Scordelis, A.C. 1967. Finite element analysis of reinforced concrete beams. *Journal of the American Concrete Institute*, 64(3):152-163.

NOMURA, N., Mihashi, H. & Izumi, M. 1991. Correlation of fracture process zone and tension softening behaviour in concrete. *Cement and Concrete Research*, 21:545-550.

NORMAN, C.D. & Anderson, F.A. 1985. Reanalysis of cracking in large concrete dams in the US Army Corps of Engineers. *COMMISSION INTERNATIONALE DES GRANDS BARRAGES, Lausanne, Switzerland*, 57(9):157-171.

NW-IALAD website: Integrity Assessment of Large Concrete Dams. (2005). http://nw-ialad.uibk.ac.at/

OCONNOR, J. P. 1985. The finite element analysis of arch dams in wide valleys including the effect of crack formation at the concrete rock interface. *Institution of Civil Engineers Proceedings, Part 2: Research and Theory (London, UK)*, 79:511-532.

ONATE, E., Oller, S., Oliver, J. & Lubliner, J. 1988. A constitutive model for cracking of concrete based on the incremental theory of plasticity. *Engineering Computations (Swansea UK)*, 5(4):309-319.

OLIVER, J. 1989. A consistent characteristic length for smeared cracking models. *International Journal for Numerical Methods in Engineering*, 28:461-474.

OLIVER, J., Huespe, AE., Pulido, MDG. & Chaves, E. 2002. From continuum mechanics to fracture mechanics: The strong discontinuity approach. *Engineering Fracture Mechanics*, 69:113-136.

OWEN, D.R.J. & Hinton, E. 1980. *Finite elements in plasticity: theory and practice*. Swansea: Pineridge Press.

PEERLINGS, RHJ., Geers, MGD., de Borst, R. & Brekelmans, WAM. 2001. A critical comparison of nonlocal and gradient-enhanced softening continua. *International Journal of Solids Structure*, 38:7732-7746.

PEKAU, O.A. & Batta, V. 1994. Seismic cracking behaviour of concrete gravity dams. *Dam Engineering*, 5(1):5-29.

PEKAU, O.A., Zhang, Z.X. & Liu, C.T. 1990. Constitutive model for concrete in strain space. *Journal of Engineering Mechanics*, 118(9):1907-1927.

PEKAU, O.A., Zhang, C. & Feng, L. 1991. Seismic fracture analysis of concrete gravity dams. *Earthquake Engineering and Structural Dynamics*, 20(4):335-354.

PETERSSON, P.E., 1981. *Crack growth and development of fracture zones in plain concrete and similar materials*. Technical report TVBM 1006, Lund Institute of Technology, Lund, Sweden.

PETTERSSON, D., Alemo, J. & Thelandersson, S. 2002. Influence on crack development in concrete structures from imposed strains and varying boundary conditions. *Construction and Building Materials*, 16:207-213.

PIJAUDIER-CABOT, G. & Bažant, Z.P. 1987. Nonlocal damage theory. *Journal of Engineering Mechanics (NY)*, 113(10):1512-1533.

PLANAS, J. & Elices, M. 1990. Fracture criteria for concrete: Mathematical approximations and experimental validation. *Engineering Fracture Mechanics*, 35(1-3):87-94.

PLANAS, J., Elices, M., Guinea, G.V., Gomez, F.J., Cendon, D.A. & Arbilla, I. 2003. Generalizations and specializations of cohesive crack models. *Engineering Fracture Mechanics*, 70:1759-1776.

PLIZZARI, G.A. 1997. LEFM applications to concrete gravity dams. *Journal of Structural Engineering*, 123(8):808-815.

PLIZZARI, G.A. 1998. On the influence of uplift pressure in concrete gravity dams. *Engineering Fracture Mechanics*, 59(3):253-267.

PLIZZARI, G.A., Waggoner, F & Saouma, V.E. 1995. Centrifuge modeling and analysis of concrete gravity dams. *Journal of Structural Engineering*, 121(10):1471-1479.

RAPHAEL, J.M. 1984. Tensile strength of concrete. *Journal of the American Concrete Institute*, 81(2):158-165.

REICH, R.W., Saouma, V.E. & Cgasten, C. 1994. Fracture mechanics based analysis of lock and dam 27 on the Mississippi river. *Dam Engineering*, 5(3):59-77.

REINHARDT, H.W. & Walraven, J.C. 1982. Cracks in concrete subject to shear. *ASCE Journal of the Structural Division*, 108(ST1):207-224.

RASHID, Y.R. 1968. Analysis of prestressed concrete pressure vessels. *Nuclear Engineering and Design*, 7(4):334-344.

RIGGS, H.R. & Powell, G.H. 1986. Rough crack model for analysis of concrete. *Journal of Structural Engineering (New York)*, 112(5):448-464.

ROSSI, P. 1990. Coupling between the cracking process and viscous phenomena in concrete. *Engineering Fracture Mechanics*, 35(1-3):79-86.

ROTS, J.G. 1988. *Computational modeling of concrete fracture*. PhD thesis, Delft Univ. of Technology, Delft, The Netherlands.

ROTS, J.G. 1989. Smeared crack approach. *Fracture Mechanics of Concrete Structures: From Theory to Applications*, RILEM Report. Editor L. Elfgren. London: Chapman and Hall, pp.138-146.

ROTS, J.G. 2002. Comparative study of crack models. *Proceedings of the DIANA Conference*, http://www2.tnodiana.com/specifications1.htm, pp.17-28.

ROTS, J.G. & de Borst, R. 1987. Analysis of mixed-mode fracture in concrete. *Journal of Structural Engineering (New York)*, 113(11):1739-1758.

ROTS, J.G. & Blaauwendraad, J. 1989. Crack model for concrete: Discrete or smeared? Fixed, multidirectional or rotating?. *Heron*, 34(1):1-59.

SALEH, A.L. & Aliabadi, M.H. 1998. Crack growth analysis in reinforced concrete using BEM. *Journal of Engineering Mechanics (New York)*, 124(9):949-958.

SAOUMA, V.E. 2005. Reliability based nonlinear fracture mechanics analysis of a concrete dam; a simplified approach. *Dam Engineering*, XVI(3):219-241.

SAOUMA, V.E., Broz, J.J., Bruhwiler, E. & Boggs, H.L. 1991. Effect of aggregate and specimen size on fracture properties of dam concrete. *ASCE Journal of Materials in Civil Engineering*, 3(3):204-218.

SAOUMA, V.E., Bruhwiler, E. & Boggs, H. 1990. A review of fracture mechanics applied to concrete dams. *Dam Engineering*, 1(1):41-57.

SAOUMA, V., Linner, J., Milner, D. & Cervenka, J. 1995. Deterministic & reliability based linear and nonlinear fracture mechanics based safety analysis of Bluestone dam. *Dept of Civil, Environmental and Architectural Engineering, Univ. of Colorado, Boulder, CO 80309-0428, USA*.

SAOUMA, V.E. & Milner, D. 1996. On why fracture mechanics should be adopted for dam safety investigation. *Dam Engineering*, 7(3):215-231.

SAOUMA, V. & Morris, D. I. 1996a. Fracture mechanics; the future of concrete dam safety evaluation; Part I: Summary of Research. *Dept of Civil, Environmental and Architectural Engineering, Univ. of Colorado, Boulder, CO, EPRI, Palo-Alto, CA, Submitted to: Hydro Review*.

SAOUMA, V. & Morris, D. I. 1996b. Fracture mechanics; the future of concrete dam safety evaluation; Part II: A Case Study. *Dept of Civil, Environmental and Architectural Engineering, Univ. of Colorado, Boulder, CO, EPRI, Palo-Alto, CA, Submitted to: Hydro Review*.

SAOUMA, V.E. & Morris, D.I. 1998. Application of fracture mechanics to concrete dams: A detailed case study. *Dam Engineering*, 9(4):321-344.

SCHLANGEN, E. & Van Mier, J.G. 1993. Mixed-mode fracture propagation: A combined numerical and experimental study. *Fracture and Damage of Concrete and Rock*, Editor H.P. Rossmanith, London: E & FN Spon, pp.166-175.

SCOTTA, R., Vitaliani, R., Saetta, A., Onate, E. & Hanganu, A. 2001. A scalar damage model with a shear retention factor for the analysis of reinforced concrete structures: Theory and validation. *Computers & Structures*, 79:737-755.

SEDDON, C.V., Shelly, A.J., Moore, D.R. & Forbes, A. 1998. *Report on the safety inspection of Van Ryneveld's Pass dam.* Report No. 2835/7938, Ninham Shand Consulting Engineers, Cape Town, South Africa.

SHALL, A. 1988. Second geological maintenance report on Van Ryneveld's Pass dam. *Report No. 1988-0129*, Geological Survey, Pretoria, South Africa.

SHI, Z.H., Ohtsu, M., Suzuki, M. & Hibino, Y. 2001. Numerical analysis of multiple cracks in concrete using the discrete approach. *Journal of Structural Engineering*, 127(9):1085-1091.

SHI, Z.H., Suzuki, M. & Nakano, M. 2003. Numerical analysis of multiple discrete cracks in concrete dams using extended fictitious crack model. *Journal of Structural Engineering*, 129(3):324-336.

SIMSCIENCE web site. http://www.simscience.org/cracks/thesis/chapter3.htm, Background on fracture mechanics and dams.

SMADI, M.M., Slate, F.O. & Nilson, A.H. 1987. Shrinkage and creep of high-, medium- and low-strength concretes, including overloads. *ACI Materials Journal (Detroit)*, 84(3):224-234.

SLOWIK, V. & Saouma, V.E. 2000. Water pressure in propagating concrete cracks. *Journal of Structural Engineering*, 126(2):235-242.

STEVENS, D.J. & Liu, D. 1992. Strain-based constitutive model with mixed evolution rules for concrete. *Journal of Engineering Mechanics (New York)*, 118(6):1184-1200.

SUARIS, W. & Shah, S.P. 1985. Constitutive model for dynamic loading of concrete. *Journal of Structural Engineering (New York)*, 111(3):563-576.

SUIDAN, M. & Schnobrich, W.C. 1973. Finite element analysis of reinforced concrete. *Journal of the Structural Division, ASCE*, 99(ST10):2109-2122.

SWARTZ, S.E. 1978. Compliance monitoring of crack growth in concrete. *Journal of the Engineering Mechanics Division, Proceedings ASCE (New York)*, 104(4):789-800.

SWARTZ, S.E. & Taha, N.M. 1990. Mixed mode crack propagation and fracture in concrete. *Engineering Fracture Mechanics*, 35(1-3):137-144.

SWENSON, D.V. and Ingraffea, A.R. 1991. The collapse of the Schoharie Creek bridge: A case study in concrete fracture mechanics. *Int. Journal of Fracture*, 51:73-92.

THOMAS, H.H. 1976. The Engineering of Large Dams Part I. London: *John Wiley & Sons*.

TRUNK, B. & Wittmann, F.H. 1998. Influence of element size on fracture mechanics parameters of concrete. *Dam Engineering*, IX(1):3-24.

VALENTE, G. 2003. Fracture mechanics for the reconstruction of Noto Cathedral. *Construction and Building Materials*, 17:579-593.

VAN DER SPUY, D. 1992. Alternative for improvement: Risk-based investigation of Van Ryneveld's Pass dam. *Dam safety report, Report No. N120-01-DY03*, Department of Water Affairs & Forestry, South Africa.

VECCHIO, F.J. & Deroo, A. 1995. Smeared-crack modelling of concrete tension splitting. *Journal of Engineering Mechanics (New York)*, 121(6):702-708.

WECHARATANA, M. & Shah, S.P. 1983. Predictions of nonlinear fracture process zone in concrete. *Journal of Engineering Mechanics (New York)*, 109(5):1231-1246.

VELTROP, J.A., Yeh, C.H. & Paul, W.J. 1990. Evaluation of cracks in a multiple arch dam. *Dam Engineering*, 1(1):5-13.

WEPT, D.H., Feltrin, G. & Bachmam, H. 1993. Influence of time-domain dam-reservoir interaction on cracking of concrete gravity dams. *Earthquake Engineering and Structural Dynamics*, 22(7):573-582.

WILLAM, K.J. et al. 1984. Identification of strain-softening properties and computational predictions of localized fracture. *Report No. 8404*, Department of Civil, Environmental and Architectural Engineering, Univ. of Colorado, Boulder, CO.

WITTMANN, F.H., Rokugo, K., Brühwiler, E., Mihashi, H. & Simonin, P. 1988. Fracture energy and strain softening of concrete as determined by means of compact tension specimens. *Materials and Structures*, 21:21-32.

XIE, M. & Gerstle, W.H. 1995. Energy-based cohesive crack propagation modeling. *Journal of Engineering Mechanics (New York)*, 121(12):1349-1358.

XIE, M., Gerstle, W.H. & Rahulkumar, P. 1995 Energy-based automatic mixed-mode crack-propagation modeling. *Journal of Engineering Mechanics (New York)*, 121(8):914-923.

YAMAGUCHI, E. & Chen, W.F. 1990. Cracking model for finite element analysis of concrete materials. *Journal of Engineering Mechanics*, 116(6):1242-1260.

YAMAGUCHI, E. & Chen, W.F. 1991. Microcrack propagation study of concrete under compression. *Journal of Engineering Mechanics*, 117(3):653-673.

YANG, Z.J. & Proverbs, D. 2003. A comparative study of numerical solutions to non-linear discrete crack modeling of concrete beams involving sharp snap-back. *Engineering Fracture Mechanics*, xxx:1-23.

YON, J.H., Hawkins, N.M., & Kobayashi, A.S. 1991. Numerical simulation of mode I dynamic fracture of concrete. *ASCE Journal of Engineering Mechanics*, 117 (7): 1595-1610.

YON, J.H., Hawkins, N.M. & Kobayashi, A.S. 1997. Comparisons of concrete fracture models. *Journal of Engineering Mechanics*, 123(3):196-203.

YOSHIKAWA, H., Wu, Z. & Tanabe, T.A. 1989. Analytical model for shear slip of cracked concrete. *Journal of Structural Engineering (New York)*, 115(4):771-788.

ZHOU, J. & Lin, G. 1992. Seismic fracture analysis and model testing of concrete gravity dams. *Dam Engineering*, 3(1):35-48.

ZUBELEWICZ, A. & Bažant, Z.P. 1987. Constitutive model with rotating active plane and true stress. *Journal of Engineering Mechanics (NY)*, 113(3):398-416.